Modelling of Sorption Enhanced Chemical Looping Steam Reforming (SE-CLSR) of Methane in a Packed Bed Reactor

JULY 2016

SYED ZAHEER ABBAS

Submitted in accordance with the requirements for the degree of

Doctor of Philosophy

The University of Leeds

School of Chemical and Process Engineering

ACKNOWLEDGEMENT

First praise is to Allah, the Almighty, on whom ultimately we depend for sustenance and guidance. Second, I would like to express my deep sense of gratitude to my supervisor Dr. Valerie Dupont and Dr. Tariq Mehmood, for their support, guidance and encouragement throughout the course of this research work. Their timely and efficient contribution helped me to shape this work into its final form. Their assistance, in any way that I may have asked, is highly appreciated and regarded.

I am also deeply indebted to all my friends and colleagues namely Shoaib Hassan (Project Engineer Descon Ltd.), Dr. Gaurav Nahar, Dr. Cheng Feng, Oluwafemi A Omoniyi, Zainab Ibrahim S G Adiya, Hafizah Yun and Sergio Ramirez for their help and support. The assistance of all the technical staff at University of Leeds is greatly appreciated.

I would like to thank Prof. Mojtaba Gadhiri, University of Leeds, for providing the license for gPROMS model builder 4.1.0®.

I also wish to thank the University of Engineering and Technology, Lahore Pakistan for providing me scholarship for PhD work. I am particularly grateful to Prof. Shahid Naveed (Ex-Dean Chemical Engineering Department, UET Lahore) and Prof. Hassan Javed Naqvi (Ex-Chairman Chemical Engineering Department, UET Lahore) for their guidance and providing me an academic base.

Finally, I'm forever indebted to my family who understanding the importance of this work and supported me in all ups and downs. They always encouraged, loved and supported me whenever I needed them. I place on record, my sincere gratitude to my fiance (Syeda Muqadassa Batool) for her prayers, moral support and consistent encouragement throughout my work.

ABSTRACT

In the sorption enhanced steam methane reforming (SE-SMR) process, hydrogen (H_2) can be produced in concentration up to 98 vol. % (dry basis) in a single reactor packed with a mixture of reforming catalyst and carbon dioxide (CO_2) sorbent. This is defined as pre-combustion capturing of CO_2 and the high purity H_2 produced can be used as a fuel for electricity generation, synthesis of ammonia-derived fertilisers, or hydrotreating of naphtha and other heavy gas oil in petroleum refinery. A cyclic operation between the production of H_2 and regeneration of CO_2 sorbent is required, but the energy demand for the sorbent regeneration is high. A proposed method to decrease this energy demand is to couple SE-SMR with chemical looping (CL), which naturally separates the nitrogen (N_2) from the syngas via the highly exothermic cyclic oxidation with air of a metallic material, which acts as the reforming catalyst when reduced (oxygen transfer material or 'OTM'). The combination of SE-SMR and CL makes the process energy efficient and eliminates the need for (i) high temperature as compared to the conventional steam methane reforming (SMR) process (typical temperature range is 750- 950°C), (ii) the water gas shift (WGS) reactors downstream of the reformer, and (iii) external heating using the natural gas fuel in the reformer. However the H_2 generation of a high purity from one reactor operation is intermittent, as part of a cyclic operation, with the reactor alternately operating in Fuel Reactor mode (FR), with fuel and steam feed or Air Reactor mode (AR), with air feed. Adsorption of CO_2 shifts the equilibrium of reaction towards more H_2 production and ultimately increases the efficiency of the process towards H_2 production. Production of H_2, CH_4 conversion and overall efficiency of the process depend upon many operating parameters. The effects of inlet temperature, reactor pressure, molar steam to carbon ratio (S/C) in the feed, and gas mass velocity on the SE-SMR and the sorption enhanced chemical looping steam reforming (SE-CLSR) of methane processes is reported in this thesis.

The formulation of the SE-CLSR process model requires the modelling of packed bed reactors. This mathematical modelling covers various individual models (sub-models) for; SMR, SE-SMR, OTM reduction and oxidation of reduced OTM. The gPROMS model builder 4.1.0® is used to solve the model equations. In this work, an experimental

kinetics study and model of SMR process over 18 wt. % NiO/α-Al_2O_3 catalyst are presented for an adiabatic fixed bed reactor in the temperature range of 300-700°C at 1 bar pressure. The model is validated by comparing the results with the experimental data obtained as part of this work. The simulation results are in excellent agreement with the experimental results. The equilibrium results are generated using Chemical Equilibrium with Applications (CEA) software. The effect of various operating parameters (temperature, pressure and S/C) on the CH_4 and water conversion (%) is modelled and compared with the equilibrium values. The mathematical model of SE-SMR was developed based on the industrial operating conditions of temperature and pressure. The 873-973 K was found to be the optimum range of temperature, under the high pressure (30 bar) conditions, for the production of H_2 of purity exceeding 85%. The developed model of SE-SMR was validated against the literature data.

The mathematical model of SE-CLSR process was developed under adiabatic conditions. This model is the combination of reduction of catalyst followed by oxidation of the reduced catalyst. The individual models of reduction and oxidation are developed by using kinetic data available in the literature and later on validated with experimental results proposed in the literature. The already developed model of SE-SMR process is combined with the OTM reduction model to mimic the dynamic process occurring in the fuel reactor (FR) system. This FR is combined with air reactor (AR) and the combined model is run for 10 cycles. The sensitivity of the process is studied under the various operating conditions of temperature (873-1023 K), pressure (1-30 bar), molar S/C (2-6) and mass flux of the gas phase (G_s = 2-7 kg m^{-2} s^{-1}). In this work, the operating conditions used for the production of H_2 represent realistic industrial production conditions. The sensitivity analysis demonstrates that the developed model of SE-CLSR process has the flexibility to simulate a wide range of operating conditions of temperature, pressure, S/C and G_s.

The candidate confirms that the work submitted is his own, except where work which has formed part of jointly-authored publications has been included. The contribution of the candidate and the other authors to this work has been explicitly indicated below. The candidate confirms that appropriate credit has been given within the thesis where reference has been made to the work of others.

LIST OF PUBLICATIONS

A list of publications is listed below that are part of this present study. The contribution of the candidate and the other others to this work has been explicitly indicated below. Chapter 4, 5 and 6 within the thesis have been based on work from jointly authored publications. These publications are:

- **Syed Zaheer Abbas**, Valerie Dupont and Tariq Mahmud. Kinetics study and modelling of steam methane reforming process over a NiO/Al_2O_3 catalyst in an adiabatic fixed bed reactor. International Journal of Hydrogen Energy, 2016. (Under review)
- **Syed Zaheer Abbas**, Valerie Dupont and Tariq Mahmud. Modelling of high purity H_2 production via sorption enhanced chemical looping steam reforming of methane in a packed bed reactor. Fuel Journal, 2016. (Under review)
- **Syed Zaheer Abbas,** R. Bloom, V. Dupont, T. Mahmud and S. J. Milne. Packed bed chemical looping and sorption enhanced steam reforming research at Leeds. Oral presentation at 6th High Temperature Solid Looping Cycles Conference, Politecnico Di Milano, Milan, Italy (1^{st} - 2^{nd} September 2015)
- **Syed Zaheer Abbas**, Valerie Dupont and Tariq Mahmud. Modelling of packed bed sorption enhanced steam reforming (SE-SMR). Oral presentation at UKCCSRC Manchester Biannual Meeting on 14^{th} April 2016.
- **Syed Zaheer Abbas**, Valerie Dupont and Tariq Mahmud, Steve J. MILNE, Zainab I. S. G. ADIYA and Robert BLOOM. Novel Materials and Reforming Process Route for the Production of Ready-Separated $CO_2/N_2/H_2$ from Natural Gas Feedstocks. Poster presented at UKCCSRC Call Projects Showcase Poster reception in London on 27^{th} June 2016.

The candidate as primary author for this publication led the experimental and modelling work and writing up of the publications. Dr. Valerie Dupont and Dr. Tariq Mahmud were co supervisors of the research work, participated in the analysis of results and proof-read the publications.

TABLE OF CONTENTS

LIST OF FIGURES

LIST OF TABLES

NOMENCLATURE

A	Cross sectional area of empty column, m^2
a	Empirical coefficient
a’	Empirical coefficient, factor of proportionality
a_v	Interfacial area per unit volume of catalyst bed, m^2/m^3
b	Empirical coefficient
b’	Empirical coefficient, factor of proportionality
C_A	Concentration of component A, mol/m^3
$C_{A,i}$	Concentration of component A at solid gas interface , mol/m^3
C_i	Concentration of component ‘i’, mol/m^3
$C_{i,in}$	Inlet concentration of component ‘i’, mol/m^3
$C_{i,o}$	Concentration of component ‘i’ at t=0, mol/m^3
C_{pg}	Heat capacity of gas at constant pressure, J/(kg.K)
$C_{p,bed}$	Heat capacity of bed at constant pressure, J/(kg.K)
D_i	Effective diffusion coefficient, m^2/s
D_m	Average molecular diffusivity, m^2/s
d_P	Catalyst particle diameter, m
D_r	Inner diameter of the reactor, m
D_z	Axial dispersion coefficient, m^2/s
e	Combined mass flux, W/m^2
E_j	Activation energy of reaction j, J/mol
E(t)	Conversion enhancement
f	Friction factor
F_c	Coolant mass flow rate, kg/s

g_c	Gravitational constant, $m^2/(kg.s^2)$
G_s	Mass flow velocity, $kg/(m^2.s)$
H^o	Enthalpy per unit mass at reference state, J/kg
h_f	Gas o solid heat transfer coefficient, $W/(m^2.s)$
j_A	Mass flux, $kg/(s.m^2)$
J_A	Molar flux, $kmol/(s.m^2)$
$J_{D,i}$	Chilton-Colburn j-factor for mass transfer
J_H	Chilton-Colburn j-factor for heat transfer
k	Thermal conductivity, W/(m.K)
k_{eff}	Effective thermal conductivity, W/(m.K)
$k_{g,A}$	Gas to solid mass transfer coefficient of component A, m^3/m^2s
K_i	Adsorption constant of species i
k_j	Kinetic rate constant of reaction j
K_j	Thermodynamic equilibrium constant of reaction j
$K_{o,i}$	Reference adsorption constant of species i
k_z	Axial thermal conductivity, W/(m.K)
L	Reactor length, m
M_m	Average molecular mass, kg/kmol
n_A	Combined mass flux for specie A, $kg/(s.m^2)$
N_A	Combined molar flux for specie A, $kmol/(s.m^2)$
p_A	Partial pressure of specie A, bar
P	Total pressure, bar
p_i^{feed}	Partial pressure of component I in feed, bar
P^o	Pressure at z=0, bar
P_{in}	Inlet pressure of the feed, bar
P_r	Prandtl number

Q	Rate of heat flow across a surface, W
q	Heat flux vector, W/m^2
q_{CO2}	Solid phase concentration of CO_2 (average on the surface of sorbent), mol/m^3
R, R_g	Ideal gas constant, J/(mol.K)
r_A	Rate of production of component A, $mol/(kg_{cat}.s)$
r_{ad}	Rate of adsorption of CO_2, mol/(kg.s)
R_e	Reynolds number
R_j	Rate of reaction j, $mol/(kg_{cat}.s)$
S_a	Active surface area, m^2
S	Surface area, m^2
S_{ci}	Schmidt's number
T	Temperature within system, K
t_n	Number of reactor tubes
T^o	Inlet temperature, K
T_s	Temperature of catalyst particles, K
$T_{s,o}$	Temperature of solid particles at 't=0', K
T_w	Wall temperature, K
U	Overall heat transfer coefficient,
u_s, v	Superficial velocity, m/s
V_c	Volume of coolant, m^3
W_c	Flow rate of coolant, kg/s
X_{max}	Maximum fractional carbonation conversion of CaO
X_{CH4}	Fractional conversion of methane
ΔH_{rex}	Heat of reaction at standard condition, J/mol
ΔH_{ads}	Heat of adsorption reaction at standard condition, J/mol

ΔP	Pressure drop across the reactor, bar

Greek Letters

β	Coefficient of kinetic energy
Ω	Denominator term in the reaction kinetics
λ_z^f	Effective thermal conductivity, W/(m.K)
λ_g	Average gas thermal conductivity, W/(m.K)
λ_s	Solid thermal conductivity, W/(m.K)
λ_z^o	Effective thermal conductivity of motionless fluid, W/(m.K)
ψ	Particle shape factor
ρ_f	Density of fluid, kg/m^3
ρ_{cat}	Density of catalyst, kg/m^3
ρ_{ad}	Density of sorbent, kg/m^3
η_j	Effectiveness factor of reaction ‘j’
Φ_{ij}	Stoichiometric coefficient of component ‘i’ in reaction ‘j’
μ_g	Viscosity of gas, Pa.s
υ	Ratio of catalyst amount to sorbent amount
ε_b	Bed void fraction

List of Abbreviations

AEM	Avrami-Erofe’ev model
AIC	Akaike information criterion
AR	Air reactor
AR5	Fifth assessment report
ASTM	American society for testing and materials
ASU	Air separating unit

BDF	Backward differentiation formulae
BFDM	Backward finite difference method
CCCC	Capture of CO_2 in coal combustion
CCS	Carbon capture and sequestration
CDCL	Coal direct chemical looping
CEA	Chemical equilibrium and applications
CFD	Computational fluid dynamics
CGSM	Changing grain size model
CLC	Chemical looping combustion
CLH	Chemical looping hydrogen
CLOU	Chemical looping with oxygen uncoupling
CLR	Chemical looping reforming
CPO	Catalytic partial oxidation
DASOLV	Differential algebraic solver
DSU	Desulfurization unit
FDM	Finite different methods
FR	Fuel reactor
GHGs	Greenhouse gases
GHSV	Gas hourly space velocity
gPROMS	General process modelling system
HHV	Higher heating value
HROs	Heavy residual oils
HT-WGS	High temperature water gas shift
IEA	International energy agency
iG-CLC	In situ gasification chemical looping combustion
IPCC	Intergovernmental panel on climate change

K-HTC	Potassium Promoted Hydrotalcite
LHV	Lower Heating Value
LT-WGS	Low Temperature Water Gas Shift
MFC	Mass Flow Controllers
MS	Mass Spectrometer
MV	Modified Volumetric model
NG	Natural Gas
OC	Oxygen Carrier
ODEAs	Ordinary Differential Equation
OSD	One Step Decarbonisation
OTM	Oxygen Transfer Material
PEMFC	Proton Exchange Membrane Fuel Cell
PDEs	Partial differential equations
POx	Partial oxidation
PSA	Pressure swing adsorption
PT	Proute-Tompkins model
RDS	Rate determining step
RPM	Random pore model
SE-SMR	Sorption enhanced steam methane reforming
S/C	Steam to carbon ratio
SCL	Syngas chemical looping
SCM	Shrinking core model
SMR	Steam methane reforming
SE-CLSR	Sorption enhanced chemical looping steam reforming
SR	Steam reforming reactor
SR-CLC	Steam reforming integrated with chemical looping combustion

USR	Unmixed steam reforming
WGS	Water gas shift
XRD	X-Ray diffraction

CHAPTER # 1
INTRODUCTION

This chapter deals with the importance of hydrogen (H_2) as the fuel of the future and the scope of the research work presented in the thesis. Process of conventional steam methane reforming (SMR) is most widely used for the production of H_2 on an industrial scale. The issues related to the conventional SMR process are discussed and objectives of this research work are addressed in this chapter.

1.1 Global warming

In the past few decades the climate of the earth is changing drastically. The change in the orbit of earth, natural phenomena like change in the intensity of radiation from the sun and the emission of excessive greenhouse gases (GHGs) in the atmosphere are the key factors effecting the climate [1]. The activities of human have strong impact on the emission of CO_2 which is causing a strong effect on the climate of earth. In the recent report of IPCC, Fifth Assessment Report (AR5) [2], it is claimed that emission of greenhouse gases into the atmosphere in last decade are the highest in the history. The last 3 decades from 1983-2012 are considered as the warmest decades faced by human since 1850. 'Hadley Centre of the UK' [3] reported data regarding rise in the temperature of the earth from 1850 onwards. According to their data, the rise in the temperature from 1850-1910 was almost zero and later on a small increase in the temperature was observed from 1910-1940. The highest rise in the temperature was observed from 1980 onwards. The change in the land temperature due to global warming is shown in **Figure 1.1**.

The linear trend of increase in temperature of the land shows that the average rise of 0.85 °C is observed over the period of 1880 to 2012. The researchers defined CO_2 emission as the major cause of the global warming and the increase in the amount of CO_2 has put negative impact on the temperature of the earth. The increase in CO_2 has not only affected the temperature on the earth but also it raised the level of sea and resulted in many extreme weather events in the past.

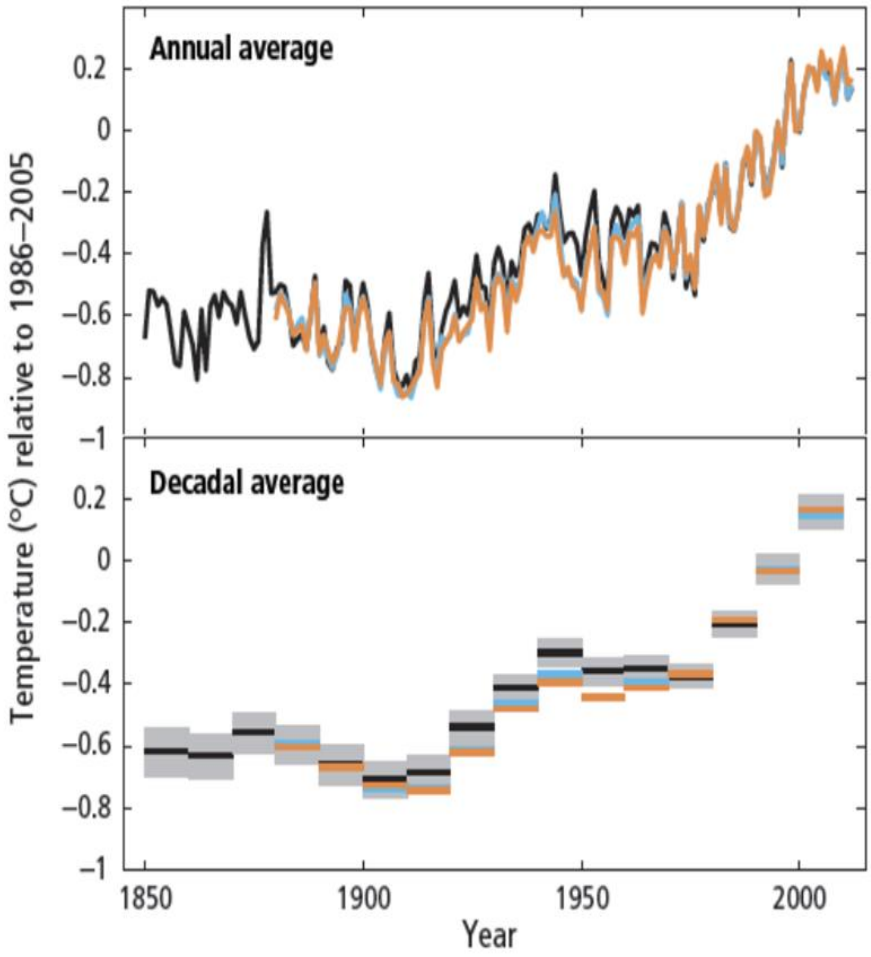

Figure 1.1: Observed globally averaged combined land and ocean surface temperature anomaly 1850–2012 (grey colour indicates an estimate of decadal mean uncertainty in data) [3]

According to IPCC report [2], the amount of CO_2, CH_4 and nitrous oxide (N_2O) are the main contributor towards climate change. Between 1750 and 2011, almost 40% of CO_2 emission remained in the atmosphere while rest is absorbed on the land (in plants and soil). Despite many mitigation techniques adopted for CO_2 emission, the amount of greenhouse gases especially CO_2 is keep on increasing. This increase in the amount of the greenhouse gases is more significant during the period of 2000 to 2010. The amount of CO_2 in the atmosphere reached 49 ± 4.5 $GtCO_2$-eq/yr in 2010. The major contribution of CO_2 in the atmosphere is the burning of fossil fuel in the thermal power plants and heavy chemical industries such as petrochemical and fertilizer. It contributed about 78% of total GHG emissions from 1970 to 2010. This increase in the amount of GHGs in the atmosphere is shown in **Figure 1.2.**

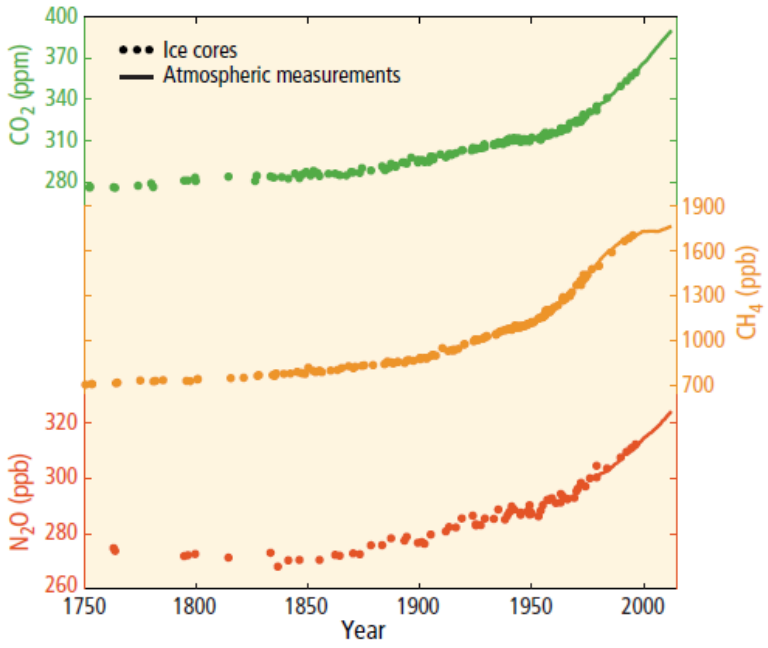

Figure 1.2: The observed concentration of GHG in the atmosphere. Data from ice cores (symbols) and direct atmospheric measurements (lines) are overlaid [4].

This rise in the amount of GHGs, especially CO_2, is due to many factors like; increase in the demand of electricity, deforestation and increase in the population of the world. The economic indicators have predicted that in coming years the demand of electricity will increase further, as currently around 3.6 billion population do not have adequate supply of electricity and around 1.6 billion people do not have any electricity. According to the report of EIA [5], by 2030 the demand of electricity will increase by more than 75%.

The data published by EIA [5] showed that in 2008 the electricity generated by coal was more than the half power generated in entire US i.e. 54% of total electricity production. The electricity generated by natural gas was 12% which is expected to increase by 32% until 2020. The other massive contributors towards the electricity generation was nuclear power (21%) and remaining was generated by oil (2%), hydropower (9%) and renewable solar or wind (2%).

As the coal and natural gas is available in abundance, this makes the industrial plants (thermal power plants and heavy chemical industries such as petrochemical and fertilizer) to run on these fuels rather than any other alternatives. But the emission of GHGs and their impact on global warming forced the companies to device a clean process of electricity production. The carbon capture and geological sequestration (CCS) is one such key techniques. The CO_2 capture and storage (CCS) process consists of capturing of CO_2 from the industrial plants and then transported to the storage location. This

technology has the provision of capturing around 85–95% of the CO_2 emitted from the industrial plant, but at the expense of large amount of energy. The CCS process needs about 10-40% more energy as compared to the plant which has no CO_2 capturing provision [6]. In 3rd assessment report (AR3) of IPCC this phenomena is discussed and comparison of both processes is shown in **Figure 1.3** [6].

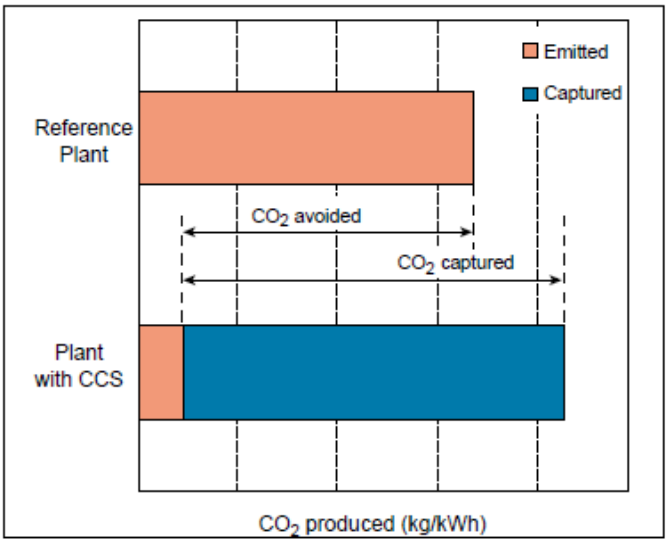

Figure 1.3: The capturing and storage of CO_2 from power plant [6]

1.2 Alternative energy sources

The fast growing demand of energy in different sectors has put enormous burden on coal, natural gas and oil. The main disadvantage of these fuels is their impact on the environment and ultimately causing global warming. At the same time due to finite sources of fossil fuels, researchers are working on alternative fuels to meet the demand of the electricity.

Currently, the renewable resources of energy are supplying 15-20% world's energy demand and in 1990 the total amount of energy produced by the renewable resources was around 2900 TWh (24% of the world's total electricity supply) [7]. According to "World Energy Outlook 2010", the use of renewable energy triples between 2008 and 2035. In this period the rise in their electricity share is predicted to be around 32% in 2035 [8]. In "IEA World Energy Outlook 2011" [9] it is predicted that in the future more energy supply shares are expected from renewable sources especially from hydropower as shown in **Figure 1.4**. It can be seen in the figure that even a considerable increase in energy share by renewable sources, still no single or combine source can fulfil the demand of energy

requirements. The electricity generated by all the renewable energy sources is mostly used for the production of hydrogen [10].

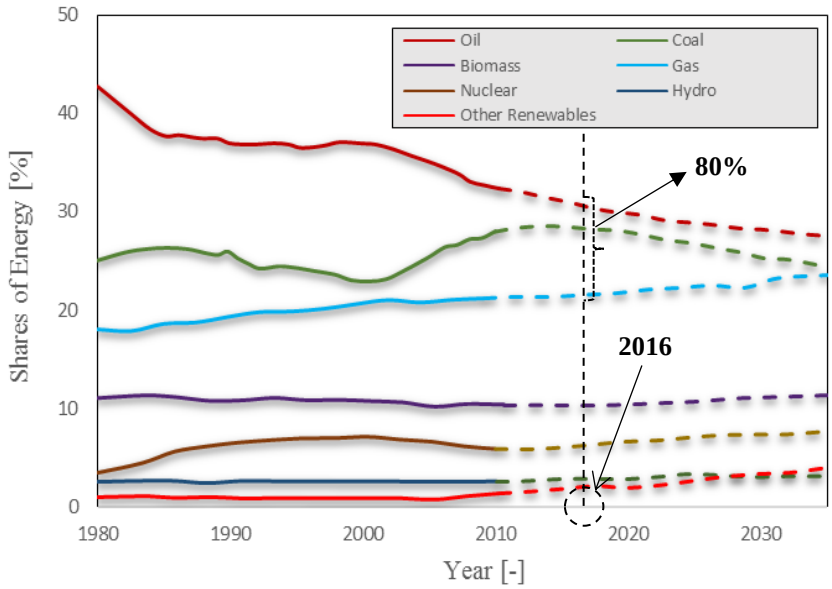

Figure 1.4: Shares of energy sources in world primary energy demand from 1980-2035 [9].

1.3 Hydrogen as a feedstock

On a broader scale H_2 can be used either as a feedstock/reactant or as a fuel. As a reactant, H_2 can be used in oil refineries to remove the sulphur contents from the hydrocarbons and in fertilizer industries for the production of ammonia.

The production of ammonia via Hyber process consumes about 60% of total world's H_2. While on the other hand in USA about 40.3% of total H_2 is used for the production of ammonia and 37.3% of total H_2 is used in the oil refineries as a reactant [1]. The worldwide captive users of H_2 are listed in **Table 1.1**.

Table 1.1: The worldwide consumption of H_2 in 2003 [1]

Captive users	**World total**	
	Billion m^3	Share (%)
Ammonia producers	273.7	61
Oil refineries	105.4	23
Methanol producers	40.5	9
Other	13.6	3
Merchant users	16.1	4
Total	449.3	100

Since 1960, the population of the world has doubled but not the supply of food per capita. The supply of food calories per capita increased from 2420 kcal/day to 2808 kcal/day from 1958 to 1999 [11]. The pace of increase in food production is very slow as compared to the growth of population. As it is already mentioned that H_2 plays a vital role in the production of ammonia, which is the backbone of any fertilizer industry [12], therefore, the need of H_2 for food supply will be higher in the future.

1.4 Hydrogen as a fuel

Increasing energy demands, depletion of fossil fuel reserves and pollution growth make H_2 an attractive alternative energy carrier. H_2 is widely considered as the fuel of the future and it has the capability to fuel the generation of electricity without emitting harmful pollutants [13]**.** H_2 is the basic raw material for fertilizer industries especially for ammonia production [14-16]. With the passage of time it may become general purpose carrier of energy for electricity, power generation and in vehicles as a transportation fuel [17, 18]. When H_2 is burnt, the only product is water vapour, without greenhouse gas or any pollutant such as SO_x, soot and particular matters emitted in the environment [19, 20]. This makes H_2 a very clean and efficient energy carrier. It can be produced from renewable and non-renewable sources. At present, reforming of natural gas and electrolysis processes are widely used for H_2 production [1, 21]. The H_2 Economy data showed that in 2004 the production of H_2 was around 50 million tons and every year this production is increasing by 10% [1]. Currently, the maximum amount of H_2 is produced from natural gas (48%) followed by petroleum (30%), coal (18%) and electrolysis process (4%) as shown in **Table 1.2** [1].

Table 1.2: World's sources of H_2 production [1]

Sources of H_2 production		Contribution [%]
Hydrocarbons	Natural gas	48
	Petroleum	30
Coal		18
Water electrolysis		4

H_2 is abundantly used as the raw fuel for fuel cells to generate electricity. Low temperature fuel cells are very efficient and environmental friendly, and they have increased the importance of H_2 because they continuously required the pure supply of H_2 and air [22]. Fuel cells are electrochemical devices and they can easily convert the chemical energy of a gaseous or liquid reactant into useful electrical energy. It consists of cathode, anode and an electrolyte. A typical schematic of a Proton Exchange Membrane Fuel Cell (PEMFC) [23] is shown in **Figure 1.5.** The fuel (H_2) is introduced at the anode surface and oxidant (O_2) is introduced at the cathode surface. H_2 splits at the anode and forms two positively charged protons. These protons move towards cathode through the electrolyte and react with oxygen to form water. The completion of this circuit generates the electricity having water as the only by product. The most important ability of the fuel cell is that it produces pollution-free energy. Europe has set a roadmap with the target of 1GW energy from fuel cells by 2015 [24].

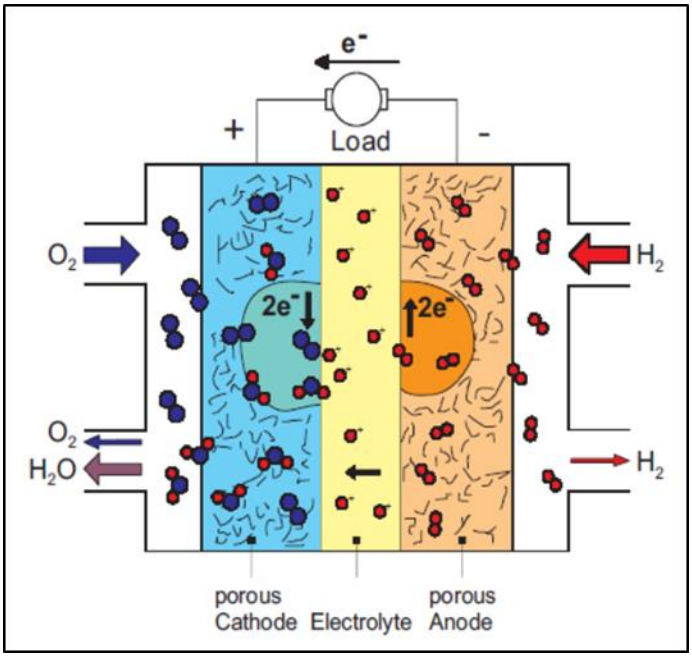

Figure 1.5: Schematic diagram of hydrogen/oxygen fuel cell [23]

1.4.1 Properties of Hydrogen fuel

Amongst all the alternative sources of fuel, H_2 is the most prominent fuel because of the properties like inexhaustibility, cleanliness and convenience of storage. These properties have promoted H_2 as one of the best replacement for gasoline, natural gas and other fuels

[25]. The flexibility of H_2 makes it more favourable fuel than the already available fuels. It can be used for transportation, power generation and for heating.

Hydrogen gas is very light weight (14 times lighter than air) and it diffuses faster than any other gases. Important physical properties of H_2 are listed in **Table 1.3**.

Table 1.3: Properties of hydrogen [1]

Property	**Value**
Molecular weight	2.02×10^{-3} kg mol^{-1}
Density of gas at 0 °C and 1 atm.	0.08987 kg m^{-3}
Density of solid at -259 °C	858 kg m^{-3}
Density of liquid at -253 °C	708 kg m^{-3}
Melting temperature	-259 °C
Boiling temperature at 1 atm.	-253 °C
Critical temperature	-240 °C
Critical pressure	12.8 atm.
Critical density	31.2 kg m^{-3}
Heat diffusion at -259 °C	58 kJ kg^{-1}
Heat of vaporization at -253 °C	447 kJ kg^{-1}
Thermal conductivity at 25 °C	0.019 kJ m^{-1} s^{-1} $°C^{-1}$
Viscosity at 25 °C	0.00892 centipoise
Heat capacity (C_p) of gas at 25 °C	14.3 kJ kg^{-1} $°C^{-1}$
Heat capacity (C_p) of liquid at -256 °C	8.1 kJ kg^{-1} $°C^{-1}$
Heat capacity (C_p) of soli at -259.8 °C	2.63 kJ kg^{-1} $°C^{-1}$

Over a wide range of temperature and pressure, H_2 is highly flammable. On reacting with oxygen, it releases high amount of energy. Unlike other fuels, H_2 fuel is not available on the earth in a free form. The energy contents in H_2 fuel are higher than any other fuel e.g. it has 3 times more energy contents as compared to gasoline (140.4 MJ/kg versus 48.6 MJ/kg). H_2 has very low ignition energy (0.02 mJ) as compared to gasoline (0.24 mJ). The comparison of different fuels is tabulated in **Table 1.4**.

Table 1.4: Comparison of hydrogen with other fuels [1]

Fuel	LHV [MJ/kg]	HHV [MJ/kg]	Stoichiom -etric air/fuel ratio [kg]	Combustible range [%]	Flame Temp. [°C]	Min. ignition energy [MJ]	Auto ignition Temp. [°C]
Methane	50.0	55.5	17.2	5-15	1914	0.30	540-630
Propane	45.6	50.3	15.6	2.1-9.5	1925	0.30	450
Octane	47.9	15.1	0.31	0.95-6.0	1980	0.26	415
Methanol	18.0	22.7	6.5	6.7-36.0	1870	0.14	460
Hydrogen	**119.9**	**141.6**	**34.3**	**4.0-75.0**	**2207**	**0.017**	**585**
Gasoline	44.5	47.3	14.6	1.3-7.1	2307	0.29	260-460
Diesel	42.5	44.8	14.5	0.6-5.5	2327		180-320

There are many processes used for H_2 production including fuel processing of hydrocarbons (natural gas, gasoline and naphtha) and non-reforming H_2 production techniques. In fuel processing techniques H_2 containing hydrocarbon fuels are converted into H_2 rich stream. These different H_2 production techniques will be discussed in **Chapter 2.**

1.5 Project scope

The conventional SMR process is the most widely used technique for H_2 production. Over 50% of the world's H_2 production comes from the SMR process [26]. The SMR process is very costly process and with the passage of time its efficiency decreases. **Cortright R et al.** [27] estimated the capital cost of the SMR plant as 254.1 M$ having 341,448 kg/day H_2 output. Furnace tubes are very costly and due to extremely high temperature in the reformer furnace, the tubes life period decreases from 11.4 to 2 years. Extremely high temperatures (800-1000 °C) in the conventional SMR process cause aging of the reformer tubes. The main reasons for damaging of the reformer tubes are; creep (inner side of the tube), carburization, thermal shocks and accidental overheating. A tube start to crack at $2/3^{rd}$ portion from the outside of tube and propagates towards the inner portion. Once that portion is damaged, cracks start to penetrate towards the outer portion [28]. In the

industry, the reformer tubes are normally designed to withstand for a period of about 100,000 h (11.4 years). High temperatures within the reformer tubes cause deterioration of catalyst and it causes tube choking and increase the gas residence time within the tubes. This choking caused overheating of the tubes and it leads to creep cavitation damage. Owing to the severe operating conditions, reformer tubes are generally fabricated from centrifugally cast creep-resistant high carbon austenitic steel of ASTM A297 Grade HK (25 Cr, 20 Ni and 0.4 C) or Grade HP (26 Cr, 35 Ni, 0.4 C). In some cases other high temperature, heat resistant alloys may be used, in general with a composition derived from the HP grade. Such materials have very high cost. Due to this problem of overheating some tubes only withstand for 2years service life and have to be replaced soon after that [29].

The vital reason of the reformer tubes failure is overheating as catalyst tubes are designed for a specific temperature range. If the operating temperature increases over the design temperature, a drastic decline in the life period of tubes is observed. **Figure 1.6** shows the effect of temperature on the expected life of reformer tubes.

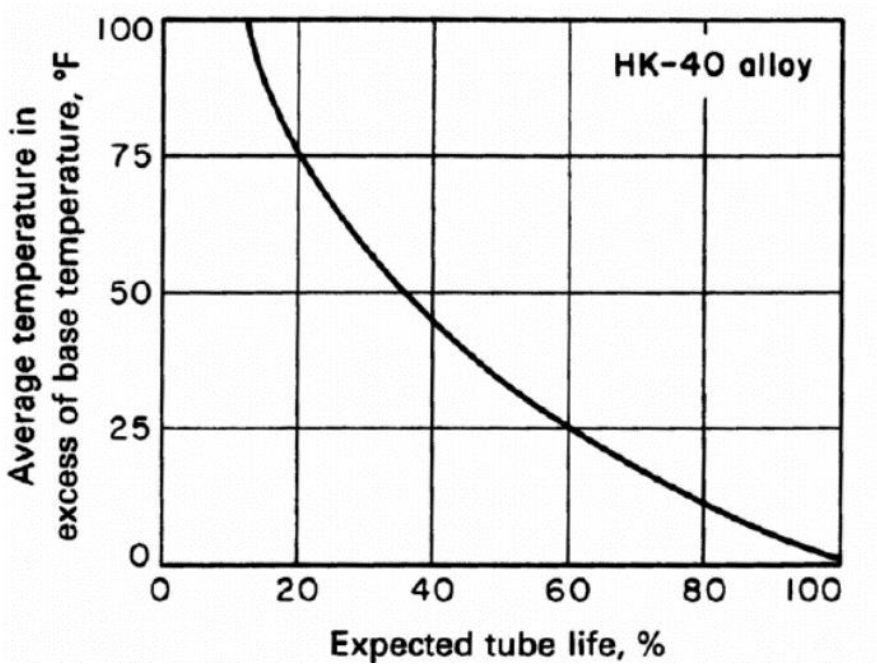

Figure 1.6: Effect of exceeding the design temperature on the expected life of HK-40 alloy reformer tubes [30]

To avoid such problems in addition to safety and environmental effect, companies have to invest significance amounts in maintenance to prevent any incident due to reformer failure. The cumulative costs to prevent the incidents are as much as $10 billion [31].

In industrial SMR process, shift reactors are needed downstream of the reformer to convert the undesired CO and CO_2 to H_2. Later on, amine scrubbing or pressure swing adsorption (PSA) process is required to achieve the higher purity of H_2 [32]. To address the issue of global warming, researchers developed the concept of combining the reforming process with in-situ CO_2 separation. This process was named sorption enhanced steam methane reforming (SE-SMR) process [32-34]. The addition of sorbent (CO_2 acceptor) along with the catalyst promotes the performance of the reforming process not only by shifting the reactions towards more H_2 production but also in terms of purity of H_2 (CO_2 free product), as well as suppressing equilibrium solid carbon by-product and permitting both lower temperatures of operations and steam demand.

In 2000, **Lyon** and **Cole** [35] proposed an interesting concept of H_2 production process. As conventional SMR process requires high temperatures, and to avoid the issues caused by the overheating and material failure of the reactor tubes, a new process was introduced which was termed as 'unmixed steam reforming' (USR) or chemical looping reforming (CLR). The CLR process operates in alternative cycles between 'steam reforming' and 'regeneration of the catalyst particles'. The heat generated during the oxidation of metal oxide is utilized in the endothermic SMR reaction (**Eq. 1.1**). The schematic of a moving bed CLR process is shown in **Figure 1.7**.

$$CH_{4(g)} + H_2O_{(g)} \leftrightarrow CO_{(g)} + 3H_{2(g)} \qquad \Delta H_{298K} = 206\ \text{kJ mol}^{-1} \qquad (1.1)$$

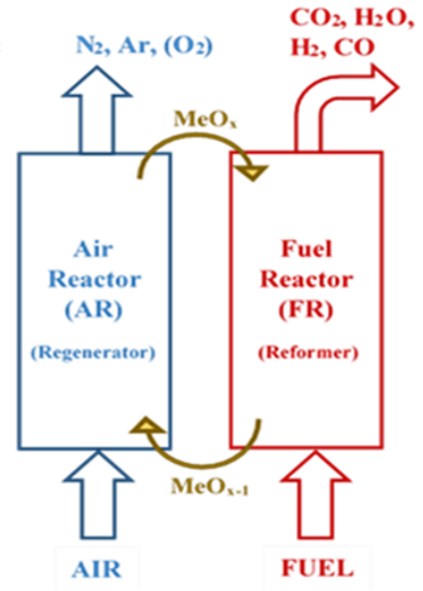

Figure 1.7: Schematic of a CLR process (MeO_x is for the oxidized metal catalyst and MeO_{x-1} is the reduced metal catalyst)

Later on, **Lyon** and **Cole** proposed another interesting approach by combining the CLR and SE-SMR process [35]. This concept was later named as the sorption enhanced chemical looping steam reforming (SE-CLSR) process. These processes will be explained in detail in **Chapter 2**. Advantages of SE-CLSR on the conventional SMR process such as high purity of H_2 (> 98 vol. %) and less energy requirement motivated the researchers to develop a pilot plant configuration of H_2 production by using the CLR technique [35-37]. Not a lot of work has been done in this field when it comes to mathematical modelling of the SE-CLSR process [37-39]. In this PhD work, the aim is to fulfil the gap in this field and model the SE-CLSR process. To address this, the following are the research objectives of this PhD work.

1.6 Research objectives

1) To investigate the performance of SE-CLSR process in a packed bed reactor, the system is divided into sub-systems. These sub-systems include the development of one-dimensional mathematical model of SMR, SE-SMR, reduction of oxygen transfer material (OTM) and re-oxidation of reduced catalyst on gPROMS model builder 4.1.0®. Develop the thermodynamic data using chemical equilibrium with application (CEA) software.

2) Conduct experimental work in the laboratory of University of Leeds, UK to develop the kinetic data for the conventional SMR process and use this kinetic data in the mathematical model of SMR process.

3) Validate SMR model against the experimental data and study the effect of operating conditions such as temperature, pressure and S/C on the performance of the process.

4) Develop a model of SE-SMR process by using the literature data for carbonation kinetics [40]. Investigate the performance of the SE-SMR process while keeping considering the high pressure (20-35 bar) industrial conditions of H_2 production.

5) Develop a mathematical model of the fuel reactor (coupling of SE-SMR and reduction of OTM processes) to check the sensitivity of the process under high pressure (20-30 bar) and temperature (873-1073 K) conditions.

6) Determine the optimum temperature, pressure, S/C and gas mass flux conditions for FR system.

7) Develop a mathematical model of the air reactor (oxidation of reduced catalyst) to investigate the performance of the SE-CLSR process.

8) Simulate the SE-CLSR process for 10 cycles to study the effect of various operating conditions, such as temperature (873-1073 K), pressure (1-30 bar), S/C (1-6) and gas mass flow velocity (2-7 kg m^{-2} s^{-1}), using the developed model of SE-CLSR process.

To meet the goal of H_2 production through the SE-CLSR process, research work is divided into different sections of modelling, simulation and experimentation. In **Chapter 2,** the techniques used in literature for H_2 production are discussed. The literature regarding mathematical modelling, reaction kinetics and methodology adopted for modelling work will be discussed in **Chapter 3**. It covers general equations across the packed bed reactor and equations for specific models like; homogeneous and heterogeneous models as well. **Chapter 4** deals with the experimental and modelling work of SMR process. gPROMS is used to carry out the mathematical modelling work. Complete description of the experimental rig and experiments performed on packed bed reactor available in University of Leeds, is also discussed in **Chapter 4**. **Chapter 5** deals with the modelling work of SE-SMR process and its validation against the literature data [40, 41]. In **Chapter 6,** the mathematical model of SE-CLSR process is illustrated. The modelling of reduction of OTM and re-oxidation of reduced catalyst is validated against the experimental literature data [42, 43]. The sensitivity of the process is studied by varying various operating conditions. **Chapter 7** covers the conclusion of the work and future recommendations.

CHAPTER # 2
HYDROGEN PRODUCTION PROCESSES

Currently, the use of hydrogen (H_2) is dominant in chemical industries but the depletion of fossil fuels and demand of electricity has enhanced the importance of H_2 as one of the promising future fuel. This chapter deals with different techniques for the production of H_2. The non-reforming and reforming techniques used in literature for the production of H_2 are reviewed. Conventional steam methane reforming (SMR), unmixed steam reforming, sorption enhanced steam methane reforming (SE-SMR) and sorption enhanced chemical looping steam reforming (SE-CLSR) of methane processes are also compared.

2.1 Introduction

The production of H_2 is one of the fast growing industrial process in the recent past. According to "hydrogen economy report" the production of H_2 in 2004 was around 50 million tons, equivalent to 170 million tons of petroleum. This production of H_2 is increasing with every year at a rate of 10%/year [44]. As discussed in previous chapter that the major sources of H_2 production are natural gas (48%) followed by petroleum (30%) and coal (18%) [45]. At present, 60% H_2 is consumed in ammonia production process and remaining 40% is used in refinery, chemicals and petrochemical sectors [46]. Hydrocarbons (natural gas and petroleum) are the major resources for H_2 production (78%), other contributors are coal and water electrolysis [47, 48]. The contributions of these resources towards H_2 production is shown in **Figure 2.1**.

In this chapter the production of H_2 from the conversion of hydrocarbons is only reviewed and discussed. The techniques for H_2 production from hydrocarbons can be classified on the basis of thermodynamic point (endothermic versus exothermic), catalytic versus non-catalytic or by the use of oxidant (oxidative versus non-oxidative). The later class is discussed in this chapter as most industrial process for H_2 production are based on this. The production of H_2 by oxidative processes occurs in the presence of oxidant such as steam, air or CO_2. The conversion of hydrocarbon to H_2 on industrial scale (e.g. steam

methane reforming [SMR], partial oxidation [POx] and auto-thermal reforming [ATR]) falls in this category. The oxidative process can be endothermic, exothermic or thermo-neutral depending upon the nature of the oxidant used. While on the other hand, non-oxidative processes do not need any oxidant to convert hydrocarbons feed stock into H_2 product stream. In these processes heat or energy is required to break the C-H bond of hydrocarbons and produced H_2. These processes are normally endothermic process such as catalytic and thermal hydrocarbon decomposition processes [1].

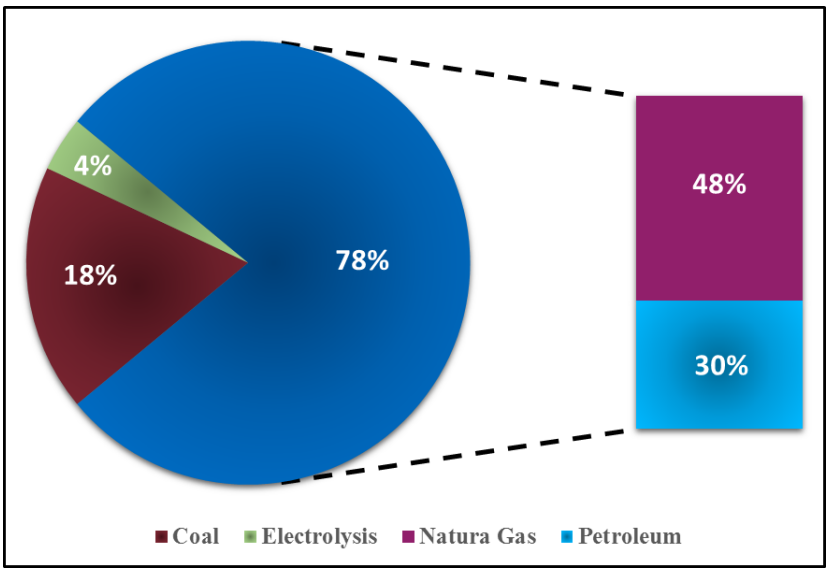

Figure 2.1: World's hydrogen production structure, after [1]

General classification of oxidative technique for H_2 production from hydrocarbon feed stock is shown in **Figure 2.2**. The most common oxidative processes that are used in industries are SMR, POx and ATR. SMR is further classified into conventional SMR, sorption enhanced SMR and H_2-membrane reforming. In the following section these process are discussed in details.

2.2 Conventional SMR process

The conventional SMR process is one of the most established and widely used industrial process for the production of H_2. It accounts to about 40% of the total world's production of H_2 [49]. Depending upon the final treatment of the product, two different approaches for SMR process are shown in **Figure 2.3 (a-b)**. In **Figure 2.3 (a)**, the bock diagram of the SMR process consists of reformer, water gas shift (WGS) reactors, CO_2 absorber and methanator while in **Figure 2.3 (b)** SMR is equipped with pressure swing adsorption

(PSA). The catalysts used for the reforming and WGS reactions are very sensitive towards sulphur contents. Sulphur can easily poison the catalysts and effect the performance of the system. Therefore, in both cases feedstock is first passed through the desulfurization unit (DSU) to remove the sulphur contents from the feed. The sulphur contents are initially converted to H_2S under the low temperature conditions (290–370 °C) in the presence of Co-Mo catalyst bed [50]. Later, this H_2S is allowed to pass over the bed of ZnO, at temperature range 340–390 °C, to remove the sulphur from the stream as shown in **Eq. 2.1**:

$$H_2S_{(g)} + ZnO_{(s)} \rightarrow ZnS_{(s)} + H_2O_{(g)} \quad (2.1)$$

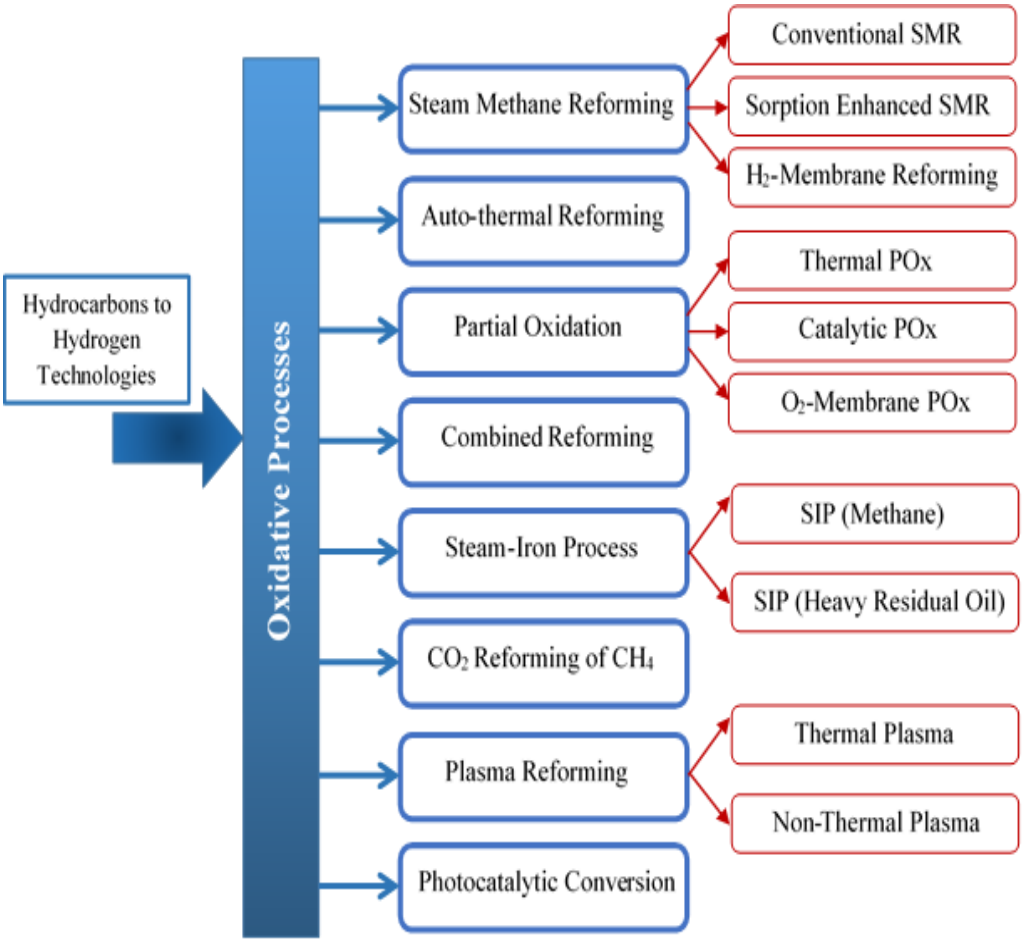

Figure 2.2: General classification of oxidative process of hydrocarbons to hydrogen production, after [45]

After DSU, the feed stock (NG: Natural gas) is fed to the reformer depending upon the carbon contents in the NG. In case when NG has higher carbon contents (C_2+), a pre-

reformer unit is used to convert the higher hydrocarbons into lower hydrocarbons (CH_4). As higher hydrocarbons have higher tendency to react than CH_4 and can easily decompose into carbon contents over the surface of the catalyst. The NG is mixed with high pressure steam (2.6 MPa) and preheated at 500 °C before introducing into the tubes of the reformer having Ni catalyst packed inside the tubes. The reformer tubes are externally heated, where feed mixture is converted to CO and H_2 at 850-900 °C according to the following reaction;

$$CH_{4(g)} + H_2O_{(g)} \leftrightarrow 3H_{2(g)} + CO_{(g)} \qquad \Delta H^{\circ} = 206 \text{ kJ mol}^{-1} \qquad (2.2)$$

This reforming reaction is highly endothermic and favoured at low pressure conditions. But as in most industrial applications, H_2 at downstream is required at high pressure conditions (2-3.5 MPa), therefore, SMR reformer is operated at such a high pressure conditions. In reaction 2.2, the steam to carbon ratio (S/C) used in feed is 1.0 which is the stoichiometric ratio. In industrial process excess of steam (S/C 2-3.0) is used to avoid the carbon deposition or decomposition of NG on the surface of catalyst in the form of coke.

The product stream leaves the reformer tubes (~15 m long and 12 cm inside diameter) at 800-950 °C. It is cooled down to 350 °C and steam is generated here. The cooled product steam is introduced into the WGS reactors. Here, CO reacts with steam according to the following reaction;

$$CO_{(g)} + H_2O_{(g)} \leftrightarrow H_{2(g)} + CO_{2(g)} \qquad \Delta H^{\circ} = -41.2 \text{ kJ mol}^{-1} \qquad (2.3)$$

Two WGS reactors are operated in series to enhance the conversion of CO as shown in **Figure 2.3 (a-b)**. The high temperature water gas shift (HT-WGS) reactor operates around 340–360 °C and low temperature water gas shift (LT-WGS) reactor operates at 200-300 °C. At the end of LT-WGS reactor, 92% CO is converted to H_2 product. The CO_2 from the product stream is separated in CO_2 absorber. On industrial scale, the most common absorbent used for the removal of acid gas (CO_2) is monoethanolamine. The target of CO_2 absorbent is to reduce the CO_2 amount to about 100 ppm. The residual amount of CO and CO_2 are removed in methanator where CH_4 is produced in the presence of H_2.

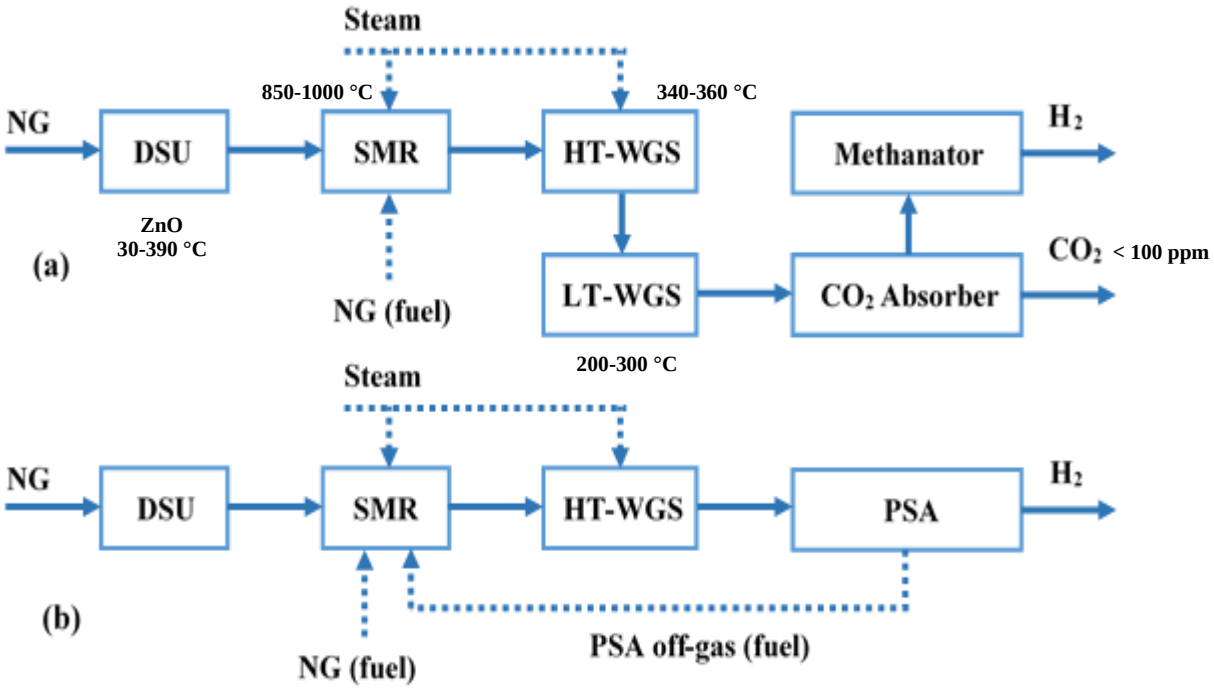

Figure 2.3: Schematic diagram of H_2 production by SMR. **a)** SMR with CO_2 removal by CO_2 absorption and **b)** SMR with a PSA unit, after [45]

In **Figure 2.3 (b)**, PSA technique is presented instead of CO_2 absorber. This is the modern technique for the purification of H_2 from the impurities like CH_4, CO and CO_2. The PSA unit consists of multiple adsorption beds and operated at pressure around 20 atm [1].

SMR process is a catalytic process, the selection of catalyst plays a vital role in the overall performance and cost of the process. Ni and different other noble metals (Ru, Rh, Ir etc.) are considered as the promising metals for SMR catalysts. Under the operating conditions of 500 °C, 0.1 MPa and S/C of 4.0, the activity of metals for SMR is as follow [51];

$$Ru > Rh > Ir > Ni > Pt > Pd$$

There are many characteristics of metals which play decisive role in the selection of the metal for the reforming process. These properties include; catalyst resistance to coke formation, robustness to withstand stress during start-up conditions, thermal stability against extreme temperature conditions and cost of the metal. Although, Ni metal is not as active as many noble gases are but it is the widely used metal in SMR catalyst because it can withstand high temperature conditions and not costly as many other noble metals are. In industrial SMR process, the Ni catalyst is supposed to permute reforming process for a 5 year continuous operation before its replacement [50]. With the increase in Ni

metal loading, the active surface area of the catalyst also increases. Although there is an optimum loading of Ni (15-20 wt. %) beyond which there is no further effect of Ni loading on the activity of the catalyst [52].

The support on the metal provides a support to the catalyst to achieve a stable active surface area. It also helps in preventing coke formation and provides resistance to the catalyst sintering. The most common supports used for SMR catalysts are α- and γ-Al_2O_3, MgO, $MgAl_2O_4$, SiO_2, ZrO_2, and TiO_2 [53]. The reaction kinetics and mechanism of SMR reactions will be discussed in next chapter.

2.3 Partial oxidation [POx]

Another commercial scale process for the production of H_2 via oxidative process is the POx of hydrocarbons [54-57]. In this process fuel and oxygen (or air) are mixed, in a desired fraction, and fuel is converted to H_2 and CO products. The POx process is highly exothermic process in nature as the oxidation reactions released considerable amount of heat. The POx process can be a catalytic reaction or non-catalytic reaction. The non-catalytic POx process is generally carried out at high temperature range (1100-1500 °C), while on the other hand catalytic POx (CPO) process is carried out in a lower temperature range i.e. 600-900 °C. The presence of the catalyst in CPO process reduces the temperature of the process but due to the exothermic reactions the formation of coke and hot spots are always there [58]. In CPO process, light hydrocarbon fuels are used as feedstock unlike heavy residual oils (HROs) in non-catalytic POx process [1]. The CPO reaction of CH_4 is exothermic reaction in nature and it is given as;

$$CH_{4(g)} + 0.5O_{2(g)} \rightarrow 2H_{2(g)} + CO_{(g)} \qquad \Delta H^{\circ} = -38 \text{ kJ mol}^{-1} \qquad (2.4)$$

In **Figure 2.4**, the thermodynamic results (generated on chemical equilibrium application software) for molar fraction (N_2 free) of product gases from CPO process are shown. The 2.0 molar ratio of carbon to oxygen (C/O) is used in feed. It can be seen that at temperature higher than 800 °C, H_2 and CO gases are the major product gases. Based on higher heating values, the typical efficiencies of POx reactors, with CH_4 as fuel, are 60-75% [54].

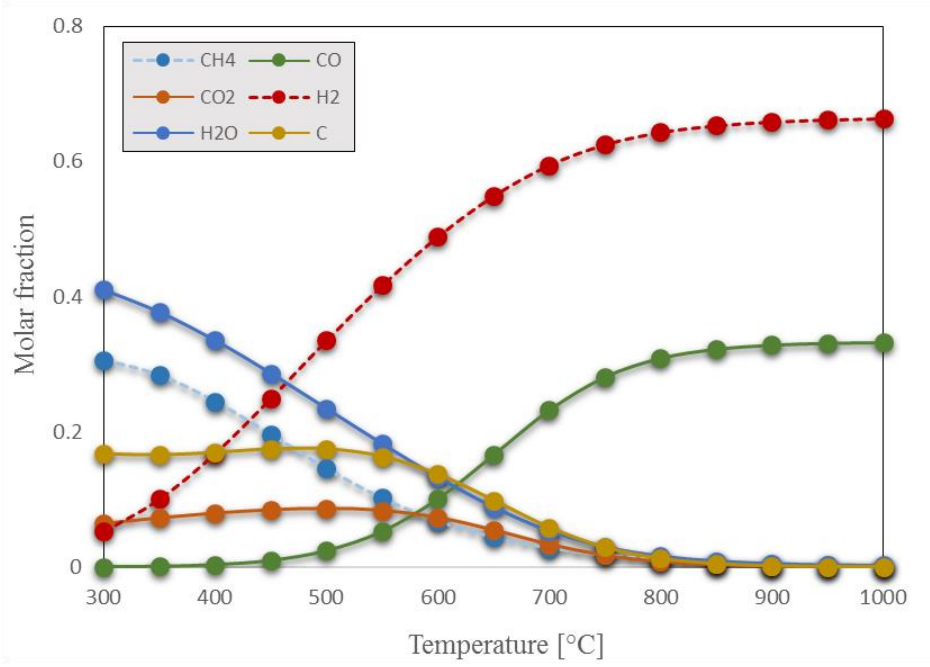

Figure 2.4: Thermodynamic analysis performed in this work for the composition of product gases (N_2 free) in POx process under the operating pressure of 1 bar and C/O of 2.0.

The most common catalysts used for CPOx process are Ni based and noble metal–based (e.g., Rh, Pt, Pd, Ir, Ru, and Re) catalysts in the form of pellets, monoliths, and foams [59]. Ni catalyst has strong tendency towards coke formation and the cost of Rh is very high as compared to Ni catalyst. **Dissanayake et al.** [60] studies the CPOx process by using 25 wt. % Ni/Al_2O_3 catalyst. The researchers observed that if POx process is performed above 700 °C, the selectivity of CO approaches 95%. **Hickman et al.** [61] showed that Rh gives higher selectivity for H_2 as compared to Pt catalysts.

2.4 Auto-thermal Reforming [ATR]

The ATR process is an oxy-steam reforming process. It combines the oxidation and reforming process to produce H_2 rich stream. It is a very old technique of H_2 production and was used in 1950 and 1960s for the production of H_2 in ammonia plants. The schematic diagram of the ATR process is shown in **Figure 2.5 [45]**. The auto-thermal reactor is divided into 3 parts. The combustion zone, thermal and catalytic zone. The feed is introduced in the combustion section where oxygen and hydrocarbon feedstock reacts and combustion reaction proceeds. The resulting combustion reaction with CH_4 as feed is given as;

$$CH_{4(g)} + \frac{3}{2}O_{2(g)} \rightarrow 2H_2O_{(g)} + CO_{(g)} \qquad \Delta H^{\circ} = -519\ \text{kJ mol}^{-1} \qquad (2.5)$$

In the thermal zone, above the surface of the catalyst, main reforming (**Eq. 2.2**) and WGS (**Eq. 2.3**) reactions occurred. The heat released during the combustion reaction provides energy for the endothermic reforming reaction. ATR process consumed less amount of oxygen than POx process (per unit of H_2 produced) [50]. If the objective of the reforming process is to control the ratio of H_2/CO in synthesis gas and reduce the consumption of oxygen, the combination of conventional SMR and ATR process is used. In this process, product stream from primary reformer is fed to the auto-thermal or secondary reformer where combustion and reforming reaction enhances the conversion of fuel. The outlet temperature in primary and secondary reformers ranges from 750-850 °C and 950-1050 °C respectively. The process of primary and secondary reformer is being used in ammonia production plants.

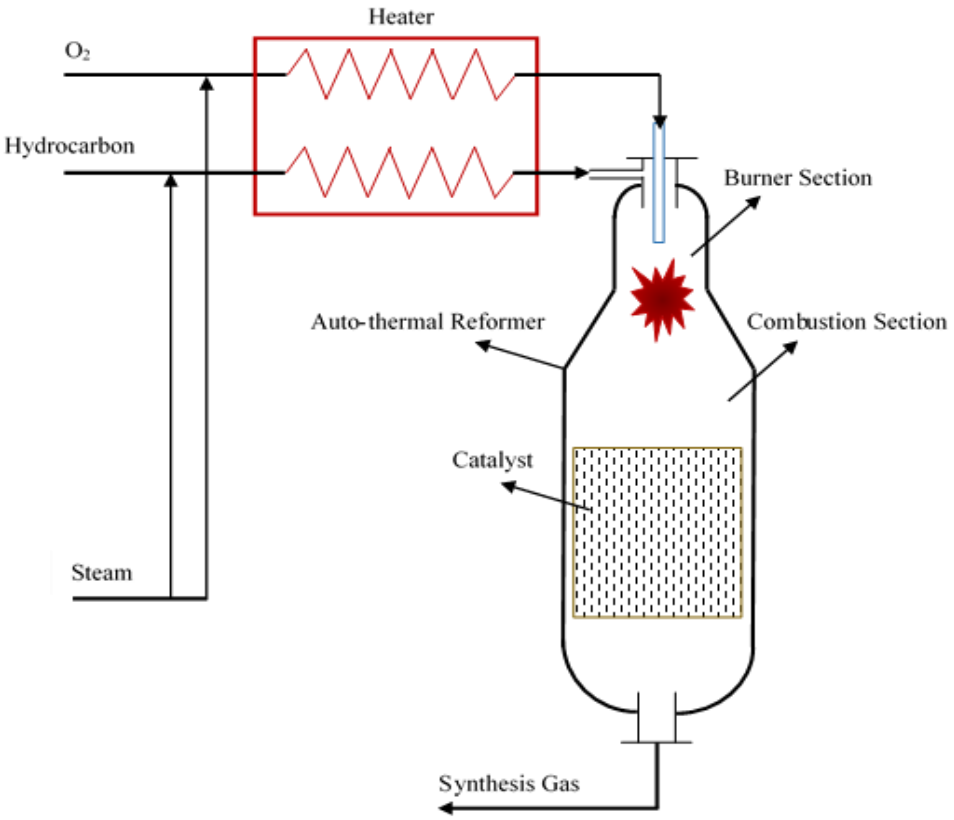

Figure 2.5: Schematic diagram of auto-thermal reformer [45]

Although steam reforming process produces the highest concentration of H_2 but the reaction is highly endothermic and thus it is not suitable for more compact and mobile

fuel cells. ATR process generates its own heat for steam reforming process [62]**.** The main features of ATR are:

a) Low energy requirement
b) Low specific consumption
c) High gas space velocity **[63]**

The comparison of all above discussed reforming technologies is listed in **Table 2.1**.

Table 2.1: Comparison of reforming technologies [64-66]

Technology	**Advantages**	**Disadvantages**
SMR	• Lower operating temperature conditions than POx and ATR process • Does not require O_2 • Produces high H_2/CO ratio (~3:1) which is beneficial for H_2 production.	• High CH_4 slippage as compared to ATR and POx process
POx	• This process has more sulphur tolerant than other reforming processes as no catalyst is required. • Low slippage of CH_4	• It has very limited industrial use • High temperature conditions caused soot formation • The ratio of H_2/CO is low
ATR	• Lower process temperature as compared to POx process • Minimum slippage of CH_4	• Requires air or oxygen

Although, SMR process is well developed process on industrial scale but still there is a room for improvement. As far as the energy efficiency, gas separation and H_2 purification is concerned, SMR process can be improved. The high temperature conditions in reformer caused malfunctioning of reformer tubes after a continuous operation of around 5 years. In the following sections some new reforming techniques are discussed to handle the problems of overheating the tubes, more production of H_2 at lower temperature than conventional SMR process.

2.5 Chemical looping reforming [CLR]

Commonly, the chemical looping term is used to describe the process of transporting oxygen. This term has been used for the cyclic process in which oxygen transfer material (OTM) is used for the conversion of fuel. The reduced metal is further oxidized to start the new cycle of chemical looping. The chemical looping process can be the combustion or reforming process depending upon the purpose of the process. The summary of chemical looping processes reported in literature is shown in **Table 2.2**.

Table 2.2: Summary of Chemical looping technologies [67]

Objective	Primary fuel	Process	Main features
Combustion	Gas	Chemical looping combustion [CLC]	In this process oxygen carrier (OC) reacts directly with the gaseous fuel (e.g. natural gas, refinery gas etc.)
	Solid	Syngas-CLC	The gasification products come in contact with the OC. Although in this process the fuel introduced in the gasifier is the gaseous fuel but the primary fuel is solid.
	Solid	In situ gasification CLC [iG-CLC]	The OC reacts with the solid gasification products inside the fuel-reactor.
	Solid	Chemical looping with oxygen uncoupling (CLOU)	The OC released the gaseous oxygen for the combustion process.
Hydrogen production	Gas	Steam reforming integrated with CLC [SR-CLC]	The heat for steam reforming is supplied by the combustion of gases.
	Gas	Chemical looping reforming [CLR]	The main products in CLR are H_2 and CO

	Gas	Chemical looping hydrogen [CLH] or One step decarbonisation [OSD]	In this process three reactors (fuel reactor, air reactor and steam reactor) are required to produce H_2 by the oxidation of OC with steam.
	Solid	Syngas chemical looping [SCL]	In this process, three reactors (reducer, oxidiser and combustor) are required for the production of H_2 from oxidation of steam
	Solid	Coal direct chemical looping [CDCL]	Like SCL process, this process also needs three reactors for the production of H_2 and regeneration of OC. Coal and O_2 are fed to the reducer reactor.

In 1951 **Lewis et al.** [68, 69] published an article on 'gasification of carbon metal oxides in a fluidized power bed'. They introduced the basic idea of CO_2 production which was quite similar to the recent technology of CLC process. In their work they proposed the idea of OC as a source of oxygen for the combustion process. They used the interconnected fluidized bed reactor scheme for the circulation of solids. Later in 1983, **Richter et al.** [70] proposed the principle of CLC process. They used the interconnected fluidized bed reactors having metal oxides as OC in these reactors. Their work was focused on enhancing the efficiency of power plants by using oxygen carriers in the fluidized bed reactors. In 1987, **Ishida et al.** [71] first time used the term 'chemical looping combustion (CLC)' in an effort to evaluate the performance of power generation system by graphic exergy analysis. **Hatanaka et al.** [72] proposed a very unique method known as MERIT (Mediator Recirculation Integrating Technology). In this method they divided the process of combustion into two section; 1) metal oxidation by air and 2) reduction of metal oxide by fuel at low temperature. For long the concept of CLC was no more than just a paper work. Later in 2001-2003, the European Union (EU) started a project 'CO_2 Capture Project (CCP)' on the concept of CLC [73]. The 'Grangemouth Advanced CO_2 Capture Project (GRACE)' was the first ever project in which 300 different metal oxides were tested and a plant having capacity of 10 kWth was run [74,

75]. Later in 2005, **Lyngfelt et al.** [76], at Chalmers University of Technology (CHALMERS), first time demonstrated a CLC process for a continuous cycles of 100 hours. They used Ni particles in their run and used natural gas as fuel for the combustion process. They achieved around 99.5% fuel conversion efficiency.

Meanwhile another EU project, 'capture of CO_2 in coal combustion (CCCC)', was developed by using the concept of CLC. The power generated through this project was 300 kWth [36, 77]. In 2006-2007, **Adánez et al.** [67, 78] used Cu particles for CLC process and it was the first time when this process was run for a continuous 120 hours.

The researchers used the technology of chemical looping for the production of H_2. This concept was used for the H_2 production in the late 19^{th} and early 20^{th} century. The term unmixed steam reforming (USR) was first introduced by **Lyon et al.** in 1996 and **Kumar et al.** in 1999 [35, 79, 80]**.** In this process, fuel and air are not directly mixed but separately passed over the surface of catalyst [35]. First air is introduced on the surface of the catalyst, and fuel is introduced after that. The USR process uses OTM to transfer the heat for endothermic SMR reaction (**Eq. 2.2**). During the reduction of OTM, metal is regenerated and undergoes the cycle of reforming with the fuel gas and steam [10, 81].

However, it was EU project 'carbon dioxide capture and hydrogen production from gaseous fuels (CACHET)' in which CLR process got more attention. This project was focused on reduction of CO_2 during power production and production of H_2 by using natural gas fuel [82]. In this project the advanced SMR, chemical looping and sorption enhanced water gas shift (SE-WGS) technologies were used. For the production of syngas, they used CLR [83], steam reforming coupled with CO_2 capture by chemical-looping combustion (SR-CLC) and one-step decarbonisation (OSD) or chemical-looping hydrogen generation (CLH) techniques [36, 84]. The focus of this project (CACHET) was to develop the CLR process for the production of syngas and studied the effect of pressure on CLR process. They used Ni based OC for the study of CLR and SR-CLC processes.

The main difference in conventional SMR and SR-CLC process is the heat requirement. In SR-CLC process no external heat is required for endothermic reforming reaction, the CLC process is used to provide the required amount of heat for reforming reaction. **Rydén et al.** [36, 85] proposed SR-CLC process. They used the circulating fluidized bed reactor for this process. The schematic diagram of SR-CLC process is shown in **Figure 2.6**. To

have more production of H_2 and almost 100% capturing of CO_2, they integrated the SR-CLC unit with WGS and PSA units as shown in **Figure 2.6**. The gases leaving from the PSA unit, can be used as fuel in the steam reactor or fuel reactor of the SR-CLC unit. So, no extra penalty on the efficiency of the process is expected.

CLR process follows the same principle as CLC process. The only difference in CLR and CLC is the desired products. In CLR process instead of heat the objective is to have H_2 and CO. During CLR process, the ratio of air to fuel is kept very low to avoid the complete oxidation of fuel to CO_2 and H_2O. In this process, unlike conventional SMR process, air separating unit (ASU) is not required. The CLR was first proposed by **Mattisson et al.** in 2001 [86]. **Rydén et al.** [85] also proposed this process and they concluded that the CLR process gives 5% more overall efficiency of the process as compared to conventional SMR process. As high pressure conditions are required at the downstream of the CLR process which ultimately caused the reduction of overall efficiency, but still it is higher than the conventional SMR process. In CLR process, the reforming reactions are the main reactions. So the most commonly used OC is the Ni-based OC. The reactions taking place in the fuel reactor are dependent upon the ratio of air to fuel. As the objective of CLR is to have H_2 and CO as the main product instead of CO_2 and water, so the ratio is adjusted accordingly. The reactions taking place in the fuel reactor and air reactor are given as;

Fuel Reactor;

$$CH_{4(g)} + NiO_{(s)} \rightarrow CO_{(g)} + 2H_{2(g)} + Ni_{(s)} \qquad \Delta H_{1200K} = 213 \text{ kJ mol}^{-1} \qquad (2.6)$$

If air is supplied in excess then CO and H_2 further react with oxygen and released CO_2 and H_2O as;

$$CO_{(g)} + NiO_{(s)} \rightarrow CO_{2(g)} + Ni_{(s)} \qquad \Delta H_{1200K} = -48 \text{ kJ mol}^{-1} \qquad (2.7)$$

$$H_{2(g)} + NiO_{(s)} \rightarrow H_2O_{(g)} + Ni_{(s)} \qquad \Delta H_{1200K} = -15 \text{ kJ mol}^{-1} \qquad (2.8)$$

The reforming and WGS reactions are as;

$$CH_{4(g)} + H_2O_{(g)} \rightarrow CO_{(g)} + 3H_{2(g)} \qquad \Delta H_{1200K} = 228 \text{ kJ mol}^{-1} \qquad (2.9)$$

$$CO_{(g)} + H_2O_{(g)} \rightarrow CO_{2(g)} + H_{2(g)} \qquad \Delta H_{1200K} = -33 \text{ kJ mol}^{-1} \qquad (2.10)$$

Air Reactor;

The reduced catalyst is regenerated in air reactor as;

$$2Ni_{(s)} + O_{2(g)} \rightarrow 2NiO_{(s)} \qquad \Delta H_{1200K} = -468\ kJ\ mol^{-1} \qquad (2.11)$$

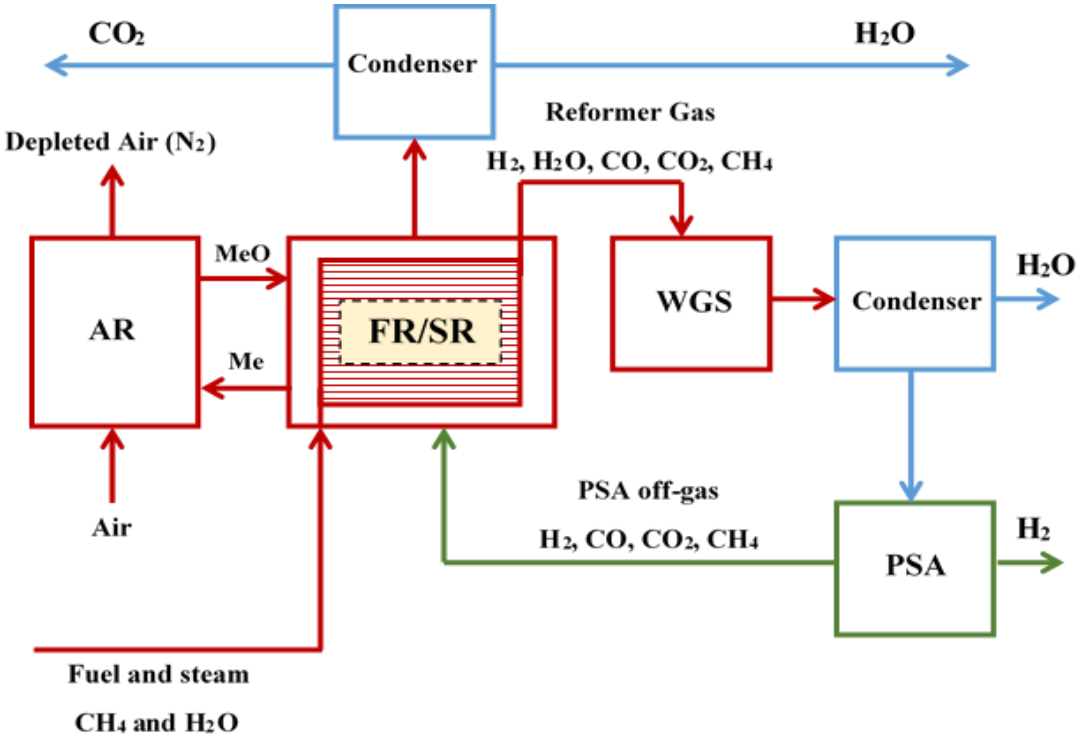

Figure 2.6: Schematic diagram of SR-CLC process. Here, **FR**: Fuel reactor; **SR**: Steam reforming reactor; **PSA**: Pressure swing adsorption unit; **WGS**: water gas shift reactor and **AR**: Air reactor [36]

As it can be seen that reduction reaction (**Eq. 2.6**) and reforming reaction (**Eq. 2.9**) are endothermic in nature and heat required for these reactions is supplied by the oxidation reaction (**Eq. 2.11**) which is highly exothermic in nature.

One of the key parameter that has vital impact on the overall performance of CLR process is the selection of OC. The good OC should have high selectivity towards CO and H_2 production, high resistance to attrition, good reactivity and high resistance to carbon formation. In **Table 2.3**, the OC used for CLR process are summarized.

Table 2.3: Oxygen carriers used in literature for CLR applications

Metal oxide [%]	Support material	Continuous plants	Reference
NiO			
18	α-Al_2O_3	CLR 500 W	[87]
		CLR 900 W	[88, 89]
21	γ-Al_2O_3	CLR 500 W	[87]
		CLR 900 W	[88, 89]
20	$MgAl_2O_4$	CLR 500 W	[87]
36	$MgAl_2O_4$		[90]
60	$MgAl_2O_4$	CLR 500 W	[91]
40	$NiAl_2O_4$+MgO	CLR 140 kW	[92]
35	SiO_2		[90]
40	ZrO_2-MgO	CLR 500 W	[93]
CuO			
43	$MgAl_2O_4$		[90]
40	SiO_2		[90]
Fe_2O_3			
32	$MgAl_2O_4$		[90]
40	$MgAl_2O_4$		[94]
39	SiO_2		[90]
Mn_2O_3			
47	SiO_2		[90]
46	$MgAl_2O_4$		[90]

Johansson et al. [95] studied the CLR process while considering two different Ni-based OC, $NiO/NiAl_2O_3$ and $NiO/MgAl_2O_4$, in a continuous process. They concluded that $NiO/MgAl_2O_4$ gives higher conversion of fuel (CH_4) and has less tendency towards the formation of carbon on the surface of the catalyst. **Diego et al.** [89] studied CLR process by using α-Al_2O_3 and γ-Al_2O_3 OC. The reactivity of α-Al_2O_3 during the reduction reaction was found to be more than the reactivity of γ-Al_2O_3 OC. In all the cases tabulated in table 2.3, Ni based OCs are found to be suitable for CLR process. It was observed that Ni-based

OCs have long lifetime and can be used for longer period of time without showing a noticeable change in the reactivity.

Modelling of fuel and air reactors are studied by many researchers. Most of the modelling work is focused on CLC process while considering the interconnected fluidized bed reactors. **Kolbitsch et al.** [96] modelled the fluidized bed reactors to study the process of CLC. In most of the literature work, CFD software is used to model the fluidized bed reactors. In these cases, the modelling of fluidized bed reactor is divided into three fields; 1) Fluid dynamics, 2) Reaction scheme and 3) heat balance. The literature regarding kinetic scheme and heat balance across the reforming process will be discussed in detail in next chapter.

2.6 SE-SMR process

As it is discussed in previous section that SMR process is responsible for about 40% world-wide production of H_2. The SMR is highly endothermic process, and researchers are moving towards CLR process to minimize the energy requirements and maximize the conversion of fuel by utilizing the heat generated within the process. The production of H_2 is increasing by a rate of 10% with every passing year. The increase in the demand of H_2 has put a negative impact on the climate by excessive emission of CO_2 during the reforming process. This makes room for a new process, which may be more economical and environmental friendly. Keeping this issue in mind, researchers developed a new process known as 'sorption enhanced steam methane reforming (SE-SMR)' process. In this process CO_2 from the SMR process is removed from the reaction zone by the sorption process. As overall reforming process is endothermic and equilibrium limited. So the complete conversion of CH_4 cannot be achieved in a single reactor under the normal operating conditions. The removal of CO_2 from the product gases shifts the equilibrium of **Eq. 2.3** towards H_2 production and enhances the conversion of fuel. **Balasubramanian et al.** [97] studied the process of CO_2 sorption in the presence of CaO as CO_2 acceptor. Thus, the presence of sorbent in the reactor causes the following reaction in the reaction zone;

$$CO_{2(g)} + CaO_{(s)} \leftrightarrow CaCO_{3(s)} \qquad \Delta H^{\circ} = -178.8\ \text{kJ mol}^{-1} \qquad (2.12)$$

The formation of carbonate not only removes the CO_2 from the product stream, it also enhances the production of H_2. This makes the sorption enhanced process a dynamic

process in nature. So continuous regeneration of sorbent is also required for continuous operation of the process. **Mayorga et al.** [98] listed the potential advantages of SE-SMR process over SMR process as following;

1) The low temperature in the reactor makes the process more economical than SMR process where expensive construction materials are required to withstand the high temperature conditions.
2) The production of H_2 is much higher than the production in case of SMR process under the same operating conditions. The amount of CO and CO_2 product gases is much lower in SE-SMR process as compared to SMR process.
3) There is no need of WGS reactor in SE-SMR process and the depositions of carbon on the surface of catalyst is almost negligible as compared to the conventional SMR process.

The concept of sorption enhanced steam reforming is not new. In 1868, **Rostrop** [52] proposed the process of hydrocarbon conversion in the presence of steam and Ca-based sorbent. Later in 1933, **William** [99] published a patent in which he discussed the process of SMR in the presence of lime as sorbent. In 1963, **Gorin et al.** [100] published a patent 'methods for the production of H_2'. They used fluidized bed reactor for the reforming reactions in the presence of Ca-based sorbent.

In literature, considerable work on SE-SMR is published while considering the fixed bed reactor system. **Balasubramanian et al.** [16] used the reforming catalyst and Ca-based sorbent to study the process of 'hydrogen from methane in a single-step process' in a fixed bed reactor system. Typical conditions used were 650 °C, 15 bar and S/C of 4 to study the performance of the sorption enhanced process. They studied the composition of product gases at the outlet of reactor as a function of time. The outlet results were divided into three sections i.e. pre-breakthrough period (sorbent is fully active), breakthrough period (sorbent reaching to its full capacity) and post-breakthrough period (sorbent is no more active and the only process taking place within the reactor in this period is reforming process). In the pre-breakthrough period the composition of product gases on dry basis was 94.7% H_2, 5.2% CH_4, and approximately 400 and 600 ppmv of CO_2 and CO, respectively. They compared the values with equilibrium results and a good agreement was observed. In the breakthrough period the CO_2 capturing efficiency dropped and ultimately in post-breakthrough period the CO_2 capturing efficiency was zero [97]. At the

end of the process they concluded that by using Ca-based CO_2 acceptor in the fixed bed reactor system can save about 20-25% energy as compared to conventional reforming process. The only disadvantage in the proposed process was the high temperature requirements in the regeneration section.

To illustrate the process of sorption enhanced reforming, **Balasubramanian et al.** used the simplified schematic diagram of adiabatic fluidized bed reactors having reforming catalyst and Ca-based sorbent. The schematic diagram is shown in **Figure 2.7**.

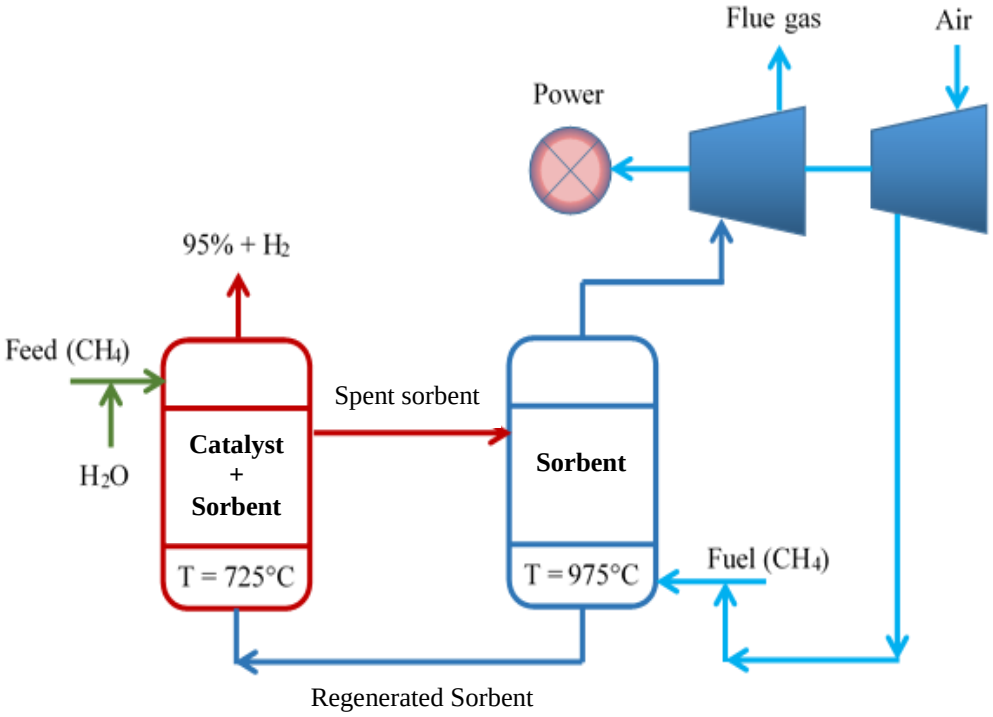

Figure 2.7: Schematic diagram of single-step hydrogen production process [97]

In primary reformer, reforming and sorption reactions take place and saturated sorbent is regenerated in regenerator reactor. The compressed air and fuel is used to regenerate the sorbent for next cycle of sorption reforming process. **Dou et al.** [101] used the fixed bed reactor system for the seam reforming of glycerol with in situ CO_2 capture process. The fixed bed reactor had an internal diameter (ID) of 0.025 m and was 0.70 m long. They used 5 g Ni-based OC and 5 g of Ca-based sorbent for the experimental work. The experimental work was run with and without sorbent to study the effect on H_2 purity and fuel conversion for a temperature range of 500-700 °C.

In literature it is reported that Ca-based sorbents and potassium promoted hydrotalcite (K-HTC) sorbents are extensively used as CO_2 acceptor for sorption enhanced reforming

process. The metal oxides of sodium and lithium are not very extensively used. The main criteria used for the selection of sorbents are as following [102];

1) High adsorption capacity
2) Low cost
3) Stability of the sorbent during reforming and regeneration cycles
4) High kinetics and thermodynamic properties

Generally, sorbents are classified as natural sorbents and synthetic sorbents. In **table 2.4**, the classification of sorbents is presented.

Table 2.4: Classification of sorbents [102]

Types	**Sorbent**	**Adsorption capacity [gCO_2/g sorbent]**
Natural Sorbents	Calcium carbonate ($CaCO_3$)	0.79
	Dolomite ($CaCO_3 \times MgCO_3$)	0.46
	Huntite ($CaCO_3 \times 3MgCO_3$)	0.25
	Hydrotalcite, promoted K_2CO_3/Hydrotalcite	0.029
Synthetic sorbents	Lithium o-silicate (Li_4SiO_4)	0.37
	Lithium Zirconate (Li_2ZrO_3)	0.29
	Sodium Zirconate (Na_2ZrO_3)	0.24

The natural sorbents (calcium carbonate and dolomite) are not expensive as compared to other sorbents and they are easily available. Calcium carbonate has very high adsorption capacity and after a run of 45 cycles, this capacity drops from 0.79 gCO_2/g sorbent to 0.316 gCO_2/g sorbent. **Ding et al.** [103] used hydrotalcite-based CO_2 adsorbent in adsorption based SMR process. In this work they used Ni-based catalyst in packed bed reactor having internal diameter (ID) 12.4 mm and length 220 mm. The experiment was run at 450 °C, 445.7 kPa and S/C of 6.0. They showed the effect of operating conditions like temperature, pressure, space velocity, particle diameter and S/C on CH_4 conversion. They found that optimum temperature, pressure and particle diameter is 445.5 °C, 721.5

kPa and 0.11-0.25 mm respectively. Increasing space velocity and S/C decreases the conversion of CH_4. Optimum values for the space velocity and S/C were found as 10.7 g-cat h mol^{-1} and 3.0 respectively. They developed the mathematical model and validated the model with experimental findings. The developed model was under the conditions of non-isothermal, non-adiabatic and non-isobaric. They concluded that by using sorbent along with catalyst in packed bed reactor, CH_4 conversion enhancement was observed.

Fernández et al. (2012) [40] developed a mathematical model of SE-SMR process in a fixed bed reactor and studied the effect of operating variables (catalyst to sorbent ratio, space velocity, steam to carbon ratio, pressure and temperature) on the composition of product gases. They use Ca/Cu looping process, CaO as sorbent in fixed bed reactor to investigate the performance of the process. It was observed that for a fixed temperature (923K), pressure (3.5 MPa), S/C (5) and gas mass flux (3.5 kg m^{-2} s^{-1}), there is a decrease in H_2 purity from 92% to 85% and decrease in CH_4 conversion from 85% to 60 % as the catalyst to sorbent ratio decreases from 0.3 to 0.1. This H_2 purity is the maximum that can be achieved by sorption enhanced reforming (SER) equilibrium under the operating condition of the system. Under the same operating conditions, increase in gas mass flux decreases H_2 purity and CH_4 conversion. The lower the gas mass flux, the higher will be the residence time of fuel within the reactor and hence the higher will be the conversion of fuel into H_2. 3.5 kg m^{-2} s^{-1} was selected as the optimum gas mass flux if the system is operated under the above said operating conditions. Increasing the S/C, temperature of the reactor and lowering the operating pressure has positive impact on H_2 purity. As high temperature favours CH_4 conversion and more H_2 is produced but as the temperature goes beyond the certain limit the H_2 purity starts decreasing. The reason behind this is that, after the certain temperature the carbonation reaction becomes ineffective and sorbent becomes saturated. So, more CO_2 leaves the system along with H_2 gas. Similarly, as the pressure of the system increases the volume will decrease for a constant temperature according to Le-Chatelier's Principle, and CH_4 conversion will not be favourable at high pressure. Optimum conditions for temperature, pressure, S/C and catalyst to sorbent ratio were 973 K, 3.5 MPa, 6 and 0.3 respectively for maximum (~95%) H_2 purity and CH_4 conversion (~90%). They studied the effect of S/C on the production of H_2. Pressure of the system was kept constant at 35 atm and the effect of S/C on H_2 production was observed by changing the temperature of the system. It was observed that 97% H_2 (dry

basis) can be produced at 650 °C in this case if S/C is as high as 5. Reducing S/C will reduce the H_2 % and same is the case with increasing temperature.

Ochoa-Fernández et al. (2007) [104] compared the performance of different sorbents on the yield of H_2. By using CaO as sorbent the process is weakly exothermic, while by using Li_2ZrO_3 the overall reaction is weakly endothermic. In order to enhance the conversion of CH_4 and get the maximum net efficiency, S/C for each process was adjusted and optimum operating temperature and pressure was derived. It was concluded from the findings that CaO is the most favourable sorbent from thermodynamics point of view and results is higher H_2 production as compared to other sorbents.

Hufton et al. [105] studied the SE-SMR process for the production of H_2 by using K_2CO_3-treated HTC sorbent. They obtained 96% purity of H_2 and CH_4 conversion of 82% in pre-breakthrough period where sorbent is active. Under the same operating conditions, the equilibrium values for CH_4 conversion and H_2 purity in SMR are 28% and 53% respectively. In **Figure 2.8**, the thermodynamic results of H_2 concentration (dry basis mole fraction) with and without sorbent are shown. It can be seen that as the temperature increases from 650°C to onwards, there is drop in the concentration of the H_2. The concentration of H_2 with and without sorbent is same in the temperature range of 750-850°C. So for the SE-SMR process with CaO as sorbent, the desired temperature range is from 500-650°C under the operating conditions of 1.0 bar and S/C of 3.0.

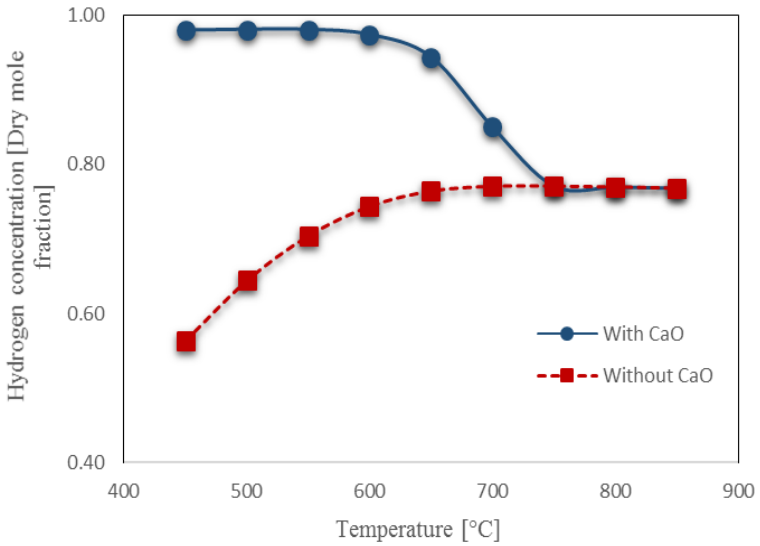

Figure 2.8: Equilibrium variation of H_2 concentration (dry basis mole fraction) with temperature at 1.0 bar, S/C of 3.0 and CaO/C ratio of 2.0 [106]

Koumpouras et al. (2007) [107] developed the mathematical model and investigated the effect of sorbent on CH_4 conversion in a fixed bed reformer. Three cases were considered to observe the effect of sorbent. In the first case, no loading of sorbent was done so it was just like a simple SMR process. In the second case, sorbent was used but its ability to absorb CO_2 was set zero. So in this case it only acts as heat carrier. In the third case, sorbent was used as heat carrier and CO_2 acceptor as well. After the investigation it was found that maximum CH_4 conversion along the axial direction of reactor was obtained in third case.

In literature many mathematical models are developed for SE-SMR process. **Ding et al.** and **Xiu et al.** [103, 108] developed numerical models and validated those models against the experimental work. In developing the model for SE-SMR process, the main section is always the modelling of reaction scheme. The kinetic model for sorption of CO_2 on the active site of CaO will be discussed in next chapter.

2.7 SE-CLSR process

The main disadvantage in SE-SMR is the regeneration of sorbent as high temperature conditions are required. But when SE-SMR is coupled with USR or CLR, the process of the calcium carbonate ($CaCO_3$) regeneration is better integrated. The CO_2 sorbent adsorbs CO_2 to produce $CaCO_3$ in an exothermic reaction (**Eq. 2.12**). This heat is utilized in the reforming reaction as a chemical potential energy. During the air regeneration step, $CaCO_3$ is decomposed into CaO and CO_2 (**Eq. 2.13**). This reaction requires the heat to proceed and oxidation of reduced catalyst (**Eq. 2.11**) provides that heat for the calcination reaction (**Eq. 2.13**) to proceed in forward direction. The heat of the Ni oxidation is stored in CaO and is used in the reforming reaction [22].

$$CaCO_{3(s)} \leftrightarrow CaO_{(s)} + CO_{2(g)} \qquad \Delta H_{298K} = 178.8 \text{ kJ mol}^{-1} \qquad (2.13)$$

As the CLR process is the cyclic process of reduction and re-oxidation of OC. This process does not need any separation unit at the downstream of the process. To make the process environmental friendly and reduce the amount of CO_2 leaving with the product stream, the concept of SE-SMR was coupled with CLR process. Hence the process of SE-CLSR used the benefits of maximizing the production of H_2 and inherent removal of CO_2. There is no need of WGS reactor and separation units at the downstream of the process. **Rydén et al.** [37] proposed this novel process for the production of H_2 by using three

interconnected fluidized bed reactors (reforming reactor, calcination reactor and air reactor). The reformer reactor was operated at low temperature and hydrocarbons were oxidized by the oxygen provided by the OC. In the reformer reactor, CO_2 produced during the reforming reactions (**Eq. 2.9** and **2.10**) was inherently removed by the sorption reaction (**Eq.2.12**). The carbonation reaction is highly exothermic reaction and released large amount of heat (-178.8 kJ mol^{-1}), this heat is utilized in the endothermic reforming reactions. So the overall reformer reactor operated under the thermo-neutral conditions. They obtained 95% + H_2 purity in the reformer reactor. The spent CO_2 sorbent (CaO) was fed to calcination reactor. The saturated sorbent was regenerated by supplying the sweep gas for the regeneration purposes. The heat required for the regeneration of the sorbent (**Eq. 2.13**) was provided by the heat of oxidation of the OC (**Eq. 2.11**). The oxidation of reduced OC was performed in the air reactor. As **Rydén et al.** [37] proposed the fluidized bed reactors, so the OC and sorbent moved between the interconnected reactors. The oxidized OC (NiO) and regenerated sorbent (CaO) were moved from the calcination reactor to the reformer reactor for the next cycle of SE-CLSR process. The detail of the process is given in literature [19]. To examine the performance of the SE-CLSR process in detail, they developed a process model on Aspen Plus. The schematic diagram of the developed model is shown in **Figure 2.9**.The connecting stream, product streams, feed stream and blocks are explained in **Table 2.5**.

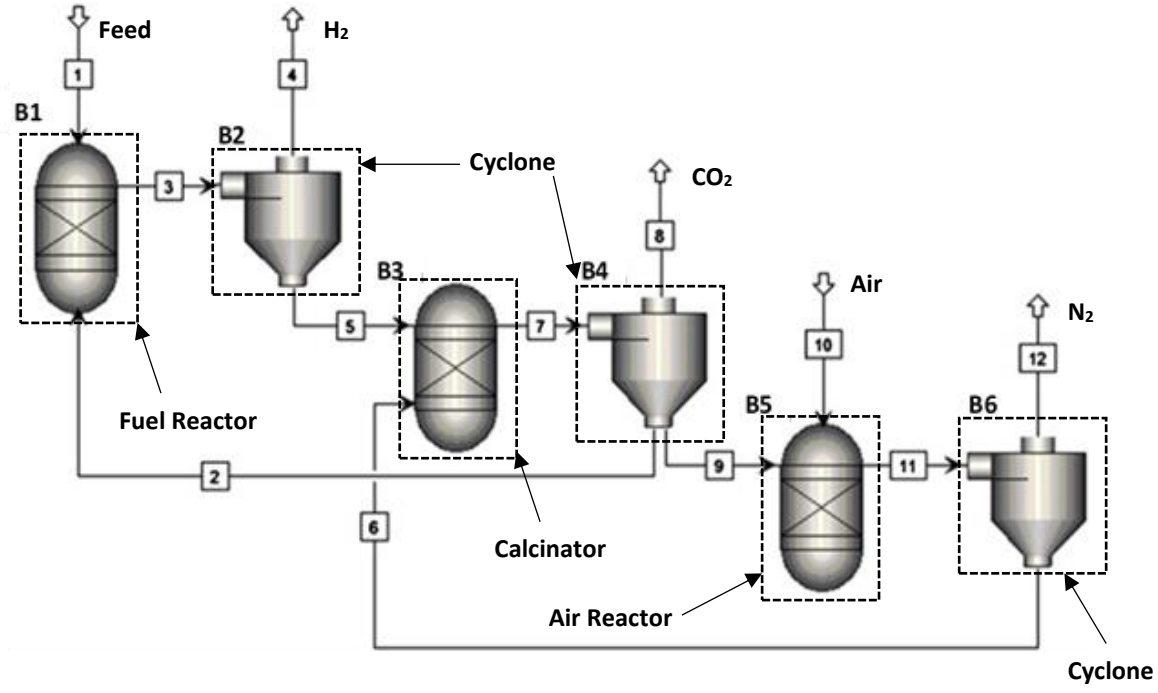

Figure 2.9: Schematic diagram of the process model of SE-CLSR [19]

Three reactors and three cyclones were used to simulate the whole process of SE-CLSR. In all of these three reactors equilibrium is reached. Hence output composition is obtained by minimizing Gibbs free energy for inlet reactants. It was observed that process operated at 580 °C and 1 bar produced almost 99% pure H_2 with 95% CO_2 capturing. CH_4 conversion under these conditions was 97%. And at 630 °C and 5 bar 98% pure H_2, 93% CO_2 capturing and 95% CH_4 conversion obtained. Overall the process is most suitable at 580 °C and 1 bar. The blocks and assumptions are listed in **Table 2.5** [19].

Table 2.5: Summary of block components and product streams

Block	**Component**	**Assumptions**
B1	Fuel reactor	Thermodynamic equilibrium is reached
B2	Cyclone	Perfect separation between solids and gas
B3	Calcination reactor	Thermodynamic equilibrium is reached
B4	Cyclone	Perfect separation between solids and gas
B5	Air reactor	Thermodynamic equilibrium is reached
B6	Cyclone	Perfect separation between solids and gas
Stream	**Type**	**Function**
1	Input stream	Fuel (CH_4, H_2O)
4	Output stream	Product (H_2, impurities)
8	Output stream	CO_2
10	Input stream	Air
12	Output stream	Oxygen depleted air (N_2)
2,3,5,6,7,9,11	Material streams	Connecting blocks

Experimental results of **Rydén et al.** (2012) showed that by varying temperature (500-700 °C) in a fluidized bed reactor using Ni (5 g) as a catalyst, CaO (10 g) as sorbent under 1 bar operating pressure, S/C of 2, O/C of 1 and CaO/C of 1.0 , CH_4 conversion increases linearly. At 500 °C, CH_4 conversion was reported as ~95% and at 700 °C it was ~98%. On the other hand, under the same operating conditions, H_2 production efficiency initially increases to a maximum value of 85% at 600 °C, and then it drops to 80% at 700 °C. This decrease in H_2 production efficiency is due to the saturation of CO_2 sorbent and decrease in its capacity to absorb CO_2. And it was quite obvious from the data of CO_2 capturing efficiency. As the temperature increase from 500-700 °C the CO_2 capturing efficiency (%) decreases from 95% to 72%. Lower the capturing of CO_2, lower will be the purity of H_2 at the outlet. Results are shown in **Table 2.6**;

The H_2 production is very sensitive to temperature, as the temperature increases the concentration of H_2 at the outlet starts decreasing. The optimum value of temperature under these conditions was found to be 580 °C. The similar effect was observed by increasing the pressure to a new value of 5 bar and keeping all other operating parameters constant.

Table 2.6: Effect of temperature on hydrogen production at 1bar [37]

Temperature, °C	500	550	600	650	700
H_2 production efficiency %	83.8	84.6	85	83.8	79.9
H_2 purity, %	97.6	96.8	96.1	93.8	83.1
CH_4 conversion, %	94.6	95.3	96.1	97.6	98.4
CO_2 capturing efficiency, %	94.6	93.8	92.3	81.5	72.3

Pimenidou et al. (2010) [39, 109] performed SE-CLSR process by using waste cooking oil as fuel in a packed bed reactor. They used 18 wt. % NiO supported on α-Al_2O_3 (0.85–2 mm size particles) and pre-calcined dolomite as CO_2 acceptor. The experimental rig they used for this work is shown in **Figure 2.10**. MKS mass flow controllers were used to control the flow of gases going into the packed bed reactor. ABB analyser and Varian 3380 gas chromatograph was used to analyse the product gases. The detail of the experimental work is given in literature. The experiment was run for 6 cycles at 600 °C and at S/C of 4. It was observed that batter conversion of fuel obtained as compared to the run without sorbent.

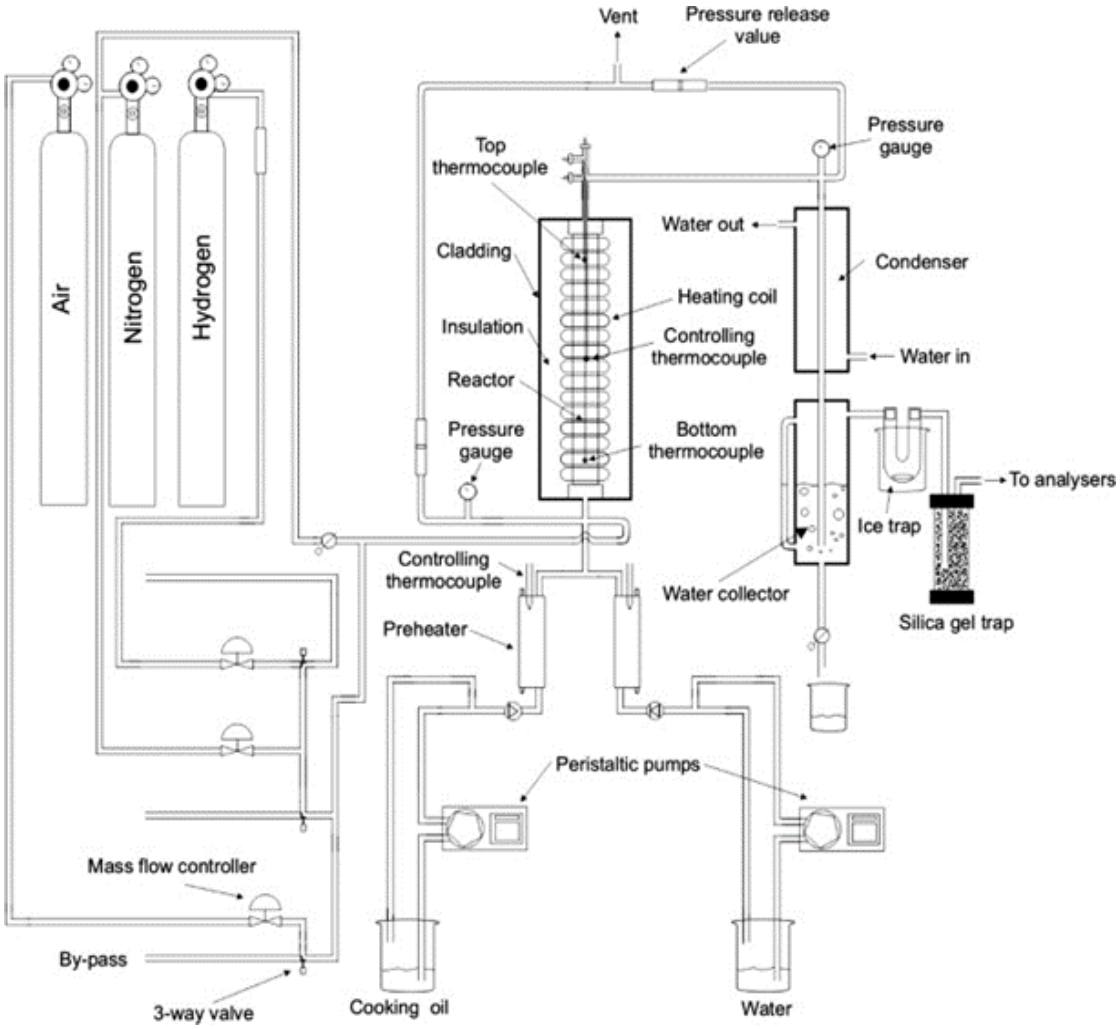

Figure 2.10: Schematic diagram of the SE-CLSR experimental set-up [109]

Kulkarni et al. [38] proposed the gasification technology for the production of H_2 and sequestration ready CO_2. The produced the high purity of H_2 with almost zero emission of CO_2. The efficiency of the process was better than the Integrated Gasification

Combined Cycle (IGCC) process with conventional CO_2 separation. In IGCC plant the heat produced during gasification is used for steam generation and ultimately this steam is used for power generation in steam turbine. While on the hand, the product gases from gasifier are passed through WGS reactor for H_2 production. H_2 has more energy content than syngas ($CO+H_2$) and it used in gas turbine for power/electricity generation.

There is no work reported on mathematical modelling of SE-CLSR process is literature. The objective of this PhD work is to develop the mathematical model of SE-CLSR process by using gPROMS model builder 4.1.0®. The kinetic data required for the modelling of SE-CLSR is reported in literature and will be discussed in next chapter.

2.8 Conclusion

The high temperature requirements, emission of CO_2, high capital cost and high regeneration temperature for sorbent in SMR, CLR and SE-SMR process respectively motivated the researcher to device the SE-CLSR process. In SE-CLSR process, the temperature for reforming process is 150-200 °C less than the conventional SMR process. The concentration of CO_2 is less than 100 ppm at the end of the process and this results in H_2 purity > 95%. The literature survey of all these H_2 production processes is covered in this chapter. The literature related to mathematical modelling of packed bed reactor is discussed in next chapter.

CHAPTER # 3
MATHEMATICAL MODELLING and SIMULATION

This chapter deals with the formulation of mathematical equations for the modelling of a packed bed catalytic reactor. This modelling includes formulation of general equations of law of conservation of mass, energy and momentum. These general formulas are then modified for different models depending upon the complexity of the system. The kinetic models reported in literature for different reforming processes are also discussed. At the end of this chapter, the methodology adopted for mathematical modelling, in next chapters, is also discussed.

3.1 Introduction

In any chemical process the mathematical modelling of diffusion and reaction scheme is considered as a very strong tool to understand the chemistry and design of the system. In order to understand the complete behaviour of the process, a detailed mathematical model needs to be developed. In industries many detailed and rigorous models are being used [110-112]. The complexity of the modelling depends upon the resemblance of the modelling with the real life process. In early days, more work was done on steady state modelling as it does not involve complexities as compared to the unsteady state modelling. The unsteady state process involved all the complexities related to physical properties and chemical reactions occurring during the process [113]. To cope with the problems of unsteady complexities, computerized based modelling software were developed for better representation of the industrial processes going on. This advancement led to considerable increase in overall efficiency of the process and reduction in manpower [114, 115]. **Elanshiae et al.** [115] adopted the 'system approach' to solve the complex fixed bed catalytic reactor problems. In their modelling, they divided the fixed bed reactor system into 'sub-systems' and solved these sub-systems separately. Every system has a boundary which isolates it from the surrounding environment. It can exchange mass or energy with the surrounding depending upon the type of the system. A

system can be classified on the basis of thermodynamic principles, continuous process and on the basis of phases involved in the process.

3.1.1 Classification of modelling systems

On the basis of thermodynamic principles, a system can be classified as an isolated, closed and open system. An 'isolated system' is one of the simplest system, no mass or energy transferred with the environment/surrounding is considered in this case. An adiabatic batch reactor is the simplest example of such system. While on the other hand, a system in which energy is transferred across the boundary but no mass transfer, is known as 'closed system'. A non-adiabatic reactor is a closed system process. There are some systems in which both mass and energy transfer with the surrounding can be observed. Such system are known as 'open systems' [116]. There are some continuous systems in which state variables are considered as invariant with respect to space dimensions. Such systems are known as 'lumped system'. In a 'discrete system', one or more state variables are either varying along the axial or radial direction of the reactor. The plug flow reactor is a good example of such system[117]. On the basis of phases involved a system can be classified as a 'homogeneous or heterogeneous system'. Only one phase is involved in homogeneous system while more than one phases are involved in heterogeneous systems.

Mathematical modelling of a heterogeneous system is considered to be more close to the real industrial processes. In modelling of a heterogeneous unsteady state system, along with reaction kinetics the diffusional processes are also considered. This makes the process more complex and close to the real life system. The fixed bed catalytic reactor is a good example of heterogeneous system [118].

The discovery of catalytic particles and later on their enormous application in chemical industry prompt the researchers to work more in this field. Now in chemical industries most of the catalytic processes are being carried out in fixed bed reactors. Catalyst particles are packed in the tubes of fixed bed reactors and bulk fluid is allowed to pass over the surface of these catalysts. The reactant particles first pass through the bulk fluid and reach at the surface of solid particles, reactants penetrate through the pores of particles and form products. These products are then desorbed and moved out of the particles towards bulk fluid.

Due to complex physical-chemical phenomena, the exact modelling of fixed bed reactors is very complex [119]. Despite of very simple appearance of fixed bed reactor, its design, operation and optimization is very complex because of complex and multiple reactions taking place within its boundary. To describe accurately the process taking place within a fixed bed reactor, a very realistic model formulation is required which demonstrates the real picture of the phenomena occurring in the reactor. This model is then validated through experimental results and then implemented on industrial scale for practical applications [120]. Modelling of catalytic fixed bed reactor involves following aspects:

a) Catalytic reactions modelling
b) Modelling of thermodynamic equilibrium
c) Mass transfer and heat transfer between the bulk gas in fluid phase and in solid phase
d) Intra particles diffusion modelling
e) Modelling of all physical properties of gases and their linkage with rest of the variables
f) Finally the combine modelling of fixed bed reactor and optimization of the process

More complex the model more parameters estimation it requires to present the real picture of the process. In modelling of reactor the most important thing is pellet modelling. One of the most commonly used models for fixed bed reactors is 'continuum model'. According to this model, differential equations for fluid phase and solid phase are developed and solved simultaneously [121]. Beside continuum model 'Cell model' is also used. In cell model the whole system is divided into small parts or cells and each cell is modelled as a single unit. The whole system is modelled by integrating these single cells. Due to wide application of continuum model in steady state simulation and optimization of fixed bed reactors, they are commonly adopted. The continuum model is classified into 2 categories: 'pseudo-homogeneous model' and 'heterogeneous model' [118].

In pseudo-homogeneous model there is no fluid-particle mass and heat transfer resistance. So this type of model is used where there are not considerable changes observed in effectiveness factor along the length of the reactor. While on the other hand heterogeneous model considered the variation of effectiveness factor and in rate equations of their model effectiveness factor is incorporated [120]. In **Figure 3.1** a schematic diagram for the classification of continuum model is shown.

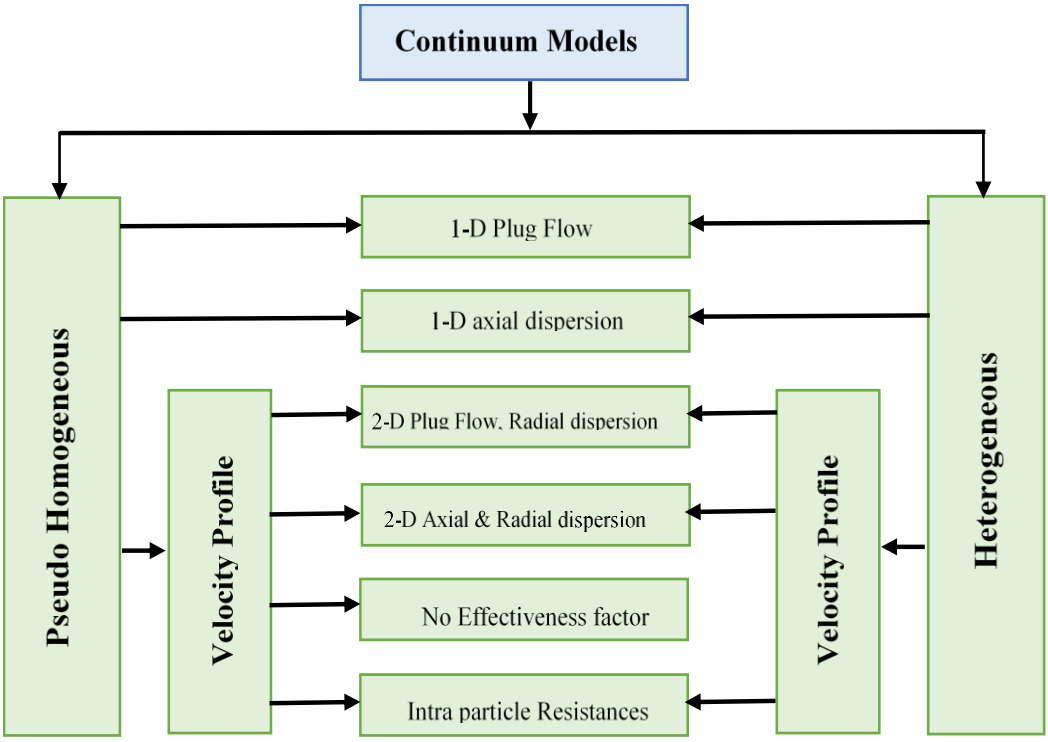

Figure 3.1: Classification of continuum model [122]

Pseudo-homogeneous and heterogeneous models are further divided into 'one-dimensional (1-D)' and 'two-dimensional (2-D)' models. 1-D models are very straight forward and simple models. They only consider the concentration and temperature variation along the axial direction and negligible gradient along the radial direction. While on the other hand, 2-D models considered the variation along both axis i.e. axial as well as radial.

3.2 Building mathematical model

In building a mathematical model for gas-solid reactive system, variety of physical and chemical relationships are considered. Law of conservation of mass and energy dictates the ultimate form of the mathematical equations for mass and energy balance within the boundaries of the system. The mathematical equations representing the overall picture of the system includes mass, energy and momentum balance equations. Mathematical model also includes equations for diffusional mechanism and reaction kinetics.

The configuration of fixed bed catalytic reactor system represented in mathematical equations form involves all the laws of mass and energy transfer from surrounding to

system, system to surrounding and within the system. The standard procedure used to develop mathematical model of fixed bed catalytic reactor can be summarized as;

a) Configuration of the system and its dependency on the surrounding
b) Identification of the variables and parameters involved in the system.
c) Formulation of the mass, energy and momentum balance equations
d) Formulation of the diffusion and reaction rate equations depending upon the type of the system.
e) Defining the boundary and initial conditions of the process to solve the partial differential equations involved in the system.

In the following sub-sections general equations for mass, energy and momentum transport are formulated and in later sections resulted equations are modified according to the requirements of the system.

3.2.1 Mass balance across the reactor

Modelling of the catalytic packed bed reactor or any other reactor involves the reaction rate equations, equations for the transfer of mass, heat and momentum. The mathematical representation of these phenomena and other interlinked parameters gives the picture of overall process happening within the boundary of the system [119].

For the derivation of following equations **Bird et al.** [123, 124] is used as a reference. First step towards the modelling of reactor is applying law of conservation of mass on a volume element of the packed bed reactor as shown in **Figure 3.2.**

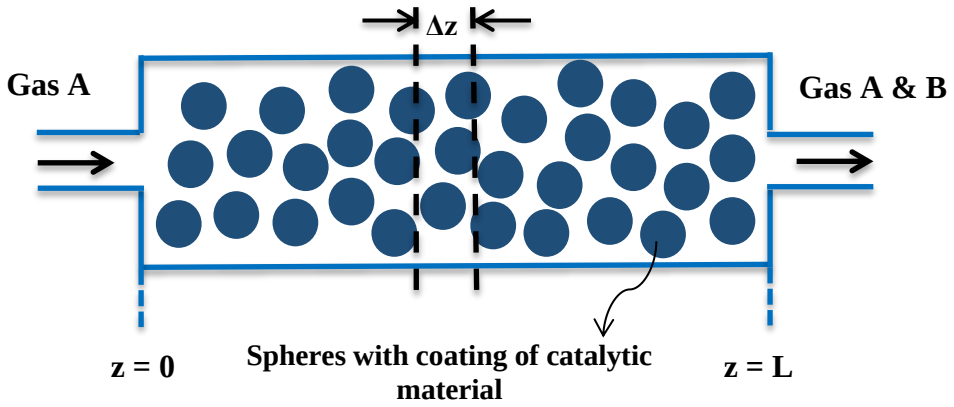

Figure 3.2: Schematic of catalytic packed bed reactor

According to the law of conservation of mass of component ‘A’,

(Rate of increase of mass of A per unit volume)

$$= \text{(Net rate of addition of A per unit volume)}$$
$$+ \text{(Net rate of production of A per unit volume)} \quad (3.1)$$

Net rate of addition of 'A' takes place either by convection or by diffusion. The convective term is introduced because of the mass motion of the fluid. To represent the law of conversation of mass in a mathematical form, let us consider the Cartesian plane;

$$\left(\frac{\partial \rho_A}{\partial t}\right)\Delta x\Delta y\Delta z = \left(n_{Ax|x}\Delta y\Delta z - n_{Ax|x+\Delta x}\Delta y\Delta z\right) + \left(n_{Ay|y}\Delta x\Delta z - n_{Ay|y+\Delta y}\Delta x\Delta z\right) + \left(n_{Az|z}\Delta x\Delta y - n_{Az|z+\Delta z}\Delta x\Delta y\right) + r_A\Delta x\Delta y\Delta z \quad (3.2)$$

The combined mass flux $'n_{Ax}'$ includes molecular flux and convective flux as well. After dividing the entire equation by $'\Delta x\Delta y\Delta z'$ and letting the size of element to approach zero, **Eq. 3.2** becomes,

$$\left(\frac{\partial \rho_A}{\partial t}\right) = -\left(\frac{\partial n_{Ax}}{\partial x} + \frac{\partial n_{Ay}}{\partial y} + \frac{\partial n_{Az}}{\partial z}\right) + r_A \qquad A = 1,2,3,\dots,N \quad (3.3)$$

This is the equation of continuity for specie 'A'. **Eq. 3.3** describes the change of mass concentration of the component 'A' with respect to time at a fixed point in a fixed bed reactor. This change in mass concentration is dependent on convective and diffusional transport of the fluid. The rate of formation or decomposition of component 'A' during the chemical reaction also effects the mass concentration of component 'A' within the system of a fixed bed reactor. **Eq. 3.3** can be written in vector form as,

$$\left(\frac{\partial \rho_A}{\partial t}\right) = -(\nabla . n_A) + r_A \quad (3.4)$$

As n_A is combined mass flux (molecular flux and convective flux) and it can be written as,

$$n_A = j_A + \rho_A v \quad (3.5)$$

Now **Eq. 3.4** can be written as,

$$\left(\frac{\partial \rho_A}{\partial t}\right) = -(\nabla . \rho_A v) - (\nabla . j_A) + r_A \quad (3.6)$$

Similarly continuity equation for molar flux is;

$$\left(\frac{\partial C_A}{\partial t}\right) = -(\nabla . N_A) + R_A \quad (3.7)$$

It is very necessary to represent the equation of continuity in both molar and mass flux form. In equation of continuity, when we are dealing with chemical reactions then molar units are preferred over mass units. In case of diffusion equations along with equation of motions, mass units are preferred.

In above equation $'R_A'$ is the rate of production of A in unit volume. **Eq. 3.7** can be written as;

$$\left(\frac{\partial C_A}{\partial t}\right) = -(\nabla . C_A v^*) - (\nabla . J_A) + R_A \qquad (3.8)$$

(A) (B) (C)

Here;

A: Net Rate of addition by convection

B: Net Rate of addition by diffusion

C: Rate of production or decomposition by reaction

This is the general form of continuity equation for packed bed catalytic reactor. Above equation can be modified for any particular system to model the mass balance across that system. In a system where only convective transport of the components are the dominant or only transport medium, then term B in **Eq. 3.8** can be ignored and vice versa.

In case of simple reforming process where no CO_2 acceptor is used, reactions taking place only on the surface of catalyst are considered. While on the other hand, when we have CO_2 acceptor along with oxygen carrier (OC) in a fixed bed reformer then the reactions occurring on the surface of the sorbent are also considered. Hence the rate equation for the production or decomposition of species will change accordingly.

3.2.2 Energy balance across the reactor

In a packed bed reactor heat transfer takes place through various transport mechanisms. Due to the molecular motion in the fluid ‘molecular energy’ transport and due to the bulk motion of the fluid ‘convective energy’ transport takes place. Similarly when fluid diffuses into each other the heat transport mechanism is known as ‘diffusion transport’. In addition to this, energy transport due to radiation is known as ‘radiation energy transport’ [123, 124]. According to the law of conservation of energy on a small element of unit volume $\Delta x \Delta y \Delta z$;

(Net rate of increase of energy per unit volume) =
(Net rate of energy addition by convection transport per unit volume) +
(Net rate of energy addition by heat conduction per unit volume) +
(Net rate of work done on system by molecular mechanism) +
(Net rate of work done on system by external forces) (3.9)

Rate of increase of energy in a unit volume $\Delta x \Delta y \Delta z$ is the summation of 'kinetic energy' and 'internal energy' of the fluid. The kinetic energy is associated with the movement of fluid while internal energy is because of rotational or vibrational movement of the fluid molecules. The internal energy also includes 'potential energy'. The mathematical form of the law of conservation of energy can be written as;

$$\Delta x \Delta y \Delta z \frac{\partial}{\partial t}\left(\frac{1}{2}\rho v^2 + \rho U\right) \tag{3.10}$$

The Convective transport, as already mentioned is the transfer of energy by the bulk motion of the fluid, is the sum of kinetic energy and internal energy of the fluid through the unit surface area. It is given as;

$$\left(\frac{1}{2}\rho v^2 + \rho U\right) v_x dS \tag{3.11}$$

In three directions the convective transport is written as;

$$\left(\frac{1}{2}\rho v^2 + \rho U\right) v \tag{3.12}$$

The volumetric flow rate across the surface element $'dS'$ perpendicular to x-axis is $'v_x dS'$.

The rate of heat transfer by molecular transport is given by 'Fourier's Law of heat conduction'. According to Fourier's Law, the rate of heat transfer per unit area is directly proportional to the temperature gradient across that unit element.

$$\frac{Q}{A} = -k\frac{dT}{dy} \tag{3.13}$$

In above equation 'k' is known as thermal conductivity and its value depends upon the temperature and pressure conditions of the system. If temperature varies in all three directions, above equation can be written as;

$$\mathbf{q} = -[k.\nabla T] \tag{3.14}$$

If fluid is moving with velocity v, then work done term is given as;

$$\textbf{Molecular Work Term} = [\boldsymbol{\pi}.\mathbf{v}] \tag{3.15}$$

In the above equation $'\boldsymbol{\pi}'$ is stress tensor. **Eq. 3.15** can be written as;

$$[\boldsymbol{\pi}.\mathbf{v}] = \mathrm{p}\mathbf{v} + [\mathrm{T}.\mathbf{v}] \tag{3.16}$$

Combine energy flux (**e**) is the sum of **Eq. 3.12, 3.14 & 3.16**. So after combining all these equations;

$$\mathbf{e} = \left(\frac{1}{2}\rho v^2 + \rho \mathrm{U}\right)\mathbf{v} + \mathrm{p}\mathbf{v} + [\mathrm{T}.\mathbf{v}] + \mathbf{q} \tag{3.17}$$

Here;

$$(\rho \mathrm{U})\mathbf{v} + \mathrm{p}\mathbf{v} = \boldsymbol{\rho}\left(\mathrm{U} + \left(\frac{\mathrm{p}}{\rho}\right)\right)\mathbf{v}$$

$$(\rho \mathrm{U})\mathbf{v} + \mathrm{p}\mathbf{v} = \boldsymbol{\rho}\left(\mathrm{U} + \mathrm{p}\acute{\mathrm{V}}\right)\mathbf{v}$$

$$(\rho \mathrm{U})\mathbf{v} + \mathrm{p}\mathbf{v} = \boldsymbol{\rho}\acute{\mathrm{H}}\mathbf{v}$$

So **Eq. 3.17** can be written as;

$$\mathbf{e} = \left(\frac{1}{2}\rho v^2 + \rho \acute{\mathrm{H}}\right)\mathbf{v} + \mathrm{p}\mathbf{v} + [\mathrm{T}.\mathbf{v}] + \mathbf{q} \tag{3.18}$$

Now the combined flux across the unit volume $\Delta x \Delta y \Delta z$ is;

$$\Delta y \Delta z\left(\mathrm{e}_{\mathrm{x}|\mathrm{x}} - \mathrm{e}_{\mathrm{x}|\mathrm{x}+\Delta \mathrm{x}}\right) + \Delta x \Delta z\left(\mathrm{e}_{\mathrm{y}|\mathrm{y}} - \mathrm{e}_{\mathrm{y}|\mathrm{y}+\Delta \mathrm{y}}\right) + \Delta y \Delta x\left(\mathrm{e}_{\mathrm{z}|\mathrm{z}} - \mathrm{e}_{\mathrm{z}|\mathrm{z}+\Delta \mathrm{z}}\right)$$

Dividing by $\Delta x \Delta y \Delta z$ and allowing unit volume to zero will give,

$$-\left(\frac{\partial \mathrm{e}_{\mathrm{x}}}{\partial \mathrm{x}} + \frac{\partial \mathrm{e}_{\mathrm{y}}}{\partial \mathrm{y}} + \frac{\partial \mathrm{e}_{\mathrm{z}}}{\partial \mathrm{z}}\right)$$

$$\text{Net Rate of combined flux} = -(\nabla.\mathbf{e}) \tag{3.19}$$

So **Eq. 3.18** will become;

$$-(\nabla.\mathbf{e}) = -\nabla.\left[\left(\tfrac{1}{2}\rho v^2 + \rho \acute{\mathrm{H}}\right)\mathbf{v} + \mathrm{p}\mathbf{v} + [\mathrm{T}.\mathbf{v}] + \mathbf{q}\right] \tag{3.20}$$

Rate of work done on system by external force is negligible in case of packed bed reactor so we can neglect that term. After re-arranging the law of conservation of energy we will get;

$$\frac{\partial}{\partial \mathrm{t}}\left(\frac{1}{2}\rho v^2 + \rho \mathrm{U}\right) = -(\nabla.\mathbf{e}) \tag{3.21}$$

Eq. 3.21 does not include the reaction and radiation term. As radiation, external field, mechanical and electrical effects are of less important in reactor so these terms are often neglected [119]. After adding heat effect of chemical reaction in **Eq. 3.21,** we will get;

$$\frac{\partial}{\partial t}\left(\frac{1}{2}\rho v^2 + \rho U\right) = -(\nabla . \mathbf{e}) + (-\Delta H)r \tag{3.22}$$

Or it can be written as;

$$\frac{\partial}{\partial t}\left(\frac{1}{2}\rho v^2 + \rho U\right) = -\nabla . \left[\left(\frac{1}{2}\rho v^2 + \rho \acute{H}\right)\mathbf{v} + p\mathbf{v} + \mathbf{q}\right] + (-\Delta H)r$$

$$= -\nabla . \left(\frac{1}{2}\rho v^2 + \rho \acute{H}\right)\mathbf{v} - \boldsymbol{\nabla} . p\mathbf{v} - \nabla . \mathbf{q} + (-\Delta H)r \tag{3.23}$$

To further simplify the **Eq. 3.23**, enthalpy term is expanded by using standard equilibrium thermodynamics formula;

$$d\acute{H} = \left(\frac{\partial \acute{H}}{\partial T}\right)_p dT + \left(\frac{\partial \acute{H}}{\partial p}\right)_T dP$$

$$d\acute{H} = C_p dT + \left[\acute{V} - T\left(\frac{\partial \acute{V}}{\partial T}\right)_p\right] dP \tag{3.24}$$

After integrating the above equation;

$$\acute{H} - H^0 = C_p(T - T^0) + \frac{1}{\rho}(p - p^0) \tag{3.25}$$

After putting all the values in **Eq. 3.23**, the new equation is of the following form;

$$\frac{\partial}{\partial t}\left(\frac{1}{2}\rho v^2 + \rho U\right) = -\nabla . \left(\frac{1}{2}\rho v^2 + \rho\left(C_p(T - T^0) + 1(p - p^0) + H^0\right)\right)\mathbf{v} - \boldsymbol{\nabla} . p\mathbf{v} - \nabla . \mathbf{q} + (-\Delta H)r$$

For constant pressure and no variation of velocity above equation will become;

$$\frac{\partial}{\partial t}\left(\rho C_p T\right) = -\nabla . \left(\rho v\left(C_p T\right)\right) - \nabla . \mathbf{q} + (-\Delta H)r \tag{3.26}$$

For 'A' number of components and 'j' number of reactions, the above equation can be written as;

$$\sum_A \rho C_p \left[\frac{\partial T}{\partial t} + v . \nabla T\right] = \sum_j \left(-\Delta H_j\right) r_j + \nabla . (k \nabla T) \tag{3.27}$$

(A) (B) (C) (D)

Here;

A: Change of heat content with time, **B:** Convective flow, **C:** Heat effect of the chemical reaction & **D:** Heat transport by conduction.

The **Eq. 3.27** is the general formulation of energy balance with assumption of constant density and heat capacity, no radiation flux, no energy flux by molecular diffusion, no heat effects due to mechanical, electrical and external field.

In later section the resulted general equation for energy balance will be modified for the simple reforming and sorption processes.

3.2.3 Pressure drop across the fixed bed reactor

There are various factors that determine the energy loss, pressure drop, in the packed bed reactor. Out of those the most important factors are;

a) Fluid flow rate
b) Fluid viscosity and density
c) Orientation and compactness of packing
d) Size, shape and surface of solid particles

Reynolds [125] observed that pressure drop in a packed column is the sum of two terms. His formulation is given as;

$$\frac{\Delta P}{L} = av + b\rho_f v^2 \tag{3.28}$$

To consider the effect of viscosity of fluid, **Eq. 3.28** was later modified into a new form (**Eq. 3.29)**;

$$\frac{\Delta P}{L} = a\mu v + b\rho_f v^2 \tag{3.29}$$

Ergun et al. [126] proposed that factor 'a' and 'b' in **Eq. 3.29** are proportional to 'viscous energy loss' and 'kinetic energy loss' respectively as shown below;

$$a = \acute{a}\left[\frac{(1-\varepsilon)^2}{\varepsilon^3}\right] \tag{3.30}$$

$$b = \acute{b}\left(\frac{1-\varepsilon}{\varepsilon^3}\right) \tag{3.31}$$

Here $'\acute{a}'$ and $'\acute{b}'$ are the factors of proportionality. By putting these values in **Eq. 3.29** we will get;

$$\frac{\Delta P}{L} = \acute{a}\left[\frac{(1-\varepsilon)^2}{\varepsilon^3}\right]\mu v + \acute{b}\left(\frac{1-\varepsilon}{\varepsilon^3}\right)\rho_f v^2 \tag{3.32}$$

This equation shows the effect of fractional void volume on the pressure drop of packed bed column. To account the effect of particle size, shape and surface area on the pressure drop of packed columns, **Ergun et al.** developed the modified equation as;

$$\frac{\Delta P g_c}{L} = 2\alpha S^2 \left[\frac{(1-\varepsilon)^2}{\varepsilon^3}\right]\mu v + \left(\frac{\beta}{8}\right) S \left(\frac{1-\varepsilon}{\varepsilon^3}\right)\rho_f v^2 \tag{3.33}$$

'S' is the specific surface area of the solid particle i.e. surface of solid particles per unit volume. It is given as;

$$d_p = \frac{6}{S} \tag{3.34}$$

So **Eq. 3.33** will become,

$$\frac{\Delta P g_c}{L} = 2\alpha \left(\frac{6}{d_p}\right)^2 \left[\frac{(1-\varepsilon)^2}{\varepsilon^3}\right]\mu v + \left(\frac{\beta}{8}\right)\left(\frac{6}{d_p}\right)\left(\frac{1-\varepsilon}{\varepsilon^3}\right)\rho_f v^2$$

$$\frac{\Delta P g_c}{L} = \frac{72\alpha}{d_p^2}\left[\frac{(1-\varepsilon)^2}{\varepsilon^3}\right]\mu v + \left(\frac{3}{4}\right)\left(\frac{\beta}{d_p}\right)\left(\frac{1-\varepsilon}{\varepsilon^3}\right)\rho_f v^2 \tag{3.35}$$

Where;

$$k_1 = 72\alpha \quad ; \quad k_2 = \left(\frac{3}{4}\right)\beta \tag{3.36}$$

After putting these values in **Eq. 3.35**;

$$\frac{\Delta P g_c}{L} = \frac{k_1}{d_p^2}\left[\frac{(1-\varepsilon)^2}{\varepsilon^3}\right]\mu v + \left(\frac{k_2}{d_p}\right)\left(\frac{1-\varepsilon}{\varepsilon^3}\right)\rho_f v^2 \tag{3.37}$$

Through the method of least square the values of $'k_1'$ *and* $'k_2'$ were found as;

$$k_1 = 150 \quad ; \quad k_2 = 1.75$$

Handley et al. [127] derived different values for 'k_1' and 'k_2' i.e. 1.24 for 'k_1' and 368 for 'k_2'. So the equation for pressure drop across the packed bed according to Ergun will become,

$$\frac{\Delta P g_c}{L} = \frac{150}{d_p^2}\left[\frac{(1-\varepsilon)^2}{\varepsilon^3}\right]\mu v + \left(\frac{1.75}{d_p}\right)\left(\frac{1-\varepsilon}{\varepsilon^3}\right)\rho_f v^2 \tag{3.38}$$

After further modification of above equation;

$$\frac{\Delta P g_c}{L} = \frac{\mu v}{d_p^2}\left[\frac{(1-\varepsilon)^2}{\varepsilon^3}\right]\left[150 + \frac{1.75 d_p \rho_f v}{(1-\varepsilon)\mu}\right]$$

$$\frac{\Delta P g_c}{L} = \frac{\mu v}{d_p^2}\left[\frac{(1-\varepsilon)^2}{\varepsilon^3}\right]\left[150 + \frac{1.75 d_p \rho_f v}{(1-\varepsilon)\mu}\right] \quad (3.39)$$

Above equation can be written in the form of friction factor 'f' as,

$$\frac{\Delta P g_c}{L} = \frac{\mu v}{d_p^2}\left[\frac{(1-\varepsilon)^2}{\varepsilon^3}\right] f \quad (3.40)$$

Eq. 3.40 gives the relation for calculation of pressure drop across the bed of the reactor and it covers all the factors affecting the loss of energy in the packed bed reactor.

Above equations for mass, energy and momentum transport can be used for any packed bed catalytic reactor. In the resulted equation (**Eq. 3.8, 3.27 & 3.40**) addition and subtraction of any term depends upon the type of system we are dealing with. In case of steady state process, all the time dependent terms will be zero.

The resulted transport equations can be solved for three different levels.

a) The macroscopic level
b) The microscopic level
c) The molecular level

The macroscopic level modelling deals with the transfer of mass, energy and momentum when entities are introduced or removed from the system. In microscopic level, more detail modelling is done to see the behaviour of fluid mixture during the transport to or from the system. The molecular level deals with the motion of molecules and intermolecular forces. This type of modelling is used when system involves complex molecules, chemically reacting system etc.

The summary of mass, energy and momentum transport equations used for modelling of 1-D heterogeneous packed bed reforming and sorption process are reported in **Table 3.1**. All these equations are derived from **Eq. 3.8, 3.27 and 3.40**.

3.2.4 Governing equations

In all mathematical modelling based literature, above equations are modified according to the nature of the system. **Singh et al.** [128] developed a mathematical model of steam-hydrocarbon reformers to check the performance of the side fired reformer. The developed mathematical model focused on the differential reformer tube section, of length Δz, filled with nickel (Ni) catalyst as shown in **Figure 3.3**. Only one tube is modelled as the representative of entire reformer. The uniform distribution of

temperature, pressure and axial diffusion of mass and energy was also assumed in this work.

Halabi et al. [129] developed a mathematical model to investigate the performance of auto-thermal reforming (ATR) process in a fixed bed reactor. In their work they assumed the variation of mass, energy and momentum terms to be in one direction i.e. along the axial direction of the reactor. The variation along the radial direction is neglected. The process is assumed to be adiabatic in nature. **Monnerat et al.** [42] presented the mathematical modelling of unsteady state oxidation of Ni gauze catalyst. In their modelling they assumed adiabatic fixed bed reactor, no heat transfer due to radiation and plug flow behaviour with no diffusional terms. In their work they modelled the system to present the effect of amount of O_2 (O_2 in Ar) on the temperature of the reactor system.

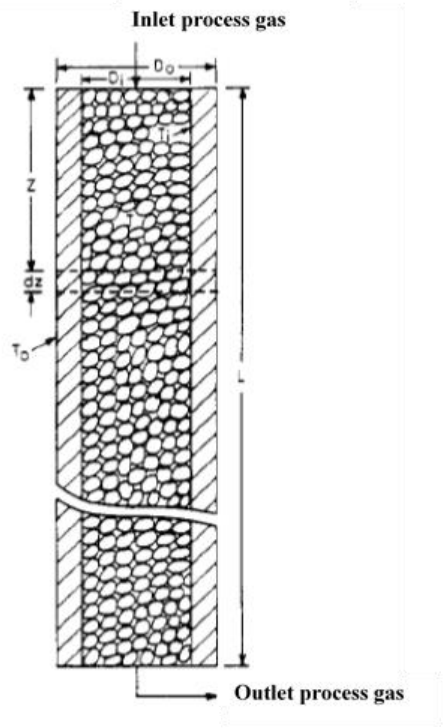

Figure 3.3: Schematic diagram of a reformer tube [128]

As explained in **Chapter 2** that the addition of sorbent enhances the reforming performance in terms of H_2 yield (wt. % of fuel) and fuel conversion. It shifts the process of conventional steam methane reforming (SMR) process beyond the equilibrium and more conversion of feed, high yield of H_2 and more pure H_2 is achieved. **Fernandez et al.** [40, 130, 131] developed a mathematical model to illustrate the performance of the adiabatic sorption enhanced steam methane reforming (SE-SMR) process. In their modelling work, they introduced the rate equations for CO_2 adsorption both in mass and

energy balance equations. **Eq. 3.8, 3.27 and 3.40** were modified according to the plug flow, 1-D heterogeneous and without axial dispersion process. The kinetic and equilibrium data reported by Twigg (1989) and Froment (1989) was used to simulate the process.

Zhou et al. used a universal nickel oxide (NiO) based catalyst and developed 1-D plug flow reactor model for reduction and chemical looping combustion (CLC) process under the assumption of isothermal and isobaric process. For reduction kinetics they used the reported data of **Iliuta et al.** and validated their modelling results with experimental data reported in literature [43, 132].

Ghouse et al. [133] focused on developing a mathematical model to investigate the performance of reforming process. They used 2-D dynamic heterogeneous model of SMR under the assumptions of no carbon deposition, ideal gas approximation and perfect mixing of the species. The mathematical modelling equations for mass and energy transfer in gas, solid and within the pellets were considered in this work. The used schematic diagram and multiscale modelling scheme is shown in **Figure 3.4.**

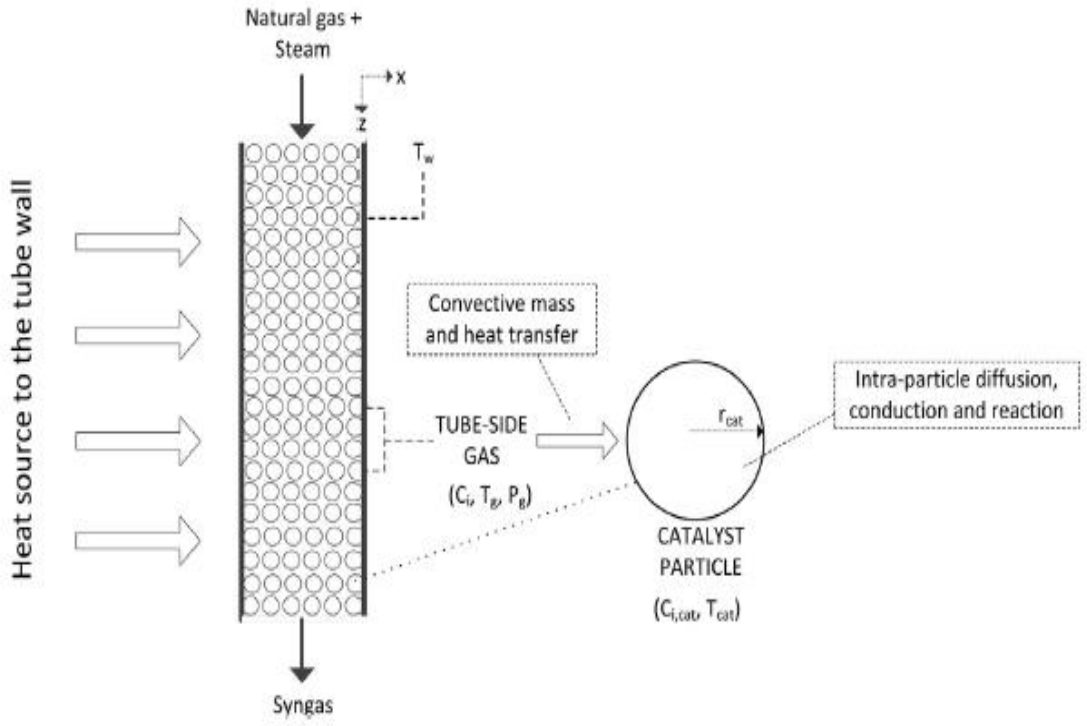

Figure 3.4: Schematic diagram of a reformer tube for a proposed multiscale modelling of SMR [133]

As shown in **Figure 3.4**, three phases were modelled to represent the 2-D variation in a fixed bed reformer. Mathematical model was developed for gas phase, catalyst phase and

for the tube wall. The mass, energy and momentum balance equations were considered for both axial and radial dimension of the reactor. The dynamic component mass balance and energy balance equations used for the modelling are tabulated in **Table 3.1**.

Adams et al. [134] presented a dynamic 2-D heterogeneous mathematical model of water gas shift (WGS) reactor. They assumed a plug flow reactor system and applied **Eq. 3.8, 3.27 and 3.40** for their experimental conditions and validated the developed model against the experimental findings.

Table 3.1: Summary of modelling equations used for simulation of 2-D heterogeneous SMR process [133]

Gas phase mass balance;

$$\left(\frac{\partial \mathrm{C_i}}{\partial \mathrm{t}}\right) = -\frac{\partial(\mathrm{u_i C_i})}{\partial \mathrm{z}} - \mathrm{k_i}\left(\mathrm{C_i} - \mathrm{C_{ci}}|_{r=Rp}\right)\left(\frac{a_v}{\varepsilon}\right) \tag{3.41}$$

Gas phase energy balance;

$$\frac{\partial\left(\mathrm{T_g}\rho_{\mathrm{g,molar}}\mathrm{C_{p,mix}}\right)}{\partial t} = -\frac{\partial\left(\mathrm{u_i}\rho_{\mathrm{g,molar}}\mathrm{C_{p,mix}}\mathrm{T_g}\right)}{\partial \mathrm{z}} + \mathrm{Q_{convwall\rightarrow gas}} - \mathrm{Q_{convgas\rightarrow cat}} + \sum_{i=1}^{Nc} \mathrm{Q}_i \tag{3.42}$$

Catalyst phase mass balance;

$$\theta_c\left(\frac{\partial \mathrm{C_{ci}}}{\partial \mathrm{t}}\right) = \frac{2}{r}\mathrm{D}_{ei,mix}\,\frac{\partial(\partial \mathrm{C_{ci}})}{\partial \mathrm{r}} + \frac{\partial}{\partial r}\left[\mathrm{D}_{ei,mix}\frac{\partial \mathrm{C_{ci}}}{\partial \mathrm{r}}\right] + \mathrm{r_i}\rho_{\mathrm{c}} \tag{3.43}$$

Catalyst phase energy balance;

$$\left[(1-\theta_c)\rho_{\mathrm{c}}\mathrm{C_{pc}} + \theta_c\sum_{i=1}^{Nc}\left(\mathrm{C_{ci}}\mathrm{C_{pc,i}}\right)\right]\frac{\partial \mathrm{T}_c}{\partial t} = \lambda_c\left(\frac{1}{\mathrm{r}^2}\right)\frac{\partial}{\partial r}\left(\mathrm{r}^2\frac{\partial \mathrm{T_c}}{\partial \mathrm{r}}\right) + \sum_{i=1}^{Nc}\mathrm{C_{pc,i}}\frac{\partial \mathrm{T_c}}{\partial \mathrm{r}}\mathrm{D}_{ei,mix}\frac{\partial \mathrm{C_{ci}}}{\partial \mathrm{r}} - \rho_{\mathrm{c}}\sum_{i=1}^{Nc}H_{c,i}\mathrm{r_i} \tag{3.44}$$

The most common mathematical models proposed in literature are either pseudo homogeneous or heterogeneous models. To solve the system of packed bed reactor, mostly reactor is divided into small sections and mathematical equations are solved for one section of the bed. This one section is assumed to represent the overall reactor. The

heterogeneous models are preferred for more detail understanding of the process as it involves various complexities and represents the real picture of the physical process. The summary of different models used in literature is presented in **Table 3.2.** The mathematical equations for mass and energy balances along with boundary conditions are listed in this table. As we move from **MODEL 1** to **MODEL 6**, complexity of the mathematical models increases. **MODEL 1- 4** are for 1-D system and **MODEL 5-6** are for 2-D systems.

The **MODEL 1** was developed by **Barkelew** [135], and in this model axial and radial dispersion is neglected. At the same time interphase and intraparticle gradients are also neglected. Later on **Liu et al.** [136] developed **MODEL 2**. This model includes interphase resistances but no intraparticle resistances. Later on, they introduced the term of axial diffusion (**MODEL 4**) to demonstrate the sensitivity of the temperature and concentration profile to axial diffusion. **McGreavy et al.** [137] developed the lumped model under the assumption of isothermal catalyst pellet. This 2-D model (**MODEL 5**) was used to solve the packed bed catalytic reactor. **Feick et al.** [138] developed a numerical technique to solve the complicated 2-D model (**MODEL 6**). They used nonlinear partial differential equations and solved them by finite different methods (FDM).

Table 3.2: Summary of modelling equations used in literature for one and 2-D heterogeneous systems [139]

Model #	**Mass and Energy balance Equations**	
MODEL 1	$\left(\frac{\partial C^*}{\partial t^*}\right) = -\frac{\partial C^*}{\partial x^*} - \frac{(1-\varepsilon_2)}{\varepsilon_2}\frac{d_p}{uC_{io}}R^*$	(3.45)
	$\left(\frac{\partial T^*}{\partial t^*}\right) = -\frac{\partial T^*}{\partial x^*} + \frac{(1-\varepsilon_2)}{\varepsilon_2}\frac{d_p}{u\rho_g c_g}(-\Delta H)\frac{R^*}{T_{io}} - \frac{Ah_w d_p}{u\rho_g c_g}(T_w^* - T^*)$	(3.46)
MODEL 2	$\left(\frac{\partial C^*}{\partial t^*}\right) = -\frac{\partial C^*}{\partial x} - \alpha(C^* - C_s^*)$	(3.47)
	$\left(\frac{\partial T^*}{\partial t^*}\right) = -\frac{\partial T^*}{\partial x} - \alpha'(T^* - T_s^*)$	(3.48)

MODEL 3

$$\left(\frac{\partial C^*}{\partial t^*}\right) = -\frac{\partial C^*}{\partial x} - \alpha(C^* - C_s^*) \quad (3.49)$$

$$\left(\frac{\partial T^*}{\partial t^*}\right) = -\frac{\partial T^*}{\partial x} - \alpha^1(T^* - T_s^*) - \frac{Ah_w d_p}{u\rho_g c_g}\,(T_w^* - T^*) \quad (3.50)$$

MODEL 4

$$\left(\frac{\partial C^*}{\partial t^*}\right) = \frac{1}{P_{eML}}\frac{\partial C^*}{\partial x^2} - \alpha(C^* - C_s^*) \quad (3.51)$$

$$\left(\frac{\partial T^*}{\partial t^*}\right) = \frac{1}{P_{eHL}}\frac{\partial T^*}{\partial x^2} - \alpha'(T^* - T_s^*) \quad (3.52)$$

MODEL 5

$$\left(\frac{\partial C^*}{\partial t^*}\right) = -\frac{\partial C^*}{\partial x} + \frac{1}{P_{eMr}}.\frac{1}{r^*}\frac{\partial}{\partial r^*}\left(\frac{1}{r^*}\frac{\partial C^*}{\partial r^*}\right) - \alpha(C^* - C_s^*) \quad (3.53)$$

$$\left(\frac{\partial T^*}{\partial t^*}\right) = -\frac{\partial T^*}{\partial x} + \frac{1}{P_{eHr}}.\frac{1}{r^*}\frac{\partial}{\partial r^*}\left(\frac{1}{r^*}\frac{\partial T^*}{\partial r^*}\right) - \alpha'(T^* - T_s^*) \quad (3.54)$$

MODEL 6

$$\left(\frac{\partial C^*}{\partial t^*}\right) = \frac{1}{P_{eML}}\frac{\partial^2 C^*}{\partial x^2} - \frac{\partial C^*}{\partial x} + \frac{1}{P_{eMr}}\frac{1}{r^*}\frac{\partial}{\partial r^*}\left(\frac{1}{r^*}\frac{\partial C^*}{\partial r^*}\right) - \alpha(C^* - C_s^*) \quad (3.55)$$

$$\left(\frac{\partial T^*}{\partial t^*}\right) = \frac{1}{P_{eHL}}\frac{\partial^2 T^*}{\partial x^2} - \frac{\partial T^*}{\partial x} + \frac{1}{P_{eHr}}.\frac{1}{r^*}\frac{\partial}{\partial r^*}\left(\frac{1}{r^*}\frac{\partial T^*}{\partial r^*}\right) - \alpha'(T^* - T_s^*) \quad (3.56)$$

All the above equations reported in literature were developed by following mass and energy conservative equations i.e. **Eq. 3.8 and 3.27**.

In **Chapter 4,** the mathematical modelling of conventional SMR is presented. The mathematical model is a 1-D heterogeneous fixed bed reactor under the assumption of plug flow behaviour. It is assumed that system obeys the ideal gas behaviour and adiabatic in nature. The variation of concentration, temperature and other variables is only considered in axial direction, all variation in radial directions are considered as negligible. In **Chapter 5,** the mathematical model of SE-SMR is presented under the conditions of adiabatic operation and plug flow in nature. In this model, CO_2 adsorption on the surface of CO_2 acceptor (CaO) is also considered. In **Chapter 6,** the reduction of oxygen carrier (OC) and oxidation of reduced nickel catalyst is modelled and coupled with already developed model of SE-SMR process. In this chapter, the fuel reactor (FR) and air reactor (AR) models are run in a cyclic way to understand the performance of the sorption enhanced chemical looping reforming (SE-CLSR) process. All models used mass, energy, momentum balance and kinetic rate equations. The mass and energy balance equations for all above mentioned processes are derived from **Eq. 3.8 and 3.27** are presented in **Table 3.3**.

Table 3.3: Summary of mass and energy balances equations used to simulate 1-D heterogeneous packed bed reactor

Mass and energy balance in the gas phase for the reforming process;

$$\varepsilon_b\left(\frac{\partial C_i}{\partial t}\right)+\frac{\partial(uC_i)}{\partial z}+k_{g,i}a_v\left(C_i-C_{i,s}\right)=\varepsilon_b D_z\frac{\partial^2 C_i}{\partial z^2} \tag{3.57}$$

$$\varepsilon_b\rho_g C_{pg}\left(\frac{\partial T}{\partial t}\right)+u_s\rho_g C_{pg}\frac{\partial(T)}{\partial z}=h_f a_v(T_s-T)+\lambda_z^f\frac{\partial^2 T}{\partial z^2} \tag{3.58}$$

Mass and energy balance in the solid phase;

$$k_{g,i}a_v\left(C_i-C_{i,s}\right)=(1-\varepsilon_b)\rho_{cat}\,r_i \tag{3.59}$$

$$\rho_{bed}C_{p,bed}\left(\frac{\partial T_s}{\partial t}\right)+h_f a_v(T_s-T)=\ (1-\varepsilon_b)\rho_{cat}\sum -\Delta H_{rxn,j}\,\eta_j R_j \tag{3.60}$$

Mass balance for Ni oxidation and reduction;

$$\left(\frac{dC_{Ni}}{dt}\right)=\pm R_j M_{Ni}\quad\&\quad\left(\frac{dC_{NiO}}{dt}\right)=\pm R_j M_{NiO} \tag{3.61}$$

Mass balance for carbon;

$$\left(\frac{dC_C}{dt}\right)=R_j M_{Ni}\,M_C \tag{3.62}$$

Mass and energy balance in the solid phase [SE-SMR];

$$k_{g,i}a_v\left(C_i-C_{i,s}\right)=\upsilon\rho_{cat}\,r_i-(1-\upsilon)\,\rho_{ads}\,r_{ads} \tag{3.63}$$

$$\rho_{bed}C_{p,bed}\left(\frac{\partial T_s}{\partial t}\right)+h_f a_v(T_s-T)=\ \upsilon\rho_{cat}\sum -\Delta H_{rxn,j}\,\eta_j R_j+(1-\upsilon)\,\rho_{ads}\sum -\Delta H_{ads}\,r_{ads} \tag{3.64}$$

Table 3.4: SE-CLSR reaction scheme used in this work

Process	Reaction	Rate equation	Ref.
Oxidation of Ni	$O_{2(g)} + 2Ni_{(s)} \leftrightarrow 2NiO_{(g)}$	$R_1 = a_0 k_1 (1 - X_{Ni})^{2/3} C_{O_2} C'_{Ni}$	[42, 140]
	$O_{2(g)} + C_{(s)} \leftrightarrow CO_{2(g)}$	$R_2 = a_0 k_2 (1 - X_C)^{1/2} C_{O_2} C'_C$	[141]
	$O_{2(g)} + 2C_{(s)} \leftrightarrow 2CO_{(g)}$	$R_3 = a_0 k_3 (1 - X_C)^{1/2} C_{O_2} C'_C$	[141]
	$O_{2(g)} + 2CO_{(g)} \leftrightarrow 2CO_{2(g)}$	$R_4 = \frac{k_4 C_{O_2} C_{CO}}{(1 + K_{CO,o} C_{CO})}$	[142]
Reduction of Oxygen carrier	$CH_{4(g)} + 2NiO_{(s)} \leftrightarrow 2Ni_{(s)} + 2H_{2(g)} + CO_{2(g)}$	$R_5 = a_0 k_5 C_{CH_4} C_{NiO} C_{Ni} (1 - X_{NiO})$	[43, 132]
	$H_{2(g)} + NiO_{(s)} \leftrightarrow Ni_{(s)} + H_2O_{(g)}$	$R_6 = a_0 k_6 C_{H_2} C_{NiO} (1 - X_{NiO})$	[43, 132, 143-145]
	$CO_{(g)} + NiO_{(s)} \leftrightarrow Ni_{(s)} + CO_{2(g)}$	$R_7 = a_0 k_7 C_{CO} C_{NiO} C_{Ni} (1 - X_{NiO})$	[43, 132, 145]
	$CH_{4(g)} + NiO_{(s)} \leftrightarrow Ni_{(s)} + 2H_{2(g)} + CO_{(g)}$	$R_8 = a_0 k_8 C_{CH_4} C_{NiO} C_{Ni} (1 - X_{NiO})$	[43, 88, 89, 91, 132]
Steam methane reforming	$CH_{4(g)} + H_2O_{(g)} \leftrightarrow CO_{(g)} + 3H_{2(g)}$	$R_9 = \frac{k_9}{p_{H_2}^{2.5}} \left(p_{CH_4} p_{H_2O} - \frac{p_{H_2}^3 p_{CO}}{K_I} \right) \left(\frac{1}{\Omega^2} \right)$	[131, 132, 146]

Water gas shift	$CO_{(g)} + H_2O_{(g)} \leftrightarrow CO_{2(g)} + H_{2(g)}$	$R_{10} = \frac{k_{10}}{p_{H_2}}\left(p_{CO}p_{H_2O} - \frac{p_{H_2}p_{CO_2}}{K_{III}}\right)\left(\frac{1}{\Omega^2}\right)$	[131, 132, 146]
Overall steam methane reforming	$CH_{4(g)} + 2H_2O_{(g)} \leftrightarrow CO_{2(g)} + 4H_{2(g)}$	$R_{11} = \frac{k_{11}}{p_{H_2}^{3.5}}\left(p_{CH_4}p_{H_2O}^2 - \frac{p_{H_2}^4 p_{CO_2}}{K_{II}}\right)\left(\frac{1}{\Omega^2}\right)$	[129, 131, 144]
Dry methane reforming	$CH_{4(g)} + CO_{2(g)} \leftrightarrow 2CO_{(g)} + 2H_{2(g)}$	$R_{12} = \frac{k_{12}p_{CH_4}p_{CO_2}}{1 + K_{CO_2}p_{CO_2}}$	[132, 138, 144]
Methane decomposition	$CH_{4(g)} + Ni_{(s)} \leftrightarrow C_{(s)} + 2H_{2(g)}$	$R_{13} = \frac{k_{13}K_{CH_{4,d}}\left(p_{CH_4} - \frac{p_{H_2}^2}{K_{p,d}}\right)}{\left(1 + \frac{1}{K_{r,d}}p_{H_2}^{\frac{3}{2}} + K_{CH_{4,d}}p_{CH_4}\right)^2}$	[132, 138, 144, 146]
Carbon gasification with steam	$H_2O_{(g)} + C_{(s)} \leftrightarrow CO_{(g)} + H_{2(g)}$	$R_{14} = \frac{\frac{k_{14}}{K_{H_2O,g}}\left(\frac{p_{H_2O}}{p_{H_2}} - \frac{p_{CO}}{K_{p,g}}\right)}{\left(1 + K_{CH_{4,g}}p_{CH_4}\frac{1}{K_{H_2O,g}}\frac{p_{H_2O}}{p_{H_2}} + \frac{1}{K_{r,g}}p_{H_2}^{\frac{3}{2}}\right)^2}$	[43, 132]
Carbon gasification with CO_2	$CO_{2(g)} + C_{(s)} \leftrightarrow 2CO_{(g)}$	$R_{15} = \frac{\frac{k_{15}}{K_{CO_2,g}K_{CO,g}}\left(\frac{p_{CO_2}}{p_{CO}} - \frac{p_{CO_2}}{K_{p,g,CO_2}}\right)}{\left(1 + K_{CO,g}p_{CO} + \frac{1}{K_{CO_2,g}K_{CO,g}}\frac{p_{CO_2}}{p_{CO}}\right)^2}$	[132, 146]
CO_2 adsorption	$CaO_{(s)} + CO_{2(g)} \leftrightarrow CaCO_{3(s)}$	$R_{16} = \frac{\eta}{M_{CaO}}\frac{dq_{CO2}}{dt}$	[40, 41, 147]

3.3 Reaction kinetics mechanism

One of the most important parameters that plays a vital role in the design and the performance of the reactor is the 'kinetic mechanism'. The overall behaviour of the reactor depends upon the specific values used for the reaction kinetics and reaction rate equations used in modelling the reactor [148].

The reaction scheme proposed in this work is summarized in **Table 3.4**. The oxidation of Ni based OC is very fast and highly exothermic in nature [R_1]. The amount of heat released during oxidation mainly depends upon the concentration of O_2 in N_2. Higher the amount of O_2, higher will be the amount of heat released. The amount of carbon deposited on the surface of catalyst during chemical looping reduction cycle is oxidized to CO and CO_2 in the oxidation cycle [R_2-R_4]. The reduction reactions [R_5-R_8] of Ni based OC along with SMR [R_9], WGS [R_{10}], overall reforming [R_{11}], dry reforming [R_{12}], methane decomposition [R_{13}], carbon gasification with steam [R_{14}], carbon gasification with CO_2 [R_{15}] and CO_2 adsorption [R_{16}] are the typical reactions included in chemical looping reduction. The reactions between gas components and the catalyst support are neglected in this work due to the lack of data available in literature [149].

3.3.1 Oxidation and reduction kinetics of Ni based OC [R_1-R_8]

In literature it has been shown that for chemical looping process NiO is an auspicious OC [146]. The wide use of NiO as an OC makes it necessary to investigate the intrinsic kinetics of its reduction and oxidation. Generally, kinetics of Ni oxidation and reduction involves various chemical steps. Depending upon different reaction mechanism, different solid state models are reported in literature. The most abundantly used models are the 'reaction order model' (F), 'geometrical contracting model' (R), 'diffusion model' (D) and 'Avrami-Erofe'ev (AE) model' as shown in **Figure 3.5** [150-153]. In **Table 3.5,** different solid-state kinetic models are tabulated. The reaction order models (F) are developed under the assumption of homogeneous reaction process. Most of the models listed in table 3.5 are one parameter models, only the AE model and the random pore model (RPM) contains two parameters. Many of the listed models are classical examples of shrinking core models (SCM) like R2 and R3. The model R2 is for two dimensional and R3 is for three dimensional growth/shrinkage [154]. In diffusion models (D), transfer of gases from or to the active metals is considered as rate determining step [155]. On the

other hand AE models involves the formation of nuclei. In addition to these models, the ProuteTompkins (PT) model is an autocatalysis model [156]. The random pore model is based on the pore growth phenomena [157, 158].

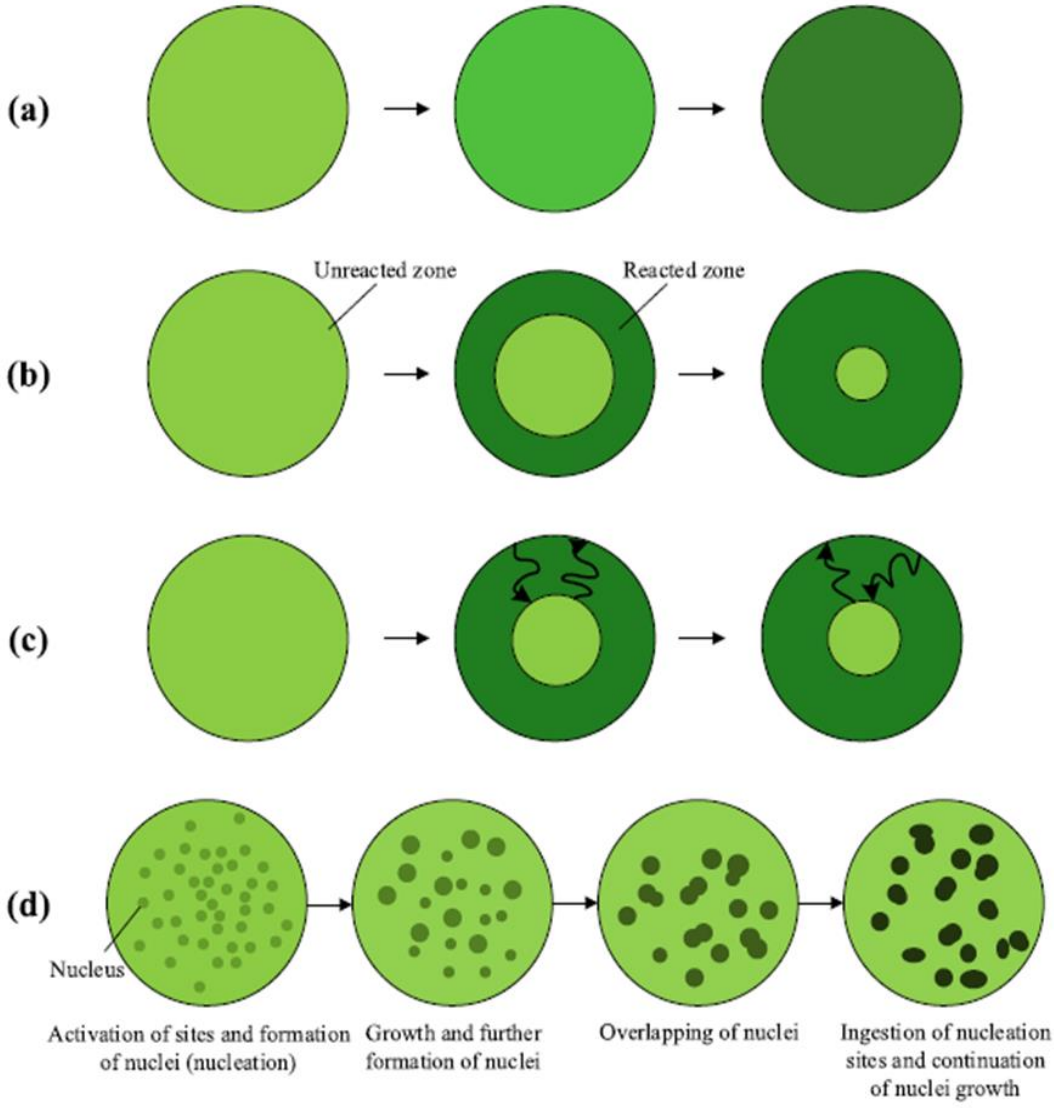

Figure 3.5: Models applicable to Ni based oxygen carrier a) Reaction order Model; (b) Geometrical contracting Model; (c) Diffusion Model and (d) Avrami-Erofe'ev Model [155]

The changing grain size model (CGSM) involves the diffusion of gases from bulk of gases to the surface of solid and then diffusion into the pores of solids. Here reaction takes place and formed product diffuses out in the similar manner as gases diffuse into the system [159]. In SCM a layer of product is formed outside the grain and with the passage of time size of core reduces, as shown in **Figure 3.6**. This model is used when the resistance to gas diffusion within the unreacted particle is very high [160]. Oxidation and reduction

reactions of OC can be addressed by nucleation growth model. Most commonly AE model is used for getting conversion vs time curve [144].

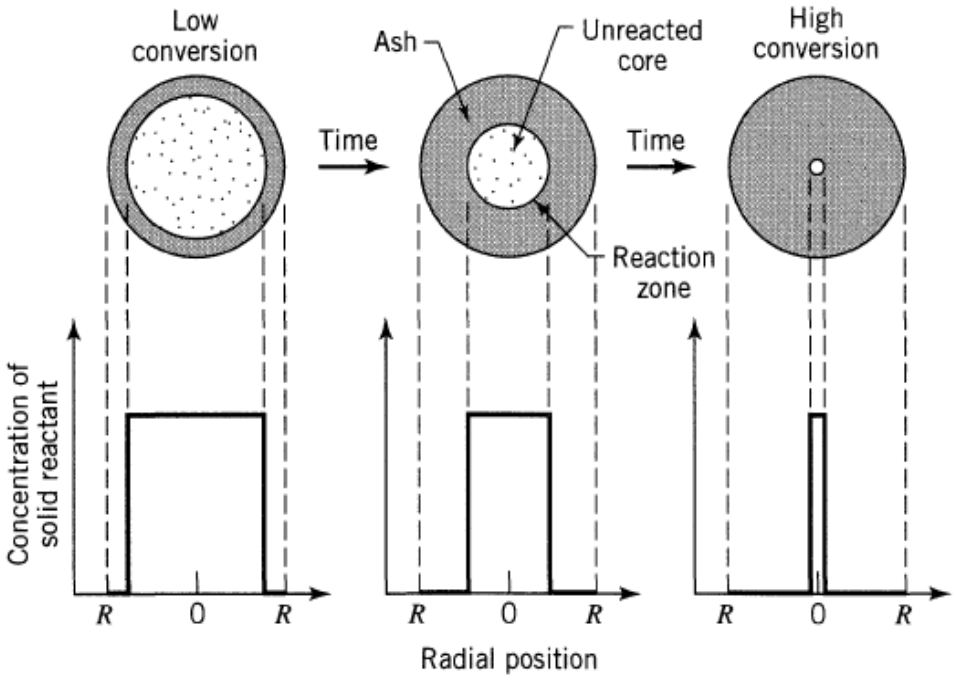

Figure 3.6: Scheme of shrinking core model (SCM) [161]

Khawam et al. [162] discussed the solid state kinetic modelling. The mechanism used for the verification of selected model comes from experimental results. Ideally, experiments like X-ray diffraction (XRD), scanning electron are used to get the results and are used in empirical models listed in **Table 3.5**. Commonly, to evaluate the kinetics parameter for solid state reduction or oxidation process, **Hancock and Sharp** method is used. **Zhou et al.** [155] explained this method by using literature data. The empirical models reported in table 3.5 were used against the experimental data to find out the best suitable model for different solid state reactions. The method of Hancock and Sharp works on the principle of nucleation model expressed as;

$$\ln[-\ln(1-x)] = \ln a + n\ln t \qquad (3.65)$$

In above equation **'x'** is for solid conversion, **'a'** is a constant that depends upon the frequency of nuclei formation and **'n'** is Avrami-Erofe'ev exponent [163]. A linear plots of ln [– ln (1-x)] vs. ln (t) gives straight line and slope of the line gives the value of 'n'. For different kinetic models, the value of n is different. The resulted value of 'n' dictates the range of models to be used for fitting. **Zhou et al.** [155] used twenty solid state models

in their work and fitted the experimental results on these models. Finally, a statistical approach was used to decide the ultimate model for different solid state catalysts. They performed Akaike Information Criterion (AIC) and the F-test in their statistical approach.

Table 3.5: The solid state kinetic models and their rate expressions [162]

Reaction model	$\mathbf{f(x) = \frac{1}{k}\frac{dx}{dt}}$	**n**
Three halves order [F1.5]	$(1-x)^{3/2}$	0.91
Second order [F2]	$(1-x)^{2}$	0.83
Third order [F3]	$(1-x)^{3}$	0.70
Zero order (Polany-Winger equation) [R1]	1	1.24
Phase boundary controlled reaction (contracting area) [R2]	$2(1-x)^{1/2}$	1.11
Phase boundary controlled reaction (contracting volume) [R3]	$3(1-x)^{2/3}$	1.07
One dimensional diffusion [D1]	$1/(2x)$	0.62
two dimensional diffusion [D2]	$1/[-\ln(1-x)]$	0.57
Three dimensional diffusion [D3]	$3(1-x)^{\frac{1}{3}}/[2(1-x)^{-\frac{1}{3}}-1]$	0.54
Avrami-Erofe'ev (n=1) [AE1]	$(1-x)$	1
Avrami-Erofe'ev (n=0.5) [AE0.5]	$\left(\frac{1}{2}\right)(1-x)[-\ln(1-x)]^{-1}$	0.5
Avrami-Erofe'ev (n=1.5) [AE1.5]	$\left(\frac{3}{2}\right)(1-x)[-\ln(1-x)]^{1/3}$	1.5
Avrami-Erofe'ev (n=2) [AE2]	$2(1-x)[-\ln(1-x)]^{1/2}$	2
Avrami-Erofe'ev (n=3) [AE3]	$3(1-x)[-\ln(1-x)]^{2/3}$	3
Avrami-Erofe'ev (n=4) [AE4]	$4(1-x)[-\ln(1-x)]^{3/4}$	4
Random pore model [RPM]	$(1-x)[1-\emptyset\ln(1-x)]^{1/2}$	---
Prout-Tompkins [PT]	$x(1-x)$	---

The reaction rate equations used for modelling oxidation of Ni catalyst and reduction of Ni based oxygen carrier are reported in **Table 3.4**. The reduction of Ni based oxygen carrier in the presence of CH_4, produces higher amount of H_2 as compared to CO, CO_2 and H_2O. **Iliuta et al.** [43] proposed 2 options of NiO reduction. In first route/option they considered direct formation of CO_2 without the formation of CO during reduction of NiO

(R_5 and R_6). In the second option they considered the formation of CO_2 via CO (R_7 and R_8).

Normally, the reduction of Ni is a high temperature process and it may cause the formation of carbon on the surface of the catalyst. To enhance the performance of the catalyst and study the effect of carbon formation on the reforming process, rate equations for carbon deposition (R_{13}) during the reforming process and carbon removal (R_2-R_4) during the oxidation process are also used in this work. The kinetic rate constants reported for oxidation and reduction are calculated by using following temperature dependence expressions [43, 140-142];

$$k_1 = k_{0,1}\exp\left(\frac{-E_1}{RT}\right) = 0.46\exp\left(\frac{-22000}{RT}\right) \quad (3.66)$$

$$k_2 = k_{0,2}\exp\left(\frac{-E_2}{RT}\right) = 20.6\exp\left(\frac{-99000}{RT}\right) \quad (3.67)$$

$$k_3 = k_{0,3}\exp\left(\frac{-E_3}{RT}\right) = (4.21\times10^{3})\exp\left(\frac{-127000}{RT}\right) \quad (3.68)$$

$$k_4 = k_{0,4}\exp\left(\frac{-E_4}{RT}\right) = (6.21\times10^{21})\exp\left(\frac{-29000\times4.184}{RT}\right)/(60\times100^{6}) \quad (3.69)$$

$$k_5 = k_{0,5}\exp\left(\frac{-E_5}{RT}\right) = 4.66\exp\left(\frac{-77416}{RT}\right) \quad (3.70)$$

$$k_6 = k_{0,6}\exp\left(\frac{-E_6}{RT}\right) = (1.31\times10^{-4})\exp\left(\frac{-26413}{RT}\right) \quad (3.71)$$

$$k_7 = k_{0,7}\exp\left(\frac{-E_7}{RT}\right) = (1.097\times10^{-4})\exp\left(\frac{-26505}{RT}\right) \quad (3.72)$$

$$k_8 = k_{0,8}\exp\left(\frac{-E_8}{RT}\right) = (4.18\times10^{-3})\exp\left(\frac{-23666}{RT}\right) \quad (3.73)$$

The kinetic parameter and the rate equations used for the oxidation and reduction process are taken from literature and the developed models are validated against the literature data. In SE-CLSR process, reduction and reforming process takes place in parallel. The kinetics for reforming process is discussed in the following section.

3.3.2 SMR and WGS reactions [R_9-R_{11}]

The SMR reaction is highly endothermic and WGS reaction is exothermic in nature. These reactions are catalysed by Ni based catalyst. In a chemical looping process, Ni reduction reactions are considered as more dominant in initial stages than reforming

reactions. The reforming reactions become dominant as the NiO starts converting to Ni. In 1955, first attempt to develop the reaction kinetics for SMR was published. This publication considered Ni catalyst supported on Kieselguhr – chalk-like stone [164]. Later in 1964, **Bodrov et al.** [165, 166] reported reaction kinetics for SMR reaction. **Eq. 3.74** is the expression that was presented to describe the reaction rate of SMR. They studied SMR kinetics on the surface of nickel foil in the temperature range of 800-900 °C.

$$R_{SMR} = \frac{k_{SMR} p_{CH_4}}{1 + a\frac{p_{H_2O}}{p_{H_2}} + b p_{CO}} \tag{3.74}$$

In the above equation 'a' and 'b' are temperature dependent constants. Later **Denken et a**l. [166] used Ni/Al_2O_3 catalyst (12% Ni) for SMR process and determined kinetics in the temperature range of 550-680 °C. In 1989, **Xu et al.** [131, 167] proposed a kinetic model, using a nickel catalyst supported on $MgAl_2O_4$. This kinetic reaction model is considered as most promising and widely employed model in the literature for the simulation of SMR process. **Hou et al.** [168] later proposed a model, which was similar to **Xu et al.,** to study the kinetics of a $Ni/\alpha\text{-}Al_2O$ catalyst, but that model was bit complex as more parameters were required to simulate the process of SMR.

Elnashaie et al. compared the work of **Bodrov et al.**, **Denken et al.** and **Xu et al.** It was concluded that different models have different dependency when it comes to partial pressure of the steam. The kinetic reaction model has negative dependency on steam partial in **Bodrov et al.** work, positive in **Denken et al.** work and **Xu et al.** work incorporated both negative and positive effects. **Elnashaie et al.** [166] concluded that the kinetic model presented by **Xu et al**. is more universal than the SMR kinetics proposed by other researchers. In chapter 4, **Xu et al**. kinetic model is used to simulate the SMR process.

There are two most important and widely used schemes for the reaction mechanism of SMR process proposed by **Xu et al**. In reaction 'scheme I' parallel formation of CO and CO_2 takes place. Although, it too takes place in reaction 'scheme II' but the mechanism of formation is different. These two reaction schemes are based on few assumptions and on the basis of these assumptions reaction rate equations for SMR coupling with WGS

reaction are developed. On the basis of following assumptions the reaction schemes are developed and shown in **Figure 3.7** and **3.8** [131].

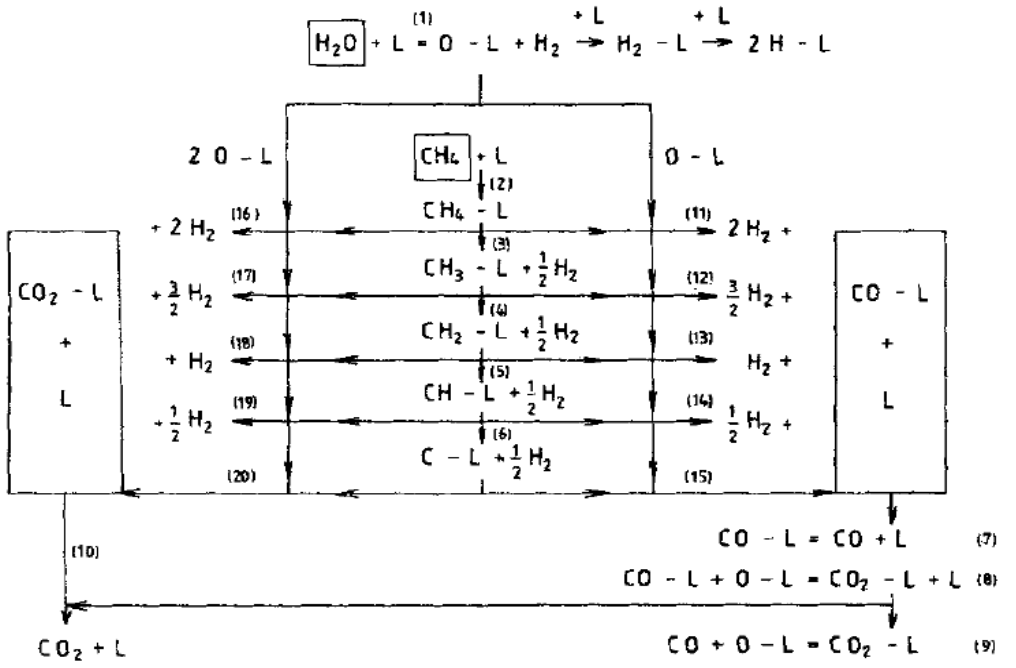

Figure 3.7: Reaction Scheme I [131]

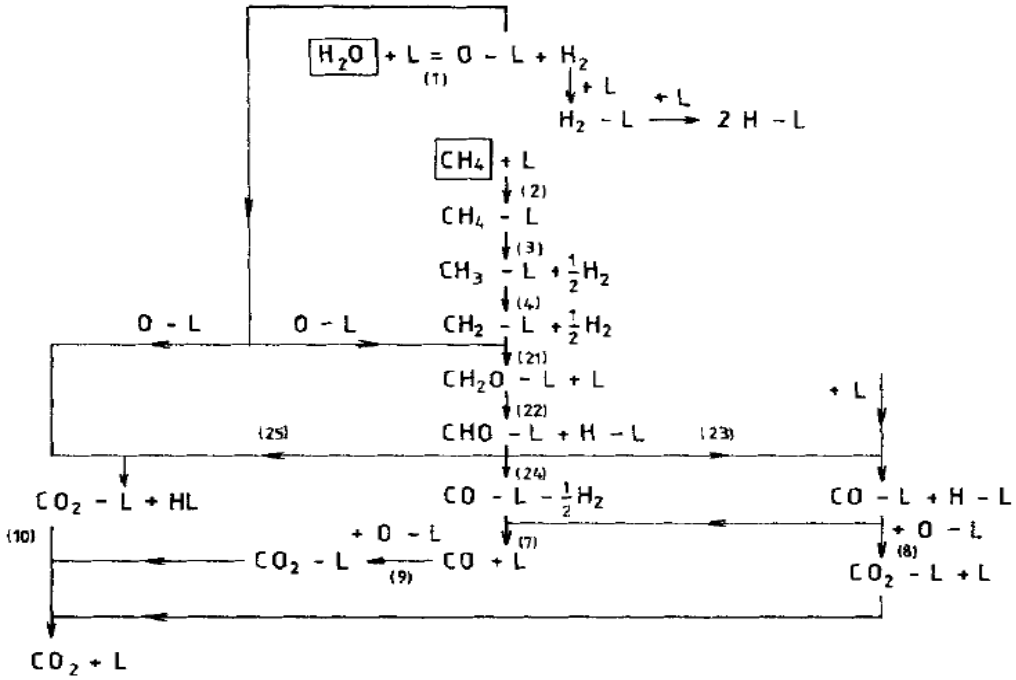

Figure 3.8: Reaction Scheme II [131]

a) Water reacts with the surface of Ni metal, adsorbed oxygen and gaseous H_2 formation takes place.

a) Similarly methane reacts on the surface and dissociated into its radicals known as chemisorbed radicals.

b) Or CH_4 reacts with adsorbed O_2 and form CO and CO_2 in result.

By following these assumptions and reaction scheme II, following 13 reaction steps were proposed that show the real picture of the reaction mechanism or scheme taking place in the SMR and WGS reactions.

$$H_2O + S_a = O - S_a + H_2 \quad \text{(I)}$$

$$CH_4 + S_a = CH_4 - S_a \quad \text{(II)}$$

$$CH_4 - S_a + S_a = CH_3 - S_a + H - S_a \quad \text{(III)}$$

$$CH_3 - S_a + S_a = CH_2 - S_a + H - S_a \quad \text{(IV)}$$

$$CH_2 - S_a + O - S_a = CH_2O - S_a + S_a \quad \text{(V)}$$

$$CH_2O - S_a + S_a = CHO - S_a + H - S_a \quad \text{(VI)}$$

$$CHO - S_a + S_a = CO - S_a + H - S_a \quad (R.D.S.;\ R_9) \quad \text{(VII)}$$

$$CO - S_a + O - S_a = CO_2 - S_a + S_a \quad (R.D.S.;\ R_{10}) \quad \text{(VIII)}$$

$$CHO - S_a + O - S_a = CO_2 - S_a + H - S_a \quad (R.D.S.;\ R_{11}) \quad \text{(IX)}$$

$$CO - S_a = CO + S_a \quad \text{(X)}$$

$$CO_2 - S_a = CO_2 + S_a \quad \text{(XI)}$$

$$2H - S_a = H_2 - S_a + S_a \quad \text{(XII)}$$

$$H_2 - S_a = H_2 + S_a \quad \text{(XIII)}$$

On the basis of this mechanism and experimental estimation of parameters, **Xu et al.** [131] proposed the rate equations for SMR. The rate equations (R_9-R_{11}) are listed in **Table 3.4**. These rate equations are on the basis of three rate determining steps (R.D.S) shown in steps (VII), (VIII) and (IX). Where:

$$\Omega = 1 + K_{CO}p_{CO} + K_{H_2}p_{H_2} + K_{CH_4}p_{CH_4} + K_{H_2O}\frac{p_{H_2O}}{p_{H_2}} \quad (3.75)$$

Here, 'K_i' is the adsorption constant of specie 'i' and 'p_i' is the partial pressure for specie 'i'. More detail is presented in **Chapter 4.** The kinetic rate constants used for the reforming process are given in **Eq. 3.76, 3.77 and 3.78**. These rate equations and rate

constants are used in the modelling work and results are validated against the experimental outputs.

$$k_9 = k_{0,9}\exp\left(\frac{-E_9}{RT}\right) = (1.17 \times 10^{15})\exp\left(\frac{-240100}{RT}\right) \quad (3.76)$$

$$k_{10} = k_{0,10}\exp\left(\frac{-E_{10}}{RT}\right) = (5.43 \times 10^{5})\exp\left(\frac{-67130}{RT}\right) \quad (3.77)$$

$$k_{11} = k_{0,11}\exp\left(\frac{-E_{11}}{RT}\right) = (2.83 \times 10^{14})\exp\left(\frac{-243900}{RT}\right) \quad (3.78)$$

These values for rate constants are reported in **Xu et al.** [131] work. The reforming reactions (R_9-R_{11}) are equilibrium reactions. The expressions used for the reaction equilibrium constants are presented in **Eq. 3.79, 3.80 and 3.81**.

$$K_I = \exp\left(\frac{-26830}{T_s} + 30.114\right) \quad (3.79)$$

$$K_{II} = \exp\left(\frac{4400}{T_s} - 4.036\right) \quad (3.80)$$

$$K_{III} = K_I K_{II} \quad (3.81)$$

The formation of CO_2 during reforming reaction can promotes the dry reforming (R_{12}) process. The kinetic rate expression and rate constant for dry reforming process is presented in next section.

3.3.3 Dry reforming [R_{12}]

The dry reforming reaction (R_{12}) is one of the important reaction in the looping reforming as far as the production of energy and chemicals are concerned. In past, many researchers did enormous work in developing the reaction kinetics for dry reforming reactions. Initial studies were focused more on Rh or mixed metal catalysts than Ni based catalysts [169-171]. **Wei et al.** [172] and **Wang et al.** [173] proposed dry reforming kinetics on the surface of Ni based catalyst. Commonly it is believed that the formation of CH_4 radical (CH_x, x = 0-3) and its reaction with the oxidant (from CO_2 dissociation) is one of the slowest step during dry reforming. **Zhang et al.** [174] used Ni/La_2O_3 catalyst for dry reforming and found that activation of CH_4 radical (CH_x, x=0-3) is the R.D.S, while in case of Ni/γ-Al_2O_3 catalyst the R.D.S is the reaction between oxidant and the surface carbon species (CH_4 radicals). **Bradford et al.** [175] reported reaction kinetics of dry

reforming for various Ni based catalysts and found that the activation of CH_4 and its reaction with oxidant is the slowest step.

In majority of dry reforming literature, 'Langmuir-Hinshelwood' type mechanism is proposed as fundamental mechanism for the reaction rate equations. **Wang et al.** [173] proposed the mechanism of CH_4 and CO_2 reaction on the surface of Ni/γ -Al_2O_3 catalyst. On the basis of their investigation, the reaction mechanism of dry reforming is given as;

$$CH_4 + * \rightarrow CH_4^* \quad \text{(I)}$$

$$CO_2 + * \rightarrow CO_2^* \quad \text{(II)}$$

$$CH_4^* \rightarrow CH_3^* + H \quad \text{(III)}$$

$$CH_3^* \rightarrow CH_2^* + H \quad \text{(IV)}$$

$$CH_2^* \rightarrow CH^* + H \quad \text{(V)}$$

$$CH^* \rightarrow C^* + H \quad \text{(VI)}$$

$$C^* + CO_2^* \rightarrow 2CO + 2* \quad \text{(VII)}$$

$$CO \rightarrow C + O \quad \text{(VIII)}$$

$$2H + O \rightarrow H_2O \quad \text{(IX)}$$

$$H + H \rightarrow H_2 \quad \text{(X)}$$

Wang et al. proposed a reaction rate equation (R_{12}) depending upon the above mentioned mechanism by using Langmuir-Hinshelwood mechanism. According to their finding, rate of reaction is first order with respect to partial pressure of CH_4, and it is first order with respect to partial pressure of CO_2 at low pressure and zero order at high pressure. The resulted rate equation is listed in **Table 3.4**. The adsorption coefficient of CO_2 and kinetic rate constant for dry reforming is given as:

$$k_{12} = k_{0,12}\exp\left(\frac{-E_{12}}{RT}\right) = 0.207\exp\left(\frac{-9920}{RT}\right) \quad (3.82)$$

$$K_{CO2} = (2.4 \times 10^{-3})\exp\left(\frac{77500}{RT}\right) \quad (3.83)$$

To find out the adsorption coefficient 'Freundlich's adsorption concept' was used.

3.3.4 Methane decomposition [R_{13}]

The study of decomposition of carbon containing gases on the surface of metals has been carried out for many years [176]. The formation of carbon on the surface of catalyst is highly undesirable as it causes catalyst deactivation and fouling of the reactor tubes. The amount of carbon formed on the surface of OC is vastly dependent on the amount of oxygen available. Normally, carbon is formed on the surface of catalyst at the end of the reduction period when almost entire NiO reduced to Ni catalyst [43, 94].

Snoeck et al. [176] proposed the mechanism to derive the rate equation for carbon decomposition. In **Figure 3.9** all the possible mechanisms for methane decomposition are shown.

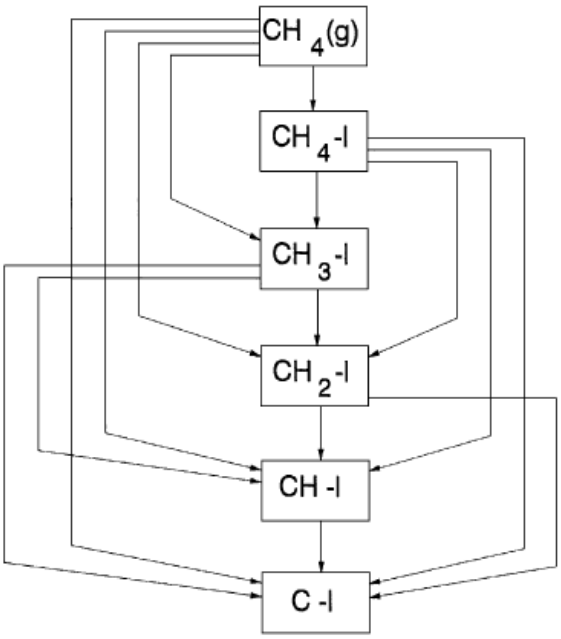

Figure 3.9: The possible reaction pathways during methane decomposition [176]

The more detailed mechanism of methane cracking includes the following steps;

Surface reactions;

$$CH_4 + l \leftrightarrow CH_4 - l \quad \text{(I)}$$

$$CH_4 - l + l \leftrightarrow CH_3 - l + H - l \qquad (R.D.S.;\ R_{13}) \quad \text{(II)}$$

$$CH_3 - l + l \leftrightarrow CH_2 - l + H - l \quad \text{(III)}$$

$$CH_2 - l + l \leftrightarrow CH - l + H - l \quad \text{(IV)}$$

$$CH - l + l \leftrightarrow C - l + H - l \quad \text{(V)}$$

$$2H - l \leftrightarrow H_2 + 2l \quad \text{(VI)}$$

Dissolution/Segregation;

$$C - l \leftrightarrow C_{Ni,f} + l \quad \text{(VII)}$$

Diffusion of carbon through Ni;

$$C_{Ni,f} \leftrightarrow C_{Ni,r} \quad \text{(VIII)}$$

Precipitation/Dissolution of carbon;

$$C_{Ni,r} \leftrightarrow C_w \quad \text{(IX)}$$

This mechanism of carbon formation on the surface of catalyst is well explained in **Figure 3.10**.

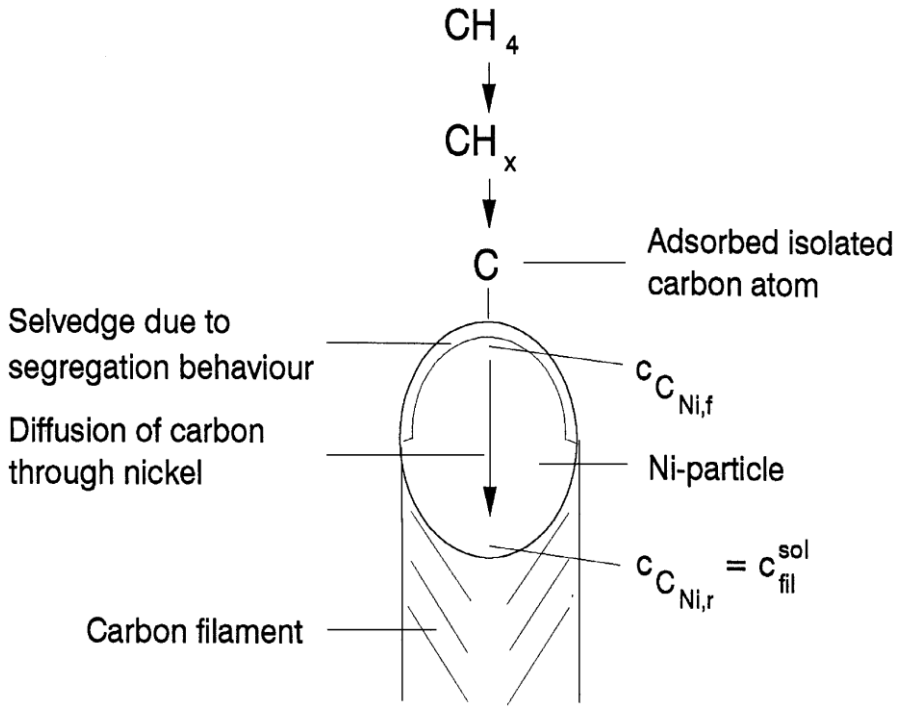

Figure 3.10: Mechanism of carbon formation on the surface of catalyst during methane decomposition/cracking [176]

Snoeck et al. [176] proposed the removal of first hydrogen atom from the CH_4 molecule with the formation of methyl group as the slowest step i.e. R.D.S (R_{13}). The amount of carbon formed dissolved in Ni at the front side of the particle, just below the selvedge ($C_{Ni,f}$ as indicated in **Figure 3.10**). The carbon keeps on diffusing in the rear end of the particle ($C_{Ni,r}$). At the end of the mechanism, carbon deposited as precipitate (solid).The rate equation developed via this mechanism is listed in **Table 3.4**. The kinetic rate

constants, equilibrium constants and adsorption coefficients for CH_4 decompositions are given as following:

$$k_{13} = k_{0,13}\exp\left(\frac{-E_{13}}{RT}\right) = 43.4\exp\left(\frac{-58900}{RT}\right) \quad (3.84)$$

$$K_{p,d} = \exp\left(\frac{104}{R}\right) \times \exp\left(\frac{-88400}{RT}\right) \quad (3.85)$$

$$K_{CH4,d} = (2.1 \times 10^{-6})\exp\left(\frac{78000}{RT}\right) \quad (3.86)$$

$$K_{r,d} = (5.18 \times 10^{7})\exp\left(\frac{-133000}{RT}\right) \quad (3.87)$$

3.3.5 Carbon gasification by steam and CO_2 [R_{14} & R_{15}]

The gasification of carbon becomes prominent when the formation of carbon on the surface of catalyst is on the higher side. The gasification reactions release H_2 and CO and promote the conversion of CH_4 by exposing more catalyst surface for the reforming reactions. **Snoeck et al.** [177] proposed the mechanism for carbon gasification by steam and CO_2 on the surface of NiO-K_2O/Ca-Al_2O_3.

The number of experiments and analysis revealed that during cracking/decomposition of CH_4, carbon formed on the surface of Ni catalyst via following steps;

a) Formation of carbon on the surface of Ni catalyst
b) Diffusion of carbon through the catalyst (Ni) particles
c) The particles of Ni are lifted by the growing filament of carbon

The carbon gasification sequence is inverse of the carbon formation. It caused Ni particles to settle down on the support again. The reaction mechanism of carbon gasification by steam is dependent on the partial pressure of the steam. The rate equation for the carbon gasification by steam (R_{14}) is presented in **Table 3.4**, the R.D.S for this rate equation is the reaction of adsorbed carbon atom with adsorbed oxygen atom. The modelling of rate equation for carbon gasification by steam is always accompanied by the carbon gasification by hydrogen. The reaction mechanism is given as;

$$C_{Ni,f} + l \leftrightarrow C - l \quad (I)$$

$$H_2 + 2l \leftrightarrow 2H - l \quad (II)$$

$$C - l + 3H - l \leftrightarrow CH_3 - l + 3l \quad (III)$$

$$CH_3 - l + H - l \leftrightarrow CH_4 - l + l \quad (IV)$$

$$CH_4 - l \leftrightarrow CH_4 + l \quad \text{(V)}$$

$$H_2O + l \leftrightarrow H_2O - l \quad \text{(VI)}$$

$$H_2O - l \leftrightarrow O - l + H_2 \quad \text{(VII)}$$

$$C - l + O - l \leftrightarrow CO - l + l \qquad (R.D.S.;\ R_{14}) \quad \text{(VIII)}$$

$$CO - l \leftrightarrow CO + l \quad \text{(IX)}$$

The rate equation of carbon gasification by CO_2 is also based on reaction of adsorbed carbon atom with adsorbed oxygen atom. The reaction mechanism of carbon gasification by CO_2 is presented as;

$$C_{Ni,f} + l \leftrightarrow C - l \quad \text{(I)}$$

$$CO_2 + 2l \leftrightarrow CO - l + O - l \quad \text{(II)}$$

$$C - l + O - l \leftrightarrow CO - l + l \qquad (R.D.S.;\ R_{14}) \quad \text{(III)}$$

$$CO - l \leftrightarrow CO + l \quad \text{(IV)}$$

The kinetic rate parameters and equilibrium constant for carbon gasification by steam and CO_2 (R_{14} and R_{15}) are given as [43];

$$k_{14} = k_{0,14}\exp\left(\frac{-E_{14}}{RT}\right) = (3.08 \times 10^4)\exp\left(\frac{-166000}{RT}\right) \quad (3.88)$$

$$K_{H2O,g} = (4.73 \times 10^{-6})\exp\left(\frac{97700}{RT}\right) \quad (3.89)$$

$$K_{CH4,g} = 3.49 \quad (3.90)$$

$$K_{r,g} = (1.83 \times 10^{13})\exp\left(\frac{-216000}{RT}\right) \quad (3.91)$$

$$K_{p,g} = \exp\left(\frac{137}{R}\right)\exp\left(\frac{-126000}{RT}\right) \quad (3.92)$$

$$k_{15} = k_{0,15}\exp\left(\frac{-E_{15}}{RT}\right) = (8.37 \times 10^{10})\exp\left(\frac{-312000}{RT}\right) \quad (3.93)$$

$$K_{CO,g} = (37.8 \times 10^{-6})\exp\left(\frac{100000}{RT}\right) \quad (3.94)$$

$$K_{CO2,g} = (8.17 \times 10^{7})\exp\left(\frac{-104000}{RT}\right) \quad (3.95)$$

$$K_{p,g,CO2} = \exp\left(\frac{178}{R}\right)\exp\left(\frac{-169000}{RT}\right) \quad (3.96)$$

3.3.6 Carbonation kinetics [R_{16}]

In this study, CaO based sorbent is used to capture CO_2 formed during the reforming process. The details about the selection criteria, importance and classifications of sorbent is given in **Chapter 2**.

In past, many efforts were made to describe the kinetics of CO_2 adsorption on the surface of CaO based sorbent [41, 147, 178, 179]. **Rodriguez et al.** [180] proposed the first order carbonation reaction rate and developed the rate equation for CO_2 adsorption on the surface of CaO sorbent (R_{16}).

$$\frac{dq_{CO2}}{dt} = k_{carb}(X_{max} - X)\left(\upsilon_{CO2} - \upsilon_{CO2,eq}\right) \tag{3.97}$$

In above equation 'X_{max}' is the maximum conversion of CaO and **'$\upsilon_{CO2,eq}$'** is the volume fraction of CO_2 in equilibrium and it is given as [178];

$$\upsilon_{CO2,eq} = (4.137 \times 10^{7})\exp\left(\frac{-20474}{T}\right) \tag{3.98}$$

3.4 Summary of nominated kinetics

The kinetic rate equations reported in above sections are used in modelling the SE-CLSR process. The mechanism proposed by **Dueso et al.** [140] is used for Ni oxidation (R_1); the reaction mechanism of **Keskitalo et al.** [141] is selected for partial and complete oxidation of the carbon (R_2 and R_3); the reaction mechanism of **Subramaniam et al.** [142] is used for the oxidation of CO to CO_2 (R_4); the kinetic mechanism of **Iliuta et al.** [43] is used for the partial oxidation of CH_4 (R_5 and R_8), H_2 oxidation (R_6) and CO oxidation (R_7); the reaction model proposed by **Xu et al.** [131] for SMR and WGS process (R_9-R_{11}) is used; the model proposed by **Becerra et al.** [181] is selected for the dry reforming (R_{12}); for the kinetic mechanism of methane decomposition (R_{13}), the model proposed by **Snoeck et al.** [176] is used; **Snoeck et al.** [177] is used for the kinetics of carbon gasification by steam and CO_2 (R_{14} and R_{15}); and for the kinetics of carbonation process (R_{16}) the mechanism proposed by **Rodriguez et al.** [180] is used. All the rate equations are presented in **Table 3.4**.

3.5 Boundary conditions

In many papers, the boundary conditions are assumed without having a detailed discussion. **Danckwerts et al**. (1953) and **Wehner et al.** (1956) were the pioneers who discussed the boundary conditions across the packed bed reactors. In their work, they divided the packed bed reactor in three zones. **1)** Entry section; **2)** the middle section where reactions take place; and 3) the exit section of the reactor [139].

Danckwerts et al. proposed the boundary conditions by neglecting the effect of dispersion in 1st and 3rd section of the reactor i.e. at the entrance and the exit. The boundary conditions proposed by Danckwerts are as;

$$uC - D_L \frac{\partial C}{\partial z} = uC_i \qquad z = 0 \qquad (3.99)$$

$$\frac{\partial C}{\partial z} = 0 \qquad z = L \qquad (3.100)$$

Cauwenberghe (1966) used the concept of Danckwerts and presented the boundary conditions for unsteady state process in the packed bed reactor. Later on, **Amundson** (1956) proposed the boundary conditions for heat transfer under the conditions of non-isothermal packed bed reactor. These conditions were used by many authors for modelling of their processes. Amundson derived these conditions on mass transfer analogy basis without any proof.

$$u\rho_g c_g T - K_L \frac{\partial T}{\partial z} = uT_i \qquad z = 0 \qquad (3.101)$$

$$\frac{\partial T}{\partial z} = 0 \qquad z = L \qquad (3.102)$$

In this work, only 1-D variation of variables is considered. So boundary conditions along the radial direction are not discussed.

In the next chapters, the boundary and initial conditions for different processes are presented depending upon the conditions of the system.

3.6 Mathematical modelling methodology

As discussed in previous chapter, SE-CLSR process consists of FR and AR cycles. To develop the mathematical model of SE-CLSR process, first individual models (SMR, SE-

SMR, reduction of Ni catalyst and oxidation of reduced catalyst) are developed. The FR comprises of combine mathematical model of SMR, SE-SMR and reduction of Ni catalyst processes.

The methodology and mechanism used to develop the individual models is already presented in above sections of this chapter. The hierarchy of mathematical modelling is shown in **Figure 3.11**. Firstly, the 1-D SMR model is developed. The modelling results are validated against the experimental data. The details of experimental work performed in laboratory and the SMR model is discussed in **Chapter 4**. The mechanism used for the reaction kinetics and governing equations is presented under 3.3.2 section. The mathematical model developed in this chapter is validated against the experimental work performed in the laboratory and against the equilibrium calculations performed by using chemical equilibrium application (CEA) software. By coupling the mathematical model of SMR with the modelling equations of CO_2 sorbent, the mathematical model of SE-SMR is developed. The SE-SMR is developed on the basis of adiabatic and non-adiabatic conditions. The developed model of SE-SMR is validated against the experimental results reported in the literature. More detail of this model is discussed in **Chapter 5**.

The mathematical modelling of NiO reduction is developed under the assumption of plug flow behaviour. The developed model includes R_5-R_{15} rate equations and it is validated against the literature data. In the FR model, SE-SMR and reduction models are combine and solved simultaneously. On the other hand, AR model is developed by considering oxidation rate equations (R_1-R_4) and it is also validated against the literature data. At the end, both FR and AR models are combine to run the mathematical model of SE-CLSR process in a cyclic way. The details of this model are discussed in **Chapter 6**.

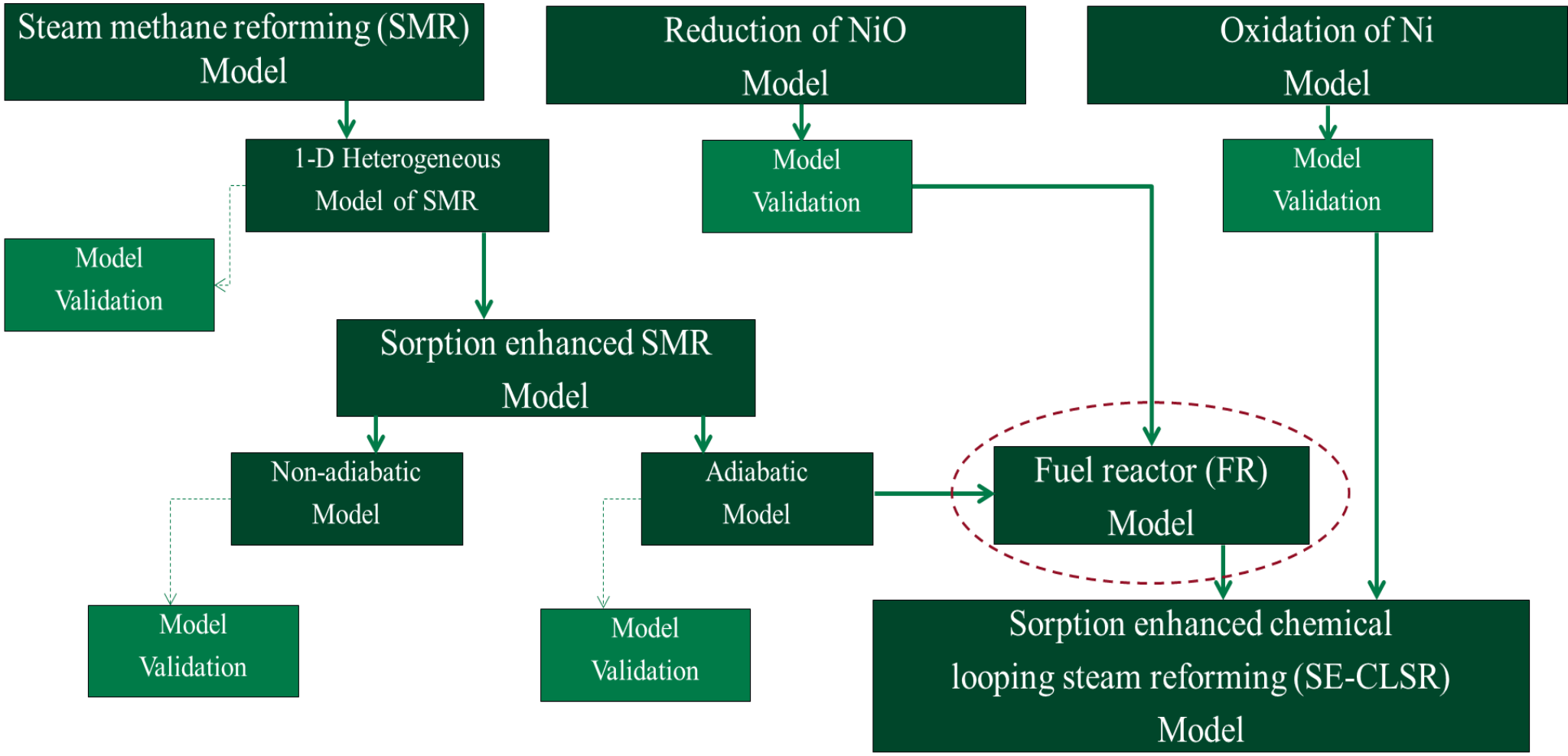

Figure 3.11: Hierarchy of modelling methodology adopted for SE-CLSR process

3.7 Conclusion

The mathematical modelling of SE-CLSR process comprises a combination of individual models. These models are SMR model, SE-SMR model, reduction of OTM model and oxidation of reduced catalyst model. The mathematical modelling of a packed bed reactor on gPROMS model builder requires the information of mass, energy and momentum balance equations across the boundary of the packed bed reactor. The generalized mass and energy balance equations for both gas and solid phase are presented in this chapter and later on modified for different types of reactor systems. The most vital part in the modelling of reactor system is the reaction kinetics for various chemical reactions involved in the reactor. A detail kinetic literature survey for various reaction systems is discussed with their rate equations and the rate constants data. This data will be used in next chapters for modelling the SMR, SE-SMR and eventually the SE-CLSR process.

CHAPTER # 4
STEAM METHANE REFORMING

This chapter focuses on the catalytic steam methane reforming (SMR) process. A brief introduction of SMR process followed by the catalysts used for the SMR process is provided. The conventional SMR process is the most widely used process for the production of hydrogen (H_2) on industrial scale.

A detail description of the experimental rig available in University of LEEDS and preliminary SMR experimentation performed in the laboratory are discussed. The mathematical modelling of a packed bed catalytic reactor developed on gPROMS model builder® is also presented in this chapter. The mathematical model of SMR process is validated by comparing the results with the experimental values. The chemical equilibrium with applications (CEA) software was used to generate the equilibrium results.

4.1 Steam methane reforming: Introduction

All hydrocarbon fuels can be used as raw materials for the production of H_2 [37]. Steam reforming of hydrocarbons, gasification of coal, enzymatic decomposition of sugar, conversion of glucose and alcohol are the few important processes of H_2 production [26]. At present, almost 90% of the worldwide H_2 originates from the fossil fuels [13]. Natural gas, naphtha and coal are the most common feedstocks for the production of H_2, but currently natural gas is the major source of H_2 production [103, 182]. Natural gas is found to be the most suitable source for H_2 production because of its low molecular weight and high H/C ratio [183].

There are various options available for the production of H_2 by using natural gas as feedstock. Steam reforming, partial oxidation and auto-thermal reforming are the primary methods used for the production of H_2 by using hydrocarbons source [184]. During the last world war, **Fischer et al.** [185] developed a process of production of important industrial chemicals by using synthesis gas. And the most attractive process for the

production of synthesis gas appeared to be partial oxidation (POx). POx of methane (CH_4) produces H_2 and carbon monoxide (CO) instead of carbon dioxide (CO_2) and water. POx reaction is exothermic reaction in nature and is given as**;**

$$CH_{4(g)} + \frac{1}{2}O_{2(g)} \leftrightarrow CO_{(g)} + 2H_{2(g)} \qquad \Delta H_{298K} = -35.7 \text{ kj mol}^{-1} \qquad (4.1)$$

Carbon to oxygen ratio (C/O) is very important in this case. Higher C/O gives more CO instead of CO_2 and this is the major disadvantage of POx process [186]. Complete oxidation of CH_4 is highly exothermic reaction and is given as [63];

$$CH_{4(g)} + 2O_{2(g)} \leftrightarrow CO_{2(g)} + 2H_2O_{(g)} \qquad \Delta H_{298K} = -890.3 \text{ kj mol}^{-1} \qquad (4.2)$$

Amongst all the available processes steam methane reforming (SMR) is the most established and commonly used process to produce syngas on a large scale [182]. Over 50% of the world's H_2 production comes from the SMR process [26]. While on the other hand, POx process is considered to be the lowest fuel processing efficiency process [183]. But POx process has the advantage of giving suitable H_2/CO ratio for production of liquid fuel by Fischer Tropsch process. The SMR process intakes CH_4 and steam as feed, in a required ratio, and converts feed into mixtures of mixtures of H_2, CO and CO_2.

Davy [187] was the first researcher who observed a catalytic interaction between hydrocarbons and the metals in 1817. He also observed the effect of sulphur and carbon on the performance of the metal which may lead to prodigious difficulties during the reforming process.

In **1868, Tessie et al.** [188] introduced the concept of steam reforming. Later in **1889, Mond et al.** [52] claimed nickel (Ni) as a promising catalyst for steam reforming process. Meanwhile, **Lang et al.** [52] studied the homogeneous SMR reaction. Initially, experiments were performed by keeping steam to carbon ratio (S/C) unity. They observed that conversion of CH_4 was very low even at very elevated temperature (947-1047 °C). Moreover, the reaction was accompanied by the formation of coke.

Neumann et al. [189] were the first in the history who studied the detail analysis of catalytic SMR process and published their work in 1924. This breakthrough unlocked new horizon and inspired many researchers to explore this field. As a result, plentiful patents published around 1930. In the same era, the first industrial steam reformer was commissioned by "Standard Oil of New Jersey" in 1930. United States was rich in natural gas resources and they adopted this process in their reforming industry for H_2 production.

At the start, SMR process was studied at atmospheric pressure. In 1962, reformers operating at 15 atm using higher hydrocarbons as feed were installed by ICI [52, 190].

The conventional SMR process is a multistep process: in first step endothermic SMR reaction (**Eq. 4.3**) takes place in the reformer at high temperature (800-1000 °C) and medium pressure (20-35 atm). The reforming reaction (**Eq. 4.3**) is highly endothermic and it requires a large amount of heat to proceed. This heat is provided by feeding supplemental natural gas to the furnace/reformer. Heating burners can be arranged in different position within the reformer to facilitate the better heat flow. Feed (CH_4 and steam) is fed to large number of tubes (40-400 tubes); these tubes are the integral part of the reformer and high number of tubes favours better and efficient heat transfer to the catalyst. The reformer tubes are normally up to 12 m long filled with Ni/Al_2O_3 catalyst [52].

In reformer higher pressure harms the conversion of CH_4 to H_2. The effluent gas from the reformer contains H_2, unconverted CH_4, CO, CO_2 and unconverted steam. These effluent gases are then fed to a water gas shift (WGS) reactor.

In the second step the exothermic WGS reaction (**Eq. 4.4**) at lower temperature (200-400 °C) and pressure (10-15 atm) takes place [52, 130, 191, 192]. This reaction regulates the amount of CO and CO_2 produced during the process. A Schematic diagram of conventional SMR process is shown in **Figure 4.1**. Beside these two reactions there is another reaction known as global SMR reaction (**Eq. 4.5**). This reaction is necessary because CO_2 can be produced directly from CH_4. Although, there are many other reactions that can take place during reforming process but the most important three reactions i.e. SMR, WGS and global SMR reactions are given below;

$$CH_{4(g)} + H_2O_{(g)} \leftrightarrow CO_{(g)} + 3H_{2(g)} \qquad \Delta H_{298K} = +206 \text{ kj mol}^{-1} \qquad (4.3)$$

$$CO_{(g)} + H_2O_{(g)} \leftrightarrow CO_{2(g)} + H_{2(g)} \qquad \Delta H_{298K} = -41 \text{ kj mol}^{-1} \qquad (4.4)$$

$$CH_{4(g)} + 2H_2O_{(g)} \leftrightarrow CO_{2(g)} + 4H_{2(g)} \qquad \Delta H_{298K} = +165 \text{ kj mol}^{-1} \qquad (4.5)$$

This two-step process of SMR enhances the hydrogen production by shifting the SMR reaction (Eq. 4.3) in the forward direction at a high temperature followed by WGS reaction (Eq. 4.4) at a lower temperature. The overall SMR process is endothermic in nature and requires additional heat to proceed. Conventional steam methane reformer consists of a furnace that contains tubes in it, with catalyst loaded in these tubes, to speed up the rate of the reaction [22].

The high temperature shift (HTS) reactor, as shown in **Figure 4.1**, is loaded with iron catalyst and operated at high temperature in the range of 377-527 °C. The unconverted CO is then introduced in the low temperature shift (LTS) reactor for further conversion of CO into CO_2. The LTS reactor is operated at relatively low temperature (200-300 °C) and loaded with copper based catalyst. The shift reactor is separated into two reactors to maintain the temperature inside the catalyst bed. The effluent gases from the process undergo absorption process and CO_2 is removed from the gases in the absorption column using amines or other absorbents as CO_2 acceptor [52].

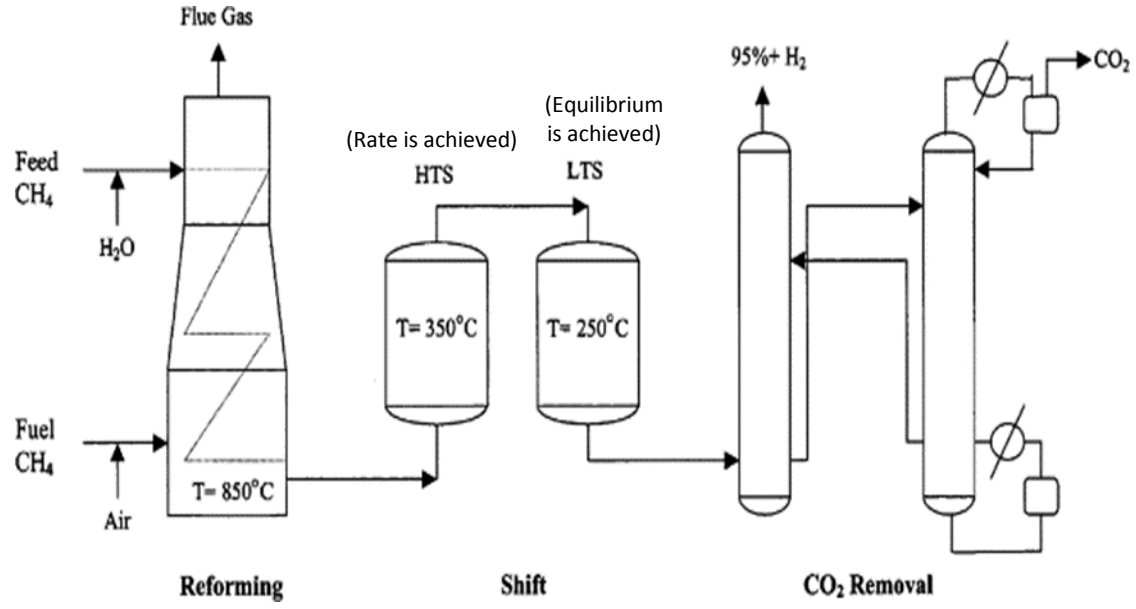

Figure 4.1: Schematic diagram conventional SMR process [102]

Extremely high temperature (800-1000 °C) in the conventional SMR process causes aging of the reformer tubes. The main reason for damaging of the reformer tubes are; creep (inner side of the tube), carburization, thermal shocks and accidental overheating. A tube start to crack at 2/3rd portion from the outside of tube and propagates towards the inner portion. Once that portion is damaged, cracks start to penetrate towards outer portion [28]. In the industry, the reformer tubes are normally designed to withstand for a period of about 100,000 h (11.4 years). High temperature within the reformer tubes causes deterioration of catalyst and this damaging of catalyst in the tubes causes choking and increase the gas residence time within the tubes. The choking causes overheating of the tubes and it leads to creep cavitation damage. Owing to the severe operating conditions, reformer tubes are generally fabricated from centrifugally cast creep-resistant high carbon austenitic steel of ASTM A297 Grade HK (25 Cr, 20 Ni and 0.4 C) or Grade HP (26 Cr,

35 Ni, 0.4 C). In some cases other high temperature, heat resistant alloys may be used, in general with a composition derived from the HP grade. Such materials have very high cost. Due to this problem of overheating, some tubes only withstand for 2years service life and have to be replaced soon after that [29].

At the same time all of the heat supplied to the reformer is not entirely utilized, hence the process becomes less efficient. The vital reason of reformer tubes failure is overheating as catalyst tubes are designed for a specific temperature range. If the operating temperature increases over the design temperature, a drastic decline in the life period of tubes is observed. **Figure 1.6** shows the effect of temperature on the expected life of reformer tubes.

To avoid such problems in addition to safety and environmental effect, companies have to invest significance amounts in maintenance to prevent any incident due to reformer failure. The cumulative costs to prevent the incidents are as much as $10 billion [31].

4.2 Steam reforming catalyst

Steam reforming process is greatly promoted by the use of catalyst. Selection of the catalyst for this process is dependent on the type of fuel used, as it is reported in **Table 4.1**.

Table 4.1: Catalyst and supports used for different feed in steam reforming process [33, 131, 164, 193-199]

Feed	Metal	Support
Methane	Ni, Rh, Mo, Pt,Ce, Zr, Co, Nb	Al_2O_3, ZrO_2, Ce-ZrO_2,Ce ZrO_2/Al_2O_3, SiO_2
Methanol	Cu, Pd, Cu/Zn/Al, CuO-ZnO, Cu-Cr_2O_3	ZnO/Al_2O_3, Al_2O_3, ZrO_2
Ethanol	Ni, Rh, Rh-Ce, Co, CuO, Cu-NiK	MgO, Al_2O_3, SiO_2, ZnO/Al_2O_3

There are many criteria that need to be considered while selecting the catalyst for reforming process. Steam reforming process is a high temperature process and requires

lot of heat to proceed. Therefore, catalyst needs to withstand a high temperature conditions without losing its thermodynamic characteristics in terms of fuel and steam conversion. The catalyst should have a long lifetime and good resistance to attrition. An environmental friendly and less costly catalyst is always attractive as compared to costly catalysts.

One of the decisive parameter, other than reactivity, is economic cost of the catalyst metal. The cost includes the cost of metal and manufacturing cost of the catalyst. Cobalt (Co) and Ni are the most expensive metals used for catalyst, followed by copper (Cu). **Figure 4.2** shows the comparison of different metals used as catalyst for reforming process.

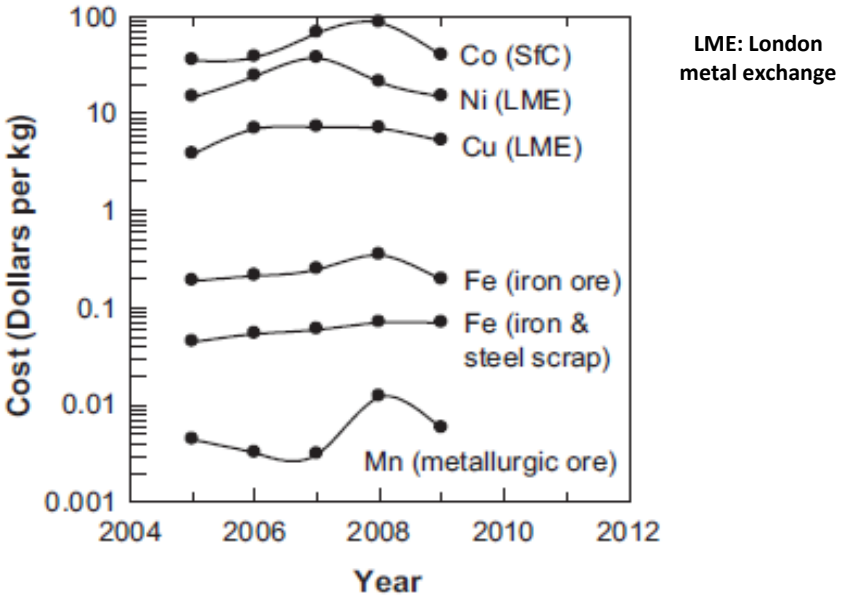

Figure 4.2: Average annual cost of materials used for catalysts [200]

Ni is expensive as compared to few other available options, such as Mn, Fe and Cu, but this is compensated by using a lower percentage of Ni in the catalyst. Ni based catalyst can withstand very high temperature (900-1100 °C) and exhibits good mechanical strength. The use of alumina based supporting material has been investigated extensively in literature. It has been found that α-Al_2O_3 shown good reactivity and no agglomeration [87].

The attrition characteristics of the catalyst are very important as it determines the reactivity of the catalyst without losing of fine particles. The cost of makeup solid, to replace the loss fines, is highly dependent on lifetime of the catalyst. A catalyst having high attrition resistance is considered to have high lifetime, hence can sustain severe

conditions for longer period of time. Lifetime of some of the catalysts is tabulated in **Table 4.2.** Different catalysts have different advantages over one another; Ni is widely used as catalyst for SMR process on industrial scale due to its high reactivity with all fuel gases, no agglomeration problem, low attrition rates and avoidance of carbon deposition [52, 130].

Table 4.2: Lifetime of catalysts used for reforming process

Catalyst	Lifetime [hr]	Reference
NiO/Al_2O_3	40,000	[201]
$NiO/NiAl_2O_4$+ $MgAl_2O_4$	33,000	[202, 203]
$NiO/NiAl_2O_4$	4500	[204]
NiO/α-Al_2O_3	100,000	[205]
CuO/γ-Al_2O_3	2400	[78]
Iron ore	1600	[206]

4.3 Experimentation

4.3.1 Equipment and materials

The schematic diagram of the set-up used for the experimentation is shown in **Figure 4.3**. This unit is divided into three sections relevant to feed, reformer reactor and analysis respectively. The feed section consists of gas cylinders for CH_4, N_2, H_2 and CO. MKS mass flow controllers were used to control the flow of gases going into the reactor. The N_2 mass flow controller had the capacity of 10,000 cm^3/min (STP), CH_4 mass flow controller had 50 cm^3/min (STP) and H_2 mass flow controller had capacity of 500 cm^3/min (STP). Programmable syringe pump (New Era Pump Systems) was used to introduce a controlled amount of distilled water in the reactor to achieve a given molar steam to carbon ratio (S/C) in the reformer. The tubular reactor was made of quartz with an inner diameter of 1.2 cm and the length of 49.5 cm, held inside an electrically heated tube furnace (Elite Thermal Systems Ltd. TSV/12/50/300). The water entered into the top portion of the reformer where it evaporated and mixed with the controlled amount of gases. A known amount of catalyst (5.0 g) was placed in the middle part of the reactor. The catalyst used here is 18 wt. % NiO supported on α-Al_2O_3 provided by Johnson

Matthey Plc. It was in the pellet form and was originally crushed to an average particle sizes of 1.2 mm, 1.85 mm, and 200 μm to determine the size resulting in the absence of pore diffusion limitation, with 200 μm used later in the kinetic study. The volume of the catalyst bed and bed length calculated was 2.67 x 10^{-6} m^3 and 0.030 m respectively. The particle density and thermal conductivity of solid is 1870 kg m^{-3} and 13.8 W m^{-1} K^{-1} respectively. The temperature inside the furnace was regulated by a Eurotherm 2416 temperature controller. The temperature of catalyst in the reactor, which may be slightly different from that of furnace (5-10 °C less), was monitored by a K-type thermocouple inserted at the centre of the catalyst bed. After the reaction, the product gases entered into the spiral tube condenser. The temperature of the condenser was set to -6 °C and ethylene glycol was used as the cooling agent in the chiller (Fisher Scientific 3016S). Water condensate was collected in the condensate collector. The analysers are very sensitive to water vapours; a silica gel trap was used to capture any water vapours leaving with product gases before entering into the analysers. The composition of outlet gases was analysed by Advanced Optima gas analyser from ABB and results were recorded online after every 5 seconds. The ABB analyser consisted of three analyser modules; Uras 14, Caldos 15 and Magnos 106. The Uras 14 was capable of detecting CH_4, CO_2 and CO based on infrared adsorption principle. The Caldos was used for H_2 measurement based on thermal conductivity. When required, the concentration of O_2 was measured by Magnos 106 analyser module. The uncertainties associated with the measurements were within ± 3% on gas volume based.

The typical experimental run involved the following steps: **1)** Half an hour heating and purging of the reactor with N_2 gas. Temperature of the catalyst bed was raised to reaction temperature by using electrical furnace and simultaneously flushing the system with continuous flow of N_2 gas. **2)** After complete flushing of the system and ensuring that there was just N_2 present in the gas lines, N_2 flow was switched to the mixture of H_2 gas in N_2 (5 vol. % H_2 in N_2) for the reduction of the NiO catalyst, as the active phase of the catalyst is reduced Ni, whereas NiO is not catalytically active for steam reforming or WSG reactions. Reduction of the catalyst continued until the H_2 concentration returned to 5 vol. %, i.e. the initial concentration. **3)** Reduction was followed by flushing for an hour with N_2 gas to remove all the H_2 gas from the gas lines. **4)** The catalyst was then ready for SMR process. Before switching on the flow of fuel gas, water flow was started. Just after the introduction of water on the surface of the catalyst, the flow of the fuel gas

was switched on. This reaction process was allowed to run for a longer period of time (~4 hr). Flow of the fuel gas and water was then turned off after obtaining steady state values of the concentration of all the exit gases. **5)** The system was again set on flushing and cooling.

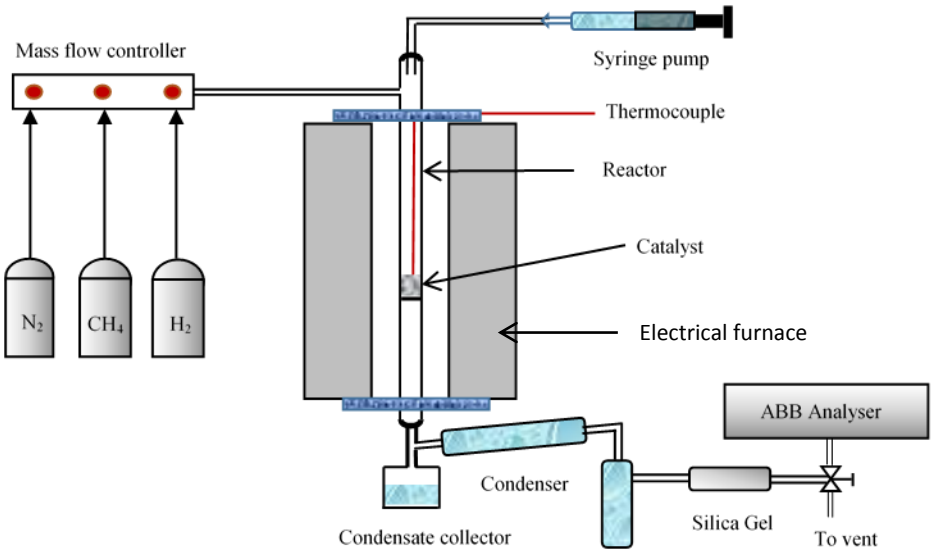

Figure 4.3: Experimental set-up for steam reforming process

4.4 Modelling methodology

Mathematical Modelling plays an important role in the development of a chemical process. It helps in understanding the experimentally observed processes by testing their models on well-established software. A one-dimensional (1-D) heterogeneous mathematical model with axial dispersion of the SMR process accounting for mass transfer in the gas phase, mass transfer in the solid phase, energy balance across the reactor system and reaction kinetics was constructed. In this model it was assumed that,

a) Operation is adiabatic in nature
b) Ideal gas law is applicable
c) Concentration and temperature gradients along the radial direction are negligible. So, only 1-D variation in concentration and temperature i.e. in the axial direction is considered.
d) Heterogeneous phase is considered and no temperature gradient existed in the catalyst particles
e) Porosity of the bed is constant

To reduce the complexity in the modelling of the reaction kinetics, only those reactions which play a significant role in the overall process were considered. The chemical reactions used in the reactor modelling are R1, R2 and R3 and their rate equations (A1-3) are given in **Appendix A**. These rate expressions are based on Langmuir-Hinshelwood methodology as described and employed by **Xu et al.** [131]. Mathematical model is composed of mass and energy balance equations both in the gas and solid phase. The mass, energy and momentum balance equations are given by:

Mass and Energy balance in the gas phase;

$$\varepsilon_b\left(\frac{\partial C_i}{\partial t}\right)+\frac{\partial(uC_i)}{\partial z}+k_{g,i}a_v\left(C_i-C_{i,s}\right)=\varepsilon_b D_z\frac{\partial^2 C_i}{\partial z^2} \tag{4.6}$$

$$\varepsilon_b\rho_g C_{pg}\left(\frac{\partial T}{\partial t}\right)+u\rho_g C_{pg}\frac{\partial(T)}{\partial z}=h_f a_v(T_s-T)+\lambda_z^f\frac{\partial^2 T}{\partial z^2} \tag{4.7}$$

Mass and Energy balance in the solid phase;

$$k_{g,i}a_v\left(C_i-C_{i,s}\right)=(1-\varepsilon_b)\rho_{cat}\,r_i \tag{4.8}$$

$$\rho_{bed}C_{p,bed}\left(\frac{\partial T_s}{\partial t}\right)+h_f a_v(T_s-T)=\ (1-\varepsilon_b)\rho_{cat}\sum -\Delta H_{rxn,j}\,\eta_j R_j \tag{4.9}$$

Pressure drop across the bed of reactor;

$$\frac{\Delta P g_c}{L}=\frac{150}{d_p^2}\left[\frac{(1-\varepsilon)^2}{\varepsilon^3}\right]\mu u+\left(\frac{1.75}{d_p}\right)\left(\frac{1-\varepsilon}{\varepsilon^3}\right)\rho_g u^2 \tag{4.10}$$

Boundary conditions;

At the reactor inlet (z = 0):

$C_i = C_{i,0}$; $T = T_o$; $T_s = T_{s,o}$; $P = P_o$

At the reactor outlet (z = L):

$\frac{\partial C_i}{\partial z} = 0$; $\frac{\partial T}{\partial z} = 0$; $\frac{\partial T_s}{\partial z} = 0$

Initial conditions;

$C_i = C_{i,0}$; $T = T_o$; $T_s = T_{s,o}$

The rates of the SMR reactions are highly dependent upon the temperature of the system and concentration of the gases. The equilibrium constants and the kinetic rate constants in the rate equations [131] are given in **Appendix A**. The values for the pre-exponential factor and activation energy were obtained from the experiments performed in the laboratory (described in section 4.5). The rate of formation or consumption of each component was obtained by combining reaction rate equations. The reaction rates for the species are given in A**ppendix A.**

In mathematical modelling many physical properties are used like thermal conductivity, dispersion coefficient, mass transfer coefficient etc. The empirical correlations used to determine these properties are listed below.

Axial mass dispersion coefficient is given as [207] ,

$$D_z = 0.73D_m + \frac{0.5ud_p}{1 + 9.49D_m/ud_p} \tag{4.11}$$

Effective thermal conductivity is given by the following relations [208],

$$\frac{\lambda_z^f}{\lambda_g} = \frac{\lambda_z^o}{\lambda_g} + 0.75PrRe_p \tag{4.12}$$

$$\frac{\lambda_z^o}{\lambda_g} = \varepsilon_b + \frac{1 - \varepsilon_b}{0.139\varepsilon_b - 0.0339 + \left(\frac{2}{3}\right)\lambda_g/\lambda_s} \tag{4.13}$$

Mass transfer coefficient is given as [209],

$$k_{g,i} = j_{D,i}ReSc_i^{1/3}\frac{D_i}{d_p} \tag{4.14}$$

$$\varepsilon_b j_{D,i} = 0.765Re^{-0.82} + 0.365Sc_i^{-0.398} \tag{4.15}$$

Dimensionless numbers are given as,

$$Re = \frac{\rho_g u d_p}{\mu} \quad ; \quad 0.01 < Re < 1500 \tag{4.16}$$

$$Sc_i = \frac{\mu}{\rho_g D_i} \quad ; \quad 0.6 < Sc < 7000 \ , \ 0.25 < \varepsilon_b < 0.96 \tag{4.17}$$

Similarly, to determine the heat transfer coefficient and its dimensional numbers, following relations were used in the model formulation [127, 209],

$$h_f = j_H \frac{C_{pg}G_s}{Pr^{2/3}} \tag{4.18}$$

Here,

$$j_H = 0.91Re^{-0.51}\psi \quad ; \quad 0.01 < Re < 50 \tag{4.19}$$

$$j_H = 0.61Re^{-0.41}\psi \quad ; \quad 50 < Re < 1000 \tag{4.20}$$

$$Pr = \frac{C_{pg}\mu_g}{\lambda_g} \tag{4.21}$$

In the reactor model linear and non-linear partial differential equations (PDEs), algebraic equations, and initial and boundary conditions are involved, and gPROMS model builder 4.1.0® was used to solve these equations. The sensitivity of the model was first checked for discretization ranging from 10-1000 intervals and model was found independent of discretization. Finally, the laboratory reactor was axially discretized by 100 uniform intervals for this paper and output results were reported after every one second. The first order backward finite difference method (BFDM) of was used to solve the PDEs and

algebraic equations using initial and boundary conditions as mentioned above. The model of the adiabatic packed bed reactor was assumed to follow the non-ideal plug flow behaviour. In gPROMS model builder 4.1.0 ® differential algebraic solver (DASOLV) was used to solve the ordinary differential equation (ODEs). DASOLV converts the PDEs into ODEs, and 4th order Runge-Kutta technique was used to solve the system.

In order to compare the modelling results with an independent model, the chemical equilibrium and applications (CEA) software was used to generate the equilibrium data [210, 211]. This software is based on minimization of Gibbs free energy (G) [212]; equation A15 in **Appendix A.** The thermodynamic analysis was done by considering the gas species involved in the reactant and product streams are CH_4, H_2, CO, CO_2, H_2O and N_2. The calculations were performed on the basis of N_2 balance. To study the effect of temperature, 1 bar and S/C of 3.0 was fixed. The thermodynamic calculations were allowed to run and outlet mole fraction data of product gases was collected for the calculations. Similarly to study the pressure effect, temperature and S/C conditions were fixed.

4.4.1 Preliminary Experiments

Prior to the design of experiments for the derivation of kinetic rate parameters, preliminary experiments were performed to find out the size of the catalyst required to virtually eliminate the diffusion control limitations, a condition necessary to obtain true reaction kinetics. In general, the size of the particle is reduced to such a size where there are no diffusion effects. To this aim, the Weisz-Prater (WP) criterion was used to determine the required size of the particle [213, 214], expressed as;

$$C_{WP} = \eta \emptyset_1^2 \tag{4.22}$$

With;

$$C_{WP} = \frac{-r'_A(obs)\rho_{cat}R_p^2}{D_e C_{A_s}} \tag{4.23}$$

If C_{WP} << 1, then there are no internal diffusion limitations and ultimately no concentration gradient exists within the catalyst particle. In order to find out how small the size of particle should be to avoid internal diffusion limitations, the Thiele Modulus ($\emptyset$) and the effectiveness factor (η) need to be calculated. The effectiveness factor is the measure of how far the reactant diffuses into the pellet before reacting. The Thiele modulus and the effectiveness factors are related to each other as follow:

$$\eta = \frac{3}{{\emptyset_1}^2}\ (\emptyset_1 \coth \emptyset_1 - 1) \tag{4.24}$$

$$\eta {\emptyset_1}^2 = 3\,(\emptyset_1 \coth \emptyset_1 - 1) \tag{4.25}$$

The reaction rate will be diffusion limited if the Thiele Modulus ($\emptyset$) is very large, i.e. if $\eta \ll 1$.

A first set of the experiments was performed by considering the size of particle (d_p) = 1.2 mm, to find out the size of the catalyst for which $\eta \cong 1$. Data for CH_4 conversion (X_{CH4}) was obtained and plotted against pseudo-contact time defined by $W/F_{CH4,o}$, to determine the rate of the reaction for this set of experiments. Weight (W) of the catalyst was kept constant in all of the experiments i.e. 5.0 g.

As expected, it was observed that as the flow rate of feed increased, keeping all the other parameters constant, conversion of CH_4 decreased due to the diminishing residence time. While keeping every parameter and operating conditions constant, except the size of the catalyst (d_p = 1.85 mm), for the second set of experiments, data for CH_4 conversion at different $W/F_{CH4,0}$ was obtained. As the size of the particle reduced, it increased the contact area and hence the conversion of CH_4 increased. **Figure 4.4** shows the effect of particle size and pseudo-contact time on CH_4 conversion, and results were compared with equilibrium values as well.

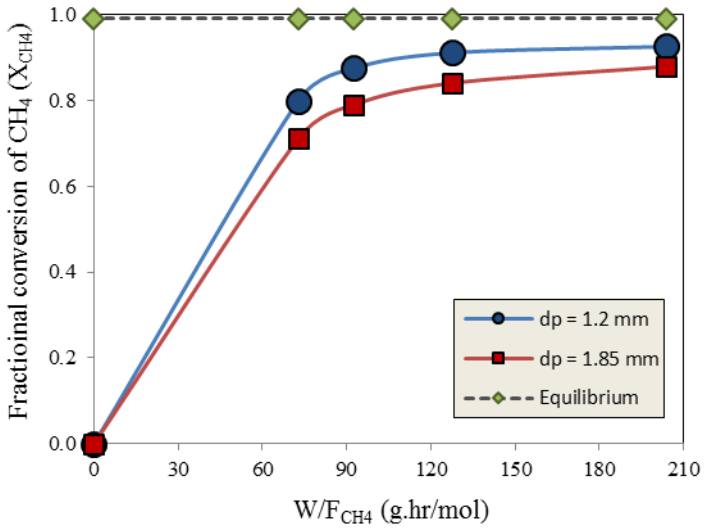

Figure 4.4: Effect of particle size and pseudo contact time on the conversion of CH_4 at constant molar S/C (3.12) and constant operating temperature (700 °C)

The slope of both CH_4 conversion curves gives the rate of reaction of CH_4 (r_{CH4} in mol hr^{-1} $kgcat^{-1}$). Values for the Thiele modulus and the effectiveness factor for both sets of experiments were used to determine the size of the catalyst required for the kinetic study.

As the size of the catalyst reduced, the effectiveness factor approached unity. Calculated values for the Thiele modulus and effectiveness factor are shown in **Table 4.3.**

Table 4.3: Calculated values for Thiele modulus and effectiveness factor

Diameter of catalyst [mm]	**Effectiveness factor**	**Thiele modulus**
1.85	0.37	6.90
1.2	0.52	4.48
0.2	**0.92**	**1.15**

Table 4.3 shows that a particle size of 0.2 mm (200 μm) is required to virtually eliminate diffusion control (i.e. η = 0.92 and Cwp = 1.22).

4.5 Results and discussion

4.5.1 Derivation of the kinetics of three SMR reactions

To ensure that the experiments were carried out in the region of intrinsic kinetics, the size of the catalyst particle was obtained in preliminary experiments. The experimental conditions used for the generation of kinetic parameters are listed in **Table 4.4**. More detail about the feed volumetric flow rates is given in **Appendix B.**

Table 4.4: Experimental conditions

Catalyst	18 wt. % $Ni/\alpha\text{-}Al_2O_3$							
Diameter of catalyst, dp [μm]	200							
Mass of catalyst [g]	2.0							
Reaction temperature [°C]	SMR				WGS			
	550	600	650	700	300	325	350	375
Pressure [atm]	1							
Molar steam to carbon ratio	3.12							
Feed mole fraction	CH_4		H_2O		N_2			
	0.075		0.234		0.691			
Feed volumetric flow rate at STP (cm^3/min)	CH_4		H_2O		N_2			
	10-28		0.023-0.064		92-258			

Typical curves of conversion of methane against pseudo contact time are shown in the **Figure 4.5** for a temperatures range between 550 °C and 700 °C. As expected for an

endothermic process, increasing temperature and pseudo contact time has a positive effect on the conversion of methane. Similarly, water gas shift (WGS) reaction is very sensitive to temperature. Experiments were performed in the temperature range of 300-375 °C. **Figure 4.6** shows the variation of CO conversion with pseudo-contact time at different temperature while keeping constant S/C (3) and pressure (1 bar).

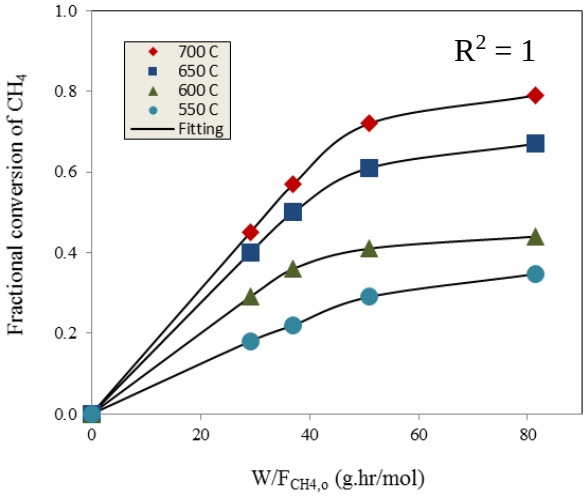

Figure 4.5: Methane conversion (X_{CH4}) vs pseudo-contact time ($W/F_{CH4,o}$) for different temperature (550-700 °C), constant pressure (1bar) and S/C (3.12)

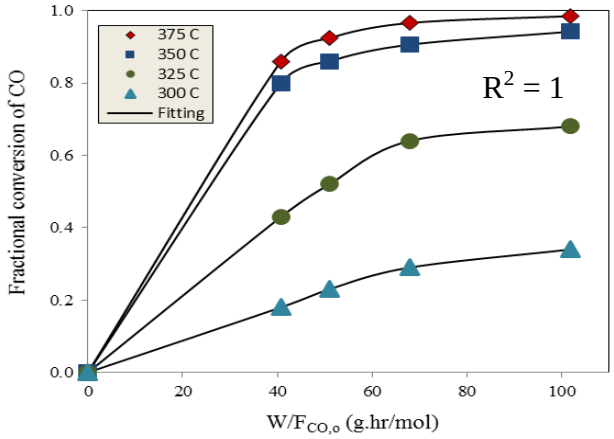

Figure 4.6: Carbon monoxide conversion (X_{CO}) vs pseudo-contact time ($W/F_{CO,o}$) for different temperature (300-375 °C), constant pressure (1bar) and S/C (3.0)

Third order polynomial regressions were used to correlate the conversion of CH_4 and conversion of CO with pseudo contact time. For a fixed temperature, pressure and molar S/C, the relationship between CH_4 and CO conversions with pseudo contact time is given as:

$$X_{CH_4} = a_0 + a_1\left(\frac{W}{F_{CH_4}}\right) + a_2\left(\frac{W}{F_{CH_4}}\right)^2 + a_3\left(\frac{W}{F_{CH_4}}\right)^3 \quad (4.26)$$

$$X_{CO} = b_0 + b_1\left(\frac{W}{F_{CO}}\right) + b_2\left(\frac{W}{F_{CO}}\right)^2 + b_3\left(\frac{W}{F_{CO}}\right)^3 \quad (4.27)$$

CH_4 and CO disappearance rate can be obtained by differentiating equation 4.26 and 4.27 w.r.t. $\left(\frac{W}{F_{CH_4}}\right)$ *and* $\left(\frac{W}{F_{CO}}\right)$. They are given as;

$$r_{CH_4} = \frac{dX_{CH_4}}{d\left(\frac{W}{F_{CH_4}}\right)} = a_1 + 2a_2\left(\frac{W}{F_{CH_4}}\right) + 3a_3\left(\frac{W}{F_{CH_4}}\right)^2 \quad (4.28)$$

$$r_{CO} = \frac{dX_{CO}}{d\left(\frac{W}{F_{CO}}\right)} = b_1 + 2b_2\left(\frac{W}{F_{CO}}\right) + 3b_3\left(\frac{W}{F_{CO}}\right)^2 \quad (4.29)$$

To estimate the kinetics parameters, a non-linear least square analysis based on minimization of the sum of the residual squares of the experimental reaction rates, obtained from equation 4.28 and 4.29, and the predicted reaction rates, obtained from equation A10 and A14, was employed. After successive iterations, the estimated values of the kinetic parameters were obtained. **Figures 4.5** and **Figure 4.6** shows the good fitting of experimental data and regression data.

Temperature dependency of the reaction rate constants is shown in **Figure 4.7**. The slope of the graphs in **Figure 4.7** gave the value of the activation energies, while the y-intercept provided the value of pre-exponential factors of the kinetic rate constant. The values for the activation energies and pre-exponential factors are listed in **Table 4.5**.

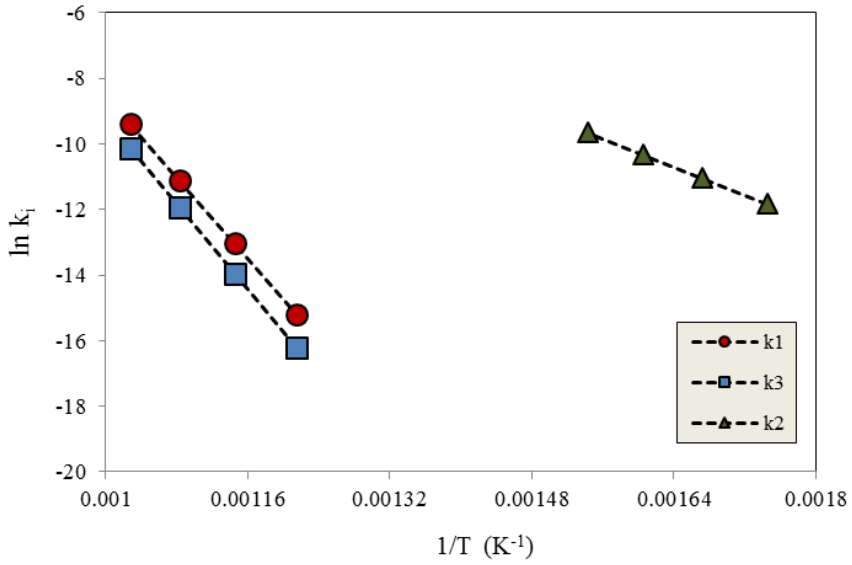

Figure 4.7: Temperature dependency of rate constants for reaction 1 (steam reforming), 2 (water gas shift) and 3 (combined steam reforming and water gas shift)

Table 4.5: Activation energies and pre-exponential factors for steam methane reforming process via reactions 1 (SMR), 2 (WGS) and 3 (SMR/WGS) over 18 wt. % $NiO/\alpha\text{-}Al_2O_3$

Reaction parameters	**This work**	**Xue and Froment [131]**
E_1 [kJ mol^{-1}]	257.01	240.10
E_2 [kJ mol^{-1}]	89.23	67.13
E_3 [kJ mol^{-1}]	236.70	243.90
$k_{o,1}$ [mol $bar^{0.5}$ g^{-1} s^{-1}]	5.19×10^{9}	1.17×10^{12}
$k_{o,2}$ [mol $bar^{-1} g^{-1} s^{-1}$]	9.90×10^{3}	5.43×10^{2}
$k_{o,3}$ [mol $bar^{0.5}$ g^{-1} s^{-1}]	1.32×10^{10}	2.83×10^{11}

4.5.2 Model validation and sensitivity

In the following sections modelling results generated via gPROMS model builder 4.1.0® are presented and model is validated against the experimental results, performed in laboratory, and equilibrium outputs.

4.5.2.1 Dynamic behaviour of the packed bed reactor under conventional SMR

The dynamic transient profiles of molar concentration of CH_4, H_2, and CO_2 along the length of the reactor are shown in Figure 6 (a-c) for inlet temperature of 700 °C at S/C of 3. These results were generated with operating conditions tabulated in **Table 4.6**.

Table 4.6: Operating conditions, parameters and average properties used in the reactor model

Bed voidage [ε_b]	0.4
Bed length [L]	0.03 m
Density of catalyst [ρ_{cat}] [215]	1870 kg/m^3

Particle diameter [d_p]	1.2 x 10^{-3} m
Gas feed temperature [T]	700 °C
Catalyst temperature [T_s]	700 °C
Pressure [P]	1 bar
Bed heat capacity [$C_{p,bed}$] [103]	850 J/(kg K)
Solid thermal conductivity [λ_s] [129]	13.8 W/(m K)
Gas thermal conductivity [λ_g]	0.56 W/(m K)
Molecular diffusivity [D_m]	1.6 x 10^{-5} m^2/s
Steam to carbon ratio [S/C]	3.0

As the overall SMR reaction is endothermic in nature (ΔH_{298} = +165 kJ mol^{-1}), therefore a drop in temperature of the reactor is expected during the conventional SMR process. In **Figure 4.8 (a)**, a dynamic profile of temperature variation along the axial direction of the reactor under the operating conditions of 700 °C and 1 bar is presented. The drop in temperature is about 50 K after a run of 50 s and is the result of an overall endothermic reaction process. The temperature within the reactor reached its steady state conditions after a run of $t \geq 100$ s. As the time period increases, the drop in temperature along the length of the reactor also increases. When the reforming process is allowed to run for 400 s, a drop of 55 °C is observed at the end of the reactor. The variation of temperature with time causes variation of the molar concentration of the product gases. As expected, CH_4 concentration decreased along the axial direction of the reactor at all times during transient behaviour because of SMR reaction (R1) (**Fig. 4.8b**). The feed temperature (700 °C) is suitable for the reforming process. Hence, less amount of CH_4 is obtained at the outlet of the reactor as higher conversion of CH_4 is achieved at such a high temperature conditions. The concentration of CH_4 along the axial direction of the reactor increases with time. This can be explained by the variation of temperature along the axial direction of the reactor. The molar concentration of H_2 increases along the axial direction of the reactor (**Fig. 4.8c**). Similarly the amount of CO_2 is increasing along the axial direction of

the reactor with the decrease in the amount of CH_4 (**Fig. 4.8d**). It can be seen that the response of molar concentration of these product gases is time dependent.

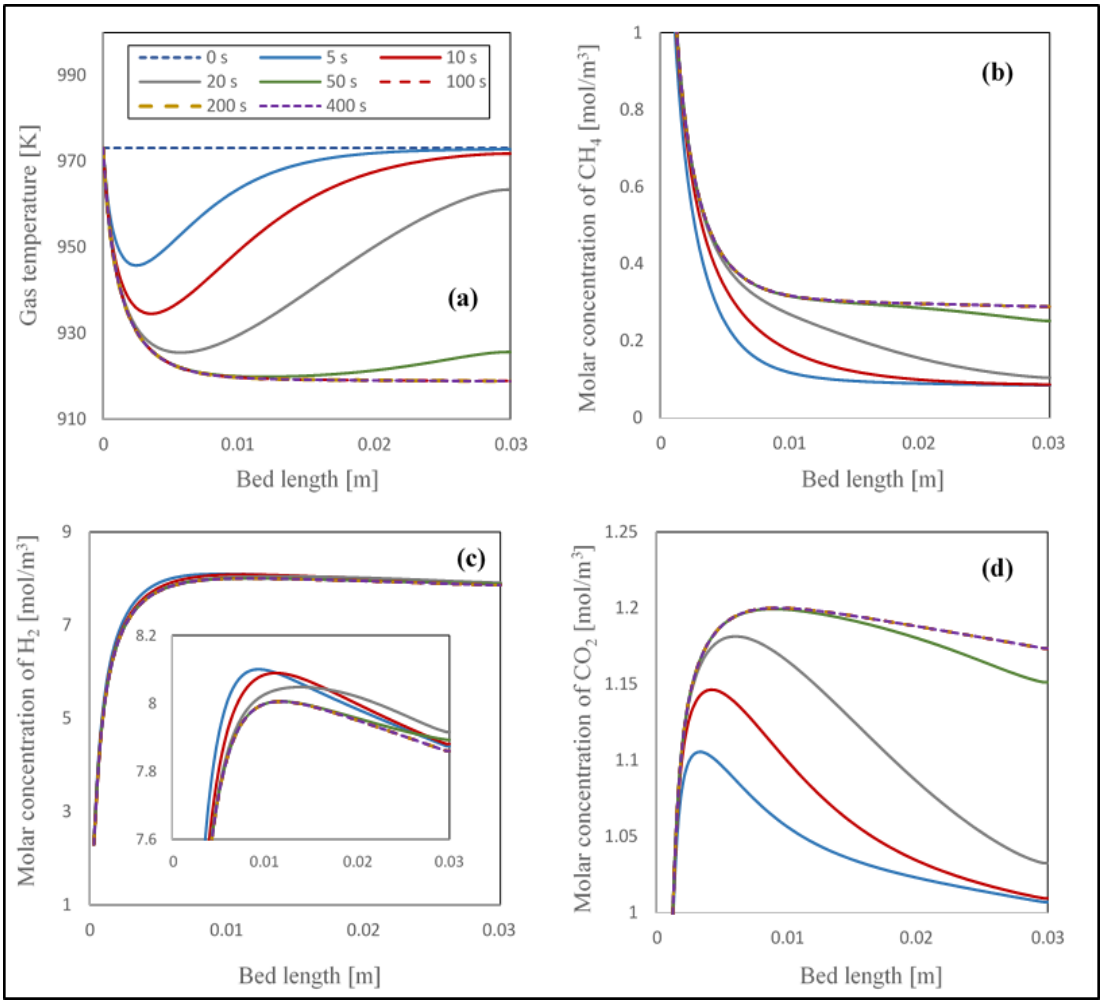

Figure 4.8: Dynamic profile of temperature profile and molar concentration of CH_4, H_2, and CO_2 in an adiabatic packed bed reactor at 700 °C, 1 bar, S/C of 3.0 and 0.05 kg m^{-2} s^{-1} mass flux of the gas phase conditions

In an effort to study the performance of the SMR and WGS reactions during SMR process, results are generated for different rate of reactions. In **Figure 4.9 (a-c)** the variations of the reforming reaction rates at different locations of the reactor are presented.

The physical properties and operating conditions used for this study are tabulated in **Table 4.6**. It can be seen that the steam methane reforming reaction (R1) is the dominant reaction at different locations within the reactor. At the very entrance of the reactor, the rate of SMR is maximum (Fig. 4.9a) and decreases drastically along the axial direction of the

reactor (Fig. 4.9b and 4.9c). It can be explained by the temperature curve, as at the upstream zone of the reactor, the temperature of the system is maximum and it causes a large rate of SMR reaction (R1). The maximum rate of SMR at the upstream zone of the reactor is 1.50 mol kg^{-1} s^{-1}. As the process is adiabatic in nature (q = 0) it causes the temperature of the system to drop from 700 °C (973.15 K) to 645.3 °C (918.15 K) along the length of the reactor. This drop in temperature confirms the decrease in the rate of the endothermic reaction. As temperature at the entrance of the reactor is very high (~ 700 °C) and WGS shift reaction is not favourable at such a high temperature conditions. So, the rate of exothermic WGS shift reaction (R2) is very low at the upstream zone of the reactor and has maximum value of 0.087 mol kg^{-1} s^{-1}

As we move along the length of the reactor, the rate of reforming reaction goes down, caused by the drop in available CH_4 reactant. The maximum rate of SMR in the middle of reactor is and it is ~0.0214 mol kg^{-1} s^{-1}. This rate of SMR is almost 70 times lower than the initial rate of the reforming reaction at the reactor's entrance. In **Figure 4.9 (b),** it can be seen that the rate of WGS reaction is on the negative side, indicating reverse reaction. This is because of temperature of the system, as higher temperature is not favourable for the WGS reaction. It can be seen that as the rate of SMR reaction decreases, the conversion of CH_4 also reduces.

At the end of reactor, the rate of SMR reaction is even lower. The maximum value of SMR at the end of reactor is 0.011 mol kg^{-1} s^{-1} i.e. almost 136 times lower than the value obtained at the entrance of the reactor. Similarly the rate of WGS reaction is higher than the previous value of the rate of WGS reaction as it can be seen in **Figure 4.9 (c). In Figure 4.9 (d),** the steady state profile of reforming reaction rate and temperature profile along the axial direction of the reactor is shown. The variation of temperature dictates the variation of the reforming reaction rates. It can be seen that at the entrance high temperature promotes the reforming reaction, but as the temperature of the system drops from 700 °C to 645 °C the SMR reaction rate also decreases. So the rate of SMR and global SMR reactions are maximum at the reactor entrance as can be seen in the figure 4.9(d).

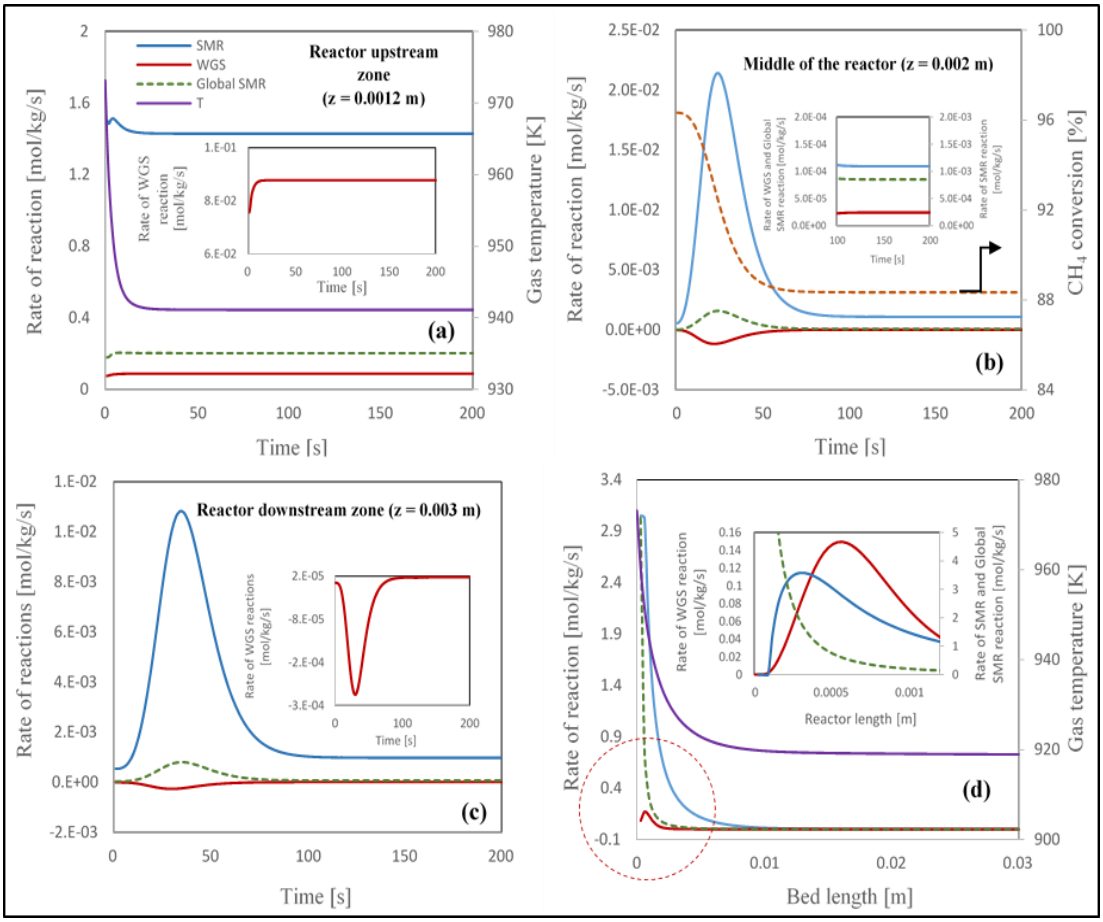

Figure 4.9: Reaction rates at different location within an adiabatic packed bed reactor (a-c) and d) variation of reactions rate along the axial direction of reactor (under steady state conditions) at 700 °C, 1 bar, S/C of 3.0, 0.05 kg m^{-2} s^{-1} mass flux of the gas phase conditions

4.5.2.2 Model validation

The modelling results first need to be validated before further analysing the sensitivity of the SMR process. The model developed in gPROMS using the parameters and conditions listed in **Table 4.6** was validated by comparing the modelling results with our experimental data. The t-value shows the percentage accuracy of the estimated parameters, with respect to 95% confidence interval. Model parameters satisfy the 95% confidence interval and weighted residual had the value (7.32) less than χ^2-value (100.75), which meant the model was a good fit to the experimental values. χ^2 (Chi square) is used for goodness of fit. The fitting data of CH_4 concentration is shown in **Appendix C**.

To validate the reactor model, two routes are adopted. In the first route, the modelling results are compared with their experimental counterparts far from the equilibrium

conditions. Later on, the model is validated against the results generated, by using chemical equilibrium software, close to equilibrium conditions.

4.5.2.2.1 CASE 1: Steady-state, away from equilibrium

In this section the experimental results generated under the steady-state conditions away from the equilibrium are compared with the equivalent modelling results. The modelling results need to satisfy both equilibrium and away from equilibrium conditions to be used as a flexible model. In the following section carbon balance results are used to validate the model.

a) Carbon balance and selectivity to carbon products

The rate equation for the carbon formation on the catalyst surface is not included in the developed model as the rate of formation of solid carbon is negligible as compared to the other rates. This is verified via the carbon balance across the reactor system for all the experiments performed for model validation and shown in **Table 4.7**. The maximum gas hourly space velocity (GHSV) used in the experimentation is 4.54 h^{-1} (equivalent to pseudo contact time of 73.1 g hr mol^{-1}) and this caused 93% recovery of the feed carbon in the form of product gases CO, CO_2 and CH_4, while only 7% was unaccounted for which represents the largest percentage of carbon unaccounted for. This is most likely caused by the propagation of errors in each of the measured variables (feed rate of CH_4, and vol. % of CO, CO_2 and CH_4).

Table 4.7: Molar carbon balance for SMR experiments over 18 wt. % NiO/α-Al_2O_3 catalyst. Experiments were run over the duration of 4500 s, at 700 °C, 1 bar pressure and S/C of 3.0. The experimental molar flow of carbon going in and carbon going out is compared with equilibrium values under the same operating conditions.

GHSV (in h^{-1}) [W/F in g h mol^{-1}]	**Feed C (mol s^{-1})**	**C in outlet gases (mol s^{-1})**			**Exp. C_{out} (mol s^{-1})**	**Exp. C_{out}/C_{in} (%)**
		CH_4	CO	CO_2		
1.62 [203.6]	0.030	Exp.: 2.2×10^{-3} Mod: 1.8×10^{-3}	Exp.: 1.38×10^{-2} Mod: 1.53×10^{-2}	Exp.: 1.35×10^{-2} Mod: 1.38×10^{-2}	0.0295	98.30

2.58 [127.4]	0.049	Exp.: 4.13×10^{-3} Mod: 5.1×10^{-3}	Exp.: 2.00×10^{-2} Mod: 2.18×10^{-2}	Exp.: 2.32×10^{-2} Mod: 2.18×10^{-2}	0.0472	96.33
4.54 [73.1]	0.086	Exp.: 1.85×10^{-2} Mod: 1.77×10^{-2}	Exp.: 2.55×10^{-2} Mod: 2.79×10^{-2}	Exp.: 3.60×10^{-2} Mod: 3.39×10^{-2}	0.0800	93.02

Selectivity (%) of CH_4 increased with increase in GHSV. As with increase in GHSV, CH_4 conversion decreased and more CH_4 went in product gases. Mathematical model was developed by ignoring the kinetics of carbon formation rate, so according to modelling results all the carbon going in feed is equal to the carbon going in outlet gases. While on other hand, in experimental results, the amount of unaccounted carbon varied from 1.7-7%, depending upon the value of GHSV. In case of 1.62 h^{-1} GHSV, the amount of unaccounted carbon is almost negligible for both experiment and modelling and hence the selectivity of all the carbon gases is quite comparable. The selectivity data for CH_4, CO and CO_2 under the operating conditions of 700 °C, 1 bar pressure and S/C of 3.0 in case of experiment and modelling is shown in **Table 4.8.**

Table 4.8: Comparison of experimental and modelling values of selectivity of C-based products at 700 °C, 1 bar pressure and S/C of 3.0.

Gases	Experimental values [%]	Modelling values [%]
CH_4	7.6	5.4
CO	47	49.8
CO_2	45.5	44.8

Selectivity of hydrogen-containing products to H_2 obtained through experiments was in good agreement with the value obtained through modelling work. For the range of GHSV (1.62-4.54 h^{-1}), H_2 selectivity in case of experiments varied from 92.6-97.7 %. In case of modelling under the same operating conditions, it varied from 93.2-98.4 %.

b) Conversion of CH_4 and H_2O

The comparisons of conversions obtained from experiments and predicted values are shown in **Figure 4.10 (a-c)**. The experimental and predicted values for methane and water conversion are compared at 700 °C, 1 bar and S/C of 3.0. The predicted values are in good agreement with the values obtained from the experiments. To calculate the value of CH_4 conversion the following relation is used;

$$X_{CH4} = \frac{(m_{CH4,i} - m_{CH4,o})}{m_{CH4,i}} \times 100 \qquad (4.30)$$

Where m_{CH4} represents the appropriate methane molar flows, with subscripts i and o standing for 'at reactor inlet and outlet' respectively. The selection of GHSV is very important here as achieving the equilibrium condition is not desirable. It can be seen that for each GHSV condition the reactor has successfully attained steady state and is closely reproduced by the model in the range of partial CH_4 conversions (0.79-0.93), i.e. far from the equilibrium. Under the same conditions, equilibrium would have yielded methane and steam conversions of 99.9% and 47% respectively.

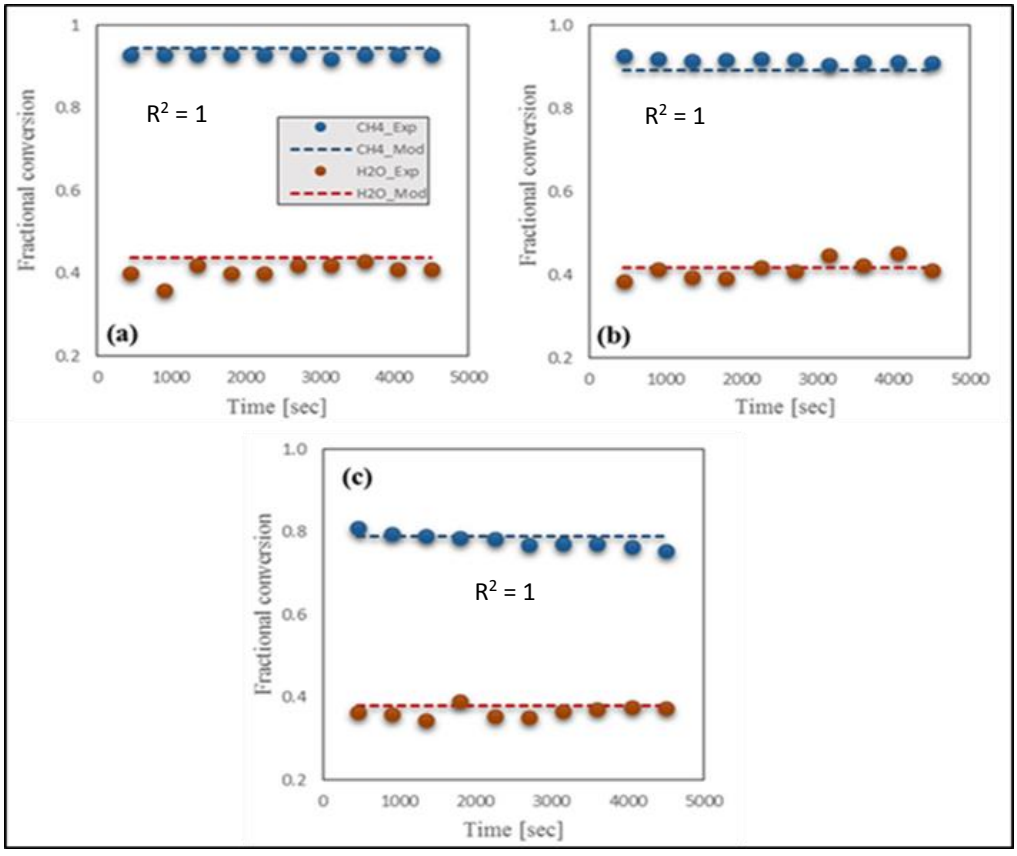

Figure 4.10: Comparison between measured and estimated CH_4 & H_2O conversion at 700 °C, 1 bar and S/C of 3. (a) 1.62 h^{-1} GHSV (b) 2.58 h^{-1} GSHV (c) 4.54 h^{-1} GHSV

c) Hydrogen Yield (wt. % of CH_4) and Purity

Hydrogen yield (wt. % of CH_4) was calculated by using equation 26:

$$H_2 \text{ yield (wt.\%)} = \frac{(\text{molar rate of } H_2 \text{ at outlet} \times \text{molar mass of } H_2)}{(\text{molar rate of } CH_4 \text{ in inlet} \times \text{molar mass of } CH_4)} \times 100 \quad (4.31)$$

Figure 4.11 (a-c) shows the variation of hydrogen purity and H_2 yield (wt. % of CH_4) with time. Modelling results are compared with experimental results and a good agreement is observed.

Together with Table 4.7 Figures 4.10 and 4.11 demonstrate the excellent agreement between experimental and predicted values and provided validation for the model based on three conditions away from chemical equilibrium.

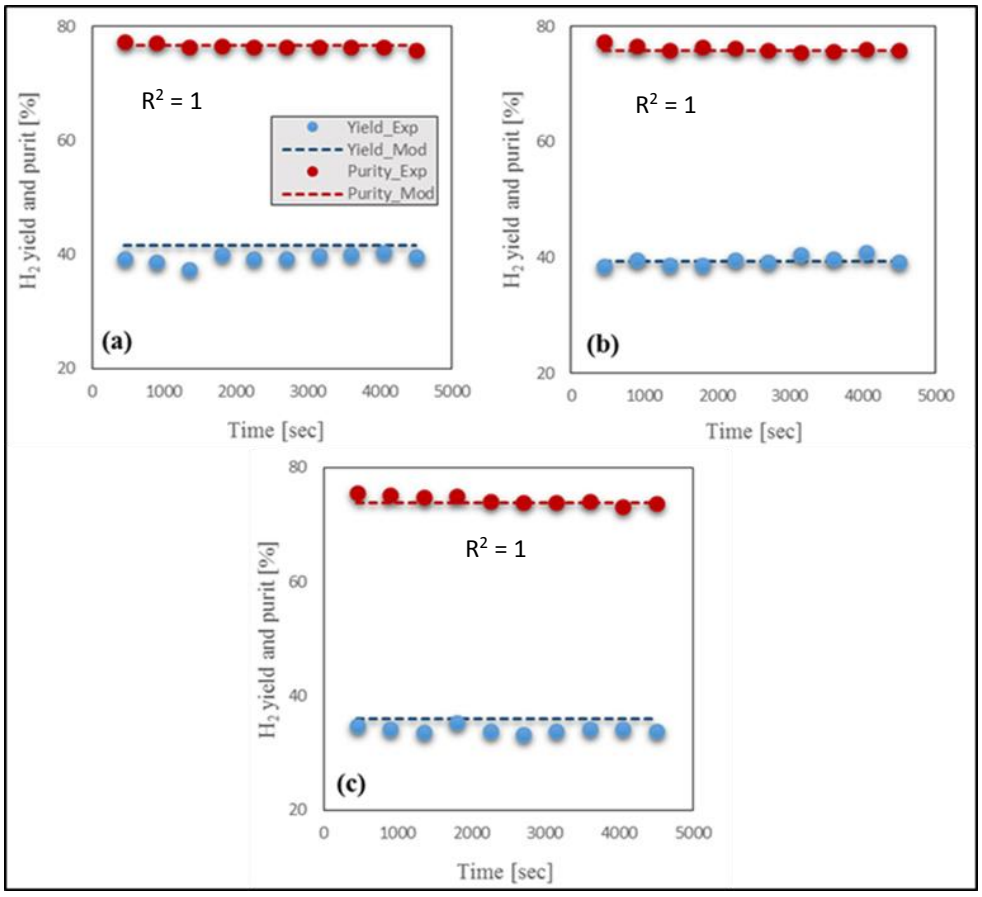

Figure 4.11: Comparison between measured and estimated values of H_2 purity (%) and H_2 yield (wt. %) at 700 °C, 1 bar and S/C 3. (a) 1.62 h^{-1} GHSV (b) 2.58 h^{-1} GSHV (c) 4.54 h^{-1} GHSV

4.5.2.2.2 CASE 2: At Equilibrium

The model's outputs at equilibrium conditions were compared against those of the CEA model provided by NASA to further its validation. The results generated on CEA are at equilibrium conditions. The validation of model at equilibrium conditions was performed in the following conditions:

a) Effect of temperature

In the SMR process at equilibrium, temperature has a positive effect on purity and yield of H_2 up to peak values corresponding to complete CH_4 conversion by steam reforming followed by WGS. Beyond the temperature of peak yield, CH_4 conversion remains maximum but reverse WGS decreases steadily the H_2 yield and purity. **Figure 4.12 (a)** shows the effect of temperature on CH_4 and H_2O conversion at constant pressure (1.5 bar) and constant S/C (3).

b) Effect of pressure

Pressure is one of the important operating parameter in SMR process. CH_4 reforming process generates a larger amount of product moles than the initial moles of reactant, thus, according to le Chatelier's principle, low pressure favours the process, as it counteracts the rise in total molar concentration. On other hand, WGS reaction is equimolar and thus is not sensitive to pressure changes once equilibrium is reached. So the conversion of CH_4 at a fixed temperature goes down as the pressure of the system increases. Effect of pressure on conversion (CH_4 and H_2O), at constant temperature (600 °C) and S/C (3), is presented in **Figure 4.12 (b).**

c) Effect of molar S/C

The S/C plays a very important role in overall performance of the system. Higher the S/C, higher will be the overall conversion of the system. But as the S/C increases, more energy is required to produce the required amount of steam and it affects the overall operational cost. Optimum S/C is required to trade-off between overall performance and cost.

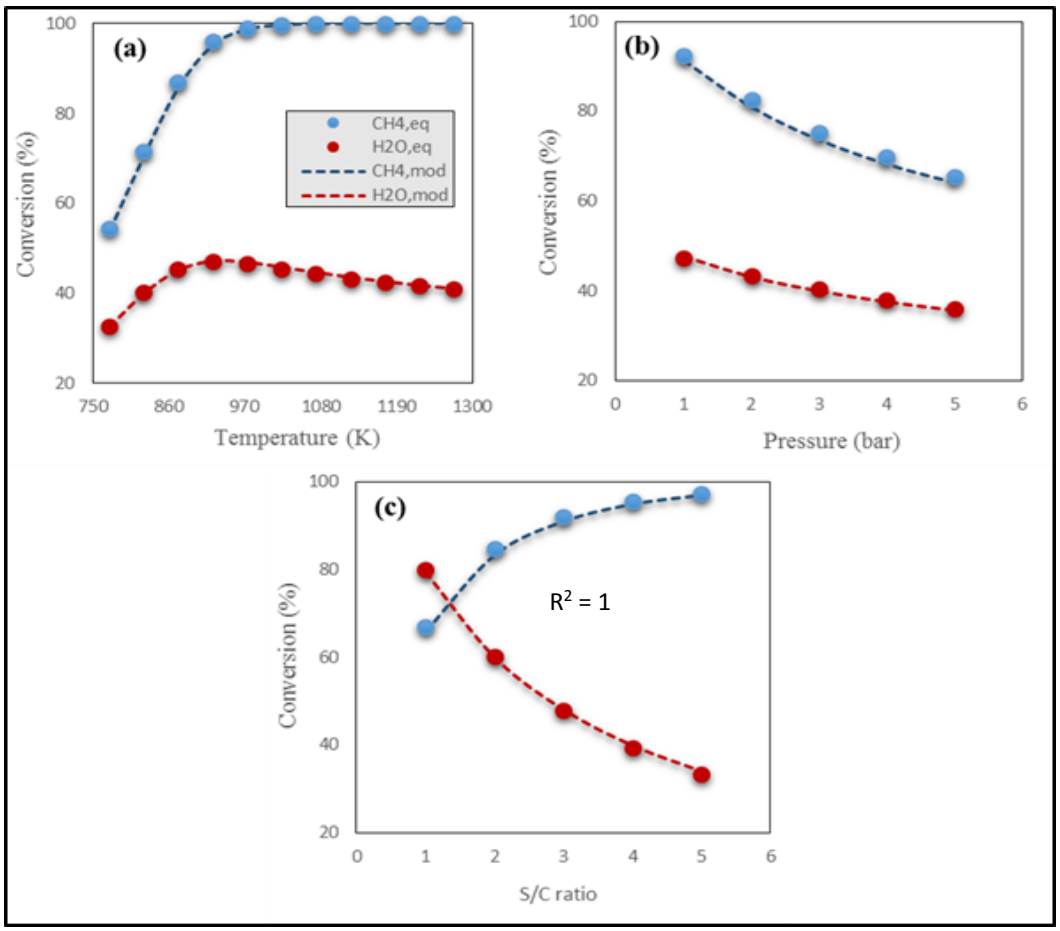

Figure 4.12: Effect on CH_4 and H_2O conversion of a) temperature, b) pressure and d) molar S/C

Effect of S/C rati on conversion (CH_4 and H_2O), at constant temperature (600 °C) and constant pressure (1 bar), is presented in **Figure 4.12 (c).**

4.5.3 Model outputs away from equilibrium

Having demonstrated the validity of the model at and away from equilibrium, the model outputs are discussed in steady-state conditions away from equilibrium outside the range of our experimental data. **Figure 4.13 (a)** shows the decrease of CH_4 and steam conversions for the increasing values of GHSV. Gas hourly space velocity (GHSV) plays a vital role in overall conversion of fuel and performance of the system. The higher the GHSV, i.e. the shorter the contact time with the catalyst throughout the reactor, the lower will be the fuel conversion. Modelling results were checked for different GHSV and results are presented in **Figure 4.13 (a-c)**. Selectivity to effluent gases was modelled according to following equations;

H_2 selectivity (%)

$$= \frac{(\text{molar rate of } H_2 \text{ at outlet})}{(\text{molar rate of } CH_4 \text{ at outlet} + \text{molar rate of } H_2 \text{at outlet})} \times 100 \qquad (4.32)$$

CH_4 selectivity (%)

$$= \frac{(\text{molar rate of } CH_4 \text{ at outlet})}{\left(\sum(\text{molar rate of all C containing gases } (CH_4, CO \text{ and } CO_2) \text{ at outlet})\right)} \times 100 \qquad (4.33)$$

CO_2 selectivity (%)

$$= \frac{(\text{molar rate of } CO_2 \text{ at outlet})}{\sum(\text{molar rate of all C containing gases } (CH_4, CO \text{ and } CO_2) \text{ at outlet})} \times 100 \qquad (4.34)$$

CO selectivity (%)

$$= \frac{(\text{molar rate of CO at outlet})}{\sum(\text{molar rate of all C containing gases } (CH_4, CO \text{ and } CO_2) \text{ at outlet})} \times 100 \qquad (4.35)$$

Thermal efficiency of reformer process is defined as;

$$\text{Thermal efficiency } (\%) = \frac{(\text{moles of } H_2 \text{ at outlet} \times LHV_{H2})}{(\text{moles of } CH_4 \text{ in inlet} \times LHV_{CH4})} \times 100 \qquad (4.36)$$

Where LHV is the relevant lower heating value.

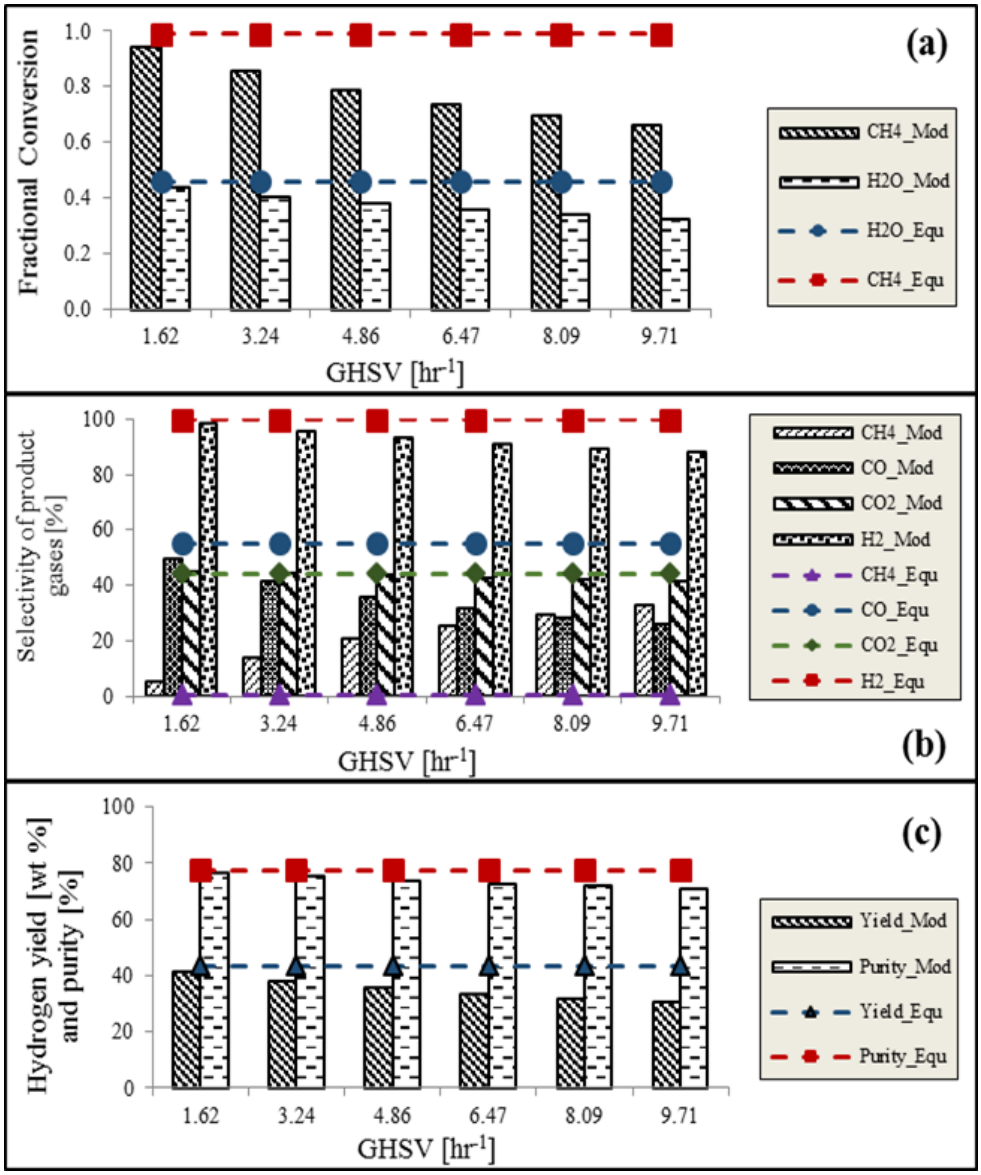

Figure 4.13: Effect of GHSV on a) conversion of methane and water, b) Selectivity to effluent gases (C-selectivity for CO, CH_4 and CO_2 and H-selectivity for H_2) & c) H_2 yield and purity, at 700 °C, 1 bar and S/C of 3.12

Figure 4.14 shows the variation of thermal efficiency of the reforming process with temperature at different S/C. The higher the S/C and temperature, the higher is the thermal efficiency of the process. Modelling results are compared with equilibrium results and it was found that at temperature 750 °C and S/C of 3, equilibrium results for thermal efficiency are equal to modelling results. At 700 °C and S/C of 3, thermal efficiency of the process is found to be 89.11%. GHSV used for **Figure 4.14** was 1.52 hr^{-1}.

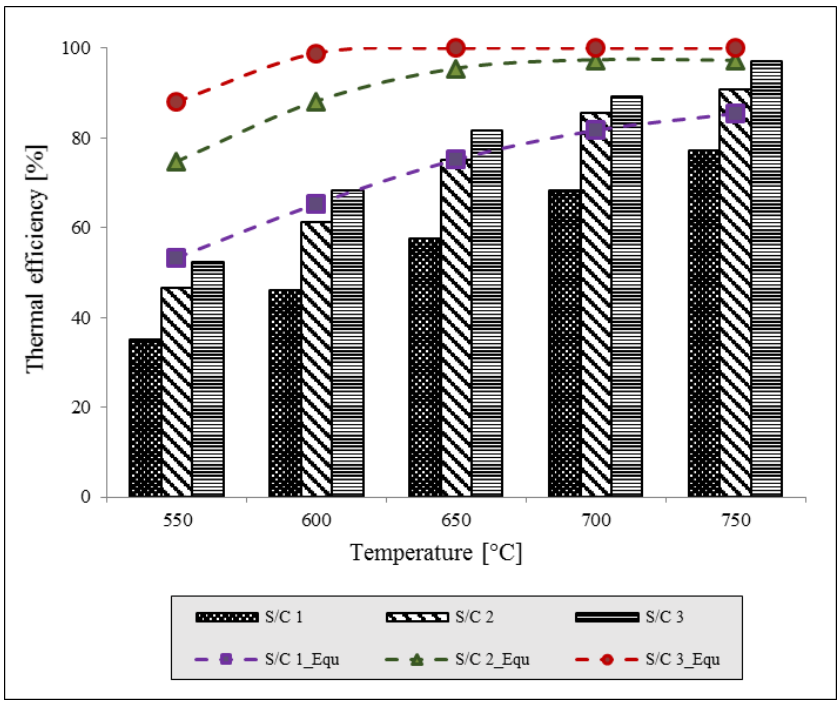

Figure 4.14: Effect of temperature and S/C on thermal efficiency (%) of reforming process at 700 °C, 1 bar and 1.52 hr^{-1} GHSV

4.6 Conclusion

An experimental study was performed over the surface of 18wt. % NiO/α-Al_2O_3 catalyst, to find out the reaction kinetics of the steam methane reforming process while keeping in mind the condition of diffusion limitations and far from the equilibrium conditions. The kinetic model proposed by **Xu et al.** is selected to fit the experimental data. A non-linear least square analysis based on minimization of the sum of the residual squares of the experimental reaction rates and the predicted reaction rates is used to estimate the kinetic parameters. The activation energies for SMR, WGS and global SMR reactions are calculated as 257.01 kJ/mol, 89.23 kJ/mol and 236.7 kJ/mol respectively.

The SMR process performance in terms of fuel conversion, selectivity of outlet gases, H_2 purity and yield (wt. % of CH_4 fed) is demonstrated in a fixed bed reformer using a 1-D heterogeneous reactor model. The modelling results are validated against the experimental results under the conditions of far from equilibrium. Later on, the modelling results are compared with the equilibrium results and an excellent agreement is observed. High temperature, lower pressure and high steam to carbon ratio gave the excellent performance of the system in terms of CH_4 conversion and purity of H_2. Results presented in this chapter gave the complete mathematical modelling of adiabatic fixed bed SMR

reactor and this model will further be used for modelling sorption enhanced steam methane reforming (SE-SMR), chemical looping steam reforming (CL-SR) and sorption enhanced chemical steam reforming (SE-CLSR) processes for H_2 production.

CHAPTER # 5

SORPTION ENHANCED STEAM METHANE REFORMING

The objective of this chapter is to develop a mathematical model of sorption enhanced steam methane reforming (SE-SMR) process by using 18 wt. % $NiO/\alpha Al_2O_3$ as a catalyst and calcium oxide (CaO) as a carbon dioxide (CO_2) sorbent. A dynamic one-dimensional (1-D) heterogeneous model of packed bed reactor is developed by using of kinetic data available in the literature [192]. In this model, along with all the steam methane reforming (SMR) reactions considered in the previous chapter, adsorption of CO_2 on the surface of CaO is also considered. The sensitivity of the developed model is studied under various operating temperature, pressure, steam to carbon ratio (S/C) and gas mass flux conditions. The mathematical model is also validated against the experimental and modelling data reported in the literature [41, 192].

5.1 Introduction

In any chemical industrial process, the reactor is considered as the heart of the process. In a catalytic reactor, reactions take place between raw materials on the surface of the catalyst. This may result in many desired and undesired products. Downstream of the reactor, an additional process unit is required to separate the desired product from the undesired ones. Separation processes are usually very costly and contribute towards higher investment and operational costs of the overall process [216].

Mayorga et al. [98] presented a concept of a reactor in which reaction and separation took place at the same time in a single reactor. This concept of "Hybrid reactor" reduces the cost of the process, as no separate unit operation is required for the separation of product streams.

Amongst all the contributors of climate change, CO_2 is the most prominent one, accounting for 99 wt. % of total air emission [102]. Almost 75% of CO_2 emission in the atmosphere for the last 20 years is due to the burning of fossil fuels [217]. Due to

increasing concern about the CO_2 emission, attention has been given to manage CO_2 emission from large industrial emitters, including conventional SMR process.

SE-SMR is the process that produces hydrogen (H_2) and at the same time captures CO_2 by adding a CO_2 adsorbent along with the reforming catalyst in the reactor. This process works on the principle of the hybrid reactor as presented by **Mayorga et al**. [98]. **Williams et al.** [99] issued a patent in which the process of SE-SMR was described for the production of H_2. **Brun et al.** [218] showed that the SE-SMR process saves the overall energy demand of the reactor system and this process has the potential of saving up to 20-25% energy as compared to conventional SMR process. The SE-SMR process has the advantage of promoting CH_4 conversion, H_2 production and CO_2 capturing efficiency. As the CO_2 captures, the equilibrium of water gas shift (WGS) reaction (R_{10}) is shifted towards more H_2 production at low temperature (723-873 K) than conventional SMR process (1073-1300 K) [104, 106]. In this process no WGS reactor is required downstream of the steam methane reformer unlike conventional SMR process used in fertilizer production plants [219]. The potential advantages of the SE-SMR process are not only improved efficiency of reforming process and elimination of the WGS reactor, it also helps to perform the reforming process at reduced temperature as compared to conventional SMR process [16]. Hence, higher CH_4 conversion and H_2 purity can be achieved at lower temperature (773-973 K).

5.2 SE-SMR sorbent

The H_2 yield depends upon the type of CO_2 sorbent used. The selection of CO_2 sorbent depends upon its CO_2 capturing capacity, its stability after multi-cycle operation and on its adequate sorption/desorption kinetics [220]. Calcium oxide (CaO) is found to be the best sorbent at high temperatures and resulted in 99% H_2 purity [104, 221]. CaO has a low cost and is considered as the most prominent sorbent for the CO_2 sorption under the reforming conditions. CaO also shows good CO_2 capturing capacity, good thermodynamics properties and good reaction kinetics as compared to the other sorbents such as Spanish dolomite, calcite and $CaCO_3$ from acetate. These are good sorbents and they show relatively very high capacity for CO_2 adsorption [10]. CaO has adsorption capacity of 0.79 g_{CO2}/g_{CaO}, while its close competitor calcined dolomite (CaO.MgO) has the adsorption capacity of 0.46 $g_{CO2}/g_{sorbent}$. But as far as the multi cycle operations are concerned, dolomite has improved performance as compared to the CaO [222]. The

carbonation of CaO is favourable in a temperature range of 600-750 °C under atmospheric pressure. While, the regeneration of the carbonated sorbent is a high temperature process and occurs at 850-1000 °C under atmospheric pressure. **Blamey J et al.** [223] found that after multi-cycle operations the reactivity of the CaO particles reduces. The main driving force for this adsorption of CO_2 on the active surface of sorbent is the partial pressure of CO_2 between the surface of sorbent and the reaction phase [224]. **Ochoa-Fernández et al.** [104] gave comparison between few most commonly used sorbent for capturing CO_2 and their finding is reported in **Table 5.1 & 5.2.** The kinetic properties of CO_2 adsorption on the surface of CaO is already reported in 3.3.6 section of **Chapter 3.**

Table 5.1: Comparison of different sorbents [104]

Properties	CaO	Li_2ZrO_3	$KLiZrO_3$	Li_4SiO_4	Na_2ZrO_3
Capacity	G	F	F	F	F
Thermodynamics	G	F	F	F	F
Stability	P	G	F	G	G
Kinetics	G	F/P	F	F	G
Regeneration T	H	M	M	M	M

Where: Good ; **F**: Fair ; **P**: Poor ; **H**: High ; **M**: Medium

Table 5.2: Performance of the CO_2 sorbents [104]

CO_2 sorbent	**Operating conditions**	**H_2 Yield [%]**
K-doped Li_2ZrO_3	848 K, 10 bar and S/C = 5	93%
Na_2ZrO_3	Same as above	90%
Li_2ZrO_3	Same as above	89%
Li_4SiO_4	Same as above	82%
CaO	Same as above	98%
CaO	848 K, 1 bar and S/C = 5	99.5%
Without sorbent	848 K, 10 bar and S/C = 5	62%

Ochoa-Fernández et al. [104] compared the performance of different sorbents on the basis of H_2 yield. They observed that by using CaO as sorbent, the process is weakly exothermic, while by using Li_2ZrO_3 the overall reaction is weakly endothermic. In order to enhance the conversion of CH_4 and get the maximum net efficiency, S/C for each process was adjusted and optimum operating temperature and pressure was derived. It was concluded from the findings that CaO is the most favourable CO_2 sorbent from thermodynamics point of view and it favours higher H_2 production during SMR as compared to other sorbents.

According to **Molinder** [225]**,** CaO undergoes three different reactions. CaO is highly hydroscopic and below 400 °C it can undergoes CaO hydration reaction (**Eq. 5.1**). Then this reaction proceed towards $Ca(OH)_2$ carbonation reaction (**Eq. 5.2**).

$$CaO_{(s)} + H_2O_{(g)} \leftrightarrow Ca(OH)_{2(s)} \qquad \Delta H_{298K} = -218.4 \text{ kJ mol}_{CaO}^{-1} \qquad (5.1)$$

$$Ca(OH)_{2(s)} + CO_{2(g)} \leftrightarrow CaCO_{3(s)} + H_2O_{(g)} \qquad \Delta H_{298K} = -64.14 \text{ kJ mol}^{-1} \qquad (5.2)$$

It was realised by **Lyon et al.** [35], that the heat required for the step of sorbent regeneration could be met by the exothermic step of unmixed steam reforming(USR) or chemical looping steam reforming (CLSR), which would reduce the temperature differences between the oxidation and reduction phases of the process and therefore can be more energy efficient by limiting the irreversibility caused by these temperature differences. More detail about the different sorbents used for the SE-SMR process is reported in **Chapter 2.**

5.3 Experimentation and materials

The mathematical model of SE-SMR process is validated by using experimental data reported in the literature [40, 41, 179]. **Lee et al.** [41] performed SE-SMR experiments in a stainless steel tubular reactor (internal diameter 24 mm). They used Ni based catalyst (1/8'' cylindrical pellet, 16.4 g) and CaO sorbent (3 mm in diameter and 83.6 g). The temperature of the system was recorded by installing two thermocouples, one at the top and one at the middle section of the packed bed reactor. The temperature of the packed bed within the reactor was controlled by two electrical heaters.

The reactor was initially heated at a rate of 5 °C/min under the atmospheric pressure conditions by using 50% flow of H_2 up to 800 °C. The reactor was kept under these conditions for 12 hr untill the entire catalyst was reduced. After the reduction of the

catalyst, the temperature of the reactor was adjusted according to the reaction temperature. Once that temperature was achieved, a HPLC pump was used to supply water in a fixed amount so that the ratio of H_2O/H_2 was the same as the ratio of H_2O/CH_4. The SE-SMR process was initiated by replacing the flow of H_2 with CH_4. **Fernandez et al.** [40] used this experimental data to build a model in MATLAB and validated their model. In this chapter, results of **Lee et al.** and **Fernandez et al.** are used for my model validation. To find out the optimum conditions for SE-SMR, further sensitivity analysis of the developed model is carried out under the conditions of adiabatic process. The effect of temperature, pressure, steam to carbon ratio (S/C) and gas mass flux (G_s) is discussed in the later part of this chapter.

5.4 Mathematical modelling of SE-SMR

The mathematical model of SMR is discussed in **Chapter 4**, this chapter deals with the modelling of the SE-SMR process. The mathematical model of the SE-SMR process is an extension of the SMR model as the only difference between both models is the sorption of CO_2 on the surface of CO_2 sorbent. A 1-D heterogeneous mathematical model of SE-SMR in an adiabatic packed bed reactor is developed on gPROMS model builder 4.1.0®. Like the model of SMR, it accounts for mass and energy transfer in both the gas and solid phase. In this model it was assumed that;

a) The flow pattern of gases in the packed bed reactor is plug flow in nature.
b) The temperature and concentration variations only along the axial direction of reactor are considered.
c) The gas follows ideal behaviour.
d) There is no energy transfer from the system to the surrounding and from the surrounding to the system, i.e. the process is considered to be adiabatic.
e) Only CO_2 is considered to be adsorbed on the surface of the sorbent.
f) The size of the catalyst and sorbent is considered uniform in the reactor.
g) The porosity of the bed is constant.

5.4.1 Governing equations

The SMR reactions, described in **Chapter 4**, are simultaneously run with the CO_2 sorption reaction. As discussed in **Chapter 2 and 3** that SMR reaction [R_9] is highly endothermic in nature, so high temperature and low pressure favour this reaction. On the other hand, WGS reaction [R_{10}] is exothermic and is favoured by low temperature and is thermodynamically insensitive to pressure variations. As the reforming reactions proceed and CO_2 is generated, the CaO based sorbent chemisorbed the CO_2 gas. Thermodynamically, the elimination of CO_2 from the gas product favours the formation of more H_2 by shifting the equilibrium of SMR reaction towards more conversion of CH_4. The adsorption of CO_2 on the surface of CaO sorbent is a highly exothermic reaction;

$$CaO_{(s)} + CO_{2(g)} \leftrightarrow CaCO_{3(s)} \qquad \Delta H_{298K} = -357.6 \text{ kJ mol}_{CaO}^{-1} \tag{5.3}$$

The overall reaction in SE-SMR is slightly exothermic in nature as shown in **Eq. 5.4**;

$$CaO_{(s)} + CH_{4(g)} + 2H_2O \leftrightarrow CaCO_{3(s)} + 4H_{2(g)} \quad \Delta H_{298K} = -55.6 \text{ kJ mol}_{CaO}^{-1} \tag{5.4}$$

On the basis of the assumptions, reported above, the mathematical equations for mass and energy balance within the reactor filled with sorbent and catalyst particles are listed in **Table 3.3**. The equations used to find out the physical properties, involved in mathematical equations, are listed in **Chapter 4**. The mass balance equation for SE-SMR process in a packed bed reactor is given as;

$$\varepsilon_b \left(\frac{\partial C_i}{\partial t}\right) + \frac{\partial (u C_i)}{\partial z} + \upsilon \rho_{cat} r_i + (1-\upsilon)\rho_{ad} r_{ad} = \varepsilon_b D_z \frac{\partial^2 C_i}{\partial z^2} \tag{5.5}$$

In the above equation, 'i' is for the gas species (CH_4, CO, CO_2, H_2, H_2O and N_2) and 'υ' is the ratio of the amount of the catalyst to the amount of the sorbent filled in the packed bed reactor. The energy balance equations, both in the gas and solid phase, for the SE-SMR process based on the above mentioned assumptions are given in **Table 3.3** (**Eq. 3.58 & 3.64**).

In literature many expressions have been reported to describe the carbonation kinetics of the CaO-based sorbents [40, 41, 179]. **Lee et al.** [41] performed experiments in a tubular reactor, having inner diameter 22 mm and bed length is 290 mm, loaded with 16.4 g Ni based reforming catalyst and 83.6 g CaO based sorbent. Through a series of experiments in the temperature range of 650-750 °C, they determined carbonation conversion data. The carbonation kinetic expression they reported is listed in **Table 3.4** [R_{16}]. In this rate

equation 'X' is the carbonation conversion of CaO. The rate of change of the carbonation conversion is already discussed in **section 3.3.6**. **Dedman et al.** [226] reported that the carbonation rate of CaO was zero order with respect to CO_2 partial pressure. **Bhatia et al.** [147] also proposed a carbonation rate expression which was independent of the partial pressure of CO_2.

The effect of carbonation reaction (Eq. 5.3) rate constant (k_{carb}) on the performance of SE-SMR is discussed in a later section of this chapter. 'X_{max}' is the ultimate carbonation conversion of CaO. **Lee et al.** [41] performed TGA (thermogravimetric) analysis and determined the maximum conversion of the active CaO at different temperatures. The experimental data revealed that the conversion of CaO is very low at a very high temperature (750 °C). It was observed that by using a large size of the pellet, there was no sign of the particle deterioration even after many cycles of carbonation and calcination. **Eq. 5.6** describes a temperature dependent expression to calculate the maximum conversion of CaO at any given temperature.

$$X_{max} = 96.34\exp\left(\frac{-12171}{T}\right) \times 4.49\exp\left(\frac{4790.6}{T}\right) \tag{5.6}$$

The rate equations used for the reforming process are listed in **Appendix A (A1-3)**. The kinetic rate constants and equilibrium constants used in this model are given **section 3.3.2** (**Eq. 3.76-3.81**). On the basis of reactions involved in SE-SMR, the rate of formation or consumption of 'i' component is given as;

$$r_i = \sum_{j=1}^{3} \eta_i \, \varphi_{ij} R_j \qquad i = CH_4, CO, CO_2, H_2 \text{ and } H_2O \tag{5.7}$$

Here 'η_j' is the effectiveness factor of the reaction j. 'φ_{ij}' is the stoichiometric coefficient of the component 'i' in the reaction 'j'. Its value is negative for the reactants and positive for the products. The rate of formation or consumption of each component is also listed in **Appendix A (A10-14)**.

The boundary conditions and initial conditions used in the mathematical modelling of SE-SMR are as follow;

Boundary conditions;

At reactor inlet (z = 0):

$C_i = C_{i,in}$; $T = T_{in}$; $T_s = T_{s,in}$; $P = P_{in}$

At reactor exit (z = L):

$$\frac{\partial C_i}{\partial z} = 0 \quad ; \quad \frac{\partial T}{\partial z} = 0 \quad ; \quad \frac{\partial T_s}{\partial z} = 0$$

Initial conditions;

$$C_i = C_{i,0} \quad ; \quad T = T_o \quad ; \quad T_s = T_{s,o} \quad ; \quad q_{CO2} = 0$$

At initial conditions, it is considered that no gas component (CH_4, CO, CO_2, H_2O and H_2) is present within the reactor so the concentration of the gas species is considered zero at the start i.e. at t = 0. But by setting the concentration of H_2 zero, it makes the reforming rate of reactions infinite (denominator equals to zero). To avoid this, a very small initial concentration (~10^{-6}) of the H_2 is used in the reactor model.

In the reactor model linear and non-linear partial differential equations (PDEs), algebraic equations, and initial and boundary conditions are involved, and gPROMS was used to solve these equations. The sensitivity of the model was first checked for discretization ranging from 10-1000 intervals and model was found independent of discretization. Finally, the reactor was axially discretized by 100 uniform intervals for and output results were reported after every one second. The first order backward finite difference method (BFDM) was used to solve the PDEs using initial and boundary conditions as mentioned above. The model of the adiabatic packed bed reactor was assumed to follow the non-ideal plug flow behavior. In gPROMS differential algebraic solver (DASOLV) was used to solve the ordinary differential equation (ODEs). DASOLV converts the PDEs into ODEs, and 4th order Runge-Kutta technique was used to solve the system of equations.

5.5 Results and discussion

5.5.1 Model validation

The developed mathematical model of SE-SMR process is first validated against the experimental and modelling data of **Lee et al.** [41] and **Fernandez et al.** [40]. Later on, the modelling results are compared with the equilibrium results generated by using chemical equilibrium with application (CEA) software. As mentioned in **section 5.3**, the experimental results of **Lee et al.** [41] and modelling results of **Fernandez et al.** [40] are used for model validation. The following parameters; length of the reactor (L), particle size (d_p), bed porosity (ε_b) and variables; S/C, operating temperature, pressure and mass flux (G_s) are adapted according to the values reported in the above mentioned literature. In these work they used temperature range of 923 K to 1023 K, pressure range between

1.0 bar and 35 bar, S/C 3 to 7 and residence time between 0.1 s^{-1} and 0.38 s^{-1}. The operating variables used for this modelling work are listed in **Table 5.3**.

Table 5.3: Operating conditions used in the reactor model

Gas feed temperature, [T_{in}]	923 K
Initial solid temperature, [T_o]	923 K
Total pressure, [P]	35 bar
Steam to carbon ratio, [S/C]	5.0
Intel gas mass flux, [G_s]	3.5 kg m^{-2} s^{-1}
Maximum fractional carbonation conversion of CaO, [X_{max}]	0.4
Apparent density of reforming catalyst, [ρ_{cat}]	550 kg m^{-3}
Apparent density of CaO based sorbent, [ρ_{CaO}]	1125 kg m^{-3}
Apparent density of two mixed solids in the reactor bed, [ρ_s]	1675 kg m^{-3}
Diameter of particles, [d_p]	0.01 m
Reactor bed length, [L]	7 m
Bed porosity, [εb]	0.5

The modelling results are checked in terms of dry gas composition of the product gases and temperature of the product gases leaving the reactor. The operating conditions mentioned in **Table 5.3** are used for this work. **Figure 5.1** shows the variation of gas compositions with time. This figure is divided into three sections; pre-breakthrough period (t < 720 s), breakthrough period (t = 720 to 1500 s) and post breakthrough period (t ≥ 1500 s). In the pre-breakthrough period, sorbent is active and it adsorbed almost all the CO_2 produced during SMR process.

$$CH_{4(g)} + 2H_2O_{(g)} \leftrightarrow 4H_{2(g)} + CO_{2(g)} \rightarrow \text{Adsorbed by CaO based sorbent}$$

The adsorption of CO_2 from the product gases shifts the reforming reaction in forward direction i.e. towards more production of H_2. In the first section of **Figure 5.3**, H_2 mole percent is 94% and CO_2 mole percent is 0.1%. In this section sorbent is at its maximum CO_2 capturing efficiency. After 720 s, the amount of H_2 in the product gases goes down and the amount of CO_2 is increasing. This is the start of breakthrough section. In this section, it is quite clear that CO_2 capturing efficiency of CaO based sorbent begins to diminish. The sorbent is approaching to the point of its maximum sorption capacity hence

the amount of CO_2 in the product gases increases. From 1500 s the sorbent is no longer active and the only process occurring within the packed bed reactor is the conventional catalytic SMR process. The process of SE-SMR is allowed to run until a steady state process is achieved.

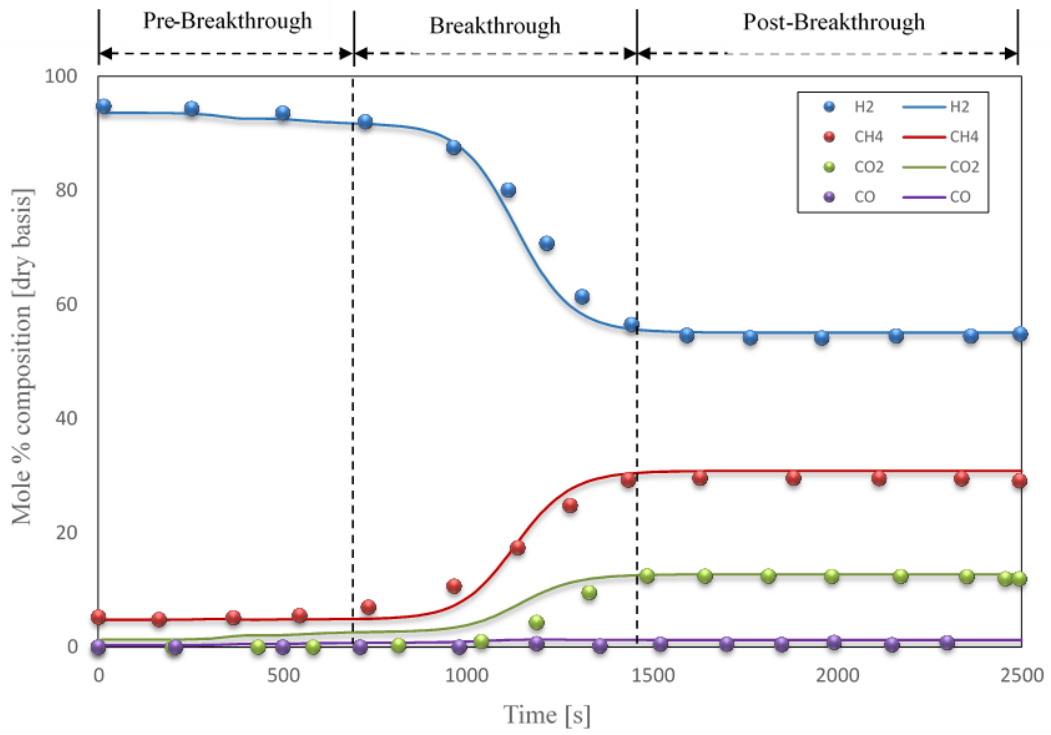

Figure 5.1: Product gases composition [dry basis] at the outlet of reactor at a feed temperature of 923 K, S/C of 5.0, 35 bar and gas mass flux of 3.5 kg m^{-2} s^{-1}. Dots represented literature values [40] and solid lines are our modelling results under the same operating conditions.

The **Figure 5.1** shows an excellent agreement between the modelling values reported in the literature [40] and the values generated in this work. Under the same conditions, equilibrium calculations were also performed on CEA for the present work. In the following section the results generated via CEA software and gPROMS are compared in terms of dry mole percent, CH_4 conversion (%) and H_2 purity (%).

In **Figure 5.1**, modelling outputs show the mole percent (dry basis) of CH_4, H_2, CO and CO_2 as 4.8%, 93.6%, 0.3% and 1.3% respectively in the pre-breakthrough period. The conversion of CH_4 and H_2 purity in this section is 86% and 93.6% respectively. These values were compared with equilibrium values and a good agreement between modelling and equilibrium results was observed. Under the same conditions, equilibrium values for mole percent (dry basis) of CH_4, H_2, CO and CO_2 are 3.9%, 95.8%, 0.1% and 0.1%

respectively. The equilibrium values for CH_4 conversion and H_2 purity are 86% and 95.8% respectively. In the post-breakthrough period, the sorbent is no longer active and the model preicted steady state mole percent (dry basis) of CH_4, H_2, CO and CO_2 after 1500 s is 30.9%, 55.1%, 1.2% and 12.8% respectively. In this section the conversion of CH_4 is reduced from 86% to 31.2%. Under the same conditions, equilibrium values for the mole percent (dry basis) of CH_4, H_2, CO and CO_2 are 20.8%, 62.8%, 2.7% and 13.6% respectively, concurrently CH_4 conversion decreases from 86% to 44%.

The overall production of H_2, conversion of CH_4 and CO_2 capturing efficiency in SE-SMR process depends upon the reactions taking place within the system and the adsorption characteristics of the sorbent. As discussed in **section 5.1**, overall SE-SMR is slightly exothermic in nature. The adsorption of CO_2 on the surface of sorbent is a highly exothermic reaction and it causes a gradual rise in the temperature of the reactor. While on other hand, the SMR process is endothermic in nature and it needs energy to proceed. The predicted temperature variation are compared with the modelling values of **Fernandez et al.** [40] and an excellent agreement was observed, as shown in **Figure 5.2.**

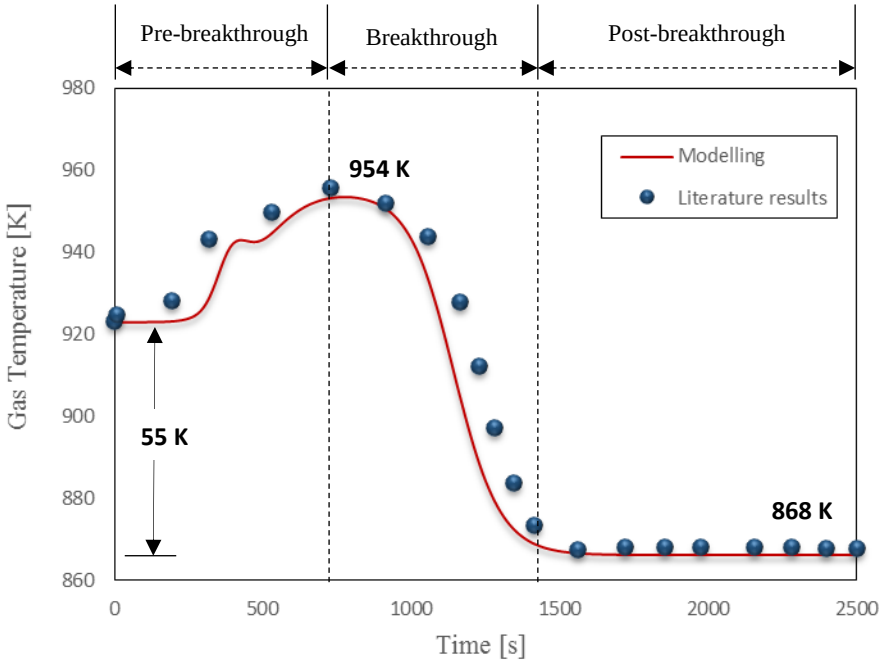

Figure 5.2: Temperature profile of gas mixture leaving at the outlet of reactor at feed temperature of 923K, S/C of 5.0, 35 bar and gas mass flux of 3.5 kg m^{-2} s^{-1} under adiabatic conditions. Dots represented literature values [40] and solid lines are our modelling results under the same operating conditions.

In the pre-breakthrough period (t < 720 s), a rise in temperature is observed because of the exothermic chemisorption process. In this section adsorption of CO_2 is maximum as the rate of carbonation reaction is high. The maximum temperature obtained in this modelling work is 954 K i.e. increase of 31 K from the feed temperature, while a rise of 32 K above the feed temperature is reported by **Fernandez et al.** [40].

In the breakthrough period, a drop in temperature is observed, and after 1500 s, the temperature profile is constant. The minimum temperature reached in this modelling work is 866 K i.e. drop of 57 K and in literature the minimum steady state temperature is reported as 868 K i.e. drop of 55 K. As discussed that sorbent is not active in the post-breakthrough period and only SMR process is happening in this section, hence the overall process is endothermic and temperature of the adiabatic reactor goes down from 923 K to 866 K.

Fernandez et al. [40] also operated the SE-SMR on non-adiabatic conditions and reported their findings. For non-adiabatic SE-SMR the energy balance equations are modified and the transfer of heat from wall to the process gas is included. The modified energy balance equation for non-adiabatic reactor is given as;

$$\rho_{bed} C_{p,bed} \left(\frac{\partial T_s}{\partial t}\right) + h_f a_v (T_s - T) = \upsilon \rho_{cat} \sum -\Delta H_{rxn,j}\, \eta_j R_j + (1-\upsilon)\rho_{ads} \sum -\Delta H_{ads}\, r_{ads} + h_w (T_w - T) \frac{4}{D_r} \quad (5.13)$$

In the above equation, the last term on the right hand side is added for non-adiabatic reactor system. This term is included to account for the transfer of heat through the wall of the reactor when external heat/energy is supplied. In this equation 'h_w' is the heat transfer coefficient across the wall of the reactor, 'T_w' is the temperature of the reactor wall and 'D_r' is the inner diameter of the reactor. This work's modelling results and the literature modelling results [40] under the same operating conditions for non-adiabatic process are compared in **Figure 5.3** and a good agreement is also observed.

By analysing both adiabatic and non-adiabatic process, it is observed that in the pre-breakthrough period of adiabatic process, the temperature is higher than the temperature in the non-adiabatic process. This higher temperature results in more CO_2 production and hence the carbonation rate is maximum. The higher carbonation rate makes the pre-breakthrough period shorter (700 s) in the adiabatic process as the sorbent reaches its total

saturation point earlier than the non-adiabatic process. Although the rise of temperature is the same in both cases, the adiabatic process has shorter pre-breakthrough period (700 s) as compared to non-adiabatic process (1200 s). This confirms that adiabatic process is more favourable for alternative reaction conditions in the SE-SMR process. Optimal duration of pre-breakthrough may be a compromise between high yield and purity of product, kinetics of adsorption, and wear and tear of flow switching controls. For instance, in the industrial pressure swing adsorption (PSA) process, after 10-15 min the valves are switched from adsorption to depressurization phase [227]. The duration of pre-breakthrough period of our adiabatic process (11.5 min), as shown in figure 5.2, is quite comparable to the industrial switching time from one phase of the process to other for the closest industrial equivalent process (PSA). On this basis, the adiabatic process was chosen for further calculations.

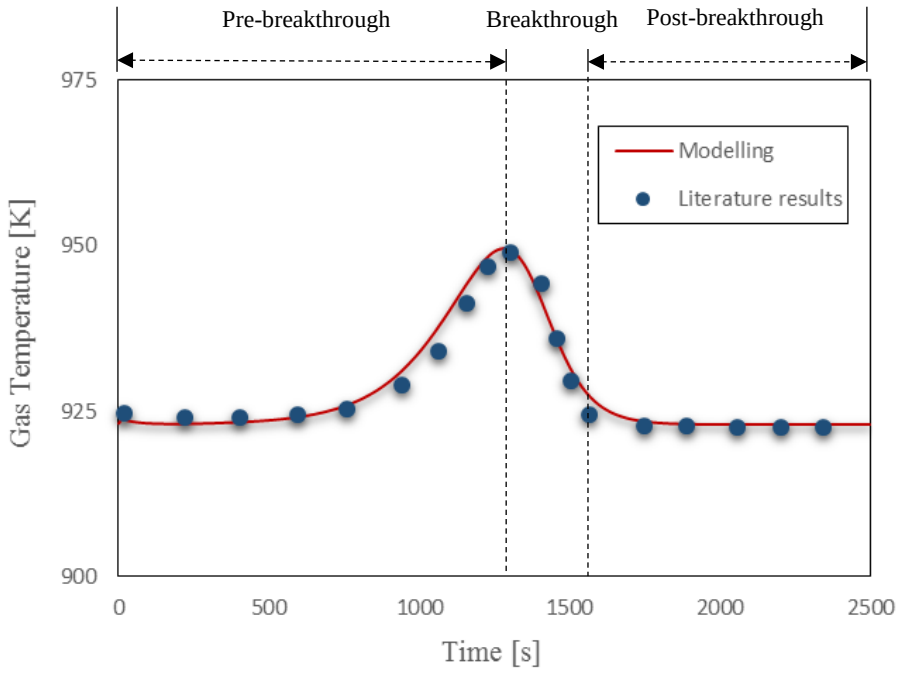

Figure 5.3: Temperature profile of gas mixture leaving at the outlet of reactor at feed temperature of 923K, S/C of 5.0, 35 bar and gas mass flux of 3.5 kg m^{-2} s^{-1} under non-adiabatic conditions. Dots represented literature values [40] and solid lines are our model results under the same operating conditions.

The reaction rate constant of CaO (k_{carb}) plays a major role in the kinetics of carbonation reactions. The effect of carbonation reaction rate constant on the temperature profile of the SE-SMR under the adiabatic conditions was studied by **Fernandez et al. [40]**, their modelling results are used here to validate the model. In **Figure 5.4,** three rate constants

are used and it is quite clear that the temperature of the system is dependent on the value of the k_{carb} (0.18, 0.35 and 0.7 s^{-1}). For smaller value of k_{CaO} (0.18 s^{-1}), the pre-breakthrough period is longer (~1500 s) than higher values of k_{CaO}, 0.7 s^{-1}, (~500 s). The lower k_{CaO} value (0.18 s^{-1}) suggests that sorbent is not highly reactive and the rate of CO_2 absorption is slow. While in case of higher value of k_{CaO} (0.7 s^{-1}), the rate of CO_2 absorption on the surface of sorbent is very fast and sorbent reached to its full absorption capacity much earlier. To achieve the maximum H_2 purity at low k_{CaO}, very low G_s is required. Therefore, longer operational period is required for the sorbent to reach at its full saturation point. Hence, higher operational cost is required. The higher value also improves the carbonation rate. In these three different values of carbonation rate constants, the final temperature of the reactor system is the same i.e. 868 K. This is because in the post-breakthrough period, the sorbent is inactive and the temperature of the system is only controlled by the conventional SMR process. The dotted lines in **Figure 5.4** are the literature modelling values and solid lines are the values generated in our modelling work. A very good agreement between values proposed in literature and our modelling values is observed.

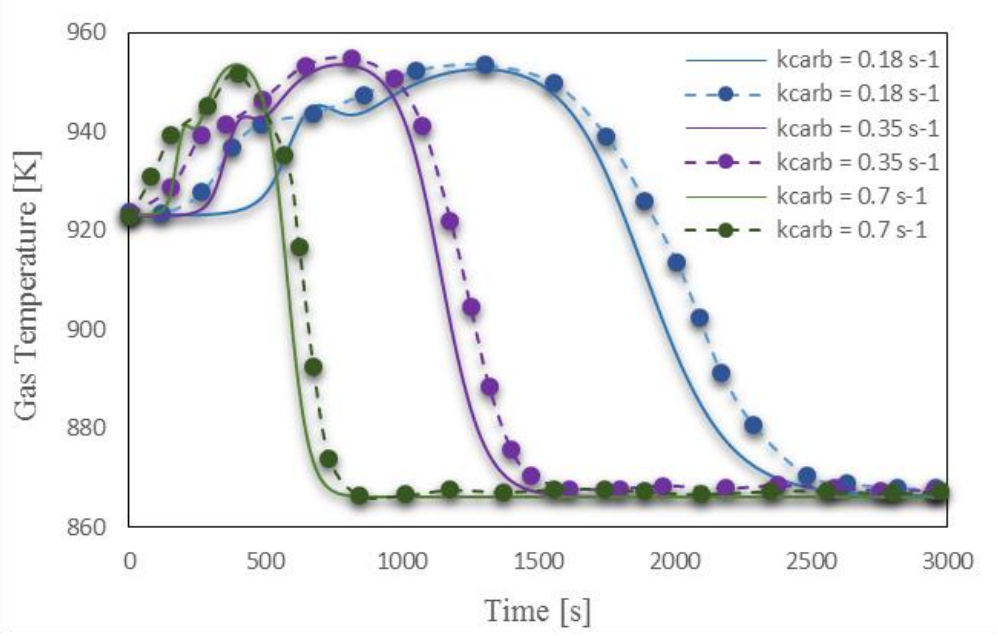

Figure 5.4: Comparison of effect of carbonation rate constant on the temperature profile of gas mixture leaving at the outlet of reactor at feed temperature of 923 K, S/C of 5.0, 35 bar and gas mass flux of 3.5 kg m^{-2} s^{-1} under non-adiabatic conditions. Dots represented literature values [40] and solid lines are our results under the same operating conditions.

5.5.2 Sensitivity analysis of the SE-SMR process

In this section optimum conditions for SE-SMR process are evaluated by operating the system under various conditions of temperature (773-1073 K), pressure (20-35 bar), S/C (1-6) and gas mass flux (2-7 kg m^{-2} s^{-1}). The outputs of modelling work are also compared with equilibrium results generated using CEA software.

5.5.2.1 Effect of temperature

As discussed in previous sections, the overall reforming process is endothermic and non-equimolar, and thus it is favourable at high temperature and low pressure. On the other hand, the sorption process is highly exothermic and it releases lot of heat (-357.6 kJ mol^{-1}_{CaO}) during the process. The overall SE-SMR is slightly exothermic (-55.6 kJ mol^{-1}_{CaO}) in nature. The effect of temperature on the conversion of CH_4, H_2 purity, CO_2 capturing efficiency and H_2 yield at atmospheric pressure under equilibrium conditions is presented in **Appendix D**. From the equilibrium results it is concluded that maximum conversion of CH_4 (99%) is achieved at high temperature (700-800 °C), S/C of 3 and 1 bar conditions. But at such a high temperature, H_2 purity goes down to 76%, because CO_2 capturing efficiency is almost zero. Therefore, there is a trade-off between conversion of CH_4 and H_2 purity. As the temperature decreases, the conversion of CH_4 decreases but at the same time H_2 purity increases as shown in **Figure D1 (a & b)**. From **Figure D1,** in **'Appendix D',** it is observed that under the conditions of 1 bar and S/C of 3.0 the optimum temperature is 600-650 °C. In this range of temperature, CH_4 conversion; H_2 purity and CO_2 capturing efficiency is 94-95%, 94-97% and 78-90% respectively. As the temperature goes higher, CO_2 capturing efficiency drops hence the H_2 purity diminishes as well. This shows that the SE-SMR is favourable at low temperature as higher temperatures favour de-carbonation reaction. **Balasubramanian et al.** [16] proposed that capturing of CO_2 above 1123 K is not effective and the Ca-sorbent becomes inert at such a high temperature.

The industrial SMR process is carried out under high temperature (800-1000 °C) and medium-high pressure (20-35 bar) conditions [52, 228]. While keeping in mind the pressure requirements of industrial plants, calculations of CH_4 conversion; H_2 purity; CO_2 capturing and H_2 yield (wt. % of CH_4) are done under high pressure conditions (20-35 bar). The SE-SMR process is run under various temperatures (500-750 °C) at S/C ratio

of 3.0 and pressure as high as 30 bar. In **Figure 5.5 (a-d)** the effect of temperature on CH_4 conversion, H_2 purity, H_2 yield (wt. % of CH_4) and CO_2 capturing efficiency is presented. Modelling results are compared with equilibrium results.

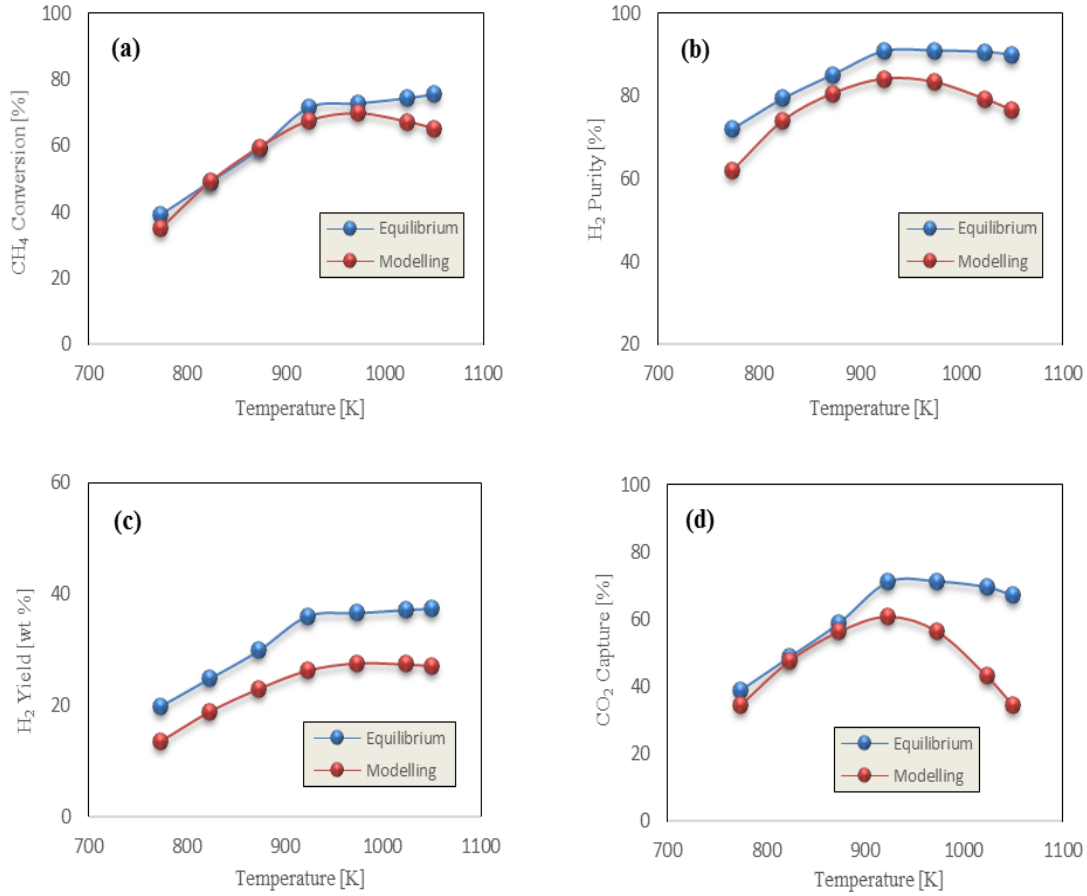

Figure 5.5: The effect of temperature on the a) CH_4 conversion; b) H_2 purity; c) H_2 yield (wt. % of CH_4) and d) CO_2 capturing efficiency at 30 bar, S/C of 3.0, CaO/C of 1.0 and mass flux of 3.5 kg m^{-2} s^{-1}

The maximum CH_4 conversion achieved at 30 bar and S/C of 3.0 is 70% at 973 K. Under these conditions the equilibrium conversion of CH_4 is 73 % as shown in **Figure 5.5 (a)**. The higher conversion of CH_4 at 973 K results in higher H_2 yield (wt. % of CH_4) i.e. 28% but lower CO_2 capturing efficiency and lower H_2 purity i.e. 56% and 83% respectively. While on the other hand, conversion of CH_4 at 923 K is slightly lower than the conversion at temperature 973 K i.e. 67% and equilibrium conversion of CH_4 at 923 K and 30 bar is 71%. But at this temperature and pressure condition, H_2 purity and CO_2 capturing efficiency according to modelling work is 84% and 61% respectively. The decrease in H_2 purity at higher temperature (973K) is due to the release of more CO_2 in the product gases

as compared to the amount of CO_2 at lower temperature. As temperature is increased from 973 K to 1050 K the drop in H_2 purity is observed from 83% to 77%. This confirms that CaO based sorbent is not efficient at temperature higher than 973 K under the conditions of 30 bar and S/C of 3.0. The optimum temperature range for SE-SMR at 30 bar and S/C of 3.0 is 873 K to 973 K. This range is used for further modelling results.

In **Figure 5.6** the dynamic profile of dry mole percent of H_2 and CO_2 at temperature range of 873-973 K is presented.

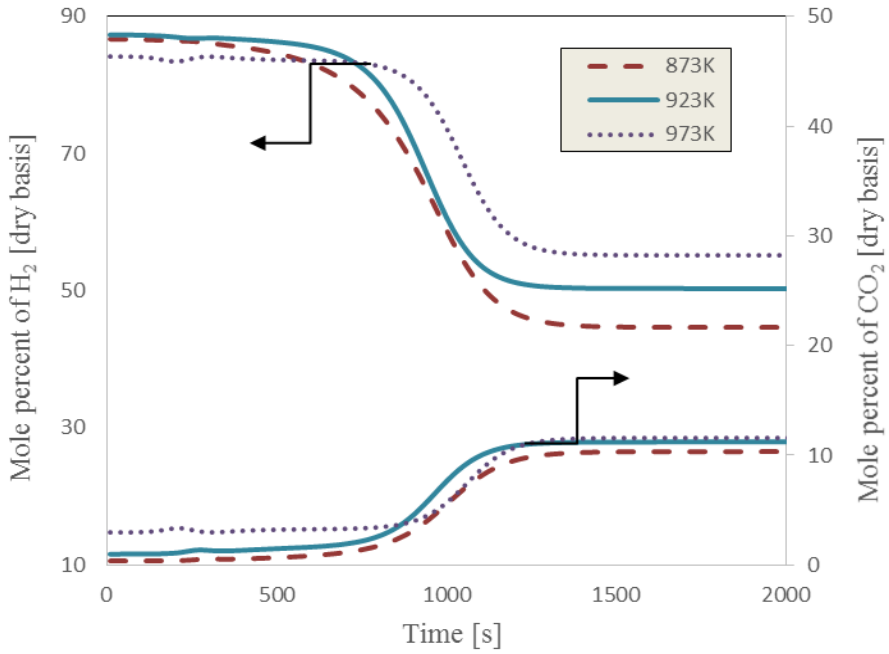

Figure 5.6: Composition profile of H_2 and CO_2 on dry basis at temperature range of 873-973 K, 30 bar, S/C of 3.0 and gas mass flux of 3.5 kg m^{-2} s^{-1}

The activity of the sorbent is higher at lower temperature (873K and 923K) while as the temperature increases beyond 923 K, the activity of sorbent decreases. In **Figure 5.6** it is quite clear that the pre-breakthrough period in case of 873 K and 923 K are smaller than the pre-breakthrough period at 973 K. The higher activity of sorbent makes the lower temperature system more preferable in cyclic process as less time is required for sorbent to reach its maximum efficiency. The mole percent of CO_2 and H_2, in the pre-breakthrough period, for SE-SMR process having 973 K as feed temperature is 2.9% and 84.1% respectively. While on the other hand, in case of 923 K the mole percent of CO_2 and H_2 is 0.3% and 87.3% respectively. Keeping in mind the activity of CaO based

sorbent, 873-923 K is the optimum range of temperature for SE-SMR under the conditions of 30 bar and S/C of 3.0.

In the post-breakthrough period, the amount of H_2 is higher at 973 K as compared to lower temperatures, as in this period only the SMR reaction is taking place and higher temperature favours the SMR process. The effect of temperature on the reforming reactions is illustrated in **Figure 5.7**.

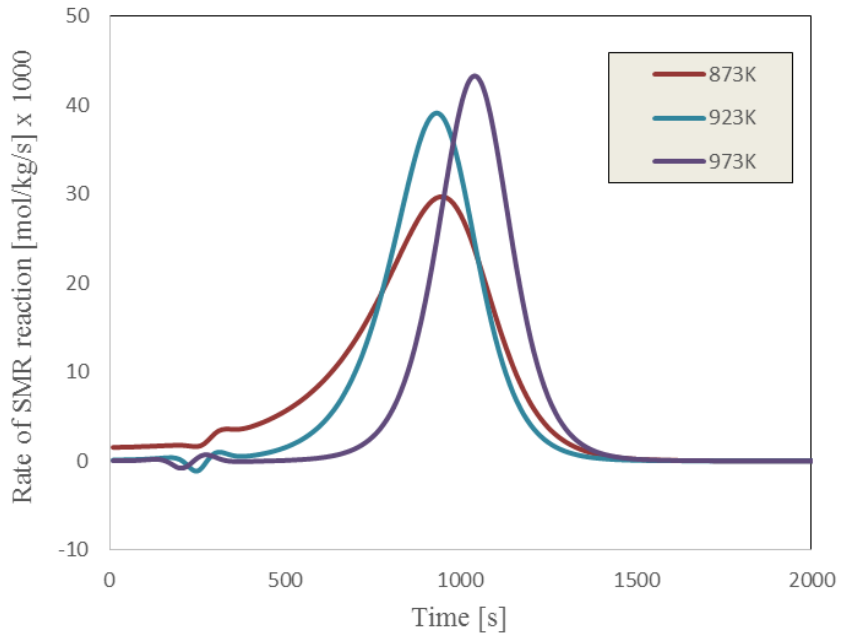

Figure 5.7: Rate of reaction profile for SMR reaction at 30 bar, S/C of 3.0 and in temperature range of 873-973 K

The rate of reforming reaction is maximum at 973 K as compared to 873 K and 923 K. The maximum values of rate of reaction at 973, 923 and 873 K are 0.04328, 0.03910 and 0.02971 mol kg^{-1} s^{-1} respectively.

The modelling results presented in **Figure 5.5, 5.6** and **5.7** portray that 923 K is the optimum temperature in terms of CH_4 conversion, H_2 purity, H_2 yield (wt. % of CH_4), CO_2 capturing efficiency and activity of sorbent for the SE-SMR process operating at 30 bar and S/C of 3.0. This temperature is favourable for SMR process as well and it is shown in **Figure 5.7.**

5.5.2.2 Effect of pressure

Temperature has a positive effect on the reforming process as seen in the previous section but according to Le Chatelier's principle, pressure has negative effect on the reforming process. Pressure has positive effect on the sorption process as absorption of CO_2 on the surface of sorbent is favourable at a pressure higher than 1 bar [19]. Thermodynamics analysis of CH_4 conversion, H_2 yield (wt. % of CH_4), H_2 purity and CO_2 capturing efficiency at different pressures is presented in **Appendix B**. These equilibrium results are reported at various pressure conditions and it is quite obvious from the results that CO_2 capturing efficiency of SE-SMR process drops from 78% to 71.0% as pressure increases from 1 bar to 30 bar. The conversion of CH_4 goes down from 95.6% to 71.0% as pressure increases from 1 bar to 30 bar. Although the equilibrium results suggest that SE-SMR process should be operated in a pressure range of 1-5 bar, the system is modelled in this section according to the conditions of a typical industrial process at 20-35 bar range. In an industrial process, highly pressurised H_2 is required downstream of the reactor and it is not feasible to generate H_2 at a lower pressure and then use high pressure compressors to pressurize it to meet the downstream pressure requirements [229]. Furthermore, high pressures are also used in the industrial SMR process in order to reduce the size of reactors, piping and storage tanks, thus saving on capital expenses and occupied space. This is the reason why in this work the performance of SE-SMR is studied at elevated pressures.

In the previous section, 923 K was selected as an optimum temperature. So the pressure effect is studied here at this constant temperature. It is observed that with the increase in pressure from 20 bar to 35 bar the conversion of CH_4 reduces from 73% to 65% whilst H_2 purity and CO_2 capturing efficiency reduce from 86 to 83% and from 64 to 59% respectively. The equilibrium results in **Figure C2 (Appendix D**) show that pressure has a positive effect on CO_2 capture and H_2 purity till 5 bar, but that as the pressure goes beyond 5 bar, the production of H_2 drops down and the amount of unconverted CH_4 rises. This results in less pure H_2 at the outlet and less partial pressure of CO_2 makes the CO_2 capture decline as well. For CO_2 to adsorb on the sorbent, the partial pressure of CO_2 in the exit of the reactor needed to be higher than the partial of CO_2 at equilibrium.

The dynamic behaviour of SE-SMR in the packed bed reactor under changing pressure and adiabatic conditions is reported in **Figure 5.8 (a-d).** The modelling results are

analysed while considering equilibrium results as reference. It is quite obvious that such high pressure can give maximum CH_4 conversion as 73.5% under the specific operating conditions of 20 bar and S/C of 3.0. To mimic the industrial scale process 30 bar pressure is picked to study the effect of other operating variables on the performance of the SE-SMR process in a packed bed reactor.

Under the conditions of 30 bar and 923 K, the equilibrium CO_2 capturing efficiency and H_2 purity are 71 % and 91% respectively. At the same operating conditions the modelling work yields 61% CO_2 capturing efficiency and 84% H_2 purity.

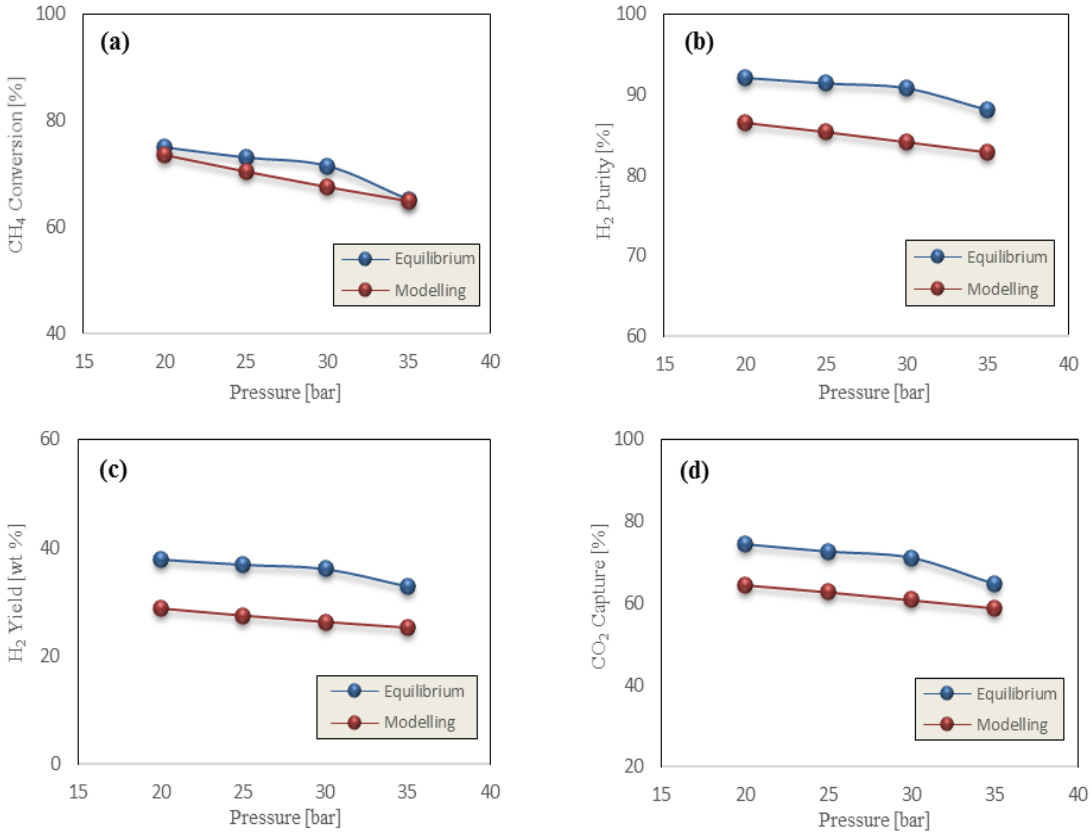

Figure 5.8: The effect of pressure on the a) CH_4 conversion; b) H_2 purity; c) H_2 yield (wt. % of CH_4) and d) CO_2 capturing efficiency at 923 K, S/C of 3.0, CaO/C of 1.0 and mass flux of 3.5 kg m^{-2} s^{-1}

The capture of CO_2 varies with pressure because pressure has significant effect on the rate of adsorption of CO_2 on the active site of the CaO based sorbent. In **Figure 5.9** the effect of pressure on the carbonation rate is illustrated. The rate of carbonation is higher at 20 bar as compared to 35 bar, hence more capture of CO_2 is expected at this pressure as compared to the higher pressures. The maximum values of carbonation rate for 20 bar

is 7.63×10^{-4} mol kg^{-1} s^{-1} and the maximum value for the carbonation rate at 35 bar is 6.27×10^{-4} mol kg^{-1} s^{-1}. This suggests that the carbonation rate is almost 1.2 times higher in case of 20 bar than 35 bar. The pre-breakthrough period at 20 bar and 35 bar is 600 s and 700 s respectively. So the sorbent reaches its maximum activity much earlier at 20 bar than 35 bar.

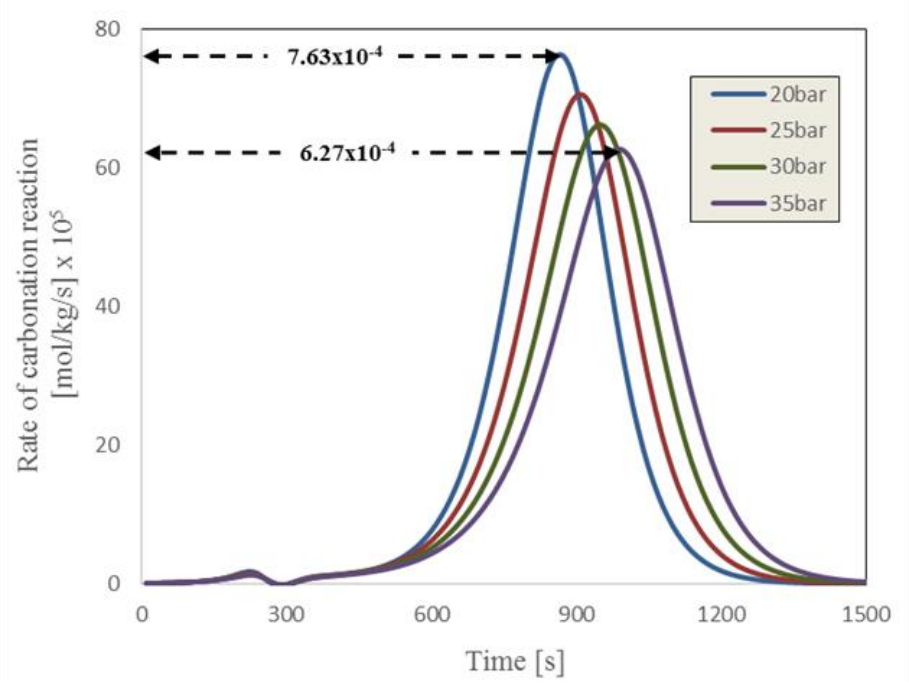

Figure 5.9: The effect of pressure on the rate of carbonation at 923 K, S/C of 3.0, CaO/C of 1.0 and mass flux of 3.5 kg m^{-2} s^{-1}

5.5.2.3 Effect of S/C

One of the parameters that plays a major role in the performance of the SE-SMR process is the amount of steam with respect to the carbon going into the reactor i.e. the molar steam to carbon ratio (S/C). The equilibrium results generated for different S/C (1-5) under atmospheric pressure conditions are presented in **Fig. D3 (Appendix D**). It is quite clear from the results that higher S/C favours the production of H_2. The sensitivity of the SE-SMR model is studied under the adiabatic conditions. Modelling results are compared with equilibrium results generated using CEA. The high pressure conditions are used for this sensitivity analysis. The comparison of modelling and equilibrium results in terms of CH_4 conversion, H_2 purity, H_2 yield (wt. % of CH_4) and CO_2 capturing efficiency is presented in **Table 5.4**. The maximum CH_4 conversion achieved is at S/C of 3.0 i.e. 67%

and under this condition H_2 purity is 84%. In **Table 5.4** results are presented for S/C range of 1-3.

Table 5.4: Effect of S/C on the CH_4 conversion, H_2 yield (wt. % of CH_4), H_2 purity and CO_2 capturing efficiency at 923 K, 30 bar and gas mass flux of 3.5 kg m^{-2} s^{-1}

S/C	CH_4 Conversion [%]		H_2 yield [wt. % of CH_4]		H_2 purity [%]		CO_2 capture [%]	
	M	E	M	E	M	E	M	E
1	32.4	34.4	12.5	17.4	58.2	67.6	28.9	34.0
2	51.7	56.2	20.1	28.3	74.7	83.5	46.1	55.8
3	67.5	71.4	26.2	36.1	84.1	90.8	60.8	71.0

** M: gPROMS modelling values; E: CEA Equilibrium values*

Tabulated results show that the higher S/C is favourable for higher conversion of CH_4. The maximum conversion of CH_4 is achieved at S/C of 3.0 and the same occurs with the purity of H_2. In **Figure 5.10**, dynamic profiles of H_2 and CO_2 are presented for various S/C (2-6). It is quite clear from the results that more steam enhances the purity of H_2. The H_2 purity increases from 74.7% to 97.5% as S/C increases from 2 to 6. The higher amount of steam in the SE-SMR process enhances the selectivity of H_2 and the less amount of CO_2 delays the carbonation rate. As can be seen in **Figure 5.10**, the pre-breakthrough period is shorter at S/C of 2 as compared to higher S/C. The pre-breakthrough period for S/C of 2 and 6 are 600 s and 1000 s respectively. It is concluded from the results that higher S/C is preferred for higher purity of H_2, CH_4 conversion and H_2 yield (wt. % of CH_4), but it reduces the overall efficiency of the process, as more energy is required to produce higher amount of steam [230]. So there is always a trade-off between the H_2 purity and the overall efficiency of the process. While keeping this in mind, in industrial processes the S/C of 3.0 is usually selected as the optimum value [231].

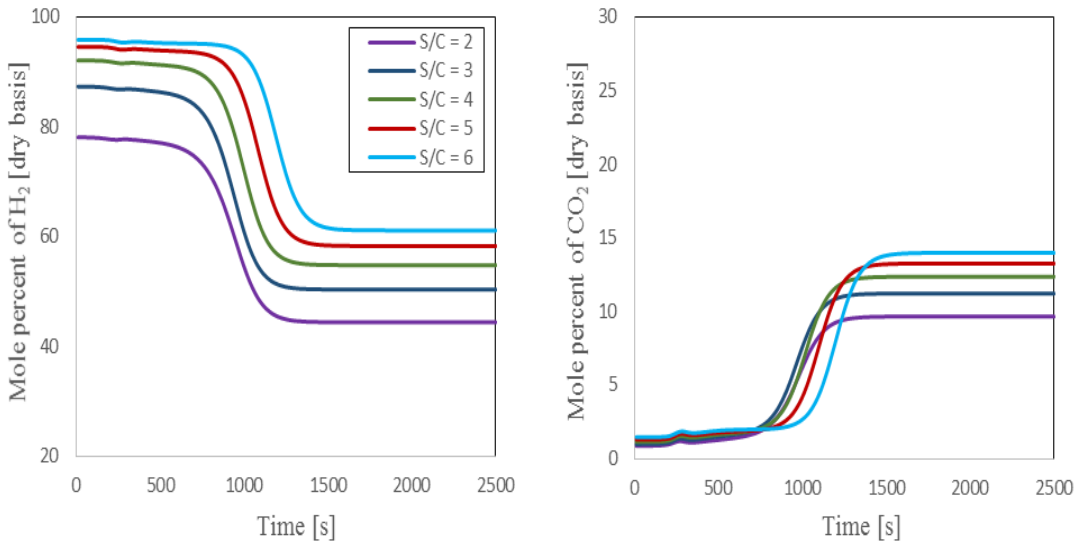

Figure 5.10: Dynamic profile of H_2 and CO_2 composition (dry basis) at the outlet of reactor for various S/C under the adiabatic conditions, at 923 K, 30 bar and 3.5 kg m^{-2} s^{-1} gas mass flux

Fernandez et al. [40] modelled the SE-SMR process for a Ca/Cu looping system and they studied the variation of temperature at the exit of the reactor for various S/C. They proposed that temperature variation is almost negligible for different S/C and the only difference they reported was the length of pre-breakthrough period [192]. In **Figure 5.11**, the dynamic profiles of temperature are presented for various S/C (2-6) and it is in excellent agreement with the literature modelling results [192]. In the initial stage, there is a slight rise in the temperature, it is because of the exothermicity of the SE-SMR process. The rise in temperature for all the S/C is about 20 K from the feed temperature. As expected from the **Figure 5.10**, the pre-breakthrough period is longer in case of higher S/C than for a lower S/C.

The minimum temperature is reached in the post-breakthrough period when all the sorbent is saturated. At this point only the conventional SMR process is taking place. In all the cases, the minimum temperature achieved is 881 K i.e. drop of 42 K from the feed temperature. **Fernandez et al.** used the high pressure conditions (35 bar) and they reported a minimum temperature of 868 K in post-breakthrough period. This shows that S/C has almost negligible effect on the overall temperature of the system.

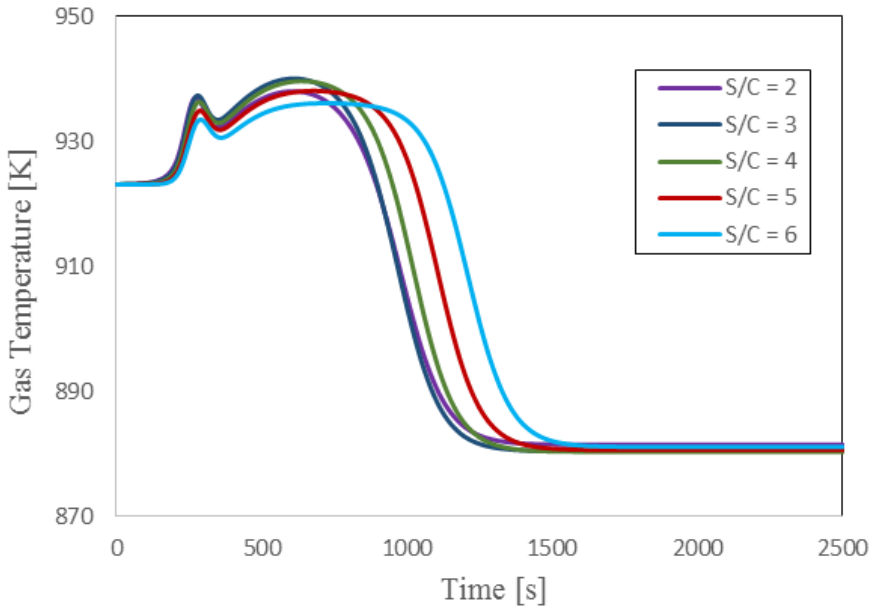

Figure 5.11: Dynamic profile of temperature at the exit of reactor for various S/C at 30 bar, 923 K feed temperature and 3.5 kg m^{-2} s^{-1} gas mass flux

5.5.2.4 Effect of gas mass flux [G_s]

The gas mass flux is another important operating variable that dictates the performance of the reactor. The selection of gas mass flux is highly dependent upon the length of the reactor and the scale of the process.

In this work, various gas mass flux conditions are used to study the effect on the performance of the SE-SMR process. In **Figure 5.12**, the dynamic variation of CO_2 and H_2 composition (dry basis) profiles are presented for various mass flow flux. The lower mass flux results in longer pre-breakthrough period as the reactants stay longer within the reactor and higher conversion of CH_4 is achieved. At mass flux of 2 kg m^{-2} s^{-1}, the conversion of CH_4 is 71%. This value is very close to the equilibrium value of 71.4% under the same operating conditions. While as the gas mass flux increases, the CH_4 conversion decreases because reactants remain for a shorter time in the reactor as compared to the lower gas mass flux. The variation in the performance of the process makes it necessary to select an optimum gas mass flux for an optimum CH_4 conversion. Although lower mass flux results in higher CH_4 conversion and H_2 purity, the pre-breakthrough period is longer as the sorbent requires more time to reach to full saturation. The pre-breakthrough period increases from 90 to 1200 s as the gas mass flux decreases

from 7 to 2 kg m^{-2} s^{-1}. In the conventional SMR process, the equilibrium concentration of the product gases at the exit of the reactor reaches at the gas velocity of 1.5-2 m/s [232]. While the carbonation reaction is slower reaction as compared to SMR, longer residence time or slow gas velocity are required to reach the equilibrium concentration of the product gases at the outlet of the reactor. Considering that for industrial PSA the switching time between adsorption and de-pressurization is 10-15 minutes, thus 3.5 kg $m^{-2}s^{-1}$ mass flux (gas velocity equivalent to 0.448 m/s) is selected as the optimum value for the SE-SMR process as it gives considerable time (11.5 min) for the sorbent to react to its full capacity without disturbing the cycle duration of the SE-SMR process. This pre-breakthrough period (11.5 min) is then comparable with the industrial time (10-15 min) required during PSA process, indicating adequate flow switching controls are possible without excessive wear and tear. At this gas mass flux CH_4 conversion and H_2 purity are 67.5% and 84.2% respectively, while the values are 71.4% and 90.8% respectively under the equilibrium conditions.

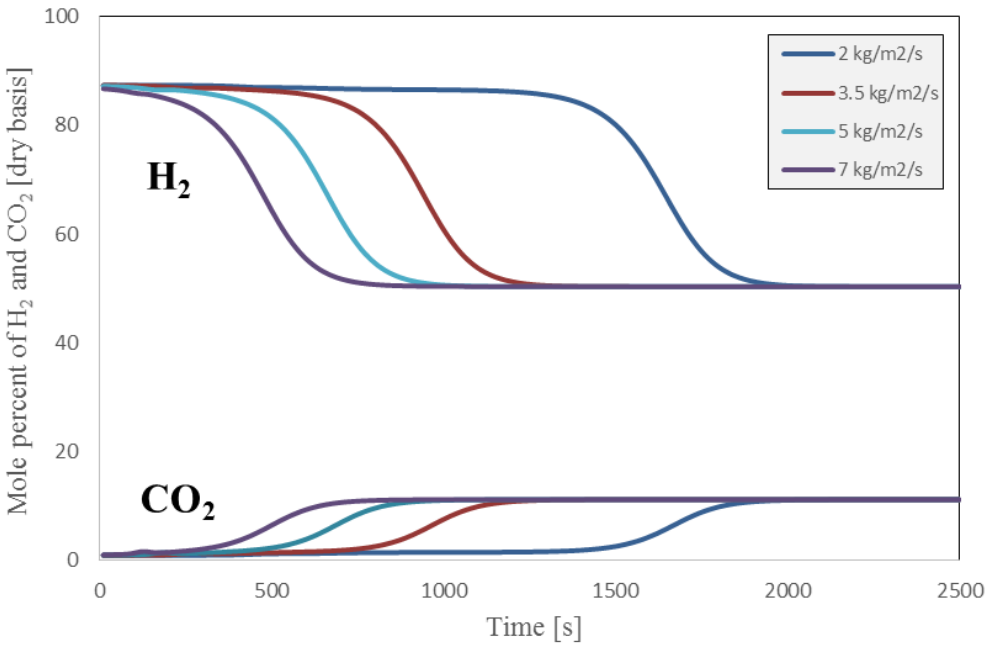

Figure 5.12: Dynamic profile of H_2 and CO_2 composition (dry basis) at the outlet of reactor for various gas mass flux under the adiabatic conditions, at 923 K, 30 bar and S/C of 3.0

5.5.3 Comparison of SE-SMR and SMR processes

The outputs of SE-SMR model, obtained on gPROMS, favour high temperature, low pressure, high S/C and low gas mass flux for a better performance of the system in terms

of CH_4 conversion and H_2 purity. To compare the performance of the SE-SMR system with the conventional SMR process, optimum values obtained through sensitivity analysis in previous sections are used. The equilibrium values for SE-SMR and SMR under various operating conditions are presented in **Appendix D**.

In **Figure 5.13** the effluent composition (dry basis) profiles are presented for SE-SMR and SMR under the operating conditions of 923 K, 30 bar, S/C 3.0 and gas mass flux of 3.5 kg m^{-2} s^{-1}. The percent compositions of H_2 and CO_2 at equilibrium under the same operating conditions are also presented in this figure. The modelling results show that the composition of CO_2 is almost zero until 700 s in the case of SE-SMR process and after ~1500 s (~25 min) CO_2 composition in the SMR and SE-SMR process becomes equal to each other. This indicates that the sorbent is active at the start and adsorption of CO_2 makes the profile of CO_2 different than the CO_2 profile in the SMR process. In case of the SE-SMR model, the composition of H_2 is 87% while in SMR model its value is almost 50%. In the post-breakthrough period ($t \geq 1500$ s) the sorbent is not inert hence both SE-SMR and SMR processes yield the same composition for CO_2 and H_2.

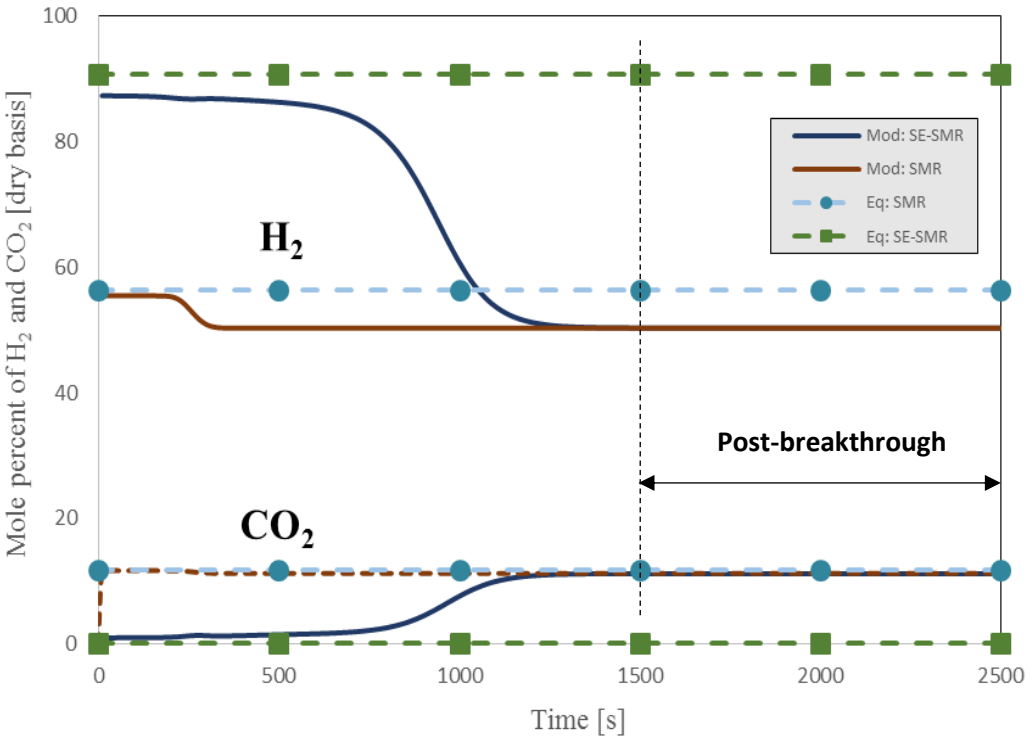

Figure 5.13: Effluent mole percent profile of H_2 and CO_2 in SE-SMR and SMR process at 923 K, 30 bar, S/C of 3.0 and gas mass flux of 3.5 kg $m^{-2}s^{-1}$

The adsorption of CO_2 on the active site of the sorbent is highly exothermic reaction and it releases considerable amount of heat (-357.6 kJ mol^{-1}_{CaO}). This heat is favourable for reforming reactions. The excessive heat makes the SE-SMR process more favourable than conventional SMR process. The enhancement in conversion of CH_4 due to CO_2 sorption is calculated. The CH_4 conversion enhancement in SE-SMR process shows the advantage of using a sorbent within the system as shown in **Figure 5.14**. The conversion enhancement factor 'E (t)' is calculated as;

$$E(t) = \frac{(X_{CH4})_{ad} - (X_{CH4})_{nad}}{(X_{CH4})_{nad}} \times 100 \quad (5.14)$$

$(X_{CH4})_{ad}$ is the conversion of CH_4 achieved in the presence of adsorbent (ad) and $(X_{CH4})_{nad}$ is the conversion of CH_4 achieved in the absence of adsorbent (nad). The value of E(t) > 0 indicates conversion enhancement because of the sorbent. The enhancement in CH_4 conversion decreases at the onset of the breakthrough period when the sorbent begins to saturate. As can be seen, conversion enhancement is zero in the post-breakthrough period.

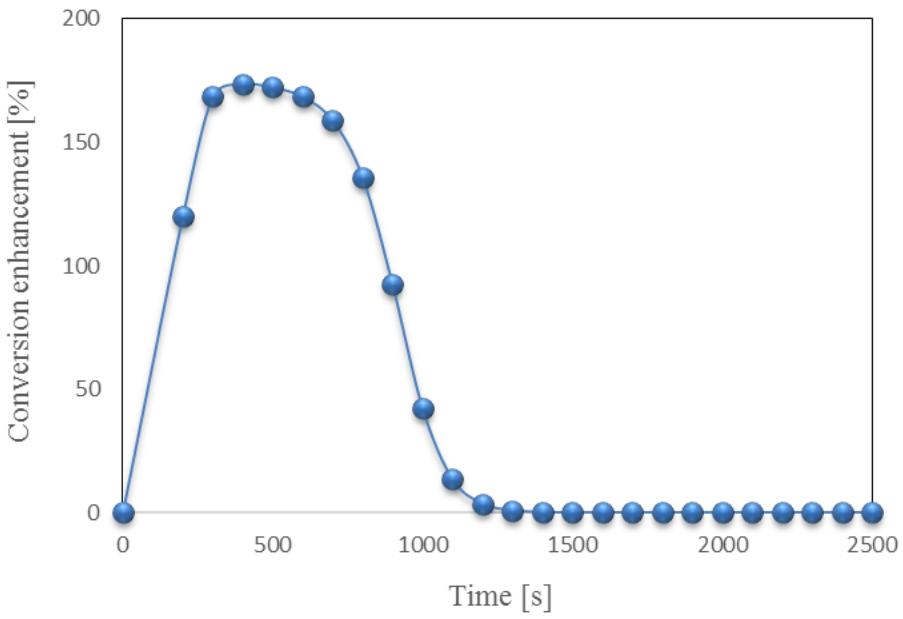

Figure 5.14: CH_4 conversion enhancement at 923 K, 30 bar, S/C of 3.0 and mass flux of 3.5 kg $m^{-2}s^{-1}$

The presence of sorbent with catalyst actually enhances the overall reaction rates by shifting the temperature of the system and eliminating the negative effect of the reverse reaction. The comparison of the temperature profile for both SE-SMR and SMR is presented in **Figure 5.15.**

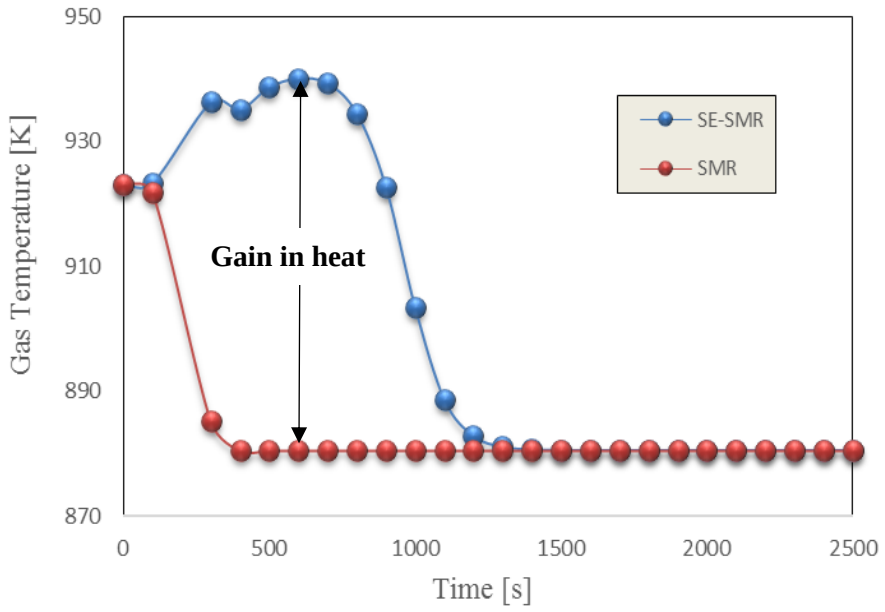

Figure 5.15: Comparison of temperature profiles generated at the exit of the packed bed reactor in SE-SMR and SMR processes under the operating conditions of 923 K, 30 bar, S/C of 3.0 and gas mass flux of 3.5 kg $m^{-2}s^{-1}$

5.6 Conclusion

The one-dimensional SE-SMR model developed on gPROMS model builder shows an excellent agreement with the experimental data reported in the literature. The mathematical model under both adiabatic and non-adiabatic conditions behaves well according to the literature data. Operating parameters, such as; temperature, pressure, S/C and gas mass flux have strong influence on the performance of the SE-SMR process. The optimum temperature obtained under the high pressure (30 bar) conditions is 923 K. This temperature yields 67.5% CH_4 conversion at S/C of 3.0 and 30 bar. The purity of H_2 achieved at the same conditions is 84.1%. While studying the effect of pressure at this optimum temperature, it is observed that pressure higher than 5 bar has negative effect on the conversion of CH_4 and H_2 purity. The selection of optimum pressure for industrial scale is a trade-off between the couple (H_2 purity, CH_4 conversion) and the couple (downstream pressure requirements, plant size). The pressure as high as 30 bar is considered as an optimum in this study as it fulfils the requirement of industrial constraints and gives a considerable purity of H_2 (84.1%). It is concluded from the results that higher S/C is preferred for higher purity of H_2, CH_4 conversion and H_2 yield (wt. %

of CH_4), but it reduces the overall efficiency of the process, as more energy is required to produce the required amount of steam. The S/C higher than 4 has no significant effect on CH_4 conversion, so the S/C of 3.0 is selected as the optimum value. The selection of optimum gas mass flux is done on the basis of operational time of the process and H_2 purity achieved at the outlet of reactor. The gas mass flux of 2 kg m^{-2} s^{-1} has onset of pre-breakthrough period at 1200 s while in case of gas mass flux of 7 kg m^{-2} s^{-1}, this period is 90 s. The gas mass flux of 3.5 kg m^{-2} s^{-1} is selected as the optimum value having pre-breakthrough period 700 s and 67.5% CH_4 conversion against equilibrium conversion of 71.4%. Furthermore, the comparison of SE-SMR and SMR process shows the CH_4 conversion enhancement due to the presence of the sorbent in the reactor. The adsorption of CO_2 on the active surface of the sorbent is highly exothermic process and it releases considerable amount of heat (-357.6 kJ mol^{-1}_{CaO}). This heat promotes the reforming reactions and CH_4 conversion above conventional SMR is achieved (180% CH_4 conversion enhancement). The developed model of SE-SMR will be further modified for sorption enhanced chemical looping steam reforming (SE-CLSR) process in the next chapter.

CHAPTER # 6

SORPTION ENHANCED CHEMICAL LOOPING STEAM METHANE REFORMING

The objective of this chapter is to develop the mathematical model of sorption enhanced chemical looping steam methane reforming (SE-CLSR) process by using 18 wt. % $NiO/\alpha Al_2O_3$ as a catalyst and calcium oxide (CaO) as a carbon dioxide (CO_2) sorbent. This model is the combination of the sorption enhanced steam methane reforming (SE-SMR), reduction of the catalyst followed by the oxidation of the reduced catalyst models. The individual models of the reduction and oxidation are developed by using kinetic data available in the literature and later on validated against the experimental results published in the literature. The model of SE-SMR process is combined with the reduction model to study the process happening in the fuel reactor (FR). This FR model is combined with the air reactor (AR) and complete model is run for 10 cycles. At the end of the chapter, a comparison is made between conventional steam methane reforming (SMR), SE-SMR and SE-CLSR process in terms of CH_4 conversion, H_2 purity, H_2 yield (wt. % of CH_4) and CO_2 capturing efficiency.

6.1 Introduction

Steam methane reforming (SMR) process is a well-known industrial process for hydrogen (H_2) production. The higher endothermicity of the process makes it to operate at high temperature (800-1000 °C) and pressure (20-35 atm) conditions. In industrial SMR process for H_2 production, shift reactors are needed at the downstream to convert the undesired CO and CO_2 into desired H_2 product. Later on, amine scrubbing or pressure swing adsorption (PSA) process is required to achieve the higher purity of H_2 product [32]. Keeping in mind the issue of global warming, researchers developed the concept of combining the reforming process with in-situ CO_2 separation. This process was named as sorption enhanced steam methane reforming (SE-SMR) process [32-34]. As discussed in **Chapter 5,** the addition of sorbent (CO_2 sorbent) along with the catalyst promotes the

performance of the reforming process not only by shifting the process towards more H_2 production but also in terms of purity of H_2 (CO_2 free product) as well as suppressing equilibrium solid carbon by-product and permitting both lower temperatures of operations and steam demand.

The H_2 yield depends upon the type of CO_2 sorbent used. The selection of CO_2 sorbent or acceptor depends upon its CO_2 capturing capacity, its stability after multi-cycles of operation and on its adequate sorption/desorption kinetics [220]. Calcium oxide (CaO) is found to be the best sorbent of CO_2 and resulted in 99% H_2 purity [104, 221]. CaO is a low cost sorbent and is considered as the most prominent sorbent for the CO_2 sorption under the reforming conditions. CaO shows good capacity of CO_2 capturing, good thermodynamics properties and good kinetics as compared to the other sorbents such as Li_2ZrO_3, $KLiZrO_3$, Li_4SiO_4 and Na_2ZrO_3. Spanish dolomite and calcite are good sorbents as well and they show very high capacity for CO_2 adsorption [10]. CaO has adsorption capacity of 0.79 g_{CO2}/g_{CaO}, while its close competitor calcined dolomite (CaO.MgO) has the adsorption capacity of 0.46 $g_{CO2}/g_{sorbent}$. But as far as the multi cycle tests are concerned, dolomite has improved performance as compared to the CaO [222]. The carbonation of CaO is favourable in a temperature range of 600-750 °C under the atmospheric pressure. While, the regeneration of the carbonated sorbent is a high temperature process and occurs at 850-1000 °C under atmospheric pressure.

Blamey et al. [223] found that after multi-cycles the reactivity of the CaO particles reduces. In previous studies, researchers concluded that addition of steam can enhance the carbonation reaction. The steam first reacts with available CaO and formed intermediate product i.e. $Ca(OH)_2$. Later, this intermediate product undergoes carbonation reaction [39, 225, 233]. The reaction mechanism is as follow;

$$CaO_{(s)} + H_2O_{(g)} \rightarrow Ca(OH)_{2(s)} \qquad \Delta H_{298K} = -109.18 \text{ kj mol}^{-1} \qquad (6.1)$$

$$Ca(OH)_{2(s)} + CO_{2(g)} \leftrightarrow CaCO_{3(s)} + H_2O_{(g)} \quad \Delta H_{298K} = -69.14 \text{ kj mol}^{-1} \qquad (6.2)$$

The main driving force for this adsorption of CO_2 on the active surface of the sorbent is the partial pressure of CO_2 between the surface of the sorbent and the reaction phase [224].

In 2000, **Lyon** and **Cole** proposed an interesting concept of H_2 production process. As conventional SMR requires high temperatures, and to avoid the issues caused by the overheating and material failure, a new process was introduced which was termed as

'unmixed reforming'. **Lyon et al.** and **Kumar et al.** defined 'unmixed steam reforming' (USR) and applied it specifically to a reactor configuration in packed bed by using atlernative feed flows [35, 234, 235]**.** The USR process was defined as an auto-thermal cyclic steam reforming process for converting hydrocarbon fuels into H_2 product. In this process fuel and air are not directly mixed but separately passed over the surface of the catalyst [35]. First, air is introduced on the surface of the catalyst, then it is discontinued, and fuel with steam is introduced after that either together or consecutively. The USR process uses oxygen transfer material (OTM) to provide heat for the endothermic steam methane reaction. During the reduction of OTM, metal is regenerated and undergoes the cycle of reforming with the fuel gas and steam [10, 81]. **Kumar et al.** [22] compared the USR and conventional SMR process as shown in **Table 6.1**.

Table 6.1: Comparison of USR and SMR processes [22]

Parameters	**Conventional SMR**	**USR**
Cost	Elevated temperature (900-1100 °C) causes decline in tubes life period, a costly process	Less costly (5-10 times) than conventional SMR
Efficiency	Heat transfer is not efficient (50% of heat is used for pre-heating), lower process efficiency	Higher process efficiency (> 90%)
Equilibrium	At temperature about 600 °C CH_4 conversion is less and it increases at a very high temperature. So reaction does not reach to its completion.	Reactions reached towards more equilibrium conditions at lower temperature than SMR process
Catalyst effectiveness	Due to high L/D ratio more catalyst particles are required and this causes more pressure drop in the bed. Due to large particles most of the catalyst remains unutilized.	Effectiveness factor of the catalyst is high
Coke formation	Chances of coke formation are always there	Coke is either suppressed or cyclically burnt off under oxidation of UMR

Sulphur tolerance	Accumulates as sulphates on catalyst (poisoning)	Allegedly desorbs as SO_2 under oxidation of UMR

The concept of unmixed combustion was studied in 1950 and this gives rise to the term chemical looping combustion (CLC) [71, 236, 237]. The terminology originally applied to the reactor configurations with moving bed reactors. The CLC makes way for new process chemical looping reforming (CLR) process. The CLR process too works on the same chemical principle as that of USR. The comparison of CLC and CLR process is shown in the **Figure 6.1** [238].

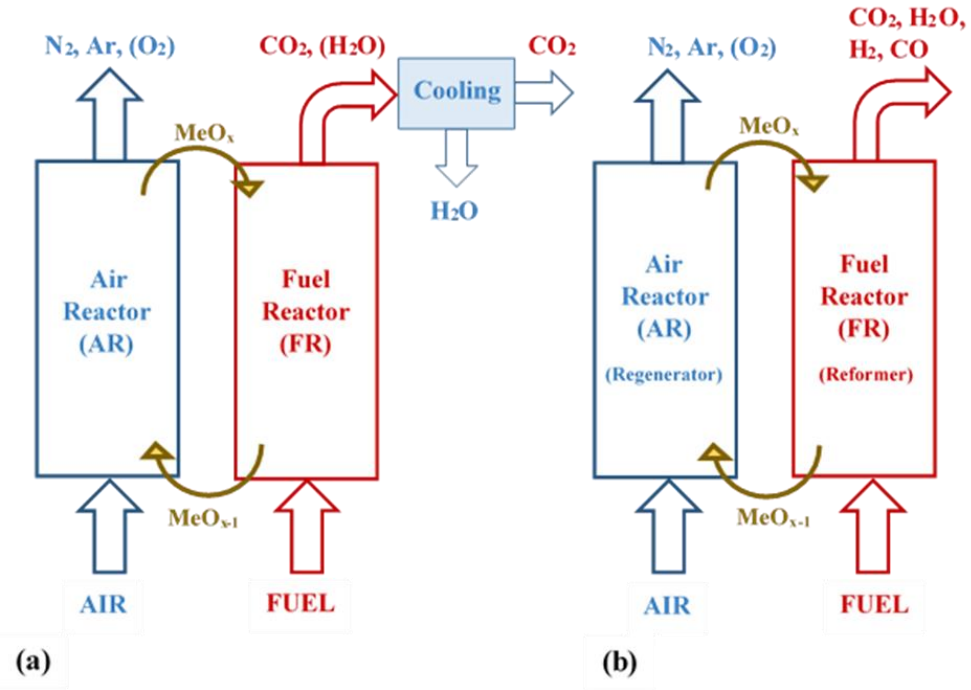

Figure 6.1: Comparison of chemical looping combustion (CLC, **a**) and chemical looping reforming (CLR, **b**) process [238]

The CLR process operates in alternative cycles between 'steam reforming' and 'regeneration of the catalyst particles'. The heat generated during the oxidation of metal oxide is utilized in the endothermic steam reforming reaction. In the fuel reactor (FR), reforming and reduction reactions take place (**Eq. 6.3-6.5**) while in the air reactor (AR) the regeneration of the catalyst takes place via oxidation reactions (**Eq. 6.6**). Iron, nickel, copper and manganese are the most promising OTM. The characteristics of all these metal oxides (Fe_2O_3, NiO, CuO and Mn_2O_3) were investigated in literature on the basis of their reactivity, regeneration ability and their ability to avoid carbon deposition. NiO was found

the best amongst all these and it shows high selectivity towards H_2 production. NiO does not agglomerate after many cycles of oxidation and reduction. Mn_2O_3 shows some minor signs of agglomeration, CuO does not show any structural change at 800 °C but Fe_2O_3 shows a complete change of its structure at 900 °C. So the reactivity was in the order of NiO/SiO_2 > CuO/SiO_2 > Mn_2O_3/SiO_2 > Fe_2O_3/SiO_2 [239]**.** Ni is the most interesting amongst all of the available OTM for reforming because of its strong catalytic properties [240]. The reaction scheme proposed by **Kumar et al.** [22] in the fuel and the air reactor is given as:

Fuel Reactor;

$$CH_{4(g)} + H_2O_{(g)} \leftrightarrow CO_{(g)} + 3H_{2(g)} \qquad \Delta H_{298K} = +206 \text{ kj mol}^{-1} \qquad (6.3)$$

$$CO_{(g)} + H_2O_{(g)} \leftrightarrow CO_{2(g)} + H_{2(g)} \qquad \Delta H_{298K} = -41 \text{ kj mol}^{-1} \qquad (6.4)$$

$$NiO_{(s)} + \frac{1}{4}CH_{4(g)} \rightarrow \frac{1}{4}CO_{2(s)} + \frac{1}{2}H_2O_{(g)} + Ni_{(s)} \qquad \Delta H_{298K} = +43.7 \text{ kj mol}^{-1} \qquad (6.5)$$

Air Reactor;

$$Ni_{(s)} + \frac{1}{2}O_{2(g)} \rightarrow NiO_{(s)} \qquad \Delta H_{298K} = -244 \text{ kJ mol}^{-1} \qquad (6.6)$$

Later on, **Lyon** and **Cole** proposed another interesting approach by combining the CLR and SE-SMR process. This concept was later named as the sorption enhanced chemical looping steam reforming (SE-CLSR) process. In this process, the carbonation reaction (**Eq. 6.7**),

$$CaO_{(s)} + CO_{2(g)} \leftrightarrow CaCO_{3(s)} \qquad \Delta H_{298K} = -178.8 \text{ kj mol}^{-1} \qquad (6.7)$$

in the FR is used to enhance the performance of the reforming reaction, and the heat of the catalyst oxidation was used for the regeneration of the sorbent [35, 37]. **Rydén et al.** [19] used three interconnected fluidized bed reactor having NiO as OTM and CaO as CO_2 sorbent. The FR or reforming reactor was operating at low temperature. They considered the SMR reactions, reduction of OTM (**Eq. 6.3-6.5**) and sorption of CO_2 on the surface of CaO (**Eq. 6.7**) in the reforming reactor system. The overall reaction heat makes the process thermo-neutral in nature. In calcination reactor, they used steam to regenerate the sorbent (reverse reaction of carbonation, **Eq. 6.7**) and catalyst was re-oxidized (**Eq. 6.6**) in the AR. As the oxidation reaction is highly exothermic reaction so the AR operated at much higher temperature as compared to FR.

Rydén et al. [19] developed a process model of SE-CLSR process on Aspen plus. Three interconnected fluidized bed reactors and three cyclones were used to simulate the whole process. The reactors were modelled on the basis of minimizing Gibbs free energy and it was observed that the process operated at 580 °C and 1 bar produced almost 99% pure H_2 with 95% CO_2 capture. **Pimenidou et al.** [39] proposed the packed bed reactor system for H_2 production from waste cooking oil. In the experimental work, reactor system contained NiO (18 wt. % NiO supported on Al_2O_3 from Johnson Matthey) as OTM and CaO as sorbent. **Kulkarni et al.** [38] proposed the gasification technology for the production of H_2 and sequestration ready CO_2. They produced the high purity of H_2 with almost zero emission of CO_2. The efficiency of the process was better than the integrated gasification combined cycle (IGCC) process with conventional CO_2 separation.

The mathematical modelling of the SE-CLSR process in a packed bed is not reported in the literature. To fill this gap, a one-dimensional mathematical model of the SE-CLSR process is developed and implemented in gPROMS model builder 4.1.0® for the solution of model equations in this work. The overall model is divided into sub-models of the FR and AR, representing the reactor operating under fuel and steam feed, and the reactor operating under air or O_2-enriched air stream, respectively. This may apply to a single reactor with alternating feed streams, or to several reactors operated with staggered feeds, similar to PSA reactors or regenerative heat exchangers. The modelling of reduction and oxidation mechanisms is discussed first, followed by the overall modelling of the SE-CLSR process as shown in **Figure 6.2**. The sub-models (oxidation/SE-SMR/reductions) are also validated against the experimental data reported in the literature [41, 43, 241]. Before starting the modelling work, equilibrium results for SE-CLSR under various operating conditions of temperature, pressure, steam to carbon ratio (S/C), CaO/C and NiO/C are generated using chemical equilibrium with application (CEA) software. The thermodynamic results for SMR, SE-SMR and SE-CLSR processes are compared in terms of CH_4 conversion, H_2 yield, H_2 purity and CO_2 capturing efficiency.

The mathematical model of SE-SMR process is already discussed in **Chapter 5**. This model is used in the FR along with the reduction model. The reactions and kinetic rate equations used to model the process, shown in **Figure 6.2**, are listed in **Table 3.4**.

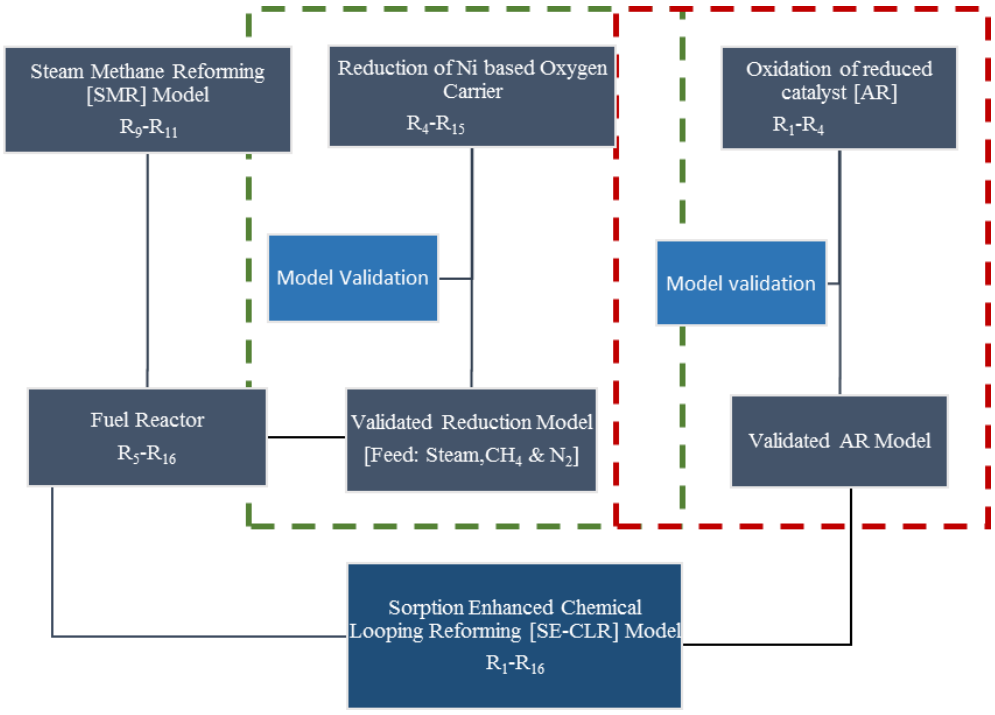

Figure 6.2: Hierarchy of modelling methodology adopted for the SE-CLSR process

6.2 Thermodynamic analysis of the SE-CLSR process

Prior to the modelling of the SE-CLSR process, sensitivity analysis under equilibrium conditions is carried out to find out the optimum conditions for the SE-CLSR process. **Andy et al.** [242] performed the thermodynamic analysis using Aspen Plus and compared SMR, SE-SMR and SE-CLSR processes. The pressure range they used for the analysis was 1-10 bar, while in the industrial processes for H_2 production the pressure range used is 20-35 bar. In this work, CEA is used to generate the equilibrium results. The effect of temperature, pressure, S/C, CaO/C and NiO/C on CH_4 conversion, H_2 purity, H_2 yield and CO_2 capturing efficiency is studied under the equilibrium conditions. To calculate the conversion of CH_4, the purity of H_2, H_2 yield (wt. % of CH_4) and CO_2 capturing efficiency following equations are used, where 'n' represents relevant molar amounts;

$$CH_4 \text{ Conversion } [\%] = \frac{(n_{CH4,in} - n_{CH4,out})}{n_{CH4,in}} \text{x } 100 \quad (6.8)$$

$$H_2 \text{ Purity } [\%] = \frac{n_{H2,out}}{(n_{H2,out} + n_{CH4,out} + n_{CO,out} + n_{CO2,out})} \text{x } 100 \quad (6.9)$$

$$H_2 \text{ Yield } [\text{wt. \% of } CH_4] = \frac{(\text{mol. weight of } H_2 \text{ x } n_{H2,out})}{(\text{mol. weight of } CH_4 \text{ x } n_{CH4,in})} \text{x } 100 \quad (6.10)$$

CO_2 Capture [%]

$$= \frac{\left(n_{CH4,in} - n_{CH4,out} - n_{CO,out} - n_{CO2,out}\right)}{n_{CH4,in}} \text{x } 100 \qquad (6.11)$$

6.2.1 Effect of pressure

Although low pressure favours both SMR and SE-SMR, to investigate the SE-CLSR process with respect to its application in industrial process, elevated pressure (20-30 bar) conditions are used. In **Figure 6.3 (a-d)** effect of pressure on CH_4 conversion, H_2 purity, H_2 yield (wt. % of CH_4) and CO_2 capturing efficiency is shown. The effect of pressure is studied in the pressure range of 1-30 bar. As it was predicted, higher pressure gives the lower conversion of CH_4 but still higher than the conversion achieved in case of SMR and SE-SMR processes under the same operating conditions. The drop in CH_4 conversion in SE-CLSR process is from 98.4% to 79.5% as the pressure increases from 1-30 bar. In the range of 20-30 bar, drop in CH_4 conversion is 85.0% to 79.5%. The effect of pressure on H_2 purity is shown in **Figure 6.3 (b)**. It is clear that H_2 purity increases as pressure increases from 1-5 bar. The increase in H_2 purity is 95.5% to 97.2% as pressure increases from 1-5 bar. As pressure increases beyond 5 bar, the drop in H_2 purity is observed. H_2 purity goes down to 92.7% at 30 bar. Under the same conditions, drop in H_2 purity for SMR and SE-SMR is 76.4-56.5% and 94.4-90.8% respectively. So the purity of H_2 is higher in case of SE-CLSR process as compared to SMR and SE-SMR processes. In **Figure 6.3 (c)**, the yield of H_2 is lower in case of SE-CLSR as compared to SE-SMR process. The reduction of NiO in SE-CLSR process yields more carbon containing products (CO and CO_2) than H_2, hence lower yield of H_2 is achieved. On the other hand, reduction process is not considered in SE-SMR process. Hence, higher yield of H_2 as compared to SE-CLSR process is observed. In **Figure 6.3 (d)**, CO_2 capturing efficiency results show that higher pressure causes drop in CO_2 capturing efficiency. In case of SE-CLSR, the drop in CO_2 capturing efficiency is from 84.08% to 79.06% as pressure moves from 1-30 bar. It can be seen that there is increase in CO_2 capturing efficiency as pressure moves from 1-10 bar, as in this range the partial pressure of CO_2 is higher than the equilibrium partial pressure, hence the carbonation reaction shifts towards product side [34].

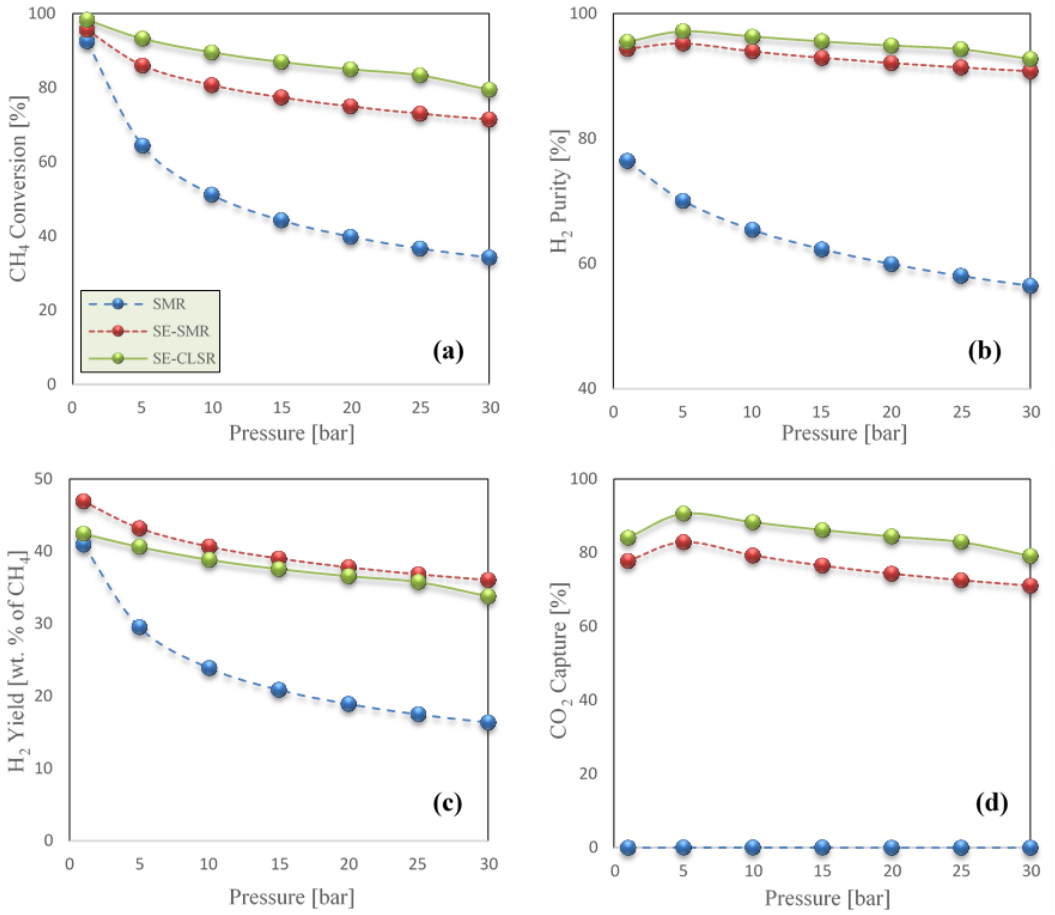

Figure 6.3: The effect of pressure on a) CH_4 conversion; b) H_2 purity; c) H_2 yield (wt. % of CH_4) and d) CO_2 capturing efficiency at 923 K, S/C of 3.0, CaO/C of 1.0 and NiO/C of 0.5

6.2.2 Effect of temperature

To study the effect of temperature on CH_4 conversion, H_2 purity, H_2 yield (wt. % of CH_4) and CO_2 capturing efficiency for SMR, SE-SMR and SE-CLSR processes, high pressure (30 bar) condition is used. The increase in CH_4 conversion is from 22.4% to 86.1% as temperature varies from 300 °C to 800 °C in the SE-CLSR process. CH_4 conversion in SE-CLSR is higher than SMR and SE-SMR. H_2 purity and CO_2 capturing efficiency follow the same trend. In **Figure 6.4 (b)**, the maximum H_2 purities achieved at 973 K are 93.9% and 91.0% in SE-CLSR and SE-SMR process respectively. The temperature of the system above 973 K causes a drop in H_2 purity as the carbonation reaction (**Eq. 6.7**) deactivates at such a high temperature in favour of calcination, hence the drop in CO_2 capturing efficiency observed as shown in **Figure 6.4 (d)**. It is concluded that under high

pressure (30 bar) condition, 923-973 K temperature range is the optimum range for SE-CLSR process.

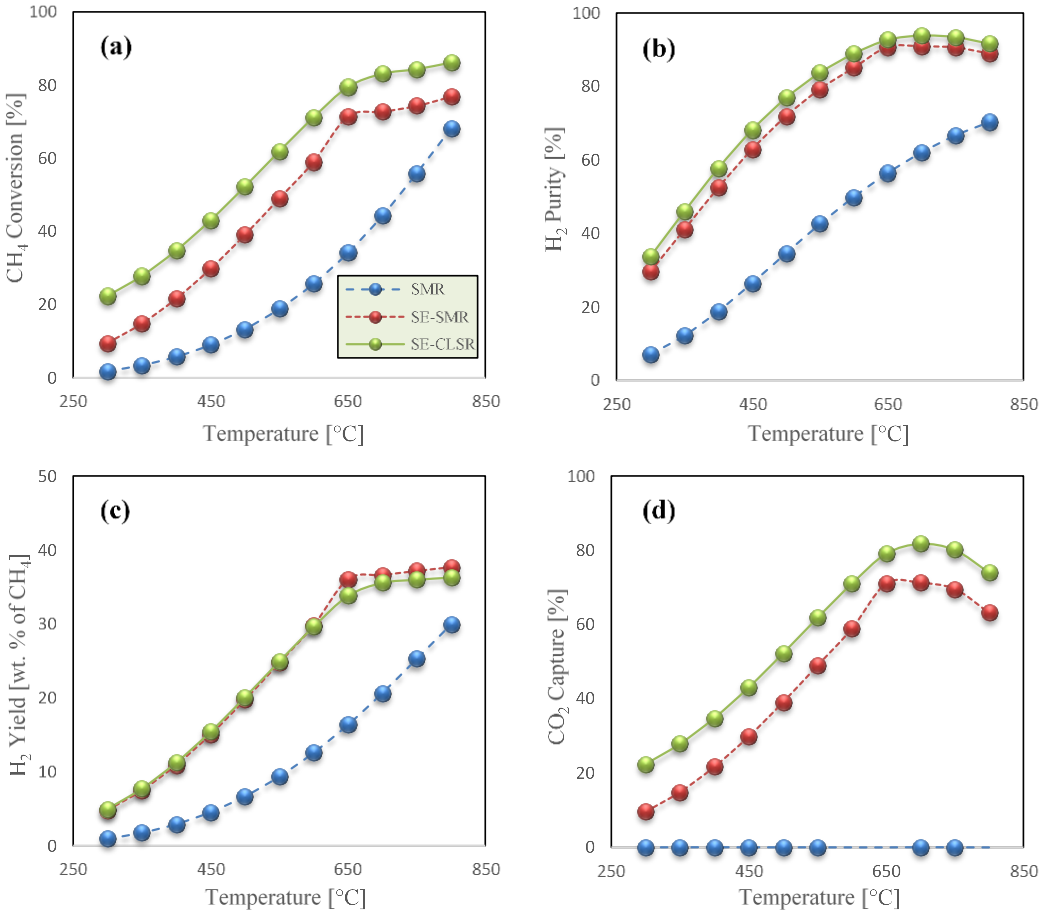

Figure 6.4: The effect of temperature on the a) CH_4 conversion; b) H_2 purity; c) H_2 yield (wt. % of CH_4) and d) CO_2 capturing efficiency at 30 bar, S/C of 3.0, CaO/C of 1.0 and NiO/C of 0.5

6.2.3 Effect of S/C

As in the reforming reactions, steam is required to convert the CH_4 into H_2 product. Excess of steam favours the reforming reaction towards more production of H_2. Although higher S/C (>2) favours CH_4 conversion and causes more formation of CO_2, this causes increase in the carbonation and hence promotes H_2 purity. But higher steam requirement has a negative impact on the overall operational cost of the process, as energy is required to produce large quantity of steam. So there is always a trade-off between the selection of S/C and overall operational cost of the process. On an industrial scale, S/C of 3.0 is preferred for reforming reactions. Under the equilibrium conditions the comparison of the

CH_4 conversion and H_2 purity in SMR, SE-SMR and SE-CLSR processes at 923 K, 30 bar and S/C of 3.0 is presented in **Table 6.2.**

Table 6.2: Comparison of SMR, SE-SMR and SE-CLSR processes in terms of CH_4 conversion and H_2 purity under the operating conditions of 923 K, 30 bar and S/C of 3.0

Process	CH_4 conversion [%]	H_2 purity [%]
SMR	34.2	56.5
SE-SMR	71.4	90.8
SE-CLSR	79.5	92.7

6.2.4 Effect of CaO/C and NiO/C

The effect of the amount of CaO based sorbent on the performance of SE-CLSR process is shown in **Figure 6.5 (a-c)**. The maximum increase in CH_4 conversion is observed at CaO/C of 0.8 i.e. 80.5%. Further increase in amount of CaO (> 0.8) has a negative effect on CO_2 capturing efficiency. Similarly, the purity of H_2 and H_2 yield (wt. %) increases with CaO/C as shown in **Figure 6.5 (b-c).** The purity of H_2 increases from 55.2% to 92.7% whereas the yield increases from 15.6% to 33.8% as CaO/C increases from 0-1. However, when H_2 yield is calculated on the basis of CH_4 available for steam reforming (i.e. not counting CH_4 used in NiO reduction), the H_2 yield varies from 17.8% to 38.6% for SE-CLSR. So the CaO/C between 0.8-1.0 is considered as the optimum ratio for SE-CLSR process under the conditions of 30 bar, 923 K and S/C of 3.0.

As the amount of NiO increases in the reactor, CH_4 conversion also increases as there is more demand in NiO reductant. But this makes less CH_4 available for reforming reactions hence lower yield of H_2 is achieved as shown in **Figure 6.6 (b)**. The yield (wt. % of CH_4) of H_2 drops from 36.1% to 31.7% as NiO/C increases from 0-1. Slight improvement in H_2 purity is observed as more conversion of CH_4 makes more H_2 and CO_2, so carbonation (**Eq. 6.7**) shifts towards solid product. This results in H_2 with higher purity. The purity of H_2 increases from 90.8% to 95.2% as NiO/C increases from 0-1.0. This makes a trade-off between the yield of H_2 and CH_4 conversion during SE-CLSR process. The NiO/C of 0.5 is picked as optimum ratio as it gives CH_4 conversion, CO_2 capturing efficiency, H_2 purity and H_2 yield (wt. % of CH_4) as 79.46%, 79.06%, 92.74% and 33.8% respectively.

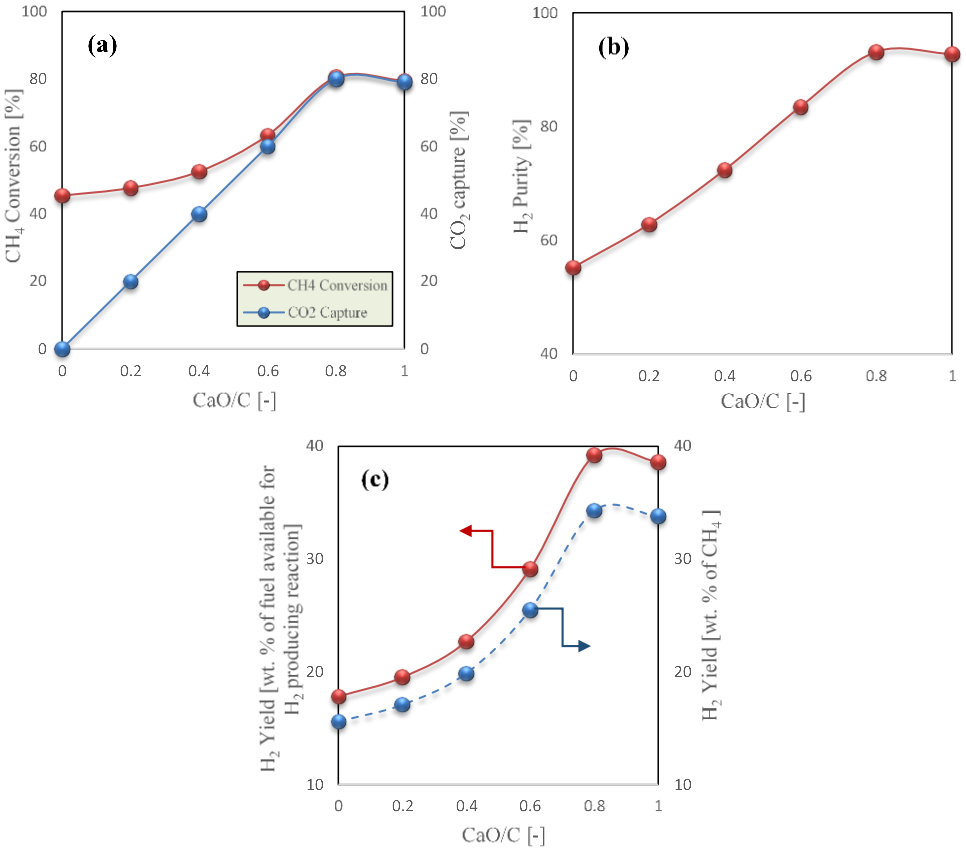

Figure 6.5: Effect of CaO/C on the a) CH_4 conversion; CO_2 capturing efficiency; b) H_2 purity; and c) H_2 yield (wt. % of CH_4); H_2 yield (wt. % of fuel available for H_2 producing reaction i.e. SR) at 30 bar, 923 K, S/C of 3.0 and NiO/C of 0.5

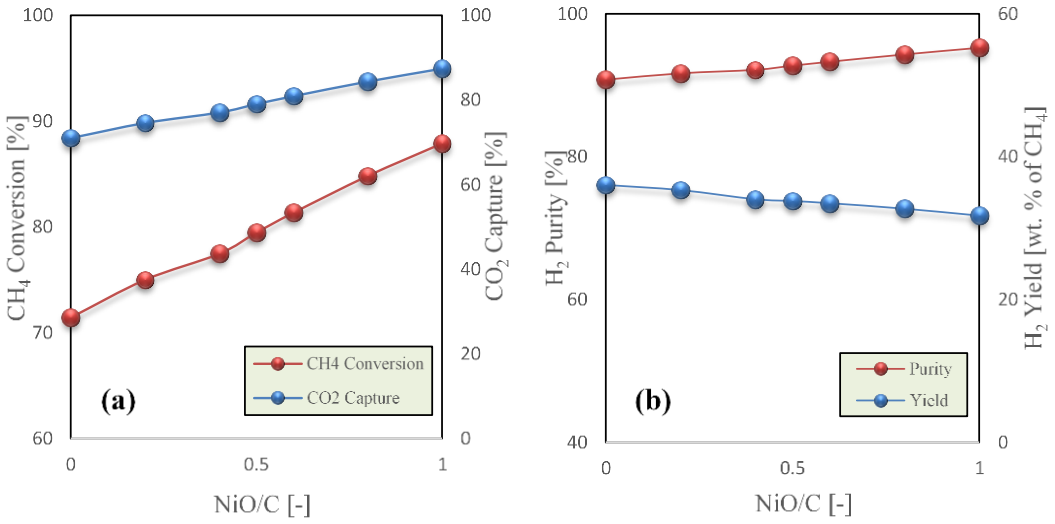

Figure 6.6: Effect of NiO/C on the a) CH_4 conversion; CO_2 capturing efficiency; b) H_2 purity; and H_2 yield (wt. %) at 30 bar, 923 K, S/C of 3.0 and CaO/C of 1.0

The above thermodynamic analysis is carried out by keeping in mind the industrial application of the SE-CLSR process. As already discussed, industrial H_2 production via

SMR is a medium-high pressure process. Therefore, the optimum conditions for temperature, pressure, S/C, CaO/C and NiO/C obtained through thermodynamic analysis are 923-973 K, 30 bar, 3.0, 1.0 and 0.5 respectively.

6.3 Mathematical modelling

A 1-D heterogeneous mathematical model of SE-CLSR in an adiabatic packed bed reactor is developed using gPROMS model builder 4.1.0®. This model accounts for mass and energy transfer in both gas and solid phase. In this model it is assumed that;

h) The flow pattern of gases in the packed bed reactor is plug flow in nature.

i) The temperature and concentration variations along the radial direction of the reactor are negligible.

j) The active surface of the catalyst and sorbent facilitates the reforming, reduction, sorption and oxidation reactions.

k) Ideal gas behaviour applies in this work.

l) There is no heat transfer from the system to the surrounding and from surrounding to the system. The operation is adiabatic in nature.

m) The size of the catalyst and sorbent are uniform and the porosity of the bed is constant.

6.3.1 Governing equations

One of the most important parameters in the design and the performance of the reactor is the kinetic mechanism. The overall behaviour of the reactor depends upon the set of reactions chosen to represent the chemical process, the values used for the pre-exponential factor and activation energy and the reaction rate equations used in modelling the reactor [148]. The reaction scheme and the rate equations used in this work are summarized in **Table 3.4**. The oxidation of Ni based oxygen carrier (OC) [R_1] is very fast and highly exothermic in nature. The amount of heat released during oxidation mainly depends upon the concentration of O_2 in N_2. Higher the amount of O_2, higher will be the amount of heat released. The amount of carbon deposited on the surface of catalyst during chemical looping reduction cycle is oxidized to CO and CO_2 in the oxidation cycle [R_2-R_4]. The reduction reactions of Ni based OC [R_5-R_8] along with the SMR [R_9], WGS [R_{10}], overall

reforming [R_{11}], dry reforming [R_{12}], methane decomposition [R_{13}], carbon gasification with steam [R_{14}], carbon gasification with CO_2 [R_{15}] and CO_2 adsorption [R_{16}] are the typical reactions included in the chemical looping reduction. The reactions between gas components and the catalyst support are neglected in this work due to the lack of data available in the literature [149]. The kinetic rate constants and the equilibrium constants used in the rate equations are temperature dependent terms and their equations as given in **APPENDIX E**. On the basis of the assumptions, reported above, the mathematical equations for mass and energy balance within the reactor filled with the sorbent and catalyst particles are listed in **Table 6.3**. The equations used to determine the physical properties, involved in the modelling, are already discussed in **Chapter 4 (Eq. 4.11-4.21).**

Table 6.3: Summary of mass and energy balance equations used to simulate 1-D heterogeneous packed bed reactor

Mass and energy balance in the gas phase ;

$$\varepsilon_b\left(\frac{\partial C_i}{\partial t}\right)+\frac{\partial(uC_i)}{\partial z}+k_{g,i}a_v\left(C_i-C_{i,s}\right)=\varepsilon_b D_z\frac{\partial^2 C_i}{\partial z^2}$$

$$\varepsilon_b\rho_g C_{pg}\left(\frac{\partial T}{\partial t}\right)+u\rho_g C_{pg}\frac{\partial(T)}{\partial z}=h_f a_v(T_s-T)+\lambda_z^f\frac{\partial^2 T}{\partial z^2}$$

Mass and energy balances in the solid phase;

$$k_{g,i}a_v\left(C_i-C_{i,s}\right)=(1-\varepsilon_b)\rho_{cat}\,r_i+\upsilon\rho_{cat}\,r_i-(1-\upsilon)\,\rho_{ads}\,r_{ads}$$

$$\rho_{bed}C_{p,bed}\left(\frac{\partial T_s}{\partial t}\right)+h_f a_v(T_s-T) = \upsilon(1-\varepsilon_b)\rho_{cat}\sum -\Delta H_{rxn,j}\,\eta_j R_j+(1-\upsilon)\,\rho_{ads}\sum -\Delta H_{ads}\,r_{ads}$$

Mass balance for Ni reduction;

$$\left(\frac{dC_{Ni}}{dt}\right)=(2R_5+R_6+R_7+R_8)M_{Ni} \qquad \& \qquad \left(\frac{dC_{NiO}}{dt}\right)=-(2R_5+R_6+R_7+R_8)M_{NiO}$$

Mass balance for carbon;

$$\left(\frac{dC_C}{dt}\right)=R_j M_{Ni}\,M_C$$

On the basis of reactions involved, the rate of formation or consumption of 'i' component is given as;

$$r_i = \sum_{j=1}^{3} \eta_i \varphi_{ij} R_j \qquad i = CH_4, CO, CO_2, H_2 \text{ and } H_2O \qquad (6.12)$$

The boundary conditions and initial conditions used in solving the mass and energy balance equations are as follows;

Boundary conditions;

At reactor inlet (z = 0)

$C_i = C_{i,in}$; $T = T_{in}$; $T_s = T_{s,in}$; $P = P_{in}$

$C_{NiO} = C_{NiO,in}$; $C_{Ni} = C_{Ni,in}$

At reactor outlet (z = L)

$\frac{\partial C_i}{\partial z} = 0$; $\frac{\partial T}{\partial z} = 0$; $\frac{\partial T_s}{\partial z} = 0$

Initial conditions;

$C_i = C_{i,0}$; $T = T_o$; $T_s = T_{s,o}$; $X = 0$; $Carbon = 0$

& $q_{CO2} = 0$

As an initial condition, it is considered that no gas component is present within the reactor so the concentration of gas species is zero at the start i.e. at t = 0. But by putting the concentration of H_2 to zero makes the rate of reforming reactions (R_9-R_{11}) infinite (denominator equals to zero). To avoid this, a very small initial concentration (~10^{-6}) of H_2 is used in the model.

In the reactor model linear and non-linear partial differential equations (PDEs), algebraic equations, and initial and boundary conditions are involved, and gPROMS was used to solve these equations. The sensitivity of the model was first checked for discretization ranging from 10-1000 intervals and model was found independent of the number of intervals. Finally, the reactor was axially discretized by 100 uniform intervals for this paper and output results were reported after every one second. The first order backward finite difference method (BFDM) was used to solve the PDEs using initial and boundary conditions as mentioned above. The model of the packed bed reactor was assumed to follow the non-ideal plug flow behaviour. In gPROMS differential algebraic solver (DASOLV) was used to solve the ordinary differential equation (ODEs). DASOLV converts the PDEs into ODEs, and 4th order Runge-Kutta technique was used to solve the system of equations.

6.4 Results and discussion

The modelling results of SE-CLSR process are divided into two parts. In the first part individual models of reduction of NiO and oxidation of reduced Ni catalyst are validated. Later, the models of FR (reduction and SE-SMR model) and AR (oxidation model) are combined and cyclic process of SE-CLSR is studied.

6.4.1 Validation of NiO reduction under CH_4 feed

The experimental data of **Iliuta et al.** [43] is used to validate the modelling of NiO reduction process. They used a fixed bed micro-reactor apparatus to investigate the reduction and oxidation (redox) of the NiO catalysts having Al_2O_3 as a support. The loading of the catalyst was 0.1 g power with particle diameter 140 μm. An electrical furnace (Hiden Catlab, Hiden Analytical Inc. Livonia, MI) was used around the fixed bed micro-reactor to maintain the temperature of the reactor. The brooks mass flow controllers (MFC) were used to measure the flow rate of gases going into the reactor. They used CH_4 in Ar as the reducing gas for the OTM. Experiment was initiated with the supply of CH_4 to the reactor and Ar to the vent. After a period of 10 min, feeds were switched off and reactor was purged for 2 min before starting the oxidation cycle. The micro-reactor was of quartz material having 4 mm internal diameter. They conducted the reduction experiments in temperature range of 800-900 °C. The schematic of the fixed bed micro-reactor system is shown in F**igure 6.7**. The experimental conditions used for the model validation are listed in **Appendix F**.

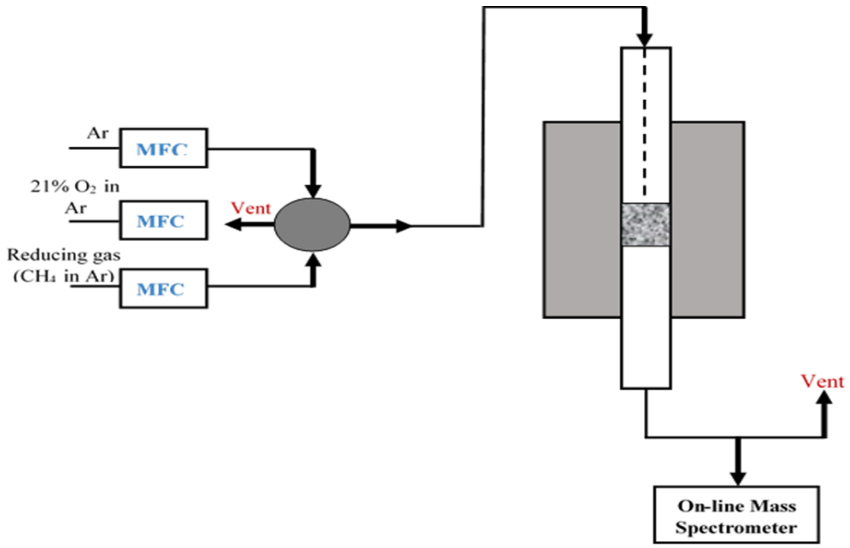

Figure 6.7: Schematic of the fixed bed micro-reactor experimental setup [43]

In this section the experimental results related to the mole fraction of CH_4, H_2, CO, CO_2 and H_2O are used to validate the modelling results. Later on, the experimental results related to the conversion of OTM are used to validate the modelling results.

In **Figure 6.8** the outlet mole fractions of product gases are shown. The length of reduction period is 60 s. In experimental work the outlet compositions of the product gases is delayed by 10-12 s, hence the results presented in figure 6.9 are adjusted accordingly. The delay in output results is because of the residence time of the gases between the 3 way valve and gas analyser. The dots in the figure are the experimental results and solid lines are the modelling results generated on gPROMS. These results are generated at 800°C and 1bar. As discussed in the experimental section, 10% CH_4 in Ar is used as the reducing gas in this process. The results show that within no time (~6s) the mole fraction of CH_4 goes to 0.007 and 0.006 in modelling and experimental case respectively. In this period entire CH_4 is converted to CO, CO_2, H_2 and H_2O. The mole fraction of H_2O is highest at the start as compared to other product gases. This is because of reduction reaction 1 and 2 (**R_5** and **R_6**). As the OTM reduced to Ni and formation of H_2 takes place, this H_2 further reduced the NiO according to **R_6** and H_2O is the dominant product at the start of the reduction process. The maximum mole fraction of H_2O obtained during modelling and experimental work is 0.083 and 0.080 respectively.

During the initial stage of the reduction process, the formation of CO_2 is dominant as compared to the formation of CO. This confirms that CO_2 formation takes place according to R_5 and R_7 at the same time. The formation CO via R_8 causes increase in the amount of CO at the outlet of the reactor but at the same time this CO takes part in the reduction of NiO and formation of CO_2 is observed. So in the initial stage of the reduction process CO_2 amount is higher than the amount of CO. The mole fraction of H_2 is the highest in later part of the reduction process and it reaches 0.101 and 0.106 in model and experiment respectively. The rise in the amount of H_2 is steep in both model and experiment. As the amount of O_2 in OTM reduces, the formation of product gases also decreases and the amount of CH_4 at the outlet of the reactor increases.

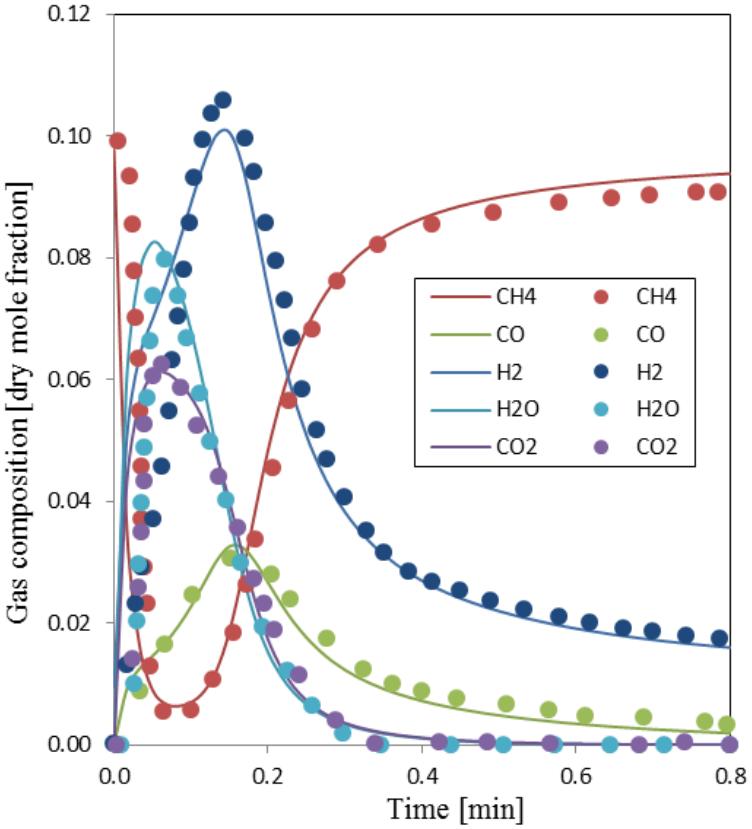

Figure 6.8: The distribution of gas products at the exit of reactor under the operating conditions of 800 °C, 1 bar and 10% CH_4 in Ar as reducing gas. Dots are the experimental values and solid lines are the modelling results.

The experimental and modelling results shown in **Figure 6.8** are in excellent agreement. Under the same operating conditions i.e. 800 °C, 1 bar and 10% CH_4 in Ar as reducing gas, the fractional conversion of NiO to Ni is reported as 0.96 in the experimental wok of **Iliuta et al. [43].** In **Figure 6.9,** the dynamic profile of NiO conversion is shown. It can be seen that the conversion of NiO reaches to its maximum value very fast. After 60 s the conversion pf NiO achieved is 0.97 in modelling work which is in excellent with experimental value of 0.96. At the conversion of NiO increases, the amount of Ni in the reactor increases hence the value of NiO with respect to initial amount of NiO decreases as shown in **Figure 6.9**. In this figure the dynamic profile of carbon formation on the surface of catalyst particle is also shown. The experimental value reported for carbon at the end of the reduction process is 8% carbon (mol% C_{total}). The modelling results are also in good agreement with experimental values. The formation of carbon is zero at the start as more O_2 is available for the formation of carbon containing product gases (CO

and CO_2). As the amount of O_2 in OTM decreases, the formation of carbon on the catalysts surface increases. By analysing the formation of carbon, it is observed that when the conversion of NiO exceeds 72% the accumulation of carbon on the surface of catalyst starts. The modelling and experimental results shown in **Figure 6.9** are in excellent agreement with each other.

In the following section the results related to the rate of reduction reactions (**R_5-R_8**) are presented. As already discussed in the above section that the reduction reactions are very fast and the formation of H_2 at initial stage promotes further reduction of the NiO and more H_2O formation takes place.

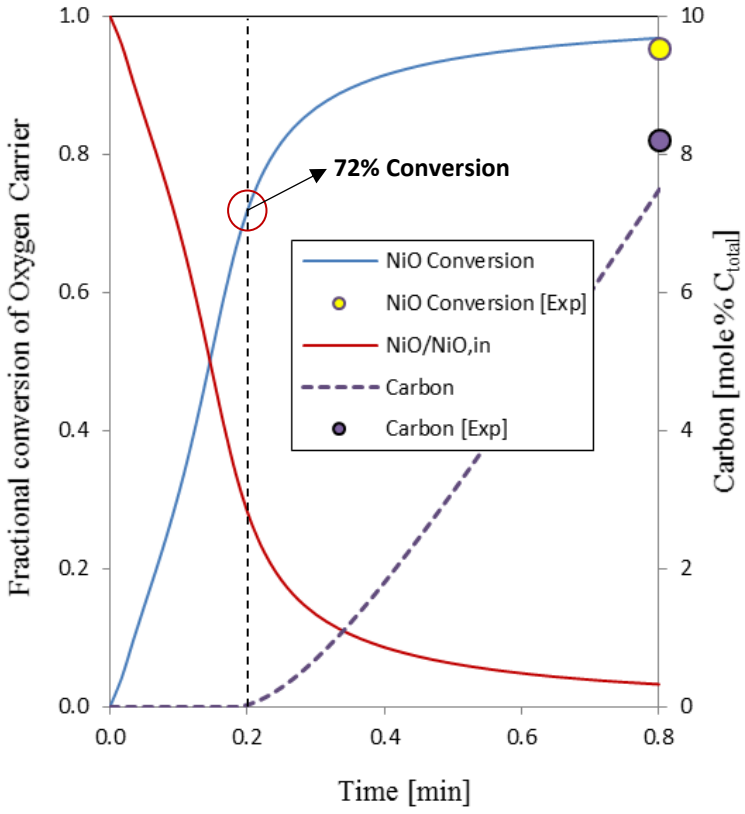

Figure 6.9: The dynamic profile of NiO conversion and carbon formation under the operating conditions of 800 °C, 1 bar and 10% CH_4 in Ar as reducing gas.

In **Figure 6.10**, the dynamic profile of the rate of reduction reactions at different location of the reactor (entrance, middle and at the exit) is demonstrated. At the entrance of the reactor the dominated reaction is R_5 i.e. partial oxidation of CH_4. According to this reaction main products are H_2 and CO_2. There is no formation of CO in this reaction. It can be seen that rate of R_7 reaction, oxidation of CO, is almost negligible here. The second

most dominating reaction at the entrance of the reactor is R_8 i.e. partial oxidation of CH_4 to CO and H_2. As we move towards the middle of the reactor R_6, NiO reduction with H_2, starts dominating the process. In the middle of the reactor enough CO is already formed, so R_7 reaction is also taking part in reducing the OTM. At the exit of the reactor again R_6 is the dominant reaction and dictates the product composition at the exit of the reactor.

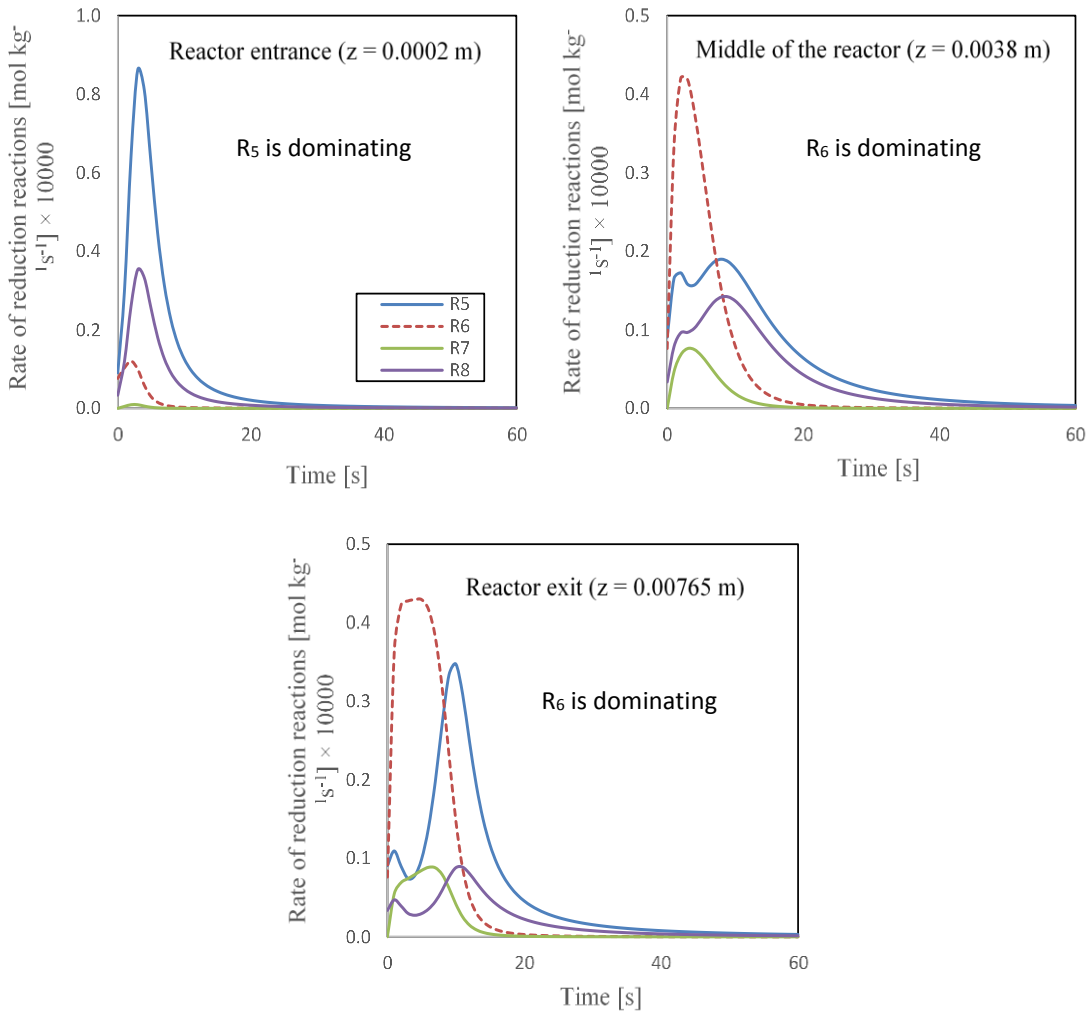

Figure 6.10: Dynamic profile of reaction rates of reduction reactions at the entrance, middle and at the exit of the reactor at 800 °C, 1 bar and 10% CH_4 in Ar as reducing gas.

In **Figure 6.11** the temperature profile at the exit of the reactor is shown. As shown in **Figure 6.10**, the dominating reduction reaction at the exit of the reactor is R_6 and this reaction is exothermic in nature hence it causes increase in the temperature of the reactor. The R_7 reaction is also an exothermic reaction and it also has a positive effect on the temperature of the reactor. The maximum temperature of the reactor achieved is 1172.7

K i.e. rise in temperature is 99.6 K. With the passage of time, R_6 and R_7 reactions are no more the dominating reaction and R_5 overtook these reactions (as shown in **Figure 6.10**), hence a drop in the temperature of the reactor is observed.

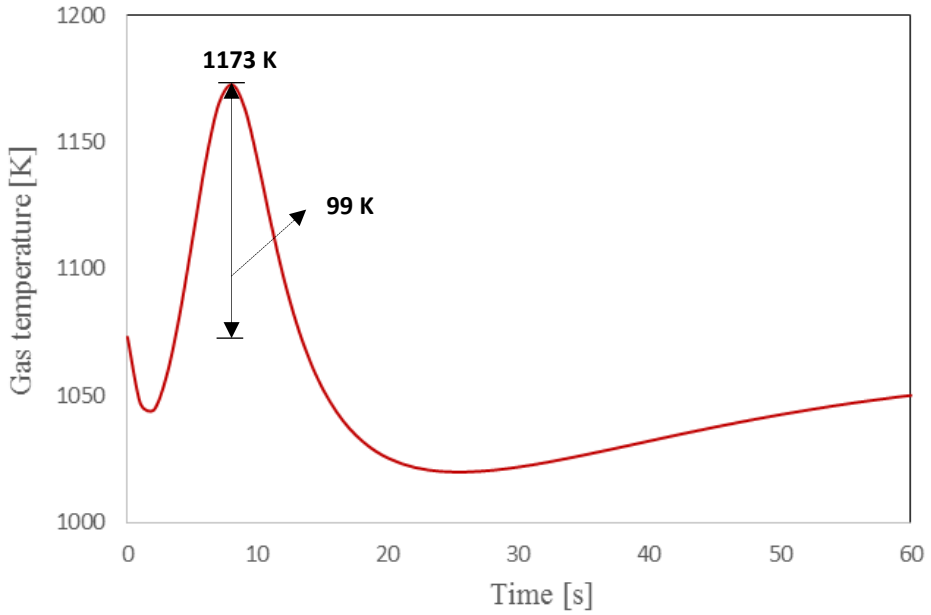

Figure 6.11: Temperature profile of the product gases at the exit of the reactor at feed temperature 800 °C, 1 bar and 10% CH_4 in Ar as reducing gas.

The effect of temperature on the conversion of NiO is presented in **Figure 6.12**. The temperature range of 773-1150 K is used in this sensitivity analysis. The conversion of NiO is less than 80% for a temperature below 773 K. Therefore, temperature higher than 773 K is used as the starting point for this analysis. At the exit of the reactor, the maximum conversion of NiO to Ni at 773 K is 80%. It increases from 91-98% as temperature increases from 873-1073 K. For temperature higher than 1073 K, there is no further increase in the NiO to Ni conversion.

It is observed that at temperature 1073 K, 90% NiO conversion in achieved within first 21 s run at the exit of the reactor. The same value of NiO conversion is achieved at 873 K and 973 K in 29 s and 51 s respectively. This shows that higher temperature favours the reduction reactions and it promotes the conversion of NiO.

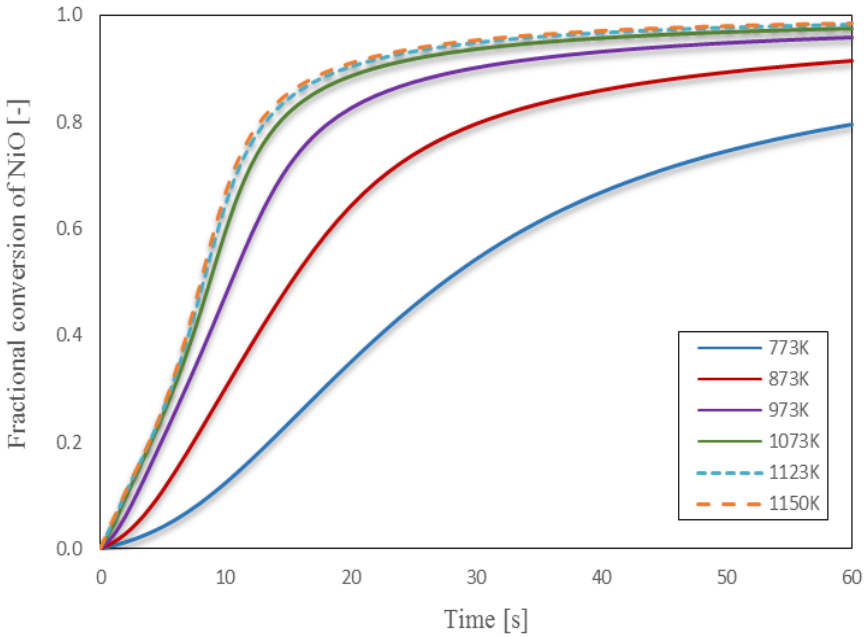

Figure 6.12: Dynamic profile of the fractional conversion of NiO to Ni in temperature range of 773-1150 K using 10% CH_4 in Ar as reducing gas

It can be seen in **Figure 6.13 (a & b)**, the rate of partial oxidation of CH_4 (**R_5**) and reduction of NiO with H_2 (R_6) increases with increase in temperature. The rate of partial oxidation of CH_4 (R_5) at 1073 K (0.347×10^{-4} mol kg^{-1} s^{-1}) is 10 times higher than the rate at 773 K (0.03×10^{-4} mol kg^{-1} s^{-1}). Similarly the rate of NiO reduction with H_2 (**R_6**) at 1073 K (0.429×10^{-4} mol kg^{-1} s^{-1}) is around 4 times higher than the rate at 773 K (0.115×10^{-4} mol kg^{-1} s^{-1}).

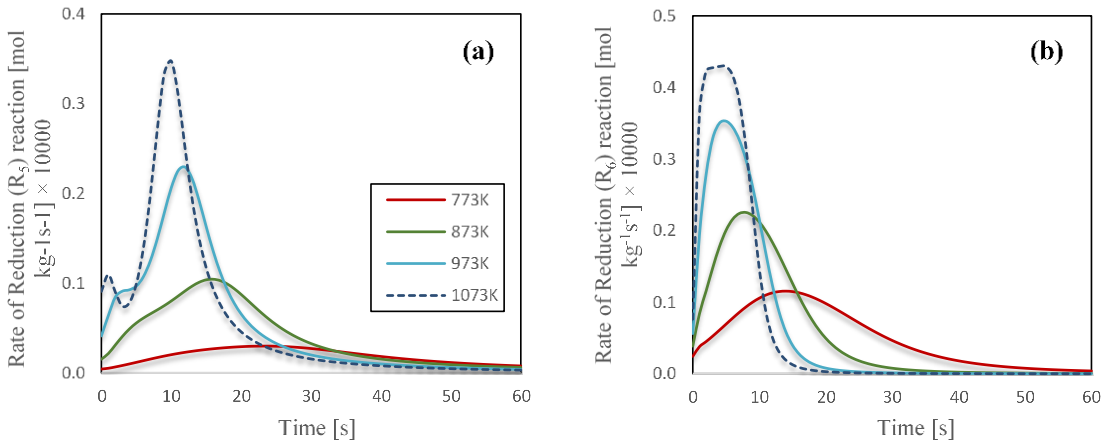

Figure 6.13: Effect of temperature on the rate of reduction reactions [a) R_5 and b) R_6]

Another important parameter that effects the conversion of NiO to Ni is the amount of CH_4 in the inert gas. As CH_4 is the reducing gas in this modelling work and the percentage of CH_4 in the feed effects the reduction rate and the conversion of NiO. In **Figure 6.14**, the effect of CH_4 concentration, in the feed gas, on the conversion of NiO is studied. The amount of CH_4 in Ar is varied from 5-20% at constant temperature (1073 K). It can been seen that higher amount of CH_4 in the feed gas promotes the conversion of NiO. The conversion of NiO is low in case of 5% CH_4 in the feed gas. The maximum conversion achieved in this case is 93% as compared to 99% when 20% CH_4 is used in the feed gas. As the amount of CH_4 in feed gas increases, it causes more supply cost of CH_4. Therefore, there is a trade-off between the selection of the amount of CH_4 in the feed and the cost of the process. The optimum value of CH_4 in the feed gas is 10% as it gives 98% conversion of NiO at 1073 K.

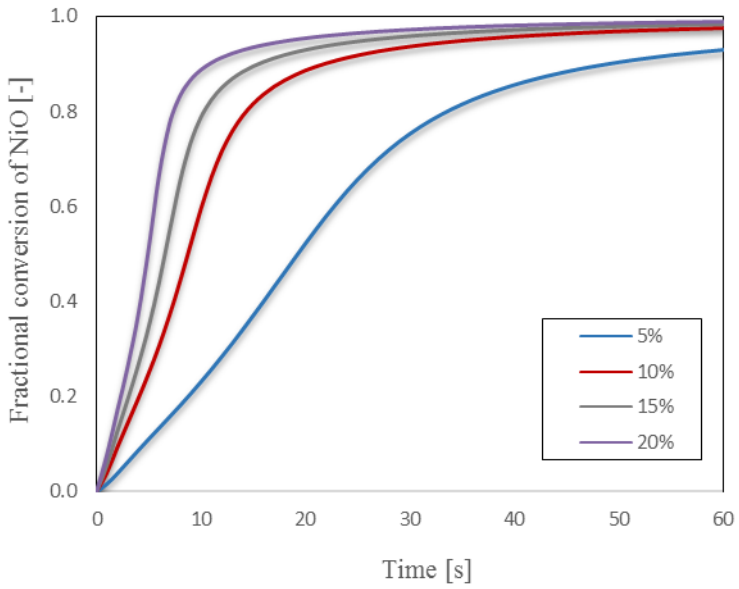

Figure 6.14: The effect of CH_4 concentration on the fractional conversion of NiO at the exit of reactor under the operating temperature of 1073 K.

In **Figure 6.15 (a-b)** the effect of temperature and NiO conversion on the rate of reduction reactions (**R_6** and **R_7**) at the exit of the reactor is presented. As in previous results the optimum temperature obtained for the reduction reactions is 1073 K and the optimum amount of CH_4 in feed is 10%, so these conditions are used in this case. It can be seen that with the increase in conversion of NiO the rate of reduction reactions (**R_6** and **R_7**) also increases. So the rate of reduction reactions is dependent on the amount of both Ni and NiO. As the conversion of NiO decreases to zero the rate of reduction of NiO with

H_2 and CO also decreases to zero. In **Figure 6.15 (b)** with the increase in the temperature from 773-1273 K, the reduction rates also increases.

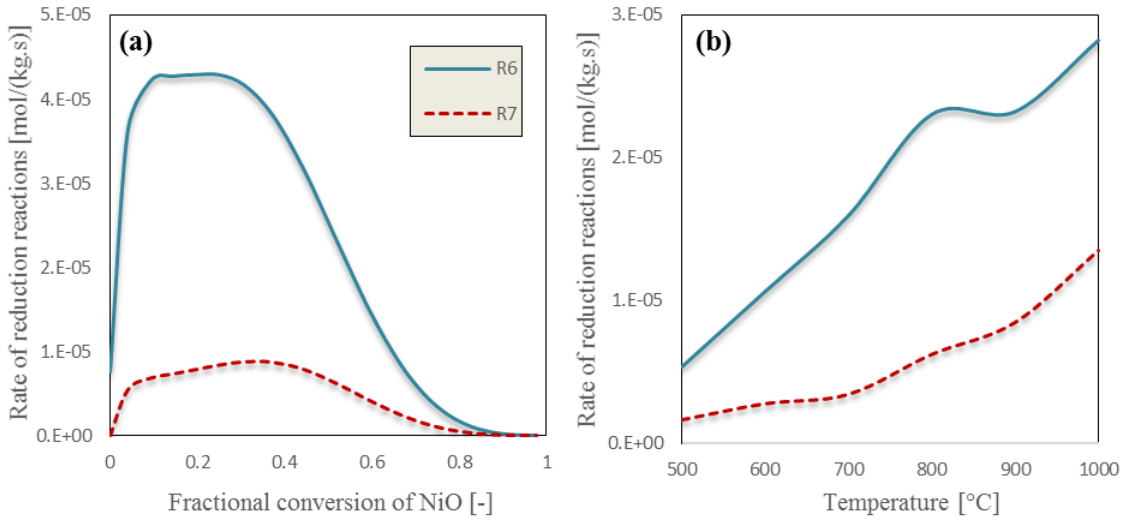

Figure 6.15: The effect of a) NiO conversion (at 800°C) and b) temperature (at 50% NiO conversion) on the rate of reduction of NiO (R_6 and R_7)

6.4.2 Validation of Ni oxidation under air and O_2 enriched air feed

In the previous section modelling of NiO reduction by using CH_4 as reducing agent is discussed and it is observed that high temperature promotes the reduction process. After the reduction of NiO, there is need to re-oxidize the reduced catalyst for the chemical looping process. In this section modelling of AR is executed.

To validate the mathematical model of the Ni oxidation, the experimental work of **Monnerat et al.** [241] is used here. The schematic diagram of their experimental work is shown in **Figure 6.16**. A fixed bed quartz reactor (ID = 9 mm and L = 230 mm), having Ni as catalyst (~210 mg), was used. To control the flow of the inlet gases mass flow controllers (Brooks Instrument B.V., Veenendaal, and Bronkhorst High-Tech B.V., Ruurlo, The Netherlands) were used. An electrical oven was used to heat up the reactor and K-type thermocouples (Philips AG, Dietikon, Switzerland) were used to monitor the temperature of the catalyst bed. Pressure gauges (Wika AG, Hitzkirch, Switzerland) were used at the upstream and downstream of the reactor to monitor the pressure of the fixed bed catalytic reactor. The effluent amount of the product gases was measured by using a

quadrupole mass spectrometer (MS) (type QMG 420, Balzers AG, Principality of Liechtenstein). The catalyst bed was heated from room temperature to 600 °C by using H_2 as feed gas. Later on, H_2 was switched off and Ar was allowed to flush the reactor and temperature of the reactor was set to the desired temperature. The oxidation of catalyst was performed by supplying controlled amount of air into the fixed bed reactor [42, 241].

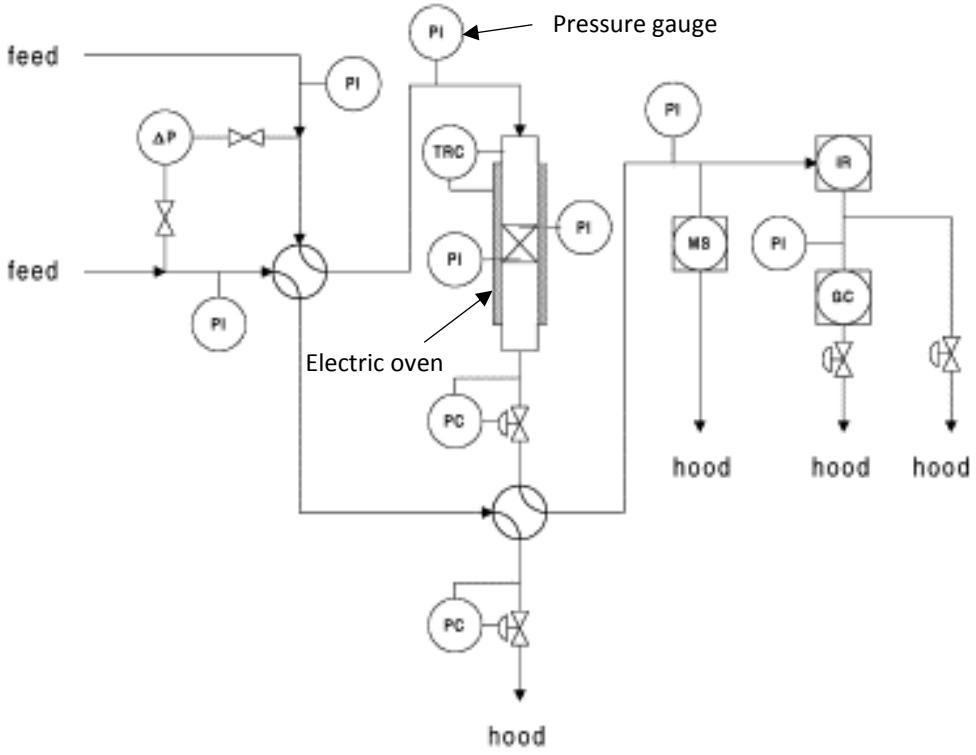

Figure 6.16: Schematic of the experimental setup [241]

The experimental output in terms of temperature and mole fraction of O_2 at the outlet of reactor is used for the validation of the model. In the following section the mathematical modelling of oxidation process is discussed. The experimental conditions used in this model are listed in **APPENDIX G**.

In **Figure 6.17,** the effect of temperature on the outlet mole fraction of O_2 is presented. The dots are experimental values and solid lines are the modelling results. The oxidation of Ni process is run at 1.5 bar using 8% O_2 in Ar as a feed gas. The oxidation process is highly exothermic in nature so it is favourable at lower temperature. The product mole fraction at the exit of the reactor shows the degree of oxidation. The amount of O_2 is almost zero at the start in all cases and it increases with the passage of time. Finally, after 100 s the outlet mole fraction of O_2 is 0.08 in all temperature cases. The steady state mole fraction of O_2 is achieved from 110 s to onwards. This confirms the complete oxidation

of Ni to NiO as the outlet mole fraction of O_2 is same as the inlet mole fraction of O_2. The modelling results are in excellent agreement with the experimental results.

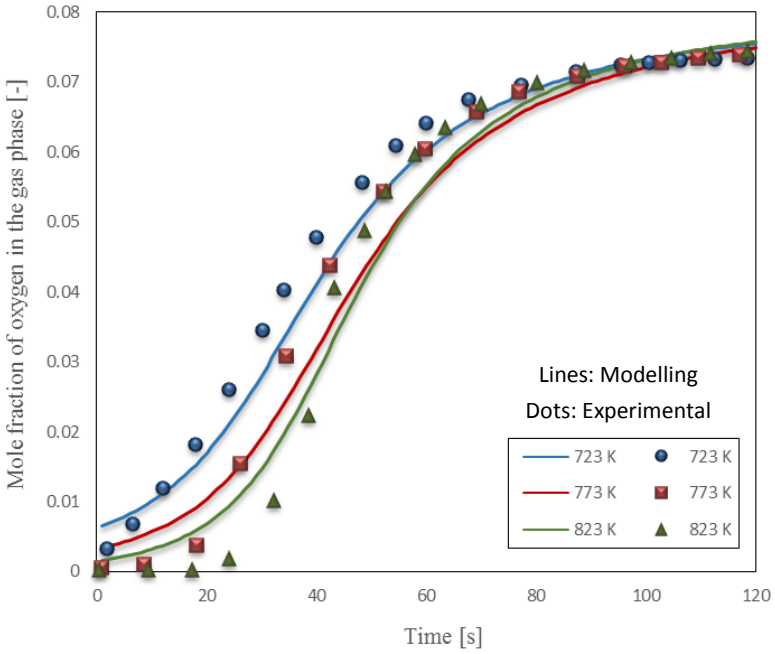

Figure 6.17: The effect of temperature on the mole fraction of O_2 at the outlet of reactor under the experimental conditions of 1.5 bar and 8% O_2 in Ar as oxidising gas.

As the Ni oxidation process is assumed to be an adiabatic process, therefore the temperature rise under the adiabatic conditions is presented in **Figure 6.18**. The modelling results are compared with the experimental variation of temperature under the conditions of 773 K feed temperature, 1.5 bar and 10% O_2 in Ar as feed gas for the oxidation process. An initial rapid rise in the temperature is observed and after 45 s of operation the temperature decreases. This is because initially all Ni is available for oxidation process but as the conversion of Ni into NiO increases, the amount of O_2 in the exit also increases and temperature of the system goes down. The maximum predicted temperature achieved the modelling is 823 K i.e. rise of 50 K from the feed temperature. The temperature of the system goes to 776 K after an operation of 180 s. It can be seen that modelling results are in excellent agreement with experimental values.

The model is further validated by varying the amount of O_2 in the feed gas. As in the oxidation process the vital parameter is the amount of O_2 in the feed, so the effect of O_2 concentration on the performance of the oxidation process is studied. In **Figure 6.19**

experimental (dots) and modelling results (solid lines) of O_2 mole fractions at the exit of the reactor for various concentration of O_2 in the feed are shown.

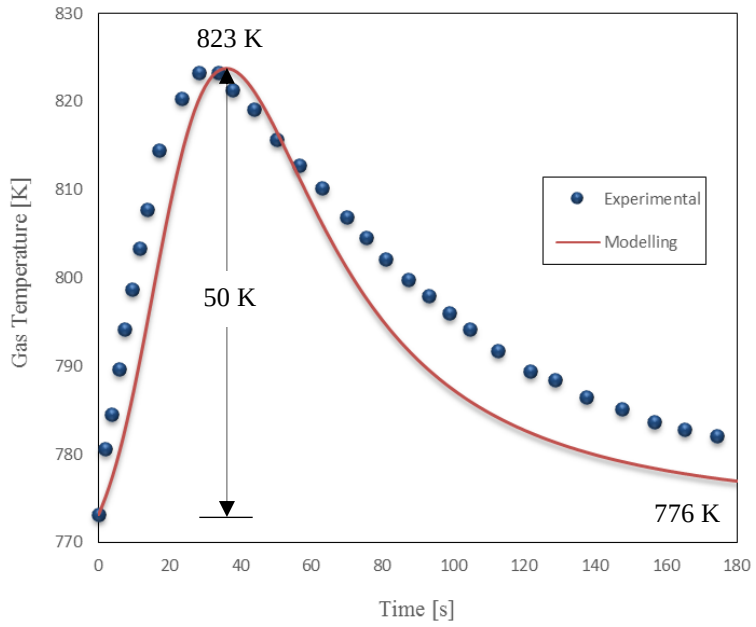

Figure 6.18: The dynamic temperature profile under the operating conditions of 773 K feed temperature, 1.5 bar and 8%O_2 in feed gas. Dots are the experimental values and solid lines are our modelling results.

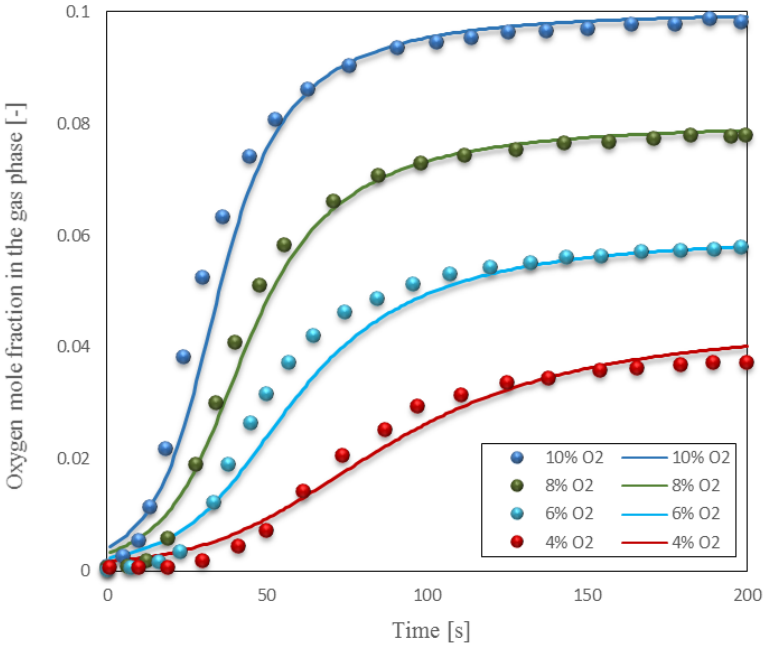

Figure 6.19: Modelling and experimental response of the outlet mole fraction of O_2 for different concentration of O_2 in feed gas under 773 K feed temperature and 1.5 bar.

The amount of O_2 in the feed has a positive effect on the rate of oxidation of Ni catalyst. The higher amount of O_2 in the feed (10%) causes the oxidation process to reach the maximum value earlier than the lower amount of O_2 (4%). The modelling results are in excellent agreement with the experimental results.

The validated model of oxidation process is run at different temperatures to observe the effect of temperature on the conversion of Ni to NiO. The feed used for this sensitivity analysis is 21% O_2 in N_2 (Air). In F**igure 6.20 (a)** the effect of temperature on Ni conversion is studied. The maximum conversion of Ni (99%) is achieved at 973 K. The higher temperature promotes the rate of oxidation reaction as can be seen **Figure 6.20 (b)**. It can be seen that there is little difference in the final conversion of Ni catalyst as the temperature increases from 673-973 K.

The higher amount of O_2 in feed promotes the oxidation reaction and hence the conversion of Ni to NiO. To investigate the effect of O_2 concentration on the rate of oxidation reaction, temperature and conversion of Ni to NiO, a sensitivity analysis is performed by varying the concentration of O_2 in feed from 5-21%.

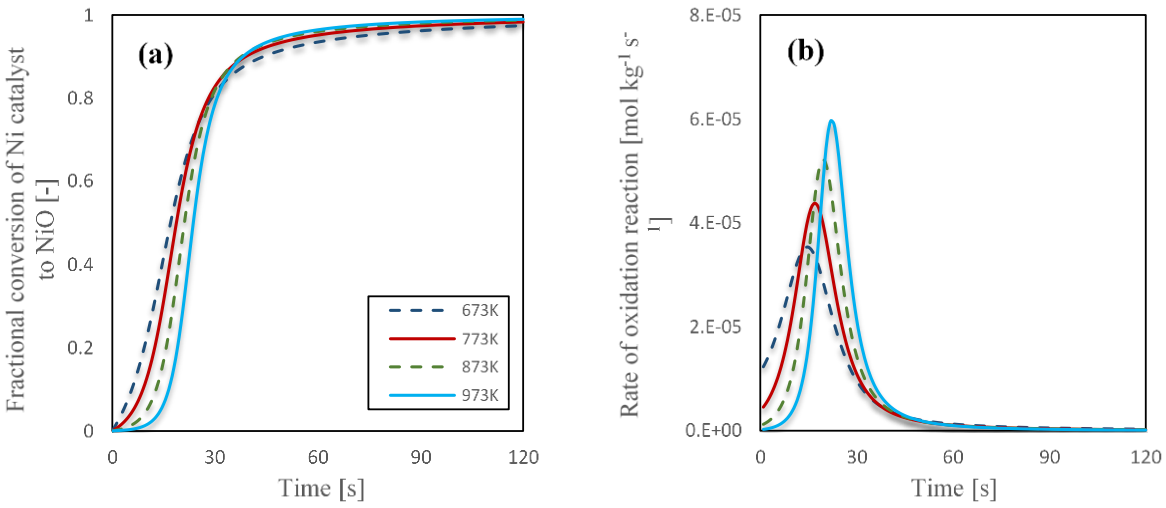

Figure 6.20: Effect of temperature on the fractional conversion of Ni catalyst and the rate of oxidation reaction under the operating conditions of 1.5 bar and 21% O_2 in N_2 as feed gas.

In **Figure 6.21 (a-d)** the dynamic profile of the temperature, rate of oxidation reaction, conversion of Ni to NiO and the maximum temperature achieved for different concentration of O_2 in the feed at the exit of the reactor is presented. As it was predicted that higher concentration of O_2 in the feed promotes the rate of conversion of Ni to NiO.

Figure 6.21 (a) shows that as the concentration of O_2 in feed increases from 5-21% in N_2, the conversion of Ni to NiO increases from 75-98% under the condition of 773 K as feed temperature. The maximum conversion of Ni (98%) is reached within 100 s in case of 21% O_2 in feed gas. In **Figure 6.21 (b)** it can be seen that when the concentration of O_2 is higher in feed, the rate of oxidation is very high as well. The rate of oxidation process is 5 times higher when the concentration of O_2 in feed is 21% as compared to the rate when the concentration of O_2 is 5% in the feed. This higher amount of O_2 in feed also causes massive rise in the temperature of the packed bed reactor. The maximum temperature achieved in case of 5%, 10%, 15% and 21% O_2 in feed is 801.8 K, 821.8 K, 835.7 K and 847.2 K respectively as shown in **Figure 6.21 (d).** The higher temperature within the system promotes the rate of reaction hence the conversion of Ni to NiO.

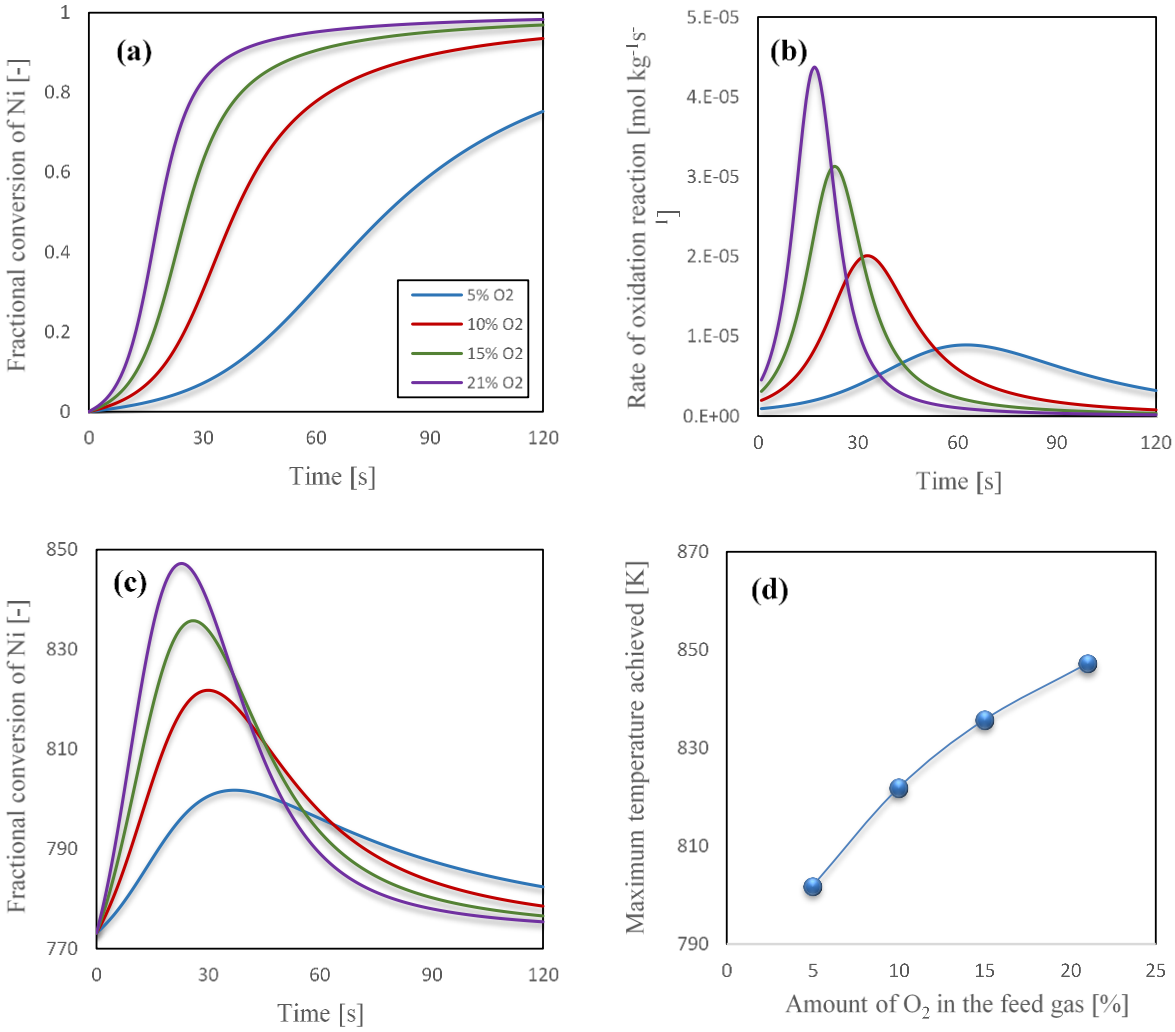

Figure 6.21: Effect of O_2 concentration in feed on a) the conversion of Ni; b) rate of oxidation reaction; c) temperature of the product gases at the outlet of reactor and d) the maximum temperature achieved under the operating condition of 773 K, 1.5 bar and mas flux of 0.4 kg m^{-2} s^{-1}

These results clearly dictate that amount of O_2 has a vital role to play in overall conversion of Ni into NiO. In modelling SE-CLSR process 21% O_2 in N_2 is used as feed for the oxidation cycle.

6.4.3 Modelling of the FR

As in the hierarchy of modelling methodology, it is explained that the FR model is the combination of SE-SMR and reduction processes. The mathematical model of SE-SMR developed in **chapter 5** is used in this work along with the reduction model developed in **section 6.4.1**. The physical parameters and operating conditions used to model the FR are given in **APPENDIX H.**

The feed in FR is steam, CH_4 and inert gas (N_2) at gas mass flux of 3.5 kg m^{-2} s^{-1}. The results developed in mathematical modelling are compared with the equilibrium results and later on FR cycle will be combined with AR cycle in order to model the entire SE-CLSR process.

In the packed bed reactor the initial amount of Ni is almost zero as it is available in the reactor in the form of NiO. Therefore, at the start the contribution of reforming reactions towards the overall performance of the system is negligible. The dynamic profile of the temperature at the exit of reactor is shown in **Figure 6.22**. The decrease is temperature from 973 K to 920 K is very sharp. In this period the dominant reaction is the reduction of NiO to Ni. As the reduction of NiO to Ni is highly endothermic in nature and process is adiabatic in nature, so a sharp decrease in the temperature is observed. During the reduction, the reforming reaction is also taking place as reforming reaction requires Ni surface to proceed. After the decrease in temperature from 973 K to 920 K, there is gradual increase in the temperature of the process. Temperature increases from 920 K to 940 K, this increase in temperature is due to the carbonation reaction. As soon as CO_2 is produced during the process, the sorbent starts working and CO_2 adsorption enhances the reforming reaction. The highly exothermic CO_2 adsorption reaction causes increase in the temperature of the packed bed reactor. As time reaches 600 s, a gradual drop in the temperature is observed from 942 K to 900 K. This drop in temperature is the clear indication that sorbent has reached to its maximum saturation. This period, from 600 s to ~1400 s, is known as breakthrough period (as discussed in chapter 5). After this breakthrough period no more adsorption of CO_2 on the surface of sorbent takes place,

hence the only process after breakthrough period is conventional SMR process. The period after 1400 s is known as post-breakthrough period and a steady state profile of the temperature is observed in this period.

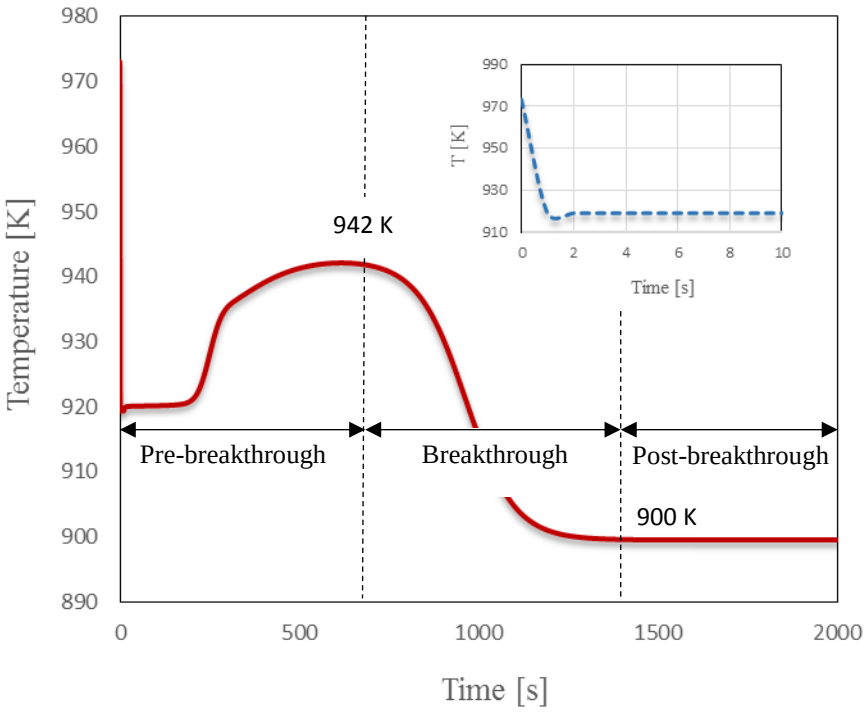

Figure 6.22: Temperature profile in the FR under the operating conditions of 30 bar, feed temperature of 973 K, S/C of 3.0 and gas mass flux of 3.5 kg m^{-2} s^{-1}.

As discussed earlier that drop in temperature at the initial stage of the FR indicates the domination of reduction reactions. At this stage of the process entire CH_4 is used for the reduction of NiO to Ni. Therefore the CH_4 conversion is almost 100% at the start of the process but with time the drop in CH_4 conversion is observed. During the pre-breakthrough period (t < 600 s), the conversion of CH_4 is 70.4% against the value of 69.4% and 28.9% CH_4 conversion in SE-SMR and SMR process respectively. Under the same operating conditions of 973 K feed temperature, 30 bar and S/C of 3.0, the purity of H_2 obtained in FR, SE-SMR and SMR process is 85.8%, 82.5% and 52.8% respectively. This shows that the CO_2 capturing efficiency is higher in FR as compare to SE-SMR process. The CO_2 capturing efficiency in the FR and SE-SMR under the same operating conditions is 64.3% and 53.6% respectively. The yield (wt. % of CH_4) of H_2 is bit higher in SE-SMR process as compared to the FR cycle of SE-CLSR process. This is because H_2 is used in the reduction of NiO to Ni in the FR while no H_2 is used as a reducing gas in the SE-SMR process. So the H_2 yield (wt. % of CH_4) is 27.3%, 27.6% and 14.1% in

the FR, SE-SMR and SMR processes respectively. The comparison of these three processes on the basis of CH_4 conversion, H_2 yield (wt. % of CH_4), H_2 purity and CO_2 capturing efficiency is presented in **Figure 6.23.**

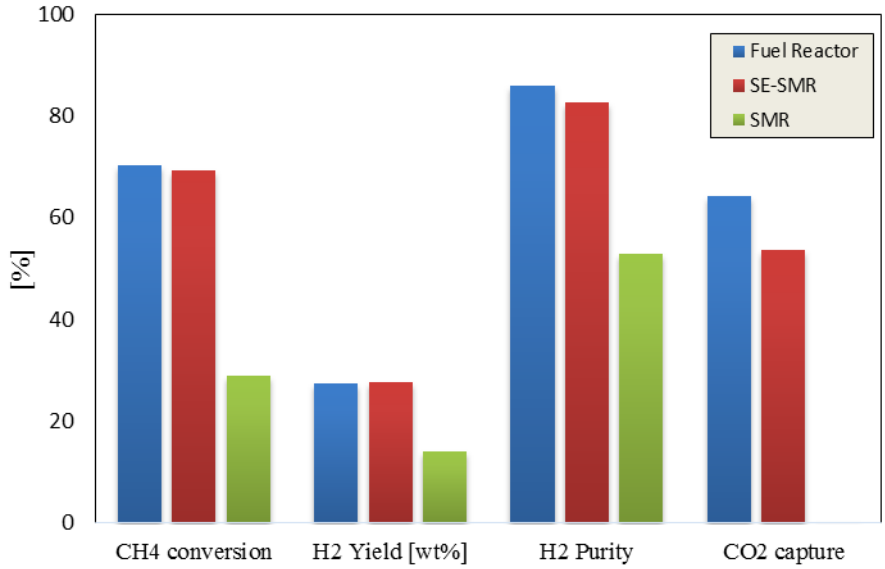

Figure 6.23: Comparison of FR, SE-SMR and SMR process on the basis of CH_4 conversion, H_2 yield (wt. % of CH_4), H_2 purity and CO_2 capturing efficiency under the operating conditions of 973 K, 30 bar, S/C of 3.0 and gas mass flux of 3.5 kg m^{-2} s^{-1}.

The higher pressure is not favourable for reforming process as discussed in **chapter 4**. So higher the pressure of the system, lower will be the conversion of CH_4. The effect of pressure on the temperature profile, CH_4 conversion, H_2 purity and CO_2 capturing efficiency is presented in **Figure 6.24 (a-d)**. The temperature profile in pre-breakthrough period is almost same for all the pressure conditions. Although the duration of pre-breakthrough period is different for different pressure conditions. In post-breakthrough period the minimum temperature is reached when pressure is 5 bar. The minimum temperature in case of 30 bar and 5 bar conditions is 900 K and 859 K respectively. That's why high pressure conditions are preferred for sorption process. The effect of pressure on CH_4 conversion, H_2 purity and CO_2 capturing efficiency is very significant. In pre-breakthrough period the conversion of CH_4 is 97.2%, 89.8%, 78.4% and 70.8% for 5 bar, 10 bar, 20 bar and 30 bar respectively. The purity of H_2 is also maximum for lower pressure conditions. The maximum purity of H_2 is achieved at 5 bar i.e. 95.8% and CO_2 capturing efficiency at the same pressure is 86.8%. The yield (wt. % of CH_4) of H_2 is also

very high at lower pressure. The yield (wt. % of CH_4) of H_2 at 5 bar, 10bar, 20 bar and 30 bar is 38.2%, 35.1%, 30.4% and 26.8% respectively.

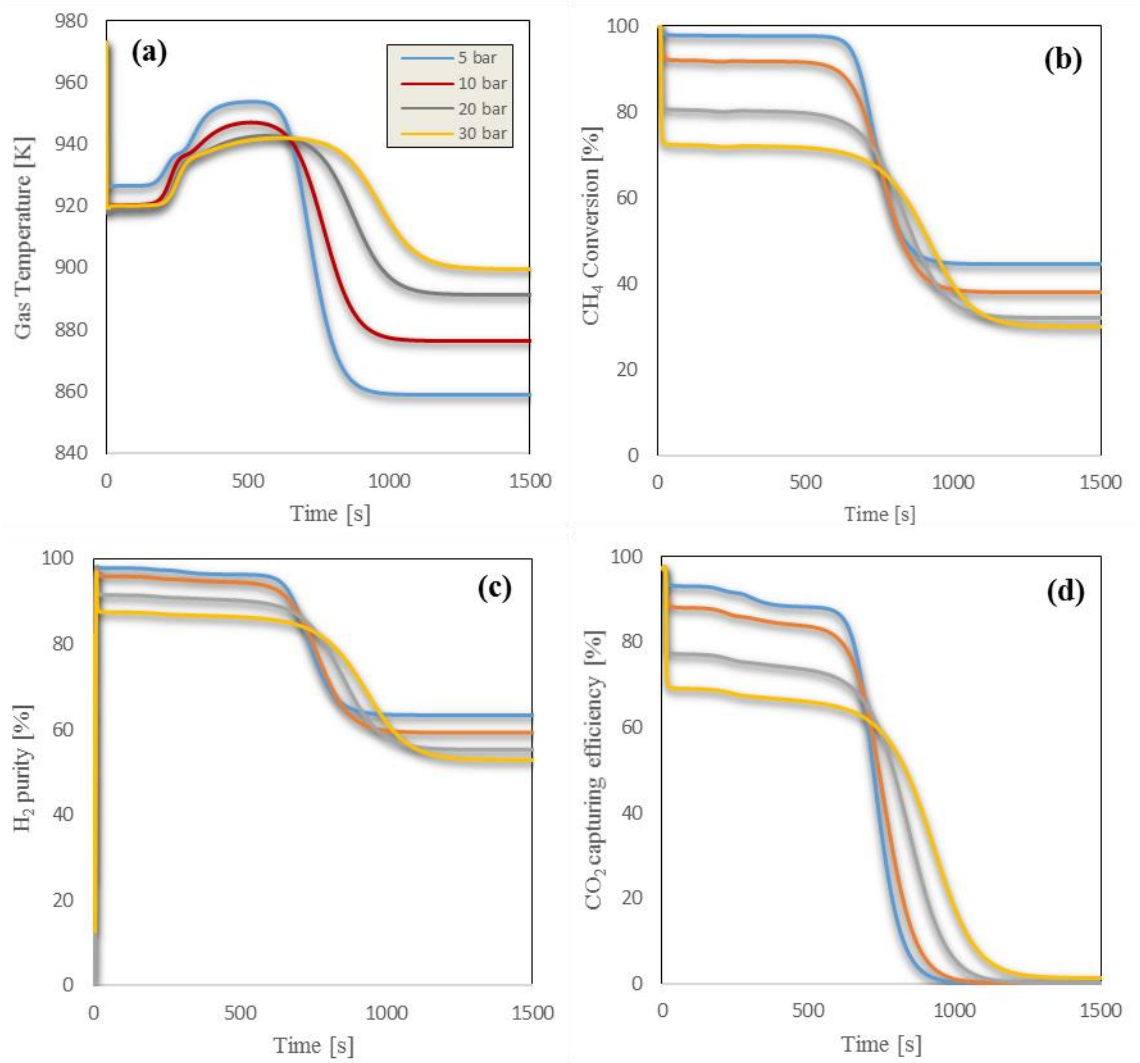

Figure 6.24: Effect of pressure on a) the temperature of the exit gases; b) CH_4 conversion; c) H_2 purity and d) CO_2 capturing efficiency under the operating conditions of 973 K, S/C of 3.0, CaO/C of 1.0 and NiO/C of 0.5

These results suggest that lower pressure conditions are favourable for better conversion of CH_4 and for more pure H_2 product. But high pressure requirements at the downstream process makes the high pressure conditions favourable for the industrial H_2 production. In the following section the combine cycles of FR and AR are run to study the performance of complete SE-CLSR process. The sensitivity of the SE-CLSR is studied under various operating conditions.

6.4.4 Sensitivity analysis of the SE-CLSR process

In previous sections, individual models of the FR and AR are developed and validated against the modelling and experimental data reported in the literature separately. As discussed in the introduction, the overall SE-CLSR process in a packed bed reactor system is based on the cyclic process between FR and AR processes. At the start of the cycle CH_4, H_2O and N_2 are introduced in the packed bed reactor (FR), loaded with NiO and CaO particles. The feed is introduced at a fixed ratio of S/C and under the specific operating conditions of temperature and pressure. The reduction of NiO to Ni is followed by reforming reactions and adsorption of CO_2. After the complete reduction of the catalyst, the feed is switched to the mixture of O_2 in N_2. The reduced catalyst is re-oxidized and saturated sorbent is regenerated by the heat of oxidation reaction. After the complete oxidation of Ni to NiO and regeneration of sorbent, the next cycle of SE-CLSR starts by shifting the feed to CH_4, H_2O and N_2. The complete coding of SE-CLSR process is given in **APPENDIX I**.

In the following section, the SE-CLSR process is studied under various operating conditions (temperature, pressure, S/C). In this modelling of SE-CLSR process the Ni deactivation by the loss of Ni element is not considered, so the effect of temperature and pressure on the catalyst deactivation is neglected.

6.4.4.1 CASE STUDY 1: Cyclic study of SE-CLSR process

In this case study, 30 bar pressure is used to evaluate the performance of the SE-CLSR process during various cycles of FR and AR. The reactor configuration used in this section is the same as that used in Chapter 5.

The SE-CLSR process starts with the FR. CH_4, H_2O and N_2 are used as feed in the FR cycle. The feed was introduced at 950 K (677 °C) and at S/C of 3.0. At the initial stage, CH_4 acts as a reducing gas and causes reduction of NiO to Ni. As reduction of NiO with CH_4 is highly endothermic process (R_5-R_8), so a drop in temperature of 50 K is observed at the start of the FR cycle as shown in **Figure 6.25**. The rise in the temperature from 900 K to 920.8 K is observed after a run of ~400 s. This rise is mainly due to the heat released during the CO_2 adsorption reaction (R_{16}). As the standard heat of carbonation reaction is -178 kJ/mol, so a rise of ~20 K temperature is observed. This temperature (921 K) remains

constant in the pre-breakthrough period (t < 550 s) and a sudden drop in the temperature is observed as the process crosses the pre-breakthrough period (t > 550 s). If the FR step is allowed to run after the breakthrough period, the steady state temperature reached in the post-breakthrough period (t >1200 s) will be ~882 K i.e. a drop of 68 K from the feed temperature. In the post-breakthrough period the sorbent is saturated, hence a sudden drop in temperature is observed. The feed gases are switched off after 550 s and at this stage the conversion of NiO to Ni is 99.9%. The red dot in **Figure 6.25** is the point where the FR cycle ends and the AR cycle begins. In this work, 21% O_2 in N_2 (air) is used as the feed for AR. The feed temperature of AR is the same as the feed temperature of FR (950 K). As in the FR, the conversion of NiO to Ni is not 100%, some NiO is present in the packed bed reactor at the start of the AR cycle. The overall oxidation of reduced Ni catalyst is a highly exothermic reaction and as the system is adiabatic, this causes the sudden rise of temperature within the packed bed reactor. The temperature during the AR cycle climbs to 1043 K (770 °C) in 450 s as shown in **Figure 6.25**. The rise in temperature is directly related to the amount of Ni left in the reactor for further oxidation. As the amount of Ni drops due to the conversion into NiO, the rate of oxidation reaction decreases and so does the temperature of the system. The conversion of Ni to NiO during this cycle is 89.8%. If more time was allowed for the AR step, a Ni conversion higher than 99% could be achieved, but this would be at the expense of lower outlet temperature of the gases. So there is a trade-off between the temperature requirement at the outlet of AR and the conversion of Ni to NiO. The optimum temperature selected for AR is 1043 K and at this point the conversion of Ni is 89.8%. To achieve this temperature, the AR cycle is run for 450 s and after this the feed gases are again switched back to the feed gases for subsequent FR step. This completes one cycle of SE-CLSR process and at the end of this cycle 70% CH_4 conversion and 86.2% H_2 purity is obtained.

This scheme of alternative cycles of FR and AR is allowed to run for 10 cycles. In 11^{th} cycle, only modelling results of FR cycle are presented. It can be seen in figure 8 that if FR is allowed to run till the steady state is achieved, the temperature of the process drops to a minimum value of 882 K. In this period, only reforming reactions are dominating as sorbent is already saturated.

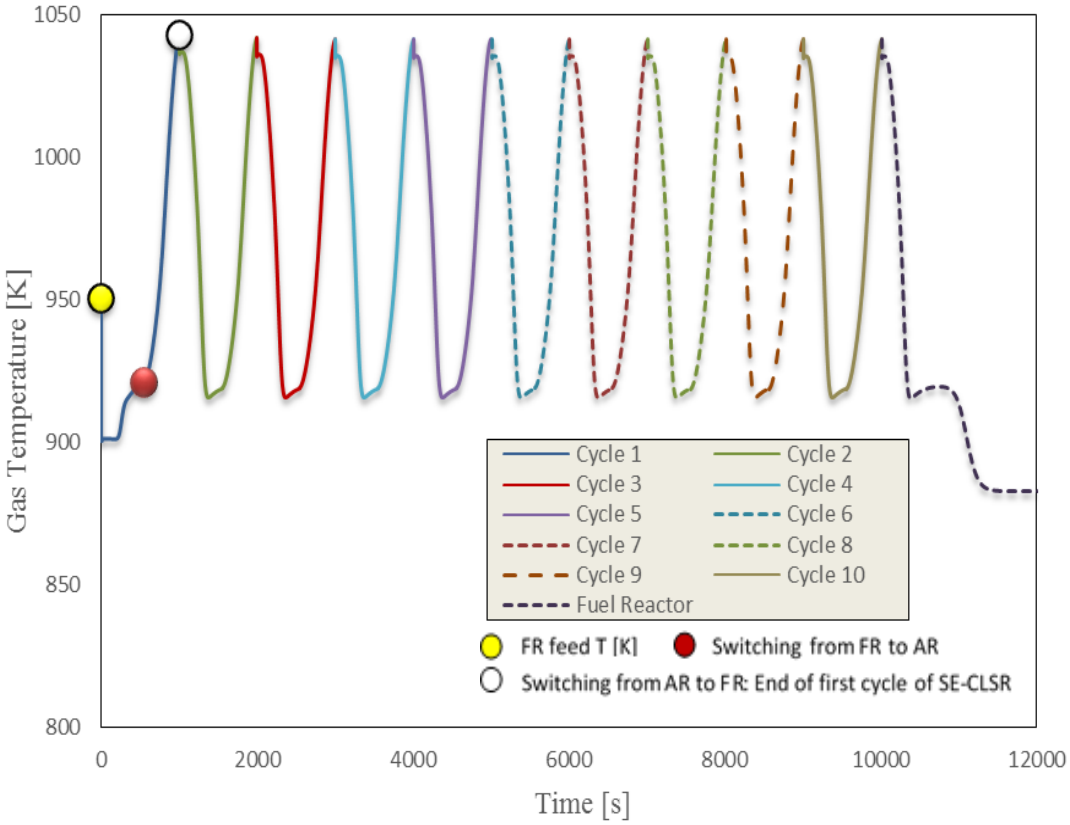

Figure 6.25: The dynamic profile of temperature in packed bed reactor system of SE-CLSR process. SE-CLSR process is run for 10 complete cycles under the operating conditions of 950 K, 30 bar, S/C of 3, CaO/C of 1, NiO/C of 0.5 and 21% O_2 in N_2 as feed for the AR.

The dynamic profiles of dry mole fraction of product gases and gas temperature, in the second FR step (cycle 2), is shown in **Figure 6.26**. It can be seen that the amount of CH_4 is almost zero at the very start of the process (first 20 s) indicating 100% conversion of CH_4 during reduction reactions. As soon as the amount of NiO decreases, the conversion of CH_4 also drops. In the pre-breakthrough period, the mole % (dry basis) of CH_4 and CO_2 at the exit of the reactor are in steady state at 11.5% and 0.9% respectively. As soon as the process approaches the breakthrough period ($t < 550$ s), the FR system is switched to AR. The red dot in the figure is the switching point from FR to AR. At this point temperature of the system is 919 K (646 °C).

In the breakthrough period ($550 < t < 1200$ s) the drop in the concentration of H_2 is observed as the sorbent is reaching towards maximum saturation and less sorbent is available for CO_2 adsorption. In the post-breakthrough period ($t > 1200$), the gases concentration reach steady state. The steady state mole % (dry basis) of H_2 is 50.7%.

Hence a drop in mole % of H_2 from 87.6% to 50.7% is observed in post-breakthrough period.

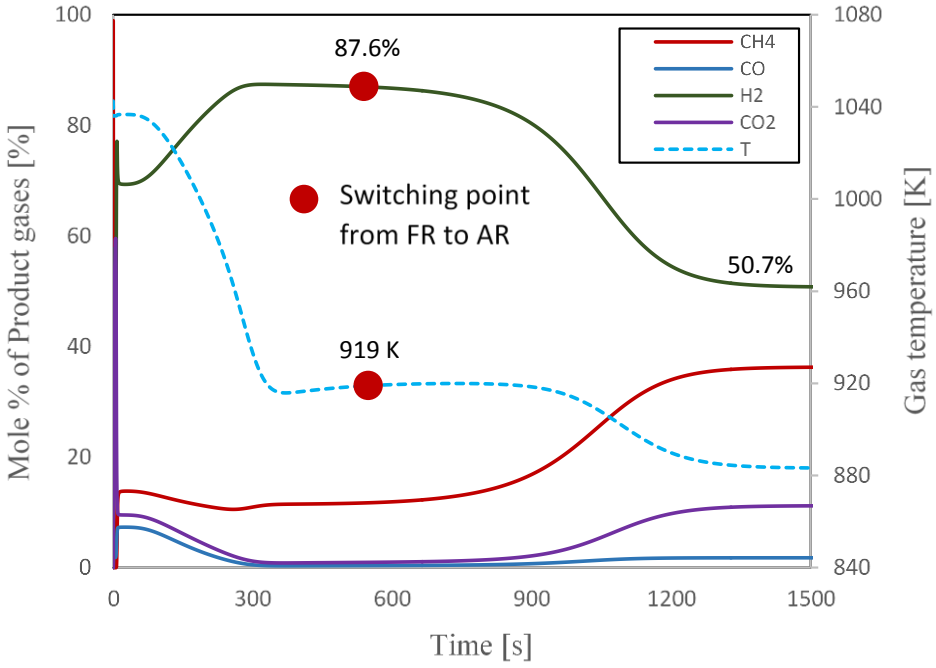

Figure 6.26: The dynamic profiles of mole% of product gases [dry basis] and gas temperature in the second cycle of FR under the operating conditions of 30 bar, 950 K feed temperature and S/C of 3.0

The variation for SMR, carbonation and reduction reaction rates along the length of the reactor during the first cycle of FR is shown in **Figure 6.27 (a)**. It shows that the reduction reactions have significant rate along the length of the reactor. The reduction of NiO to Ni produces CO_2, the sorbent captures the CO_2 and enhances the reduction reaction rate. So, the capturing of CO_2 at the start of the process promotes the reduction process and it can be seen in **Figure 6.27 (b)**. The dotted lines are the modelling results for the reduction rates in the absence of sorbent while the solid lines are for the reduction rates in the presence of sorbent. The enhancement of reduction rates in the presence of sorbent, promotes the fast conversion of NiO to Ni in the FR cycle. Later, along the length of the reactor as NiO is converted to Ni, both SMR and carbonation reactions start dominating the process.

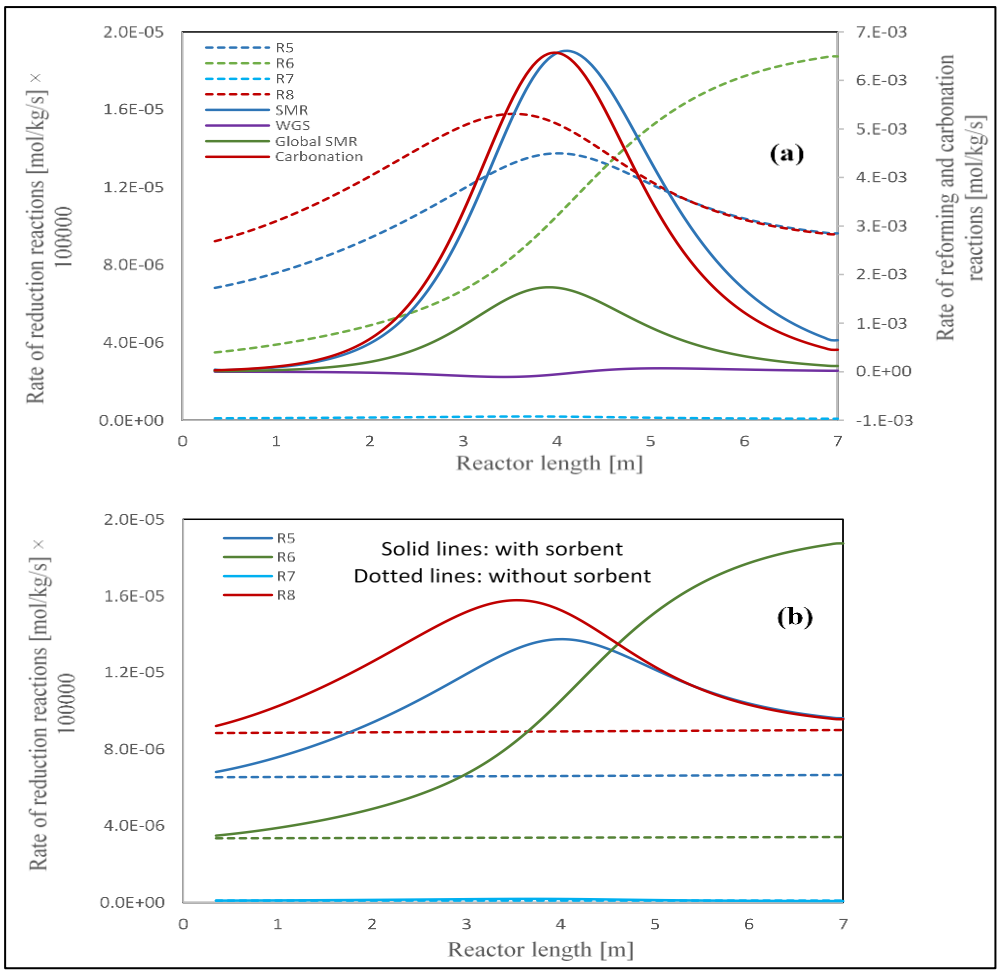

Figure 6.27: The profile of a) rate of reaction of SMR, carbonation and reduction reactions; b) rate of reduction reactions in the presence of sorbent and without sorbent along the length of reactor, in the first cycle of the FR, under the operating conditions of 30 bar, 950 K feed temperature and S/C of 3.0

The variation in CH_4 conversion, H_2 purity, H_2 yield (wt. % of CH_4) and CO_2 capturing efficiency during 11 cycles of SE-CLSR is presented in **Figure 6.28**. The change in CH_4 is very negligible as it varies from 70.81% to 70.77% during 11 cycles of the SE-CLSR process. This shows that cyclic operation of the SE-CLSR process is very stable. The equilibrium value of CH_4 conversion under the same operating conditions is ~82%. The purity and yield (wt. % of CH_4) of H_2 are also not affected during 11 cycles of the SE-CLSR process. At the end of the 11^{th} cycle the purity of H_2 and H_2 yield (wt. %) is 86.9% and 28% against the equilibrium value of 93.9% and 35% respectively. The CO_2 capturing efficiency remains constant at 67.4%, compared to the equilibrium value of 81.8%. This is caused by the kinetics used for the carbonation reaction.

Although the values of CH_4 conversion, purity yield (wt. % of CH_4) of H_2 under high pressure conditions are lower than equilibrium and significantly below 100%, keeping in mind the operational constraints of industrial process for H_2 production (scale of plant, throughput), we need to select the high pressure conditions over lower pressure. As the variation of output results with number of cycles is almost negligible, so in the next section the sensitivity of the SE-CLSR process is checked for temperature and S/C while considering only two cycles of the SE-CLSR process.

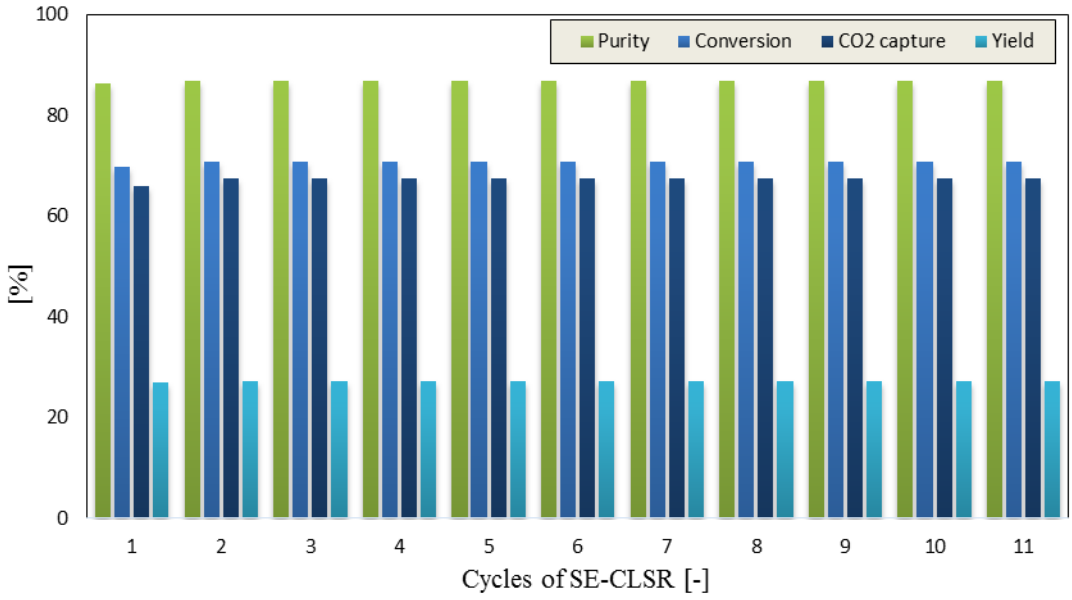

Figure 6.28: Comparison of CH_4 conversion, H_2 purity, H_2 yield (wt. % of CH_4) and CO_2 capturing efficiency achieved during 11 cycles of the SE-CLSR process under the operating conditions of 950 K, 30 bar and S/C of 3.0

6.4.4.2 CASE STUDY 2: Sensitivity analysis on temperature and S/C

In this section, the effect of temperature and S/C on the performance of SE-CLSR is first studied. The output of mathematical modelling will be compared with the equilibrium data generated using CEA. In **Figure 6.29 (a-b),** the effect of temperature on the output mole % (dry basis) of H_2 and CO_2 is shown. At 873 K temperature, the amount of CO_2 is almost zero (0.2 mole % on dry basis) in the pre-breakthrough period and the amount of H_2 is ~83 mole % on a dry basis. As the feed temperature increases from 873 K to 923 K, the amount of CO_2 in the exit gases also increases along with the amount of H_2. It can be seen in **Figure 6.29 (a-b)** that the amount of CO_2 is maximum at 1023 K temperature. This shows that the sorbent is not very active in this temperature range, hence the CO_2

capturing efficiency is not very high. The pre-breakthrough period is different for different temperature conditions. At 923 K and 973 K temperature the amount of H_2 in the pre-breakthrough period is 87.14% and 87.32% respectively and the amount of CO_2 is 0.36% and 0.96% respectively. At 1023 K, the concentration of H_2 (84.6 mole% on dry basis) is also lower than that at 973K temperature. The increase in the temperature of the SE-CLSR process promotes the CH_4 conversion as shown in **Figure 6.30**. The conversion of CH_4 at 873 K and 973 K is 62.4% and 71.7% respectively. The increase in H_2 yield (wt. %) is 23.8-27.7% as temperature increases from 873-973 K. The higher temperature shifts the reforming reaction in the forward direction and enhances the conversion of CH_4 but as the temperature increases from 973 K to 1023 K, a drop in CH_4 conversion is observed. The new value obtained at 1023 K is 70.5%. Similarly the drop in CO_2 capturing efficiency is observed as temperature increases from 973 K to 1023 K (68.3-60.0%). This drop in CO_2 capturing efficiency has a direct adverse effect on the purity of H_2. The H_2 purity drops from 87.3% to 84.6% as temperature increases from 973 K to 1023 K. This confirms that the sorption reaction is not favourable as temperature increases beyond 973 K. The kinetics used for the carbonation reactions are not favourable for such a high temperature conditions.

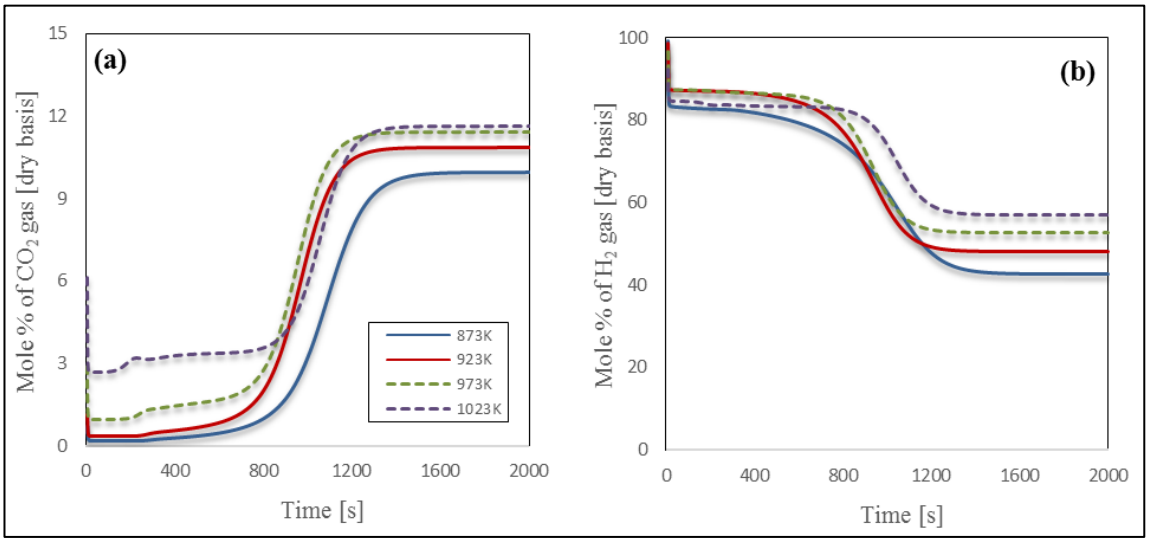

Figure 6.29: Effect of temperature on the outlet composition of a) H_2 and b) CO_2 at 30 bar and S/C of 3.0

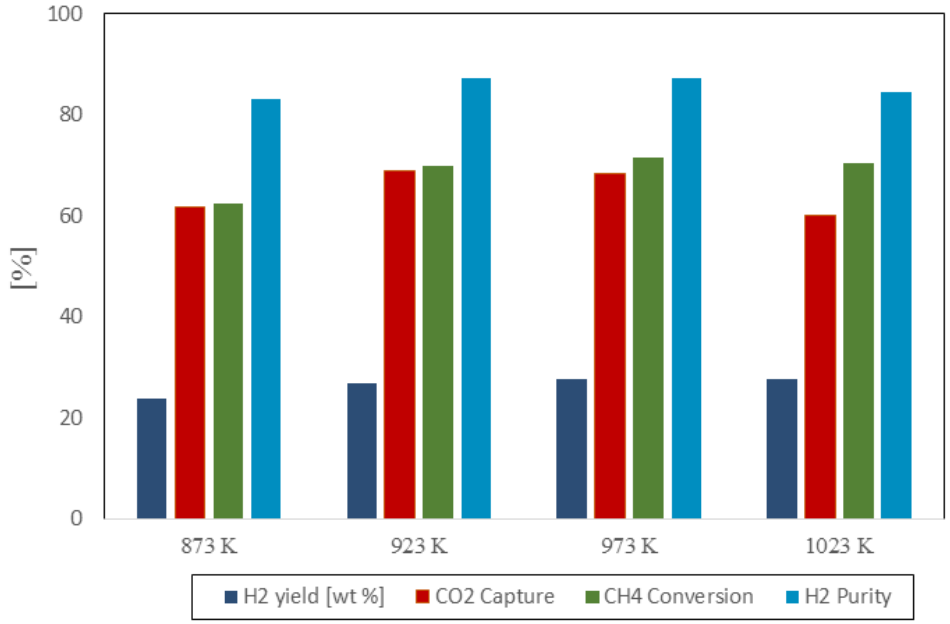

Figure 6. 30: Effect of temperature on the H_2 yield (wt. % of CH_4), CH_4 conversion, CO_2 capturing efficiency and H_2 purity at 30 bar, S/C of 3.0

In **Figure 6.31,** the effect of S/C on CH_4 conversion, H_2 purity, H_2 yield (wt. %) and CO_2 capturing efficiency is shown. The optimum temperature and pressure conditions obtained from previous sections (973 K and 30 bar) are used. It is quite clear from the graph that higher S/C favours more conversion of CH_4 to H_2 as more steam is available for the reforming reactions. The maximum CH_4 conversion is achieved at the highest S/C considered (4.0) i.e. 81.9% and under the same operating conditions, the CO_2 capturing efficiency, the purity and yield (wt. % CH_4) of H_2 are 74.9%, 91.0% and 32% respectively. Although high S/C favours the SE-CLSR process, it puts a burden on the utility cost of the process as more energy is required to generate more steam for the process. So there is a trade-off between the operational cost and the selection of S/C ratio. The optimum value picked is 3.0 as this value is also used in industrial processes of H_2 production to prevent carbon deposits.

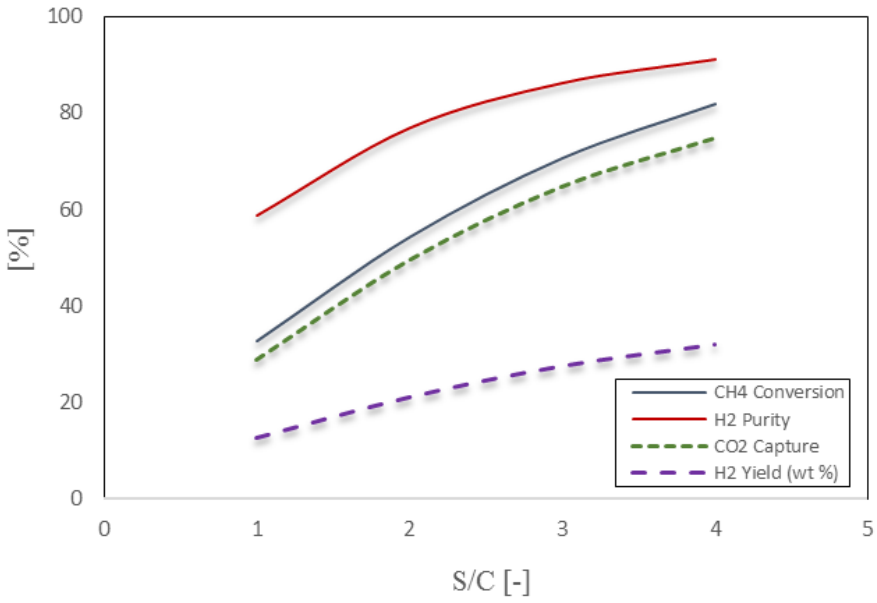

Figure 6.31: Effect of S/C on the CH_4 conversion, H_2 yield (wt. % of CH_4), H_2 purity and CO_2 capturing efficiency under the operating conditions of 973 K, 30 bar, CaO/C of 1.0 and NiO/C of 0.5.

The reduction reactions are endothermic in nature and cause drop in the temperature of the system. Later on, carbonation causes a sudden rise in the temperature because of its exothermicity. As long as the sorbent is not saturated, the temperature of the system remains higher than the feed temperature. The effect of S/C on the temperature of the SE-CLSR at the outlet of the reactor is shown in **Figure 6.32**. It can be seen that there is very negligible effect of S/C on the temperature profile of the packed bed reactor in SE-CLSR process with time. The maximum temperature is almost the same in all cases of S/C i.e. ~945 K. If the FR is allowed to run for a considerable time so that steady state is reached then the minimum temperature reached in all cases is almost the same as well i.e. ~900 K. Another important factor that can affect the performance of the SE-CLSR process is the mass flux of the gas phase (G_s). The higher G_s causes lesser time for the gases to spend within the reactor system. Hence, G_s is inversely proportional to the pseudo contact time. In **Figure 6.33,** the effect of G_s on the outlet composition (dry basis) of H_2 and CO_2 is presented. Higher G_s causes shorter pre-breakthrough period (onset of breakthrough occurs earlier). Conversely, lower G_s causes longer pre-breakthrough. The pre-breakthrough period in case of mass flux of the gas phase of 2, 3.5 and 5 kg $m^{-2}s^{-1}$ is 1300 s, 600 s and 300 s respectively. The values for CH_4 conversion, H_2 yield and H_2 purity

for mass flux of the gas phase of 2, 3.5 and 5 kg $m^{-2}s^{-1}$ are shown in **Table 6.4**. It can be seen that these variations in gas mass flow velocities do not affect the CH_4 conversion, purity and yield (wt. % of CH_4) of H_2 but the time required to complete a cycle of SE-CLSR process. In the conventional SMR process, the equilibrium concentration of the product gases at the exit of the reactor reaches at the gas velocity of 1.5-2 m/s [232]. While the carbonation reaction is slower reaction as compare to SMR, hence longer residence time or slow gas velocity is required to reach the equilibrium concentration of the product gases at the outlet of the reactor. 3.5 kg $m^{-2}s^{-1}$ mass flux (gas velocity equivalent to 0.448 m/s) is selected as the optimum value for the SE-CLSR process as it gives considerable time for the sorbent to react its full capacity without disturbing the cycle duration of the SE-CLSR process.

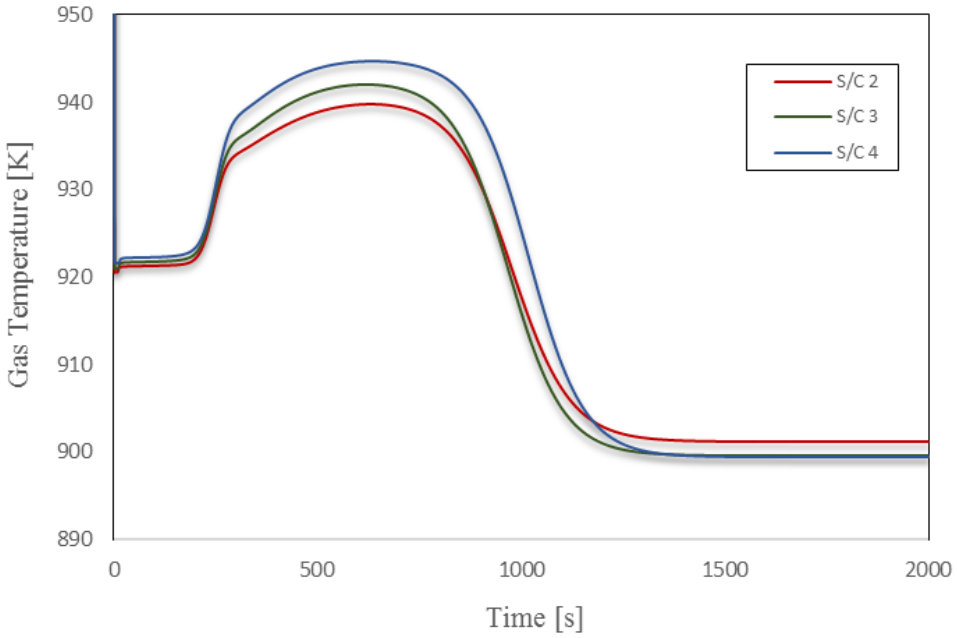

Figure 6.32: Effect of S/C on the temperature profile of the SE-CLSR process under the operating conditions of 973 K, 30 bar, CaO/C of 1.0 and NiO/C of 0.5.

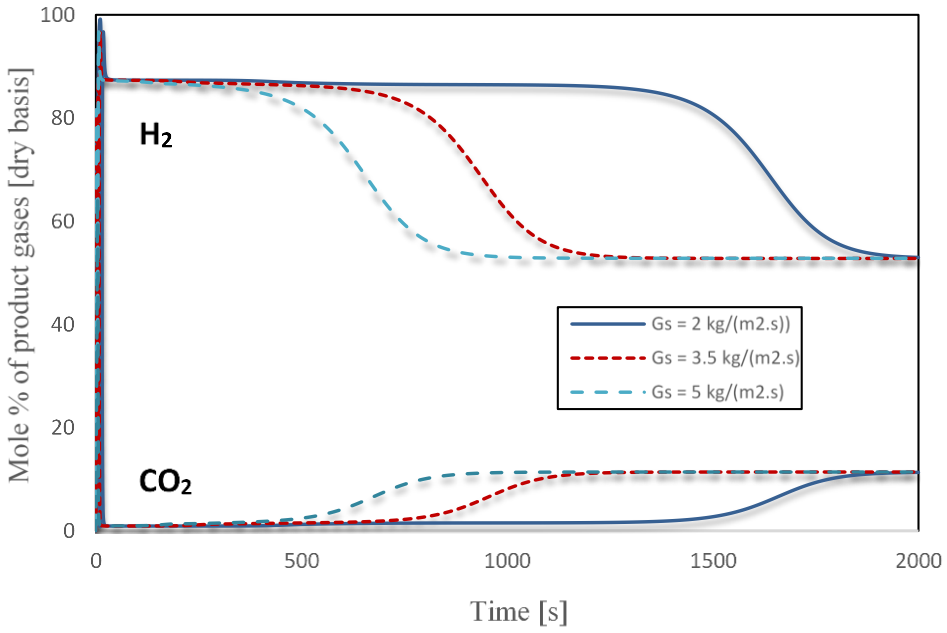

Figure 6.33: Effect of mass flux of the gas phase on the outlet composition of H_2 and CO_2 under the operating conditions of 973 K, 30 bar and S/C of 3.0

Table 6.4: Effect of mass flux of the gas phase on CH_4 conversion, yield (wt. % of CH_4) and purity of H_2 under the operating conditions of 973 K, 30 bar and S/C of 3.0

G_s [kg m^{-2} s^{-1}]	**CH_4 conversion [%]**	**H_2 yield [wt. % of CH_4]**	**H_2 purity [%]**
2	70.61	27.45	85.99
3.5	70.22	27.32	85.77
5	69.79	27.14	85.60

6.5 Conclusion

The adiabatic SE-CLSR process in a packed bed reactor using methane feedstock for H_2 production is simulated using 1-dimensional heterogeneous model of the process. The model equations are solved using the 1st order backward finite difference method in gPROMS. The model of the SE-CLSR is run for 10 cycles under the adiabatic conditions.

The FR cycle and the AR cycle are simulated and the results are validated against published experimental data. The packed bed reactor of SE-CLSR process is run under various operating conditions of temperature, pressure, S/C and mass flow velocities to study the sensitivity of the process. The effect of these operating parameters is studied under the equilibrium conditions and later on compared with the dynamic model outputs. It is concluded from the results that there is a negligible effect observed on CH_4 conversion, H_2 purity, H_2 yield (wt. %) and CO_2 capturing efficiency during the various number of the SE-CLSR cycles. The effect of pressure is positive on the performance of SE-CLSR process, but as the pressure exceeds 5 bar, the conversion and CO_2 capturing efficiency decreases. While keeping in mind the H_2 production on industrial scale, the pressure of 30 bar is used to generate data at different operating temperatures (873-973 K). At 873 K, 62% CH_4 conversion and 83% H_2 purity are achieved. As the temperature increases to 973 K, the CH_4 conversion and H_2 purity both increase to 72% and 87% respectively. The temperature higher than 973 K reduces both H_2 purity and CO_2 capturing efficiency as the carbonation reaction is not active at such a higher temperature. So 973 K is selected as the optimum temperature for the SE-CLSR process operated under 30 bar pressure. The S/C of 3.0 gives the optimum value for CH_4 conversion and H_2 purity as the higher values of S/C are not favourable as far as the operational cost of the process is concerned. The higher S/C increases steam requirement and hence more operational cost. So, despite of its positive effect on CH_4 conversion and H_2 production, S/C higher than 3 is not recommended for the industrial scale production of H_2. It is concluded that the gas mass flow velocity has no effect on the production of H_2 but the higher mass flux of the gas phase reduces the pre-breakthrough period and the cycle duration. The mass flux of the gas phase of 3.5 kg $m^{-2}s^{-1}$ is selected as the optimum value for 30 bar and S/C of 3. The sensitivity analysis demonstrates that the developed model of the SE-CLSR process gives significantly higher purity of H_2 and CH_4 conversion under high pressure (30 bar) conditions as compared to the conventional SMR process. This model can be applied to simulate continuous production of H_2 using either two or multiple packed bed reactors. In future, this model will be used to simulate the production of H_2 in ammonia plant.

CHAPTER # 7

CONCLUSIONS & FUTURE RECOMMENDATIONS

7.1 Conclusions

An experimental study was performed over the surface of 18 wt. % NiO/α-Al_2O_3 catalyst, to determine the true reaction kinetics of the steam methane reforming (SMR) process while keeping in mind the conditions of diffusion limitations and away from the equilibrium. A non-linear least square analysis, based on minimization of the sum of residual squares of the experimental reaction rates and the predicted reaction rates, was used to estimate the kinetic parameters. The activation energies for SMR, WGS and global SMR reactions were calculated as 257.0, 89.2 and 236.7 kJ mol^{-1} respectively.
The performance of the SMR process in terms of fuel conversion, selectivity of the outlet gases, purity and yield (wt. % of CH_4) of H_2 was demonstrated in a packed bed reformer using a 1-D heterogeneous reactor model. The modelling results were validated against the experimental results under conditions away from equilibrium and at equilibrium. Later on, modelling results were compared with the equilibrium results and an excellent agreement was observed. High temperature, lower pressure and high steam to carbon (S/C) ratio gave the excellent performance of the system in terms of fuel conversion and purity of H_2.

7.1.1 SE-SMR model

The 1-D SE-SMR model developed on gPROMS model builder 4.1.0® mimiqued the experimental data reported in the literature with an excellent agreement. The mathematical model under both adiabatic and non-adiabatic conditions behave well according to the literature data. Operating parameters, such as; temperature, pressure, S/C and gas mass flux (G_s) have a strong influence on the performance of the SE-SMR process. The optimum temperature obtained under the high pressure conditions (30 bar) was 923 K. This temperature resulted in 67.5% CH_4 conversion at S/C of 3.0 and 30 bar.

The purity of H_2 achieved under the same optimum temperature and operating conditions was 84.1%. While studying the effect of the pressure at this optimum temperature, it was observed that pressure higher than 5 bar had negative effect on the conversion of CH_4 and H_2 purity. The selection of optimum pressure for the industrial scale was a trade-off between H_2 purity and industrial plant constraints (pressure in 20-30 bar range). The pressure as high as 30 bar was considered as optimum in this study as it fulfilled the requirement of the industrial pressure of H_2 (20-30 bar) and gave a considerable purity of H_2 (84.1%). The selection of optimum S/C was also a trade-off between the purity of H_2 and operational cost of the plant. The higher amount of steam enhances the conversion of CH_4 and the H_2 purity but high steam requirement is not feasible in terms of operational cost of the plant. The S/C of 3.0 is selected to meet the requirements of H_2 purity at minimum operational cost. As higher S/C (>3.0) requires higher duty for steam generation and size of the reformer. The selection of optimum G_s is done on the basis of operational time of the process and H_2 purity achieved at the outlet of the reactor. The G_s of 2 kg m^{-2} s^{-1} causes the onset of pre-breakthrough period at 1200 s while at 7 kg m^{-2} s^{-1} it is 90 s. The G_s of 3.5 kg m^{-2} s^{-1} is picked as optimum value having pre-breakthrough period of 700 s and 67.5% CH_4 conversion against equilibrium CH_4 conversion of 71.4%. Furthermore, the comparison of results from SE-SMR and SMR models shows the conversion enhancement due to the presence of the sorbent in the reactor. The adsorption of CO_2 on the active surface of the sorbent is highly exothermic process and it releases considerable amount of heat (ΔH_{rex} = -178.8 kJ mol^{-1}). This heat promotes the reforming reactions and a CH_4 conversion higher than that achieved by the conventional SMR.

7.1.2 SE-CLSR model

The adiabatic SE-CLSR process in a packed bed reactor using methane feedstock for H_2 production was simulated using the model of the process. The model of the SE-CLSR was run for 10 cycles under adiabatic conditions. The fuel reactor (FR) cycle and the air reactor (AR) cycle were simulated and the results were validated against the published experimental data. The packed bed reactor of SE-CLSR process was run under various operating conditions of temperature (873-1023 K), pressure (1-30 bar), S/C (2-6) and G_s (2-7 kg m^{-2} s^{-1}) to study the sensitivity of the process. The effect of these operating parameters was studied under the equilibrium conditions and later on equilibrium results were compared with the model outputs. It was concluded from the results that there was

a negligible effect on CH_4 conversion, H_2 purity, H_2 yield (wt. % of CH_4) and CO_2 capturing efficiency from cycle to cycle over 10 cycles of SE-CLSR operation. The effect of pressure on the performance of SE-CLSR process was positive, but as the pressure exceeded 5 bar, the conversion and CO_2 capturing efficiency decreased. While keeping in mind the H_2 production on industrial scale, the pressure of 30 bar was used to generate data at different operating temperatures (873-973 K). At 873 K, 62% CH_4 conversion and 83% H_2 purity were achieved. As the temperature increased to 973 K, the CH_4 conversion and H_2 purity both increased to 72% and 87% respectively. The temperature higher than 973 K reduced both H_2 purity and CO_2 capturing efficiency as the carbonation reaction was not active at such a higher temperature. Thus 973 K was selected as the optimum temperature for the SE-CLSR process operated under 30 bar pressure. The S/C of 3.0 yielded the optimum value for CH_4 conversion and H_2 purity as the higher values of S/C were not favourable as far as the operational and capital costs of the process are concerned. So, despite of its positive effect on CH_4 conversion and H_2 production, S/C higher than 3 was not recommended for the industrial scale production of H_2. It was concluded that the G_s had no effect on the production of H_2 but the higher mass flux of the gas phase reduced the pre-breakthrough period and the cycle duration. The G_s of 3.5 kg $m^{-2}s^{-1}$ was selected as the optimum value for 30 bar and S/C of 3. The sensitivity analysis demonstrated that the developed model of the SE-CLSR process resulted in a significantly higher purity of H_2 and CH_4 conversion under high pressure (30 bar) conditions as compared to the conventional SMR process. This model can be applied to simulate continuous production of H_2 using either two or multiple packed bed reactors.

7.2 Future work

In this work, the mathematical model of the SE-CLSR process was successfully developed on gPROMS model builder 4.1.0®, and the sensitivity of the model was checked under various operating temperature, pressure, S/C and G_s while keeping in mind the realistic industrial scale conditions. This process gave high overall process efficiency, CH_4 conversion and H_2 yield (wt. % of CH_4) as compared to the conventional SMR process. The production of H_2 in industrial ammonia plants is based on the conventional SMR process. This research can be used to simulate the ammonia plant by replacing the conventional reforming process with this developed SE-CLSR process. The effect of sorbent degradation on the performance of SE-CLSR can be studied in the future to

investigate the more detail insight of the process. The current model does not incorporate the variation of temperature and concentration within the pores of the catalyst and sorbent particles. In the future, work could be done to model the behaviour of the gases within the pores of the particles. The degradation of the sorbent is not studied in this work, work could be done to model the effect of sorbent degradation on the performance of SE-CLSR process.

8. References

1. Gupta, R.B., Hydrogen fuel: production, transport, and storage2008: Crc Press.
2. Change, I.P.o.C., Climate Change 2014–Impacts, Adaptation and Vulnerability: Regional Aspects2014: Cambridge University Press.
3. Kosaka, Y. and S.-P. Xie, Recent global-warming hiatus tied to equatorial Pacific surface cooling. Nature, 2013. **501**(7467): p. 403-407.
4. Pachauri, R.K., M. Allen, V. Barros, J. Broome, W. Cramer, R. Christ, J. Church, L. Clarke, Q. Dahe, and P. Dasgupta, Climate Change 2014: Synthesis Report. Contribution of Working Groups I, II and III to the Fifth Assessment Report of the Intergovernmental Panel on Climate Change. 2014.
5. Beér, J., CO2 Reduction and Coal-Based Electricity Generation, in Fossil Energy2013, Springer. p. 475-488.
6. Metz, B., O. Davidson, H. De Coninck, M. Loos, and L. Meyer, Carbon dioxide capture and storage. 2005.
7. Painuly, J.P., Barriers to renewable energy penetration; a framework for analysis. Renewable energy, 2001. **24**(1): p. 73-89.
8. Birol, F., World energy outlook 2010. International Energy Agency, 2010. **1**.
9. Khatib, H., IEA World Energy Outlook 2011—A comment. Energy Policy, 2012. **48**: p. 737-743.
10. Dupont, V., A. Ross, E. Knight, I. Hanley, and M. Twigg, Production of hydrogen by unmixed steam reforming of methane. Chemical Engineering Science, 2008. **63**(11): p. 2966-2979.
11. Gilland, B., World population and food supply: can food production keep pace with population growth in the next half-century? Food policy, 2002. **27**(1): p. 47-63.
12. Ramachandran, R. and R.K. Menon, An overview of industrial uses of hydrogen. International Journal of Hydrogen Energy, 1998. **23**(7): p. 593-598.
13. Chiron, F.-X., G.S. Patience, and S. Rifflart, Hydrogen production through chemical looping using NiO/NiAl2O4 as oxygen carrier. Chemical Engineering Science, 2011. **66**(24): p. 6324-6330.
14. Harrison, D.P. and Z. Peng, Low-Carbon Monoxide Hydrogen by Sorption-Enhanced Reaction. International Journal of Chemical and Reactor Engineering, 2003. **1**: p. 1055.

15. Ogden, J.M., Developing an infrastructure for hydrogen vehicles: a Southern California case study. International Journal of Hydrogen Energy, 1999. **24**(8): p. 709-730.
16. Balasubramanian, B., A. Lopez Ortiz, S. Kaytakoglu, and D. Harrison, Hydrogen from methane in a single-step process. Chemical Engineering Science, 1999. **54**(15): p. 3543-3552.
17. Abrardo, J. and V. Khurana, Hydrogen technologies to meet refiners' future needs: Fuels management. Hydrocarbon Processing, 1995. **74**(2): p. 43-49.
18. Liguras, D.K., D.I. Kondarides, and X.E. Verykios, Production of hydrogen for fuel cells by steam reforming of ethanol over supported noble metal catalysts. Applied Catalysis B: Environmental, 2003. **43**(4): p. 345-354.
19. Rydén, M. and P. Ramos, H 2 production with CO 2 capture by sorption enhanced chemical-looping reforming using NiO as oxygen carrier and CaO as CO 2 sorbent. Fuel Processing Technology, 2012. **96**: p. 27-36.
20. Ritter, J. and A. Ebner, Separation technology R&D needs for hydrogen production in the chemical and petrochemical industries. report for US Department of Energy, 2005.
21. Sherif, S.A., F. Barbin, and T.N. Veziroglu, Principles of hydrogen energy production, storage and utilization. Journal of Scientific and Industrial Research, 2003. **62**(1/2): p. 46-63.
22. Kumar, R.V., R.K. Lyon, and J.A. Cole, Unmixed Reforming: A Novel Autothermal Cyclic Steam Reforming Process, in Advances in Hydrogen Energy2002, Springer. p. 31-45.
23. Carrette, L., K. Friedrich, and U. Stimming, Fuel cells–fundamentals and applications. Fuel cells, 2001. **1**(1): p. 5-39.
24. Edwards, P.P., V.L. Kuznetsov, W.I. David, and N.P. Brandon, Hydrogen and fuel cells: towards a sustainable energy future. Energy Policy, 2008. **36**(12): p. 4356-4362.
25. Kreith, F. and R. West, Fallacies of a hydrogen economy: a critical analysis of hydrogen production and utilization. Journal of Energy Resources Technology, 2004. **126**(4): p. 249-257.
26. Cortright, R., R. Davda, and J. Dumesic, Hydrogen from catalytic reforming of biomass-derived hydrocarbons in liquid water. Nature, 2002. **418**(6901): p. 964-967.

27. Rutkowski, M. Current (2005) hydrogen from SMR natural gas with CO2 capture and sequestration. 2005; Available from: http://www.hydrogen.energy.gov/h2a_prod_studies.html
28. Le May, I., T. Da Silveira, and C. Vianna, Criteria for the evaluation of damage and remaining life in reformer furnace tubes. International journal of pressure vessels and piping, 1996. **66**(1): p. 233-241.
29. Ray, A.K., S.K. Sinha, Y.N. Tiwari, J. Swaminathan, G. Das, S. Chaudhuri, and R. Singh, Analysis of failed reformer tubes. Engineering Failure Analysis, 2003. **10**(3): p. 351-362.
30. da Silveira, T.L. and I. Le May, Reformer Furnaces: Materials, Damage Mechanisms, and Assessment. Arabian Journal for Science and Engineering, 2006. **31**(2): p. 99.
31. Brightling, J.R., P.V. Broadhurst, and M.P. Roberts, Catalyst catastrophes in hydrogen plants. Petroleum technology quarterly, 2006. **11**(1): p. 39.
32. Bartholomew, C.H. and R.J. Farrauto, Fundamentals of industrial catalytic processes2011: John Wiley & Sons.
33. Xiu, G.-h., P. Li, and A.E. Rodrigues, Sorption-enhanced reaction process with reactive regeneration. Chemical Engineering Science, 2002. **57**(18): p. 3893-3908.
34. Harrison, D.P., Sorption-enhanced hydrogen production: a review. Industrial & engineering chemistry research, 2008. **47**(17): p. 6486-6501.
35. Lyon, R.K. and J.A. Cole, Unmixed combustion: an alternative to fire. Combustion and Flame, 2000. **121**(1): p. 249-261.
36. Rydén, M. and A. Lyngfelt, Using steam reforming to produce hydrogen with carbon dioxide capture by chemical-looping combustion. International Journal of Hydrogen Energy, 2006. **31**(10): p. 1271-1283.
37. Rydén, M. and P. Ramos, H< sub> 2</sub> production with CO< sub> 2</sub> capture by sorption enhanced chemical-looping reforming using NiO as oxygen carrier and CaO as CO< sub> 2</sub> sorbent. Fuel Processing Technology, 2012. **96**: p. 27-36.
38. Kulkarni, P., J. Guan, R. Subia, Z. Cui, J. Manke, A. Frydman, W. Wei, R. Shisler, R. Ayala, and G. Rizeq, Fuel-Flexible Gasification-Combustion Technology for Production of H2 and Sequestration-Ready CO2, 2008, GE Energy & Environmental Research Corporation.

39. Pimenidou, P., G. Rickett, V. Dupont, and M.V. Twigg, High purity H 2 by sorption-enhanced chemical looping reforming of waste cooking oil in a packed bed reactor. Bioresource Technology, 2010. **101**(23): p. 9279-9286.
40. Fernandez, J., J. Abanades, and R. Murillo, Modeling of sorption enhanced steam methane reforming in an adiabatic fixed bed reactor. Chemical Engineering Science, 2012. **84**: p. 1-11.
41. Lee, D.K., I.H. Baek, and W.L. Yoon, Modeling and simulation for the methane steam reforming enhanced by in situ CO 2 removal utilizing the CaO carbonation for H 2 production. Chemical Engineering Science, 2004. **59**(4): p. 931-942.
42. Monnerat, B., L. Kiwi-Minsker, and A. Renken, Mathematical modelling of the unsteady-state oxidation of nickel gauze catalysts. Chemical Engineering Science, 2003. **58**(21): p. 4911-4919.
43. Iliuta, I., R. Tahoces, G.S. Patience, S. Rifflart, and F. Luck, Chemical-looping combustion process: Kinetics and mathematical modeling. AIChE Journal, 2010. **56**(4): p. 1063-1079.
44. Badwal, S.P., S. Giddey, and C. Munnings, Hydrogen production via solid electrolytic routes. Wiley Interdisciplinary Reviews: Energy and Environment, 2013. **2**(5): p. 473-487.
45. Pant, K. and R.B. Gupta, Fundamentals and use of hydrogen as a fuel. Hydrogen fuel: production, transport, and storage, 2009: p. 3-32.
46. Davis, S.C., S.W. Diegel, and R.G. Boundy, Transportation energy data book: Edition 23, 2003, United States. Department of Energy.
47. Scholz, W.H., Processes for industrial production of hydrogen and associated environmental effects. Gas separation & purification, 1993. **7**(3): p. 131-139.
48. Solomon, B.D. and A. Banerjee, A global survey of hydrogen energy research, development and policy. Energy Policy, 2006. **34**(7): p. 781-792.
49. Rostrup-Nielsen, J.R., Production of synthesis gas. Catalysis today, 1993. **18**(4): p. 305-324.
50. Armor, J.N., The multiple roles for catalysis in the production of H 2. Applied Catalysis A: General, 1999. **176**(2): p. 159-176.
51. Rostrupnielsen, J. and J.B. Hansen, CO 2-reforming of methane over transition metals. Journal of Catalysis, 1993. **144**(1): p. 38-49.
52. Rostrup-Nielsen, J.R., Catalytic steam reforming1984: Springer.

53. Wang, S. and G. Lu, CO 2 reforming of methane on Ni catalysts: effects of the support phase and preparation technique. Applied Catalysis B: Environmental, 1998. **16**(3): p. 269-277.
54. Holladay, J.D., J. Hu, D.L. King, and Y. Wang, An overview of hydrogen production technologies. Catalysis today, 2009. **139**(4): p. 244-260.
55. Hohn, K. and L. Schmidt, Partial oxidation of methane to syngas at high space velocities over Rh-coated spheres. Applied Catalysis A: General, 2001. **211**(1): p. 53-68.
56. Krummenacher, J.J., K.N. West, and L.D. Schmidt, Catalytic partial oxidation of higher hydrocarbons at millisecond contact times: decane, hexadecane, and diesel fuel. Journal of Catalysis, 2003. **215**(2): p. 332-343.
57. Pino, L., V. Recupero, S. Beninati, A.K. Shukla, M.S. Hegde, and P. Bera, Catalytic partial-oxidation of methane on a ceria-supported platinum catalyst for application in fuel cell electric vehicles. Applied Catalysis A: General, 2002. **225**(1): p. 63-75.
58. Song, C., Fuel processing for low-temperature and high-temperature fuel cells: Challenges, and opportunities for sustainable development in the 21st century. Catalysis today, 2002. **77**(1): p. 17-49.
59. Hu, Y.H. and E. Ruckenstein, Catalytic conversion of methane to synthesis gas by partial oxidation and CO 2 reforming. Advances in Catalysis, 2004. **48**: p. 297-345.
60. Dissanayake, D., M.P. Rosynek, K.C. Kharas, and J.H. Lunsford, Partial oxidation of methane to carbon monoxide and hydrogen over a Ni/Al 2 O 3 catalyst. Journal of Catalysis, 1991. **132**(1): p. 117-127.
61. Hickman, D. and L. Schmidt, Production of syngas by direct catalytic oxidation of methane. SCIENCE-NEW YORK THEN WASHINGTON-, 1993. **259**: p. 343-343.
62. Hamid, A., M. Kamaruddin, N. Ibrahim, K.A. Ibrahim, and A. Ahmad, Simulation of hydrogen production for mobile fuel cell applications via autothermal reforming of methane. 2006.
63. Freni, S., G. Calogero, and S. Cavallaro, Hydrogen production from methane through catalytic partial oxidation reactions. Journal of Power sources, 2000. **87**(1): p. 28-38.

64. Wilhelm, D., D. Simbeck, A. Karp, and R. Dickenson, Syngas production for gas-to-liquids applications: technologies, issues and outlook. Fuel Processing Technology, 2001. **71**(1): p. 139-148.
65. Holladay, J., E. Jones, D.R. Palo, M. Phelps, Y.-H. Chin, R. Dagle, J. Hu, Y. Wang, and E. Baker. Miniature fuel processors for portable fuel cell power supplies. in MRS Proceedings. 2002. Cambridge Univ Press.
66. Navarro, R., M. Pena, and J. Fierro, Hydrogen production reactions from carbon feedstocks: fossil fuels and biomass. Chemical Reviews, 2007. **107**(10): p. 3952-3991.
67. Adánez, J., P. Gayán, J. Celaya, L.F. de Diego, F. García-Labiano, and A. Abad, Chemical looping combustion in a 10 kWth prototype using a CuO/Al2O3 oxygen carrier: Effect of operating conditions on methane combustion. Industrial & engineering chemistry research, 2006. **45**(17): p. 6075-6080.
68. Lewis, W., E. Gilliland, and M. Sweeney, Gasification of carbon-Metal oxides in a fluidized powder bed. Chemical Engineering Progress, 1951. **47**(5): p. 251-256.
69. Production of pure carbon dioxide, 1954, Google Patents.
70. Gaggioli, R.A. Second law analysis for process and energy engineering. in ACS Symposium series. 1983. Oxford University Press.
71. Ishida, M., D. Zheng, and T. Akehata, Evaluation of a chemical-looping-combustion power-generation system by graphic exergy analysis. Energy, 1987. **12**(2): p. 147-154.
72. Hatanaka, T., S. Matsuda, and H. Hatano. A new-concept gas-solid combustion system "MERIT" for high combustion efficiency and low emissions. in Energy Conversion Engineering Conference, 1997. IECEC-97., Proceedings of the 32nd Intersociety. 1997. IEEE.
73. Thomas, D.C. and S.M. Benson, Carbon Dioxide Capture for Storage in Deep Geologic Formations-Results from the CO2 Capture Project: Vol 2-Geologic Storage of Carbon Dioxide with Monitoring and Verification2015: Elsevier.
74. Lyngfelt, A., B. Kronberger, J. Adanez, J. Morin, and P. Hurst. Development of oxygen carrier particles for chemical-looping combustion design and operation of a 10 kW chemical-combustor. in 7th International Conference on Greenhouse Gas Control Technologies, Canada. 2004.

75. Adánez, J., L.F. de Diego, F. García-Labiano, P. Gayán, A. Abad, and J. Palacios, Selection of oxygen carriers for chemical-looping combustion. Energy & Fuels, 2004. **18**(2): p. 371-377.
76. Lyngfelt, A. and H. Thunman, Construction and 100 h of operational experience of a 10-kW chemical-looping combustor. Carbon dioxide capture for storage in deep geologic formations-results from the CO2 capture project, 2005. **1**: p. 625-645.
77. Mattisson, T., F. García-Labiano, B. Kronberger, A. Lyngfelt, J. Adánez, and H. Hofbauer, Chemical-looping combustion using syngas as fuel. International Journal of Greenhouse Gas Control, 2007. **1**(2): p. 158-169.
78. Luis, F., F. Garcı, P. Gayán, J. Celaya, J.M. Palacios, and J. Adánez, Operation of a 10kWth chemical-looping combustor during 200h with a CuO–Al 2 O 3 oxygen carrier. Fuel, 2007. **86**(7): p. 1036-1045.
79. Lyon, R.K., Methods and systems for heat transfer by unmixed combustion, 1996.
80. Kumar, R.V., J.A. Cole, and R.K. Lyon. Unmixed reforming: an advanced steam reforming process. in Fuel Cell Reformer Conference, South Coast Air Quality District, Diamond Bar, CA. 1999.
81. Rizeq, R., R. Kumar, J. West, V. Zamansky, and K. Das. Advanced gasification-combustion technology for production of H2, power, and sequestration-ready CO2. in Proceedings of International Pittsburgh Coal Conference, Newcastle, New South Wales, Australia, December. 2001.
82. Beavis, R., Introduction to Cachet. A pre-combustion technology, development program, co-funded by the EU and CCP. Carbon dioxide capture for storage in deep geological formationse results from the CO2 capture project, 2009. **3**.
83. Rydén, M., A. Lyngfelt, A. Schulman, L.F. de Diego, J. Adánez, M. Ortiz, T. Pröll, J. Bolhàr-Nordenkampf, and P. Kolbitsch, Developing chemical looping steam reforming and chemical looping autothermal reforming. Carbon Dioxide Capture for Storage in Deep Geological Formations–Results from the CO2 Capture Project, 2009. **3**.
84. Fang, H., L. Haibin, and Z. Zengli, Advancements in development of chemical-looping combustion: a review. International Journal of Chemical Engineering, 2009. **2009**.
85. Rydén, M., Hydrogen production from fossil fuels with carbon dioxide capture, using chemical-looping technologies2008: Chalmers University of Technology.

86. Mattisson, T. and A. Lyngfelt, Applications of chemical-looping combustion with capture of CO2. Second Nordic Minisymposium on CO2 Capture and Storage, Göteborg, Sweden, 2001.
87. Rydén, M., A. Lyngfelt, and T. Mattisson, Chemical-looping combustion and chemical-looping reforming in a circulating fluidized-bed reactor using Ni-based oxygen carriers. Energy & Fuels, 2008. **22**(4): p. 2585-2597.
88. Luis, F., M. Ortiz, F. García-Labiano, J. Adánez, A. Abad, and P. Gayán, Hydrogen production by chemical-looping reforming in a circulating fluidized bed reactor using Ni-based oxygen carriers. Journal of Power sources, 2009. **192**(1): p. 27-34.
89. Luis, F., M. Ortiz, J. Adánez, F. García-Labiano, A. Abad, and P. Gayán, Synthesis gas generation by chemical-looping reforming in a batch fluidized bed reactor using Ni-based oxygen carriers. Chemical Engineering Journal, 2008. **144**(2): p. 289-298.
90. Zafar, Q., T. Mattisson, and B. Gevert, Redox investigation of some oxides of transition-state metals Ni, Cu, Fe, and Mn supported on SiO2 and MgAl2O4. Energy & Fuels, 2006. **20**(1): p. 34-44.
91. Rydén, M., A. Lyngfelt, and T. Mattisson, Synthesis gas generation by chemical-looping reforming in a continuously operating laboratory reactor. Fuel, 2006. **85**(12): p. 1631-1641.
92. Pröll, T., J. Bolhàr-Nordenkampf, P. Kolbitsch, and H. Hofbauer, Syngas and a separate nitrogen/argon stream via chemical looping reforming–A 140kW pilot plant study. Fuel, 2010. **89**(6): p. 1249-1256.
93. Rydén, M., M. Johansson, A. Lyngfelt, and T. Mattisson, NiO supported on Mg–ZrO 2 as oxygen carrier for chemical-looping combustion and chemical-looping reforming. Energy & Environmental Science, 2009. **2**(9): p. 970-981.
94. Rydén, M., A. Lyngfelt, T. Mattisson, D. Chen, A. Holmen, and E. Bjørgum, Novel oxygen-carrier materials for chemical-looping combustion and chemical-looping reforming; La x Sr 1− x Fe y Co 1− y O 3− δ perovskites and mixed-metal oxides of NiO, Fe 2 O 3 and Mn 3 O 4. International Journal of Greenhouse Gas Control, 2008. **2**(1): p. 21-36.
95. Johansson, M., T. Mattisson, A. Lyngfelt, and A. Abad, Using continuous and pulse experiments to compare two promising nickel-based oxygen carriers for use in chemical-looping technologies. Fuel, 2008. **87**(6): p. 988-1001.

96. Kolbitsch, P., J. Bolhar-Nordenkampf, T. Pröll, and H. Hofbauer, Comparison of two Ni-based oxygen carriers for chemical looping combustion of natural gas in 140 kW continuous looping operation. Industrial & engineering chemistry research, 2009. **48**(11): p. 5542-5547.
97. Balasubramanian, B., A.L. Ortiz, S. Kaytakoglu, and D. Harrison, Hydrogen from methane in a single-step process. Chemical Engineering Science, 1999. **54**(15): p. 3543-3552.
98. Mayorga, S.G., J.R. Hufton, S. Sircar, and T.R. Gaffney, Sorption enhanced reaction process for production of hydrogen. Phase 1 final report, 1997, Air Products and Chemicals, Inc., Allentown, PA (United States).
99. Roger, W., Hydrogen production, 1933, Google Patents.
100. Retallick, W.B., Method for the production of hydrogen, 1963, Google Patents.
101. Dou, B., G.L. Rickett, V. Dupont, P.T. Williams, H. Chen, Y. Ding, and M. Ghadiri, Steam reforming of crude glycerol with in situ CO 2 sorption. Bioresource Technology, 2010. **101**(7): p. 2436-2442.
102. Barelli, L., G. Bidini, F. Gallorini, and S. Servili, Hydrogen production through sorption-enhanced steam methane reforming and membrane technology: a review. Energy, 2008. **33**(4): p. 554-570.
103. Ding, Y. and E. Alpay, Adsorption-enhanced steam–methane reforming. Chemical Engineering Science, 2000. **55**(18): p. 3929-3940.
104. Ochoa-Fernández, E., G. Haugen, T. Zhao, M. Rønning, I. Aartun, B. Børresen, E. Rytter, M. Rønnekleiv, and D. Chen, Process design simulation of H2 production by sorption enhanced steam methane reforming: evaluation of potential CO2 acceptors. Green Chemistry, 2007. **9**(6): p. 654-662.
105. Hufton, J., W. Waldron, S. Weigel, M. Rao, S. Nataraj, and S. Sircar. Sorption enhanced reaction process (SERP) for the production of hydrogen. in Proceedings of the 2000 US DOE Hydrogen Program Review. 2000.
106. Hufton, J., S. Mayorga, and S. Sircar, Sorption-enhanced reaction process for hydrogen production. AIChE Journal, 1999. **45**(2): p. 248-256.
107. Koumpouras, G.C., E. Alpay, and F. Stepanek, Mathematical modelling of low-temperature hydrogen production with in situ CO< sub> 2</sub> capture. Chemical Engineering Science, 2007. **62**(10): p. 2833-2841.

108. Xiu, G., P. Li, and A.E. Rodrigues, Adsorption-enhanced steam-methane reforming with intraparticle-diffusion limitations. Chemical Engineering Journal, 2003. **95**(1): p. 83-93.
109. Pimenidou, P., G. Rickett, V. Dupont, and M. Twigg, Chemical looping reforming of waste cooking oil in packed bed reactor. Bioresource Technology, 2010. **101**(16): p. 6389-6397.
110. Elnashaie, S.S., Modelling, simulation and optimization of industrial fixed bed catalytic reactors. Vol. 7. 1994: CRC Press.
111. Eigenberger, G., Modelling and simulation in industrial chemical reaction engineering, in Modelling of Chemical Reaction Systems1981, Springer. p. 284-304.
112. Salmi, T., Modelling and simulation of transient states of ideal heterogeneous catalytic reactors. Chemical Engineering Science, 1988. **43**(3): p. 503-511.
113. Baiker, A. and M. Bergougnan, Investigation of a fixed-bed pilot plant reactor by dynamic experimentation. Part 1. Apparatus and experimental results. The Canadian Journal of Chemical Engineering, 1985. **63**(1): p. 138-145.
114. Schnelle Jr, P. and J. Richards, A review of industrial reactor control: difficult problems and workable solutions. Chemical Process Control-CPC III, 1986: p. 749-802.
115. Elnashaie, S. and F. Alhabdan, Mathematical modelling and computer simulation of industrial water–gas shift converters. Mathematical and Computer Modelling, 1989. **12**(8): p. 1017-1034.
116. Prigogine, I., Irreversibility as a symmetry-breaking process. 1973.
117. Douglas, J.M., Process Dynamics and Control: Control System Synthesis. Vol. 2. 1972: Prentice Hall.
118. Froment, G.F. and K.B. Bischoff, Chemical reactor design and analysis. John Wiley & Sons, New York, 1979.
119. Froment, G.F., chemical reactor analysis and design, 2007, john wiley and sons, inc.
120. Eishishini, S.S.E.H.E.a.S.S., in Modelling, simulation and optimization of industrial fixed bed catalytic reactors1993, Gorden and breach science publishers.
121. Danckwerts, P.V., Continuous flow systems: Distribution of residence times. Chemical Engineering Science, 1953. **2**(1): p. 1-13.

122. Iordanidi, A., Mathematical modeling of catalytic fixed bed reactors2002: Twente University Press.
123. Bird, R.B., W.E. Stewart, and E.N. Lightfoot, Transport phenomena. Vol. 2. 1960: Wiley New York.
124. Bird, R.B., W.E. Stewart, and E.N. Lightfoot, Transport phenomena2007: Wiley. com.
125. Reynolds, O., A.W. Brightmore, and W.H. Moorby, Papers on Mechanical and Physical Subjects: 1881-1900. Vol. 2. 1901: The University Press.
126. Ergun, S., Fluid flow through packed columns. Chem. Eng. Prog., 1952. **48**: p. 89-94.
127. Handley, D. and P. Heggs, The effect of thermal conductivity of the packing material on transient heat transfer in a fixed bed. International Journal of Heat and Mass Transfer, 1969. **12**(5): p. 549-570.
128. Singh, C.P. and D.N. Saraf, Simulation of side fired steam-hydrocarbon reformers. Industrial & Engineering Chemistry Process Design and Development, 1979. **18**(1): p. 1-7.
129. Halabi, M., M. De Croon, J. Van der Schaaf, P. Cobden, and J. Schouten, Modeling and analysis of autothermal reforming of methane to hydrogen in a fixed bed reformer. Chemical Engineering Journal, 2008. **137**(3): p. 568-578.
130. Twigg, M.V. and M. Twigg, Catalyst handbook1989: CSIRO.
131. Xu, J. and G.F. Froment, Methane steam reforming, methanation and water-gas shift: I. Intrinsic kinetics. AIChE Journal, 1989. **35**(1): p. 88-96.
132. Zhou, Z., L. Han, and G.M. Bollas, Model-based analysis of bench-scale fixed-bed units for chemical-looping combustion. Chemical Engineering Journal, 2013. **233**: p. 331-348.
133. Ghouse, J.H. and T.A. Adams, A multi-scale dynamic two-dimensional heterogeneous model for catalytic steam methane reforming reactors. International Journal of Hydrogen Energy, 2013. **38**(24): p. 9984-9999.
134. Adams, T.A. and P.I. Barton, A dynamic two-dimensional heterogeneous model for water gas shift reactors. International Journal of Hydrogen Energy, 2009. **34**(21): p. 8877-8891.
135. Barkelew, C. Stability of chemical reactors. in Chem. Eng. Prog. Symp. Ser. 1959.

136. Liu, S.-L., R. Aris, and N.R. Amundson, Stability of Nonadiabatic Packed Bed Reactors. Elementary Treatment. Industrial & Engineering Chemistry Fundamentals, 1963. **2**(1): p. 12-20.
137. McGreavy, C. and D. Cresswell, A lumped parameter approximation to a general model for catalytic reactors. The Canadian Journal of Chemical Engineering, 1969. **47**(6): p. 583-589.
138. Feick, J. and D. Quon, Mathematical models for the transient behavior of a packed bed reactor. The Canadian Journal of Chemical Engineering, 1970. **48**(2): p. 205-211.
139. Karanth, N. and R. Hughes, Mathematical modeling of heterogeneous catalytic reactors. Catalysis Reviews Science and Engineering, 1974. **9**(1): p. 169-208.
140. Dueso, C., M. Ortiz, A. Abad, F. García-Labiano, F. Luis, P. Gayán, and J. Adánez, Reduction and oxidation kinetics of nickel-based oxygen-carriers for chemical-looping combustion and chemical-looping reforming. Chemical Engineering Journal, 2012. **188**: p. 142-154.
141. Keskitalo, T.J., K.J. Lipiäinen, and A.O.I. Krause, Kinetic modeling of coke oxidation of a ferrierite catalyst. Industrial & engineering chemistry research, 2006. **45**(19): p. 6458-6467.
142. Subramaniam, B. and A. Varma, Reaction kinetics on a commercial three-way catalyst: the carbon monoxide-nitrogen monoxide-oxygen-water system. Industrial & engineering chemistry product research and development, 1985. **24**(4): p. 512-516.
143. Kolbitsch, P., T. Pröll, and H. Hofbauer, Modeling of a 120kW chemical looping combustion reactor system using a Ni-based oxygen carrier. Chemical Engineering Science, 2009. **64**(1): p. 99-108.
144. Hossain, M.M. and H.I. de Lasa, Reactivity and stability of Co-Ni/Al2O3 oxygen carrier in multicycle CLC. AIChE Journal, 2007. **53**(7): p. 1817-1829.
145. Jin, H. and M. Ishida, Reactivity study on natural-gas-fueled chemical-looping combustion by a fixed-bed reactor. Industrial & engineering chemistry research, 2002. **41**(16): p. 4004-4007.
146. Mattisson, T., M. Johansson, and A. Lyngfelt, The use of NiO as an oxygen carrier in chemical-looping combustion. Fuel, 2006. **85**(5): p. 736-747.
147. Bhatia, S. and D. Perlmutter, Effect of the product layer on the kinetics of the CO2-lime reaction. AIChE Journal, 1983. **29**(1): p. 79-86.

148. De Diego, L.F., P. Gayán, F. García-Labiano, J. Celaya, A. Abad, and J. Adánez, Impregnated CuO/Al2O3 oxygen carriers for chemical-looping combustion: avoiding fluidized bed agglomeration. Energy & Fuels, 2005. **19**(5): p. 1850-1856.
149. Corbella, B.M., L.F. de Diego, F. García-Labiano, J. Adánez, and J.M. Palacios, Characterization study and five-cycle tests in a fixed-bed reactor of titania-supported nickel oxide as oxygen carriers for the chemical-looping combustion of methane. Environmental science & technology, 2005. **39**(15): p. 5796-5803.
150. Mattisson, T., A. Lyngfelt, and P. Cho, The use of iron oxide as an oxygen carrier in chemical-looping combustion of methane with inherent separation of CO 2. Fuel, 2001. **80**(13): p. 1953-1962.
151. Abad, A., J. Adánez, F. García-Labiano, F. Luis, P. Gayán, and J. Celaya, Mapping of the range of operational conditions for Cu-, Fe-, and Ni-based oxygen carriers in chemical-looping combustion. Chemical Engineering Science, 2007. **62**(1): p. 533-549.
152. Ryu, H.-J., D.-H. Bae, K.-H. Han, S.-Y. Lee, G.-T. Jin, and J.-H. Choi, Oxidation and reduction characteristics of oxygen carrier particles and reaction kinetics by unreacted core model. Korean Journal of Chemical Engineering, 2001. **18**(6): p. 831-837.
153. Moghtaderi, B. and H. Song, Reduction properties of physically mixed metallic oxide oxygen carriers in chemical looping combustion. Energy & Fuels, 2010. **24**(10): p. 5359-5368.
154. Evans, J., S. Song, and C. Leon-Sucre, The kinetics of nickel oxide reduction by hydrogen; measurements in a fluidized bed and in a gravimetric apparatus. Metallurgical Transactions B, 1976. **7**(1): p. 55-65.
155. Zhou, Z., L. Han, and G.M. Bollas, Kinetics of NiO reduction by H 2 and Ni oxidation at conditions relevant to chemical-looping combustion and reforming. International Journal of Hydrogen Energy, 2014. **39**(16): p. 8535-8556.
156. Brown, M.E., The Prout-Tompkins rate equation in solid-state kinetics. Thermochimica acta, 1997. **300**(1): p. 93-106.
157. Miura, K. and P.L. Silveston, Analysis of gas-solid reactions by use of a temperature-programmed reaction technique. Energy & Fuels, 1989. **3**(2): p. 243-249.

158. Bhatia, S.K. and D. Perlmutter, A random pore model for fluid-solid reactions: I. Isothermal, kinetic control. AIChE Journal, 1980. **26**(3): p. 379-386.
159. Szekely, J. and J. Evans, A structural model for gas—solid reactions with a moving boundary. Chemical Engineering Science, 1970. **25**(6): p. 1091-1107.
160. Adanez, J., A. Abad, F. Garcia-Labiano, P. Gayan, and L.F. de Diego, Progress in chemical-looping combustion and reforming technologies. Progress in Energy and Combustion Science, 2012. **38**(2): p. 215-282.
161. Levenspiel, O., Chemical reaction engineering, 1999, john wiley and sons.
162. Khawam, A. and D.R. Flanagan, Solid-state kinetic models: basics and mathematical fundamentals. The journal of physical chemistry B, 2006. **110**(35): p. 17315-17328.
163. Son, S.R., K.S. Go, and S.D. Kim, Thermogravimetric analysis of copper oxide for chemical-looping hydrogen generation. Industrial & engineering chemistry research, 2008. **48**(1): p. 380-387.
164. Akers, W. and D. Camp, Kinetics of the methane-steam reaction. AIChE Journal, 1955. **1**(4): p. 471-475.
165. Bodrov, N., L. Apel'Baum, and M. Temkin, Kinetics of the reaction of methane with steam on the surface of nickel. Kinet. Katal, 1964. **5**: p. 696.
166. Elnashaie, S., A. Adris, A. Al-Ubaid, and M. Soliman, On the non-monotonic behaviour of methane—steam reforming kinetics. Chemical Engineering Science, 1990. **45**(2): p. 491-501.
167. Xu, J. and G.F. Froment, Methane steam reforming: II. Diffusional limitations and reactor simulation. AIChE Journal, 1989. **35**(1): p. 97-103.
168. Hou, K. and R. Hughes, The kinetics of methane steam reforming over a Ni/α-Al< sub> 2</sub> O catalyst. Chemical Engineering Journal, 2001. **82**(1): p. 311-328.
169. Olsbye, U., T. Wurzel, and L. Mleczko, Kinetic and reaction engineering studies of dry reforming of methane over a Ni/La/Al2O3 catalyst. Industrial & engineering chemistry research, 1997. **36**(12): p. 5180-5188.
170. Barroso Quiroga, M.M. and A.E. Castro Luna, Kinetic analysis of rate data for dry reforming of methane. Industrial & engineering chemistry research, 2007. **46**(16): p. 5265-5270.

171. Yin, L., S. Wang, H. Lu, J. Ding, R. Mostofi, and Z. Hao, Simulation of effect of catalyst particle cluster on dry methane reforming in circulating fluidized beds. Chemical Engineering Journal, 2007. **131**(1): p. 123-134.
172. Wei, J. and E. Iglesia, Isotopic and kinetic assessment of the mechanism of reactions of CH 4 with CO 2 or H 2 O to form synthesis gas and carbon on nickel catalysts. Journal of Catalysis, 2004. **224**(2): p. 370-383.
173. Wang, S. and G. Lu*, A comprehensive study on carbon dioxide reforming of methane over Ni/γ-Al2O3 catalysts. Industrial & engineering chemistry research, 1999. **38**(7): p. 2615-2625.
174. Zhang, Z. and X.E. Verykios, Mechanistic aspects of carbon dioxide reforming of methane to synthesis gas over Ni catalysts. Catalysis Letters, 1996. **38**(3-4): p. 175-179.
175. Bradford, M.C. and M.A. Vannice, Catalytic reforming of methane with carbon dioxide over nickel catalysts II. Reaction kinetics. Applied Catalysis A: General, 1996. **142**(1): p. 97-122.
176. Snoeck, J.-W., G. Froment, and M. Fowles, Kinetic study of the carbon filament formation by methane cracking on a nickel catalyst. Journal of Catalysis, 1997. **169**(1): p. 250-262.
177. Snoeck, J.-W., G. Froment, and M. Fowles, Steam/CO2 reforming of methane. Carbon filament formation by the Boudouard reaction and gasification by CO2, by H2, and by steam: kinetic study. Industrial & engineering chemistry research, 2002. **41**(17): p. 4252-4265.
178. Baker, E., 87. The calcium oxide–carbon dioxide system in the pressure range 1—300 atmospheres. Journal of the Chemical Society (Resumed), 1962: p. 464-470.
179. Li, Z.-s. and N.-s. Cai, Modeling of multiple cycles for sorption-enhanced steam methane reforming and sorbent regeneration in fixed bed reactor. Energy & Fuels, 2007. **21**(5): p. 2909-2918.
180. Rodríguez, N., M. Alonso, and J. Abanades, Experimental investigation of a circulating fluidized-bed reactor to capture CO2 with CaO. AIChE Journal, 2011. **57**(5): p. 1356-1366.
181. Becerra, A.M., M.E. Iriarte, and A.E.C. Luna, Catalytic activity of a nickel on alumina catalyst in the CO2 reforming of methane. Reaction Kinetics and Catalysis Letters, 2003. **79**(1): p. 119-125.

182. Joensen, F. and J.R. Rostrup-Nielsen, Conversion of hydrocarbons and alcohols for fuel cells. Journal of Power sources, 2002. **105**(2): p. 195-201.
183. Welaya, Y., M.M. El Gohary, and N.R. Ammar, Steam and partial oxidation reforming options for hydrogen production from fossil fuels for PEM fuel cells. Alexandria Engineering Journal, 2012. **51**(2): p. 69-75.
184. Ersoz, A., H. Olgun, and S. Ozdogan, Reforming options for hydrogen production from fossil fuels for PEM fuel cells. Journal of Power sources, 2006. **154**(1): p. 67-73.
185. Bauer, S., S. Javanovic, C.-L. Yu, and H.-Z. Cheng, Upgrading of methane under homogeneous thermal conditions: An environmental and economic imperative. Energy & Fuels, 1997. **11**(6): p. 1204-1218.
186. Vernon, P.D., M.L. Green, A.K. Cheetham, and A.T. Ashcroft, Partial oxidation of methane to synthesis gas. Catalysis Letters, 1990. **6**(2): p. 181-186.
187. Davy, H., Some new experiments and observations on the combustion of gaseous mixtures, with an account of a method of preserving a continued light in mixtures of inflammable gases and air without flame. Philosophical Transactions of the Royal Society of London, 1817. **107**: p. 77-85.
188. Tessié du Motay, C. and C. Maréchal, Industrial preparation of hydrogen. Bull Mensuel de La Société Chimique de Paris, 1868. **9**: p. 334-334.
189. Neumann, B. and K. Jacob, DIE GLEICHGEWICHTSVERHÄLTNISSE BEI DER METHANBILDUNG AUS KOHLENOXYD UND WASSERSTOFF, BZW. KOHLENDIOXYD UND WASSERSTOFF. Zeitschrift für Elektrochemie und angewandte physikalische Chemie, 1924. **30**(23-24): p. 557-576.
190. Byrne Jr, P., E. Gohr, and R. Haslam, Recent Progress in Hydrogenation of Petroleum. Industrial & Engineering Chemistry, 1932. **24**(10): p. 1129-1135.
191. Adris, A., B. Pruden, C. Lim, and J. Grace, On the reported attempts to radically improve the performance of the steam methane reforming reactor. The Canadian Journal of Chemical Engineering, 1996. **74**(2): p. 177-186.
192. Fernandez, J., J. Abanades, and G. Grasa, Modeling of Sorption Enhanced Steam Methane Reforming. Part II: Simulation within a novel Ca/Cu chemical loop process for hydrogen production. Chemical Engineering Science, 2012.
193. Dirksen, H. and C. Riesz, Equilibrium in the steam reforming of natural gas. Industrial & Engineering Chemistry, 1953. **45**(7): p. 1562-1565.

194. Allen, D., E. Gerhard, and M. Likins Jr, Kinetics of the methane-steam reaction. Industrial & Engineering Chemistry Process Design and Development, 1975. **14**(3): p. 256-259.
195. Amphlett, J., M. Evans, R. Mann, and R. Weir, Hydrogen production by the catalytic steam reforming of methanol: Part 2: Kinetics of methanol decomposition using girdler G66B catalyst. The Canadian Journal of Chemical Engineering, 1985. **63**(4): p. 605-611.
196. Jiang, C., D. Trimm, M. Wainwright, and N. Cant, Kinetic mechanism for the reaction between methanol and water over a Cu-ZnO-Al 2 O 3 catalyst. Applied Catalysis A: General, 1993. **97**(2): p. 145-158.
197. Cavallaro, S. and S. Freni, Ethanol steam reforming in a molten carbonate fuel cell. A preliminary kinetic investigation. International Journal of Hydrogen Energy, 1996. **21**(6): p. 465-469.
198. Wolf, D., M. Barre-Chassonnery, M. Höhenberger, A. Van Veen, and M. Baerns, Kinetic study of the water–gas shift reaction and its role in the conversion of methane to syngas over a Pt/MgO catalyst. Catalysis today, 1998. **40**(2): p. 147-156.
199. Froment, G., Production of synthesis gas by steam-and CO 2-reforming of natural gas. Journal of Molecular Catalysis A: Chemical, 2000. **163**(1): p. 147-156.
200. Survey, G., Mineral Commodity Summaries: 20122012: Government Printing Office.
201. Lyngfelt, A. and H. Thunman, Construction and 100 h of operational experience of a 10-kW chemical-looping combustor. Carbon Dioxide Capture for Storage in Deep Geologic Formations; Results from the CO2 Capture Project, 2005. **1**: p. 625-645.
202. Linderholm, C., A. Lyngfelt, C. Béal, A. Trikkel, R. Kuusik, E. Jerndal, T. Mattison, and L. Eide, Chemical-looping combustion with natural gas using spray-dried NiO-based oxygen carriers, 2009, Citeseer.
203. Reactivity, H., Mechanical Durability of NiO/NiAl2O4 and NiO/NiAl2O4/MgAl2O4 Oxygen Carrier Particles Used for more than 1000 h in a 10 kW CLC Reactor Shulman, Alexander; Linderholm, Carl; Mattisson, Tobias; Lyngfelt, Anders. Industrial & engineering chemistry research, 2009. **48**(15): p. 7400-7405.

204. Linderholm, C., A. Abad, T. Mattisson, and A. Lyngfelt, 160h of chemical-looping combustion in a 10kW reactor system with a NiO-based oxygen carrier. International Journal of Greenhouse Gas Control, 2008. **2**(4): p. 520-530.
205. Adánez, J., C. Dueso, L.F. de Diego, F. García-Labiano, P. Gayán, and A. Abad, Methane combustion in a 500 Wth chemical-looping combustion system using an impregnated Ni-based oxygen carrier. Energy & Fuels, 2008. **23**(1): p. 130-142.
206. Wu, J., L. Shen, J. Hao, and H. Gu. Chemical looping combustion of coal in a 1 kWth reactor. in 1st International Conference on Chemical Looping. 2010.
207. Edwards, M. and J. Richardson, Gas dispersion in packed beds. Chemical Engineering Science, 1968. **23**(2): p. 109-123.
208. Yagi, S., D. Kunii, and N. Wakao, Studies on axial effective thermal conductivities in packed beds. AIChE Journal, 1960. **6**(4): p. 543-546.
209. Geankoplis, C., Drying of process materials. Transport processes and unit operations, 1993: p. 520-583.
210. Gordon, S. and B.J. McBride, Computer program for calculation of complex chemical equilibrium compositions and applications1996: Citeseer.
211. McBride, B.J. and S. Gordon, Computer Program for Calculation of Complex Chemical Equilibrium Compositions and Applications II. Users Manual and Program Description. 2; Users Manual and Program Description. 1996.
212. Kee, R.J., F.M. Rupley, and J.A. Miller, Chemkin-II: A Fortran chemical kinetics package for the analysis of gas-phase chemical kinetics, 1989, Sandia National Labs., Livermore, CA (USA).
213. Weisz, P. and C. Prater, Interpretation of measurements in experimental catalysis. Adv. Catal, 1954. **6**(143): p. 60390-9.
214. Fogler, H.S., Elements of chemical reaction engineering. 1999.
215. De Smet, C., M. De Croon, R. Berger, G. Marin, and J. Schouten, Design of adiabatic fixed-bed reactors for the partial oxidation of methane to synthesis gas. Application to production of methanol and hydrogen-for-fuel-cells. Chemical Engineering Science, 2001. **56**(16): p. 4849-4861.
216. Yang, R.T., Gas separation by adsorption processes2013: Butterworth-Heinemann.
217. Metz, B., O. Davidson, H. De Coninck, M. Loos, and L. Meyer, IPCC special report on carbon dioxide capture and storage. Prepared by Working Group III of

the Intergovernmental Panel on Climate Change. IPCC, Cambridge University Press: Cambridge, United Kingdom and New York, USA, 2005. **4**.

218. Brun-Tsekhovoi, A., A. Zadorin, Y.R. Katsobashvili, and S. Kourdyumov. The process of catalytic steam-reforming of hydrocarbons in the presence of carbon dioxide acceptor. in Hydrogen energy progress VII, proceedings of the 7th world hydrogen energy conference. 1988.
219. Han, C. and D.P. Harrison, Simultaneous shift reaction and carbon dioxide separation for the direct production of hydrogen. Chemical Engineering Science, 1994. **49**(24): p. 5875-5883.
220. Yong, Z., V. Mata, and A.r.E. Rodrigues, Adsorption of carbon dioxide at high temperature—a review. Separation and Purification Technology, 2002. **26**(2): p. 195-205.
221. Abanades, J.C., The maximum capture efficiency of CO 2 using a carbonation/calcination cycle of CaO/CaCO 3. Chemical Engineering Journal, 2002. **90**(3): p. 303-306.
222. Silaban, A., M. Narcida, and D. Harrison, Characteristics of the reversible reaction between CO2 (g) and calcined dolomite. Chemical Engineering Communications, 1996. **146**(1): p. 149-162.
223. Blamey, J., V. Manovic, E.J. Anthony, D.R. Dugwell, and P.S. Fennell, On steam hydration of CaO-based sorbent cycled for CO 2 capture. Fuel, 2015. **150**: p. 269-277.
224. Solieman, A., J. Dijkstra, W. Haije, P. Cobden, and R. van den Brink, Calcium oxide for CO< sub> 2</sub> capture: Operational window and efficiency penalty in sorption-enhanced steam methane reforming. International Journal of Greenhouse Gas Control, 2009. **3**(4): p. 393-400.
225. Molinder, R.A., CO2 capture materials for sorption enhanced steam reforming, 2012, University of Leeds.
226. Dedman, A. and A. Owen, Calcium cyanamide synthesis. Part 4.—The reaction CaO+ CO 2= CaCo 3. Transactions of the Faraday Society, 1962. **58**: p. 2027-2035.
227. De Meyer, H., R. Doclo, and J. Seynaeve, Pressure swing adsorption process, 1980, Google Patents.
228. Rostrup-Nielsen, J.R. and T. Rostrup-Nielsen, Large-scale hydrogen production. Cattech, 2002. **6**(4): p. 150-159.

229. Meyer, J., J. Mastin, T.-K. Bjørnebøle, T. Ryberg, and N. Eldrup, Techno-economical study of the Zero Emission Gas power concept. Energy Procedia, 2011. **4**: p. 1949-1956.
230. Antzara, A., E. Heracleous, D.B. Bukur, and A.A. Lemonidou, Thermodynamic Analysis of Hydrogen Production via Chemical Looping Steam Methane Reforming Coupled with in Situ CO 2 Capture. Energy Procedia, 2014. **63**: p. 6576-6589.
231. Stevens, J.F., B. Krishnamurthy, P. Atanassova, and K. Spilker, Development of 50 kW fuel processor for stationary fuel cell applications, 2007, Chevron Techology Ventures, LLC.
232. Rostrup-Nielsen, J., J. Sehested, and J.K. Nørskov, Hydrogen and synthesis gas by steam-and CO 2 reforming, in Advances in Catalysis2002.
233. Wu, S., T. Beum, J. Yang, and J. Kim, Properties of Ca-base CO2 sorbent using Ca (OH) 2 as precursor. Industrial & engineering chemistry research, 2007. **46**(24): p. 7896-7899.
234. Lyon, R. Methods and systems for heat transfer by unmixed combustion using mixed catalysts. in Fuel and Energy Abstracts. 1997.
235. Kumar, R.V., J.A. Cole, and R.K. Lyon. Unmixed reforming: an advanced steam reforming process. in Preprints of Symposia, 218th. ACS National Meeting, August. 1999.
236. Warren K. Lewis, N.a.E.R.G., Production of pure carbon dioxide. 1950.
237. Richter, H. and K. Knoche. Reversibility of Combustion Proceases, Efficiency and Costing, Second Law Analysis of Processes. in Gaggioli R A. ACS Symposium Series.
238. Pröll, T. and H. Hofbauer. Chemical Looping Combustion and Reforming. in Proceedings of the 9th European Conference on Industrial Furnaces and Boilers (INFUB-9), Estoril, Portugal. 2001.
239. Zafar, Q., T. Mattisson, and B. Gevert, Integrated hydrogen and power production with CO2 capture using chemical-looping reforming redox reactivity of particles of CuO, Mn2O3, NiO, and Fe2O3 using SiO2 as a support. Industrial & engineering chemistry research, 2005. **44**(10): p. 3485-3496.
240. de Diego, L.F., P. Gayán, J. Celaya, J.M. Palacios, and J. Adánez, Operation of a 10kWth chemical-looping combustor during 200h with a CuO–Al< sub> 2</sub> O< sub> 3</sub> oxygen carrier. Fuel, 2007. **86**(7): p. 1036-1045.

241. Monnerat, B., L. Kiwi-Minsker, and A. Renken, Hydrogen production by catalytic cracking of methane over nickel gauze under periodic reactor operation. Chemical Engineering Science, 2001. **56**(2): p. 633-639.
242. Antzara, A., E. Heracleous, D.B. Bukur, and A.A. Lemonidou, Thermodynamic analysis of hydrogen production via chemical looping steam methane reforming coupled with in situ CO 2 capture. International Journal of Greenhouse Gas Control, 2015. **32**: p. 115-128.

9. APPENDICES

9.1 APPENDIX A

The rate equations used for SMR, WGS and global SMR reactions:

$$R_1 = \frac{k_1}{p_{H_2}^{2.5}}\left(p_{CH_4}p_{H_2O} - \frac{p_{H_2}^3 p_{CO}}{K_I}\right)\left(\frac{1}{\Omega^2}\right) \quad A1$$

$$R_2 = \frac{k_3}{p_{H_2}}\left(p_{CO}p_{H_2O} - \frac{p_{H_2}p_{CO_2}}{K_{II}}\right)\left(\frac{1}{\Omega^2}\right) \quad A2$$

$$R_3 = \frac{k_2}{p_{H_2}^{3.5}}\left(p_{CH_4}p_{H_2O}^2 - \frac{p_{H_2}^4 p_{CO_2}}{K_{III}}\right)\left(\frac{1}{\Omega^2}\right) \quad A3$$

$$\Omega = 1 + K_{CO}p_{CO} + K_{H_2}p_{H_2} + K_{CH_4}p_{CH_4} + K_{H_2O}\frac{p_{H_2O}}{p_{H_2}} \quad A4$$

Equilibrium constants for SMR process, Arrhenius expression for kinetic parameters and adsorption equation are given as:

$$K_I = \exp\left(\frac{-26830}{T_s} + 30.114\right) \quad A5$$

$$K_{II} = \exp\left(\frac{4400}{T_s} - 4.036\right) \quad A6$$

$$K_{III} = K_I K_{II} \quad A7$$

$$k_j = k_{oj}\exp\left(\frac{-E_j}{R_g T}\right) \quad A8$$

$$K_i = K_{oi}\exp\left(\frac{-\Delta H_i}{R_g T}\right) \quad A9$$

Reaction rate for all species involved in the reactor system:

$$r_{CH_4} = -\eta_1 R_1 - \eta_3 R_3 \quad A10$$

$$r_{CO_2} = \eta_2 R_2 + \eta_3 R_3 \quad A11$$

$$r_{H_2O} = -\eta_1 R_1 - \eta_2 R_2 - 2\eta_3 R_3 \quad A12$$

$$r_{H_2} = 3\eta_1 R_1 + \eta_2 R_2 + 4\eta_3 R_3 \quad A13$$

$$r_{CO} = \eta_1 R_1 - \eta_2 R_2 \quad A14$$

Gibbs free energy:

$$dG = \sum_{i=1}^{N} \mu_i dn_i = 0 \quad A15$$

9.2 APPENDIX B

Table B.1: Experimental conditions used for the kinetic study of the reforming process

Catalyst	18 wt. % Ni/α-Al_2O_3							
Diameter of catalyst, dp [μm]	200							
Mass of catalyst [g]	2.0							
Reaction temperature [°C]	SMR				WGS			
	550	600	650	700	300	325	350	375
Pressure [atm]	1							
Molar steam to carbon ratio	3.12							
Feed mole fraction	CO/CH_4		H_2O		N_2			
	0.075		0.234		0.691			
Feed volumetric flow rate at STP (cm^3/min) for SMR	CH_4		H_2O		N_2			
	10		0.023		92			
	16		0.037		146			
	22		0.05		203			
	28		0.064		258			
Feed volumetric flow rate at STP (cm^3/min) for WGS	CO		H_2O		N_2			
	8		0.018		72			
	12		0.027		108			
	16		0.036		144			
	20		0.045		180			

9.3 APPENDIX C

Statistical analysis on gPROMS

CH_4 concentration [mol m^{-3}]

Time [s]	Variable Values			Deviation		
	Experimental Measurement	Model Prediction	Standard Deviation of Experimental Measurement	Absolute	Percentage	Weighted
0	1.2E+00	1.2E+00	2.0E-02	0.0E+00	0.0E+00	0.0E+00
1	4.9E-01	4.9E-01	2.0E-02	5.1E-09	1.0E-06	2.5E-07
2	4.9E-01	4.9E-01	2.0E-02	-8.1E-09	-1.6E-06	-4.1E-07
3	4.9E-01	4.9E-01	2.0E-02	-7.9E-09	-1.6E-06	-4.0E-07
4	4.9E-01	4.9E-01	2.0E-02	-7.9E-09	-1.6E-06	-4.0E-07
5	4.9E-01	4.9E-01	2.0E-02	-7.9E-09	-1.6E-06	-4.0E-07
6	4.9E-01	4.9E-01	2.0E-02	-7.9E-09	-1.6E-06	-4.0E-07
7	4.9E-01	4.9E-01	2.0E-02	-7.9E-09	-1.6E-06	-4.0E-07
8	4.9E-01	4.9E-01	2.0E-02	-7.9E-09	-1.6E-06	-4.0E-07
9	4.9E-01	4.9E-01	2.0E-02	-7.9E-09	-1.6E-06	-4.0E-07
10	4.9E-01	4.9E-01	2.0E-02	-7.9E-09	-1.6E-06	-4.0E-07
11	4.9E-01	4.9E-01	2.0E-02	-7.9E-09	-1.6E-06	-4.0E-07
12	4.9E-01	4.9E-01	2.0E-02	-7.9E-09	-1.6E-06	-4.0E-07
13	4.9E-01	4.9E-01	2.0E-02	-7.9E-09	-1.6E-06	-4.0E-07
14	4.9E-01	4.9E-01	2.0E-02	-7.9E-09	-1.6E-06	-4.0E-07
15	4.9E-01	4.9E-01	2.0E-02	-7.9E-09	-1.6E-06	-4.0E-07
16	4.9E-01	4.9E-01	2.0E-02	-7.9E-09	-1.6E-06	-4.0E-07
17	4.9E-01	4.9E-01	2.0E-02	-7.9E-09	-1.6E-06	-4.0E-07
18	4.9E-01	4.9E-01	2.0E-02	-7.9E-09	-1.6E-06	-4.0E-07
19	4.9E-01	4.9E-01	2.0E-02	-7.9E-09	-1.6E-06	-4.0E-07
20	4.9E-01	4.9E-01	2.0E-02	-7.9E-09	-1.6E-06	-4.0E-07
21	4.9E-01	4.9E-01	2.0E-02	-7.9E-09	-1.6E-06	-4.0E-07
22	4.9E-01	4.9E-01	2.0E-02	-7.9E-09	-1.6E-06	-4.0E-07
23	4.9E-01	4.9E-01	2.0E-02	-7.9E-09	-1.6E-06	-4.0E-07
24	4.9E-01	4.9E-01	2.0E-02	-7.9E-09	-1.6E-06	-4.0E-07
25	4.9E-01	4.9E-01	2.0E-02	-7.9E-09	-1.6E-06	-4.0E-07
26	4.9E-01	4.9E-01	2.0E-02	-7.9E-09	-1.6E-06	-4.0E-07
27	4.9E-01	4.9E-01	2.0E-02	-7.9E-09	-1.6E-06	-4.0E-07
28	4.9E-01	4.9E-01	2.0E-02	-7.9E-09	-1.6E-06	-4.0E-07
29	4.9E-01	4.9E-01	2.0E-02	-7.9E-09	-1.6E-06	-4.0E-07
30	4.9E-01	4.9E-01	2.0E-02	-7.9E-09	-1.6E-06	-4.0E-07
31	4.9E-01	4.9E-01	2.0E-02	-7.9E-09	-1.6E-06	-4.0E-07
32	4.9E-01	4.9E-01	2.0E-02	-7.9E-09	-1.6E-06	-4.0E-07
33	4.9E-01	4.9E-01	2.0E-02	-7.9E-09	-1.6E-06	-4.0E-07
34	4.9E-01	4.9E-01	2.0E-02	-7.9E-09	-1.6E-06	-4.0E-07
35	4.9E-01	4.9E-01	2.0E-02	-7.9E-09	-1.6E-06	-4.0E-07
36	4.9E-01	4.9E-01	2.0E-02	-7.9E-09	-1.6E-06	-4.0E-07
37	4.9E-01	4.9E-01	2.0E-02	-7.9E-09	-1.6E-06	-4.0E-07
38	4.9E-01	4.9E-01	2.0E-02	-7.9E-09	-1.6E-06	-4.0E-07
39	4.9E-01	4.9E-01	2.0E-02	-7.9E-09	-1.6E-06	-4.0E-07
40	4.9E-01	4.9E-01	2.0E-02	-7.9E-09	-1.6E-06	-4.0E-07
41	4.9E-01	4.9E-01	2.0E-02	-7.9E-09	-1.6E-06	-4.0E-07

42	4.9E-01	4.9E-01	2.0E-02	-7.9E-09	-1.6E-06	-4.0E-07
43	4.9E-01	4.9E-01	2.0E-02	-7.9E-09	-1.6E-06	-4.0E-07
44	4.9E-01	4.9E-01	2.0E-02	-7.9E-09	-1.6E-06	-4.0E-07
45	4.9E-01	4.9E-01	2.0E-02	-7.9E-09	-1.6E-06	-4.0E-07
46	4.9E-01	4.9E-01	2.0E-02	-7.9E-09	-1.6E-06	-4.0E-07
47	4.9E-01	4.9E-01	2.0E-02	-7.9E-09	-1.6E-06	-4.0E-07
48	4.9E-01	4.9E-01	2.0E-02	-7.9E-09	-1.6E-06	-4.0E-07
49	4.9E-01	4.9E-01	2.0E-02	-7.9E-09	-1.6E-06	-4.0E-07
50	4.9E-01	4.9E-01	2.0E-02	-7.9E-09	-1.6E-06	-4.0E-07
51	4.9E-01	4.9E-01	2.0E-02	-7.9E-09	-1.6E-06	-4.0E-07
52	4.9E-01	4.9E-01	2.0E-02	-7.9E-09	-1.6E-06	-4.0E-07
53	4.9E-01	4.9E-01	2.0E-02	-7.9E-09	-1.6E-06	-4.0E-07
54	4.9E-01	4.9E-01	2.0E-02	-7.9E-09	-1.6E-06	-4.0E-07
55	4.9E-01	4.9E-01	2.0E-02	-7.9E-09	-1.6E-06	-4.0E-07
56	4.9E-01	4.9E-01	2.0E-02	-7.9E-09	-1.6E-06	-4.0E-07
57	4.9E-01	4.9E-01	2.0E-02	-7.9E-09	-1.6E-06	-4.0E-07
58	4.9E-01	4.9E-01	2.0E-02	-7.9E-09	-1.6E-06	-4.0E-07
59	4.9E-01	4.9E-01	2.0E-02	-7.9E-09	-1.6E-06	-4.0E-07
60	4.9E-01	4.9E-01	2.0E-02	-7.9E-09	-1.6E-06	-4.0E-07
61	4.9E-01	4.9E-01	2.0E-02	-7.9E-09	-1.6E-06	-4.0E-07
62	4.9E-01	4.9E-01	2.0E-02	-7.9E-09	-1.6E-06	-4.0E-07
63	4.9E-01	4.9E-01	2.0E-02	-7.9E-09	-1.6E-06	-4.0E-07
64	4.9E-01	4.9E-01	2.0E-02	-7.9E-09	-1.6E-06	-4.0E-07
65	4.9E-01	4.9E-01	2.0E-02	-7.9E-09	-1.6E-06	-4.0E-07
66	4.9E-01	4.9E-01	2.0E-02	-7.9E-09	-1.6E-06	-4.0E-07
67	4.9E-01	4.9E-01	2.0E-02	-7.9E-09	-1.6E-06	-4.0E-07
68	4.9E-01	4.9E-01	2.0E-02	-7.9E-09	-1.6E-06	-4.0E-07
69	4.9E-01	4.9E-01	2.0E-02	-7.9E-09	-1.6E-06	-4.0E-07
70	4.9E-01	4.9E-01	2.0E-02	-7.9E-09	-1.6E-06	-4.0E-07
71	4.9E-01	4.9E-01	2.0E-02	-7.9E-09	-1.6E-06	-4.0E-07
72	4.9E-01	4.9E-01	2.0E-02	-7.9E-09	-1.6E-06	-4.0E-07
73	4.9E-01	4.9E-01	2.0E-02	-7.9E-09	-1.6E-06	-4.0E-07
74	4.9E-01	4.9E-01	2.0E-02	-7.9E-09	-1.6E-06	-4.0E-07
75	4.9E-01	4.9E-01	2.0E-02	-7.9E-09	-1.6E-06	-4.0E-07
76	4.9E-01	4.9E-01	2.0E-02	-7.9E-09	-1.6E-06	-4.0E-07
77	4.9E-01	4.9E-01	2.0E-02	-7.9E-09	-1.6E-06	-4.0E-07
78	4.9E-01	4.9E-01	2.0E-02	-7.9E-09	-1.6E-06	-4.0E-07
79	4.9E-01	4.9E-01	2.0E-02	-7.9E-09	-1.6E-06	-4.0E-07
80	4.9E-01	4.9E-01	2.0E-02	-7.9E-09	-1.6E-06	-4.0E-07
81	4.9E-01	4.9E-01	2.0E-02	-7.9E-09	-1.6E-06	-4.0E-07
82	4.9E-01	4.9E-01	2.0E-02	-7.9E-09	-1.6E-06	-4.0E-07
83	4.9E-01	4.9E-01	2.0E-02	-7.9E-09	-1.6E-06	-4.0E-07
84	4.9E-01	4.9E-01	2.0E-02	-7.9E-09	-1.6E-06	-4.0E-07
85	4.9E-01	4.9E-01	2.0E-02	-7.9E-09	-1.6E-06	-4.0E-07
86	4.9E-01	4.9E-01	2.0E-02	-7.9E-09	-1.6E-06	-4.0E-07
87	4.9E-01	4.9E-01	2.0E-02	-7.9E-09	-1.6E-06	-4.0E-07
88	4.9E-01	4.9E-01	2.0E-02	-7.9E-09	-1.6E-06	-4.0E-07
89	4.9E-01	4.9E-01	2.0E-02	-7.9E-09	-1.6E-06	-4.0E-07
90	4.9E-01	4.9E-01	2.0E-02	-7.9E-09	-1.6E-06	-4.0E-07
91	4.9E-01	4.9E-01	2.0E-02	-7.9E-09	-1.6E-06	-4.0E-07
92	4.9E-01	4.9E-01	2.0E-02	-7.9E-09	-1.6E-06	-4.0E-07
93	4.9E-01	4.9E-01	2.0E-02	-7.9E-09	-1.6E-06	-4.0E-07
94	4.9E-01	4.9E-01	2.0E-02	-7.9E-09	-1.6E-06	-4.0E-07
95	4.9E-01	4.9E-01	2.0E-02	-7.9E-09	-1.6E-06	-4.0E-07

96	4.9E-01	4.9E-01	2.0E-02	-7.9E-09	-1.6E-06	-4.0E-07
97	4.9E-01	4.9E-01	2.0E-02	-7.9E-09	-1.6E-06	-4.0E-07
98	4.9E-01	4.9E-01	2.0E-02	-7.9E-09	-1.6E-06	-4.0E-07
99	4.9E-01	4.9E-01	2.0E-02	-7.9E-09	-1.6E-06	-4.0E-07
100	4.9E-01	4.9E-01	2.0E-02	-7.9E-09	-1.6E-06	-4.0E-07

9.4 APPENDIX D

Thermodynamic analysis of SMR and SE-SMR process

D.1 Effect of pressure

a) CH_4 Conversion [%]

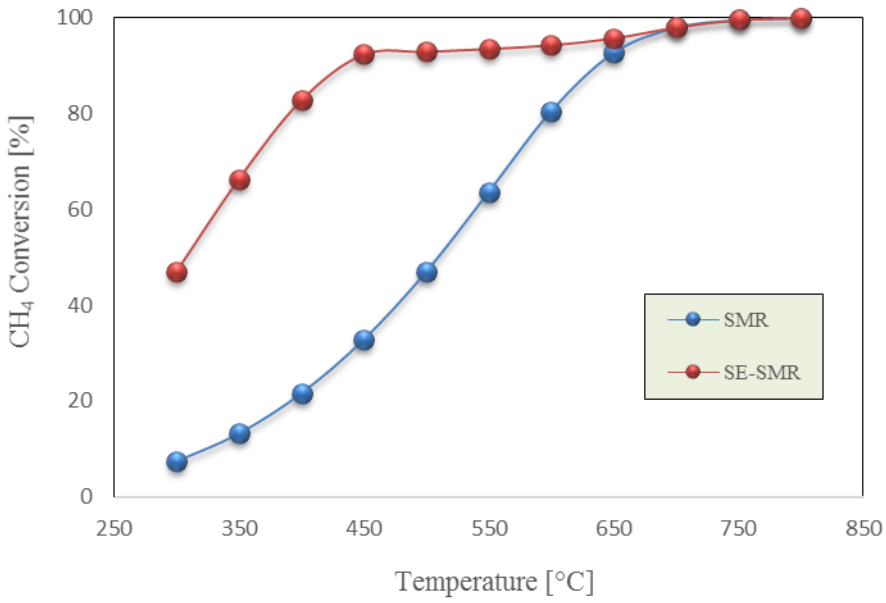

b) H_2 Purity [%]

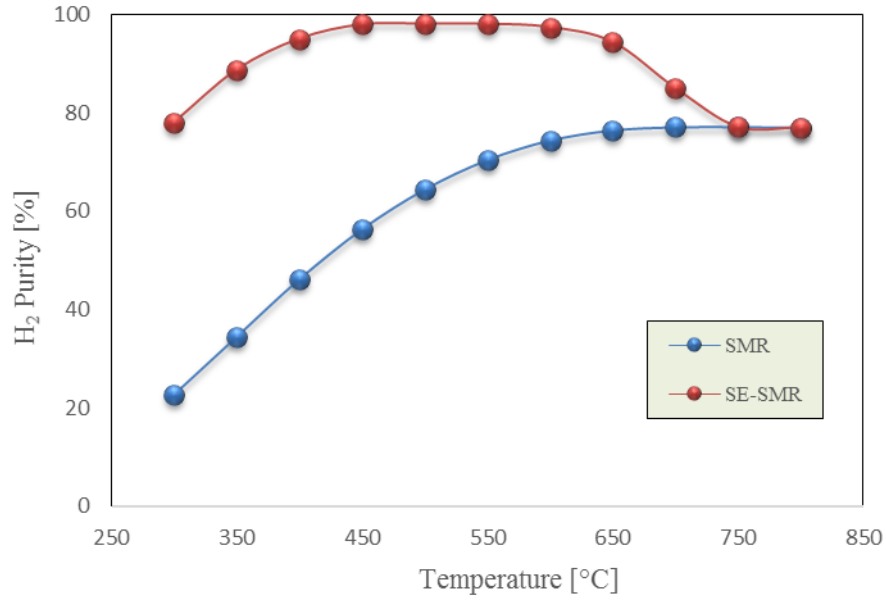

c) H_2 Yield [%]

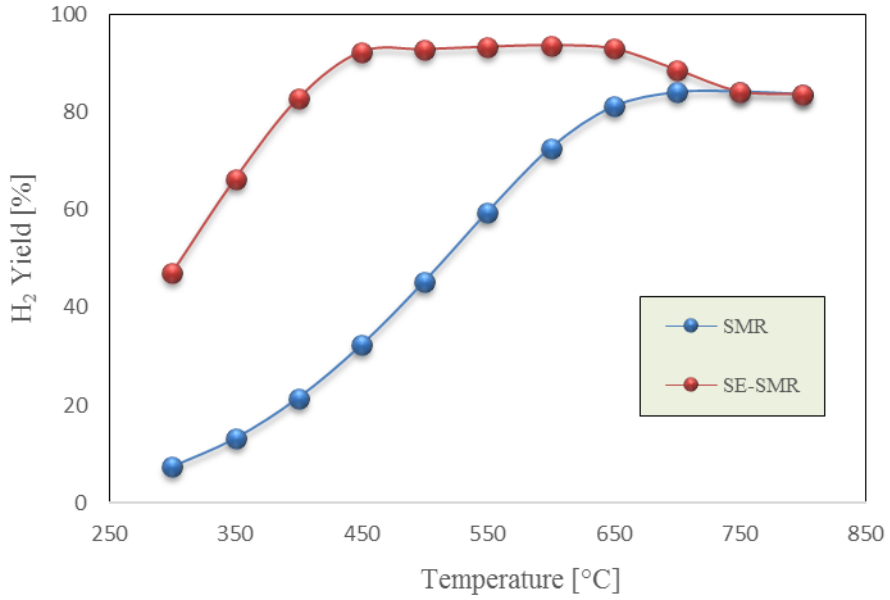

d) CO_2 capturing efficiency [%]

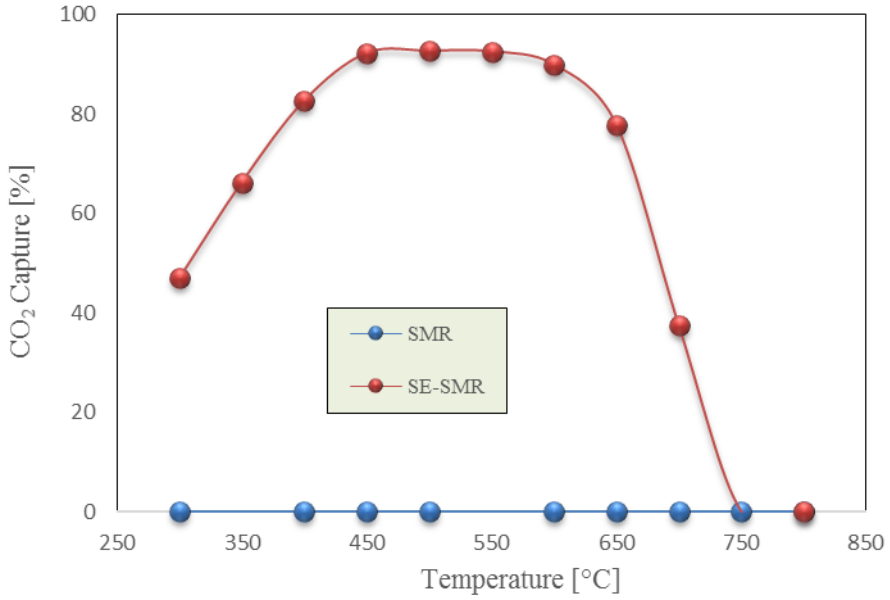

Figure D1: Effect of temperature on the a) Conversion of CH_4, b) H_2 purity, c) H_2 yield and d) CO_2 capturing efficiency under the conditions of 1 bar, S/C of 3.0 and CaO/C of 1.0.

D.2 Effect of pressure

a) CH_4 Conversion [%]

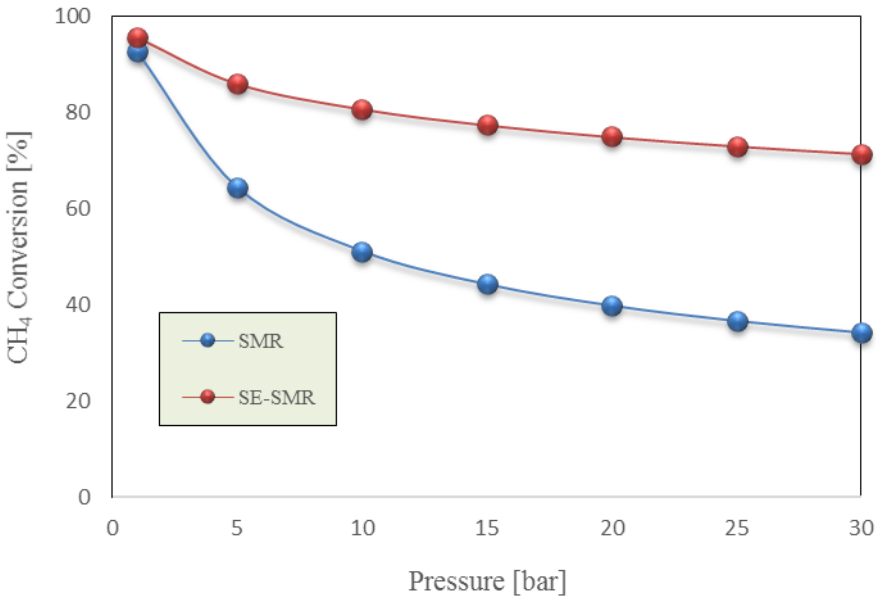

b) H_2 Purity [%]

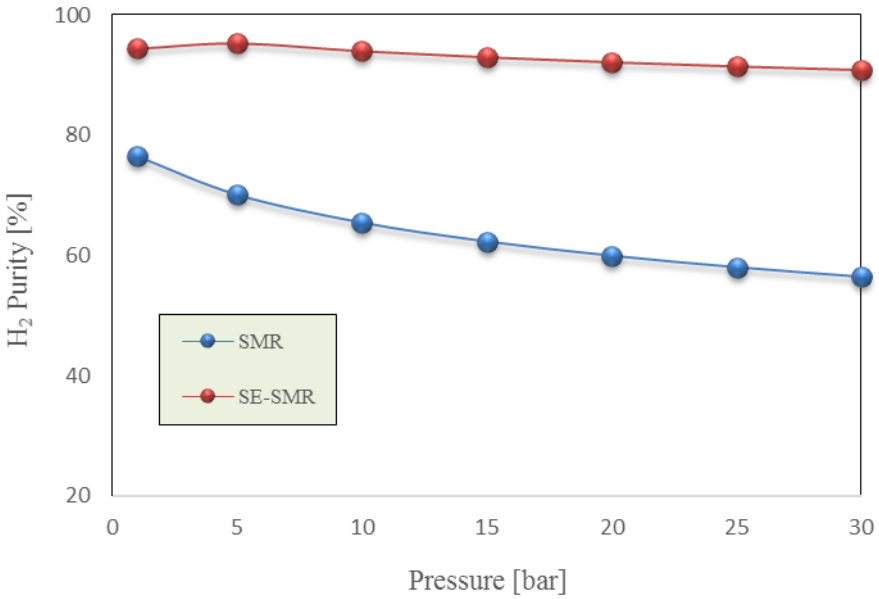

c) H_2 Yield [%]

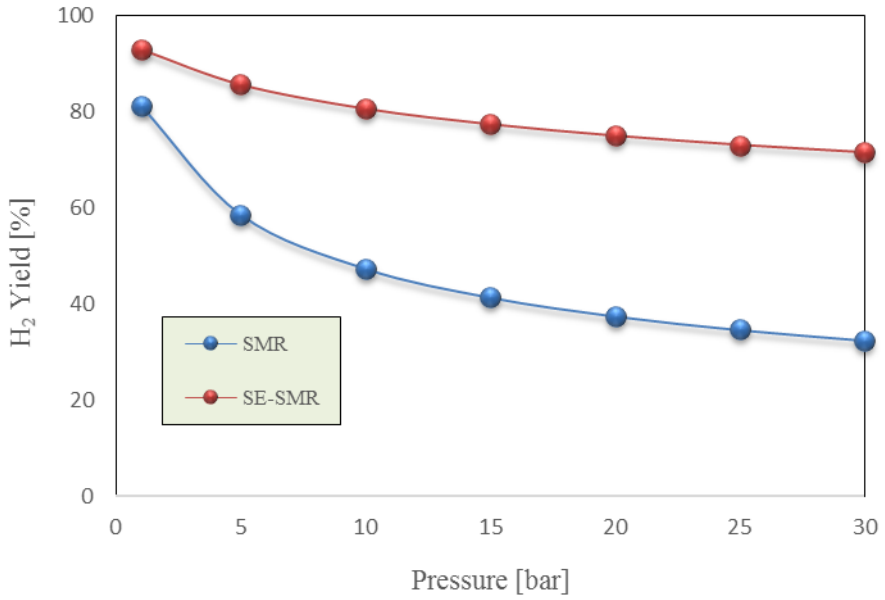

d) CO_2 Capturing efficiency [%]

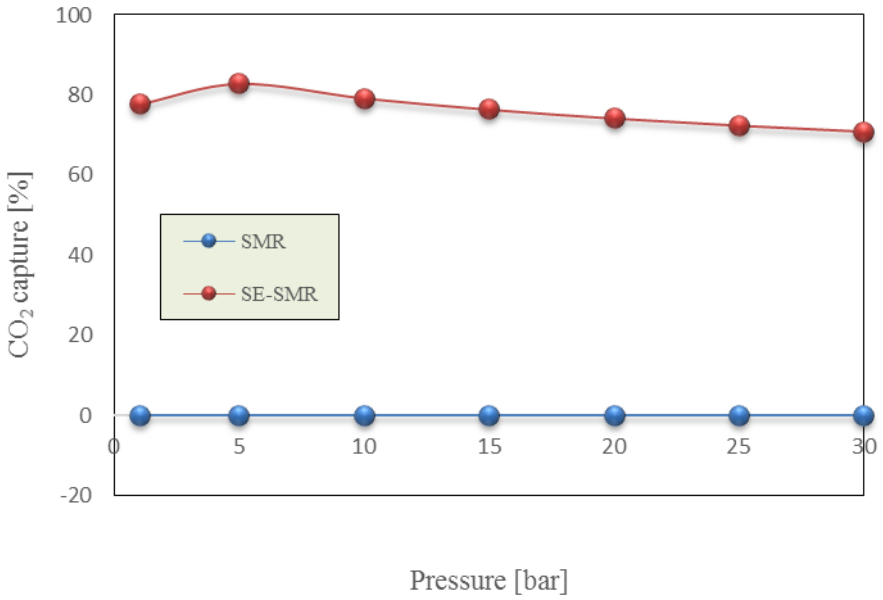

Figure D2: Effect of pressure on the a) Conversion of CH_4, b) H_2 purity, c) H_2 yield and d) CO_2 capturing efficiency under the conditions of 650 °C, S/C of 3.0 and CaO/C of 1.0.

D.3 Effect of S/C

a) CH_4 Conversion [%]

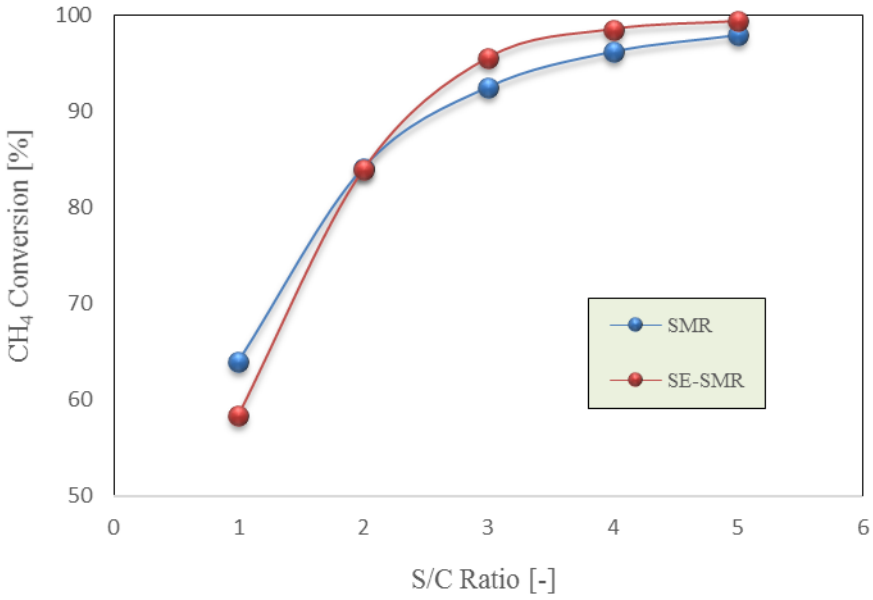

b) H_2 Purity [%]

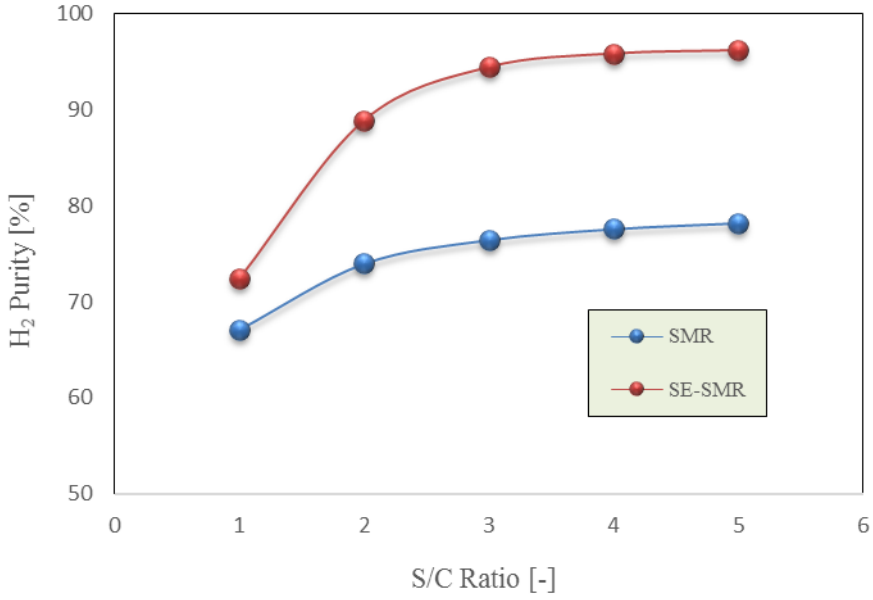

c) H_2 Yield [%]

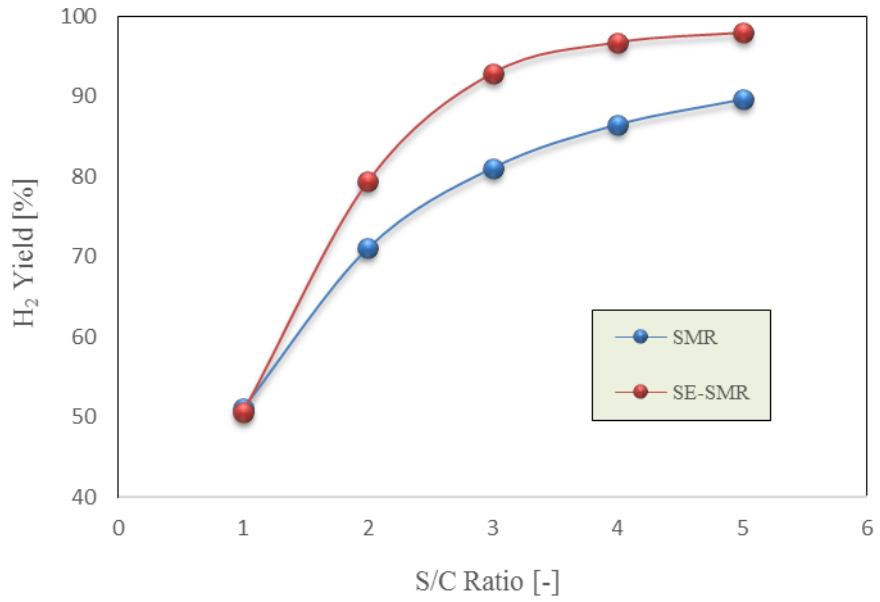

d) CO_2 Capturing efficiency [%]

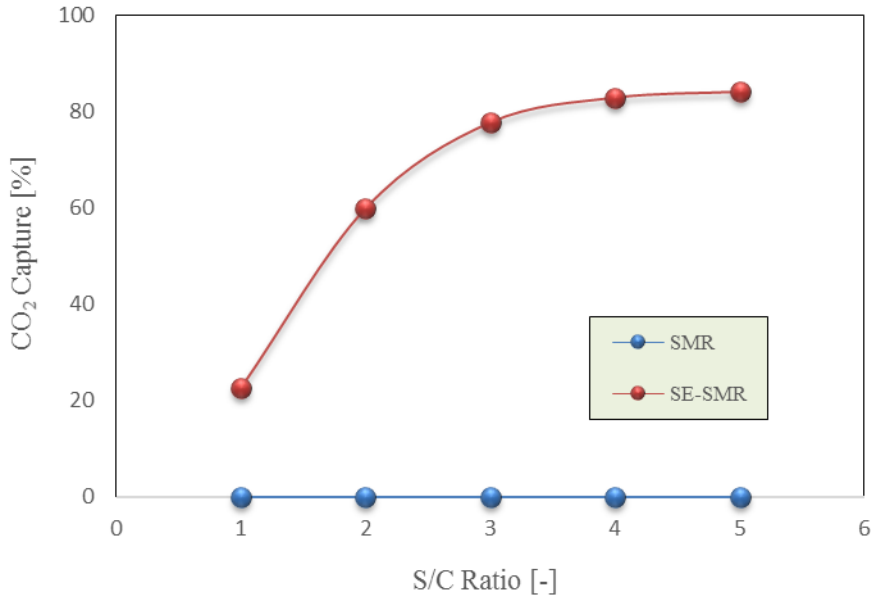

Figure D3: Effect of S/C on the a) Conversion of CH_4, b) H_2 purity, c) H_2 yield and d) CO_2 capturing efficiency under the conditions of 650 °C, 1 bar and CaO/C of 1.0

9.5 APPENDIX E

The rate constants and the equilibrium constants used in the rate equations [R_1-R_{16}]:

$$k_1 = k_{0,1}\exp\left(\frac{-E_1}{RT}\right) = 0.46\exp\left(\frac{-22000}{RT}\right) \quad (E.1)$$

$$k_2 = k_{0,2}\exp\left(\frac{-E_2}{RT}\right) = 20.6\exp\left(\frac{-99000}{RT}\right) \quad (E.2)$$

$$k_3 = k_{0,3}\exp\left(\frac{-E_3}{RT}\right) = (4.21\times10^{3})\exp\left(\frac{-127000}{RT}\right) \quad (E.3)$$

$$k_4 = k_{0,4}\exp\left(\frac{-E_4}{RT}\right) = (6.21\times10^{21})\exp\left(\frac{-29000\times4.184}{RT}\right)/(60\times100^{6}) \quad (E.4)$$

$$k_5 = k_{0,5}\exp\left(\frac{-E_5}{RT}\right) = 4.66\exp\left(\frac{-77416}{RT}\right) \quad (E.5)$$

$$k_6 = k_{0,6}\exp\left(\frac{-E_6}{RT}\right) = (1.31\times10^{-4})\exp\left(\frac{-26413}{RT}\right) \quad (E.6)$$

$$k_7 = k_{0,7}\exp\left(\frac{-E_7}{RT}\right) = (1.097\times10^{-4})\exp\left(\frac{-26505}{RT}\right) \quad (E.7)$$

$$k_8 = k_{0,8}\exp\left(\frac{-E_8}{RT}\right) = (4.18\times10^{-3})\exp\left(\frac{-23666}{RT}\right) \quad (E.8)$$

$$k_9 = k_{0,9}\exp\left(\frac{-E_9}{RT}\right) = (1.17\times10^{15})\exp\left(\frac{-240100}{RT}\right) \quad (E.9)$$

$$k_{10} = k_{0,10}\exp\left(\frac{-E_{10}}{RT}\right) = (5.43\times10^{5})\exp\left(\frac{-67130}{RT}\right) \quad (E.10)$$

$$k_{11} = k_{0,11}\exp\left(\frac{-E_{11}}{RT}\right) = (2.83\times10^{14})\exp\left(\frac{-243900}{RT}\right) \quad (E.11)$$

$$K_I = \exp\left(\frac{-26830}{T_s} + 30.114\right) \quad (E.12)$$

$$K_{II} = \exp\left(\frac{4400}{T_s} - 4.036\right) \quad (E.13)$$

$$K_{III} = K_I K_{II} \quad (E.14)$$

$$\Omega = 1 + K_{CO}p_{CO} + K_{H_2}p_{H_2} + K_{CH_4}p_{CH_4} + K_{H_2O}\frac{p_{H_2O}}{p_{H_2}} \quad (E.15)$$

$$K_i = K_{oi}\exp\left(\frac{-\Delta H_i}{R_g T}\right) \quad (E.16)$$

$$k_{12} = k_{0,12}\exp\left(\frac{-E_{12}}{RT}\right) = 0.207\exp\left(\frac{-9920}{RT}\right) \quad (E.17)$$

$$K_{CO2} = (2.4 \times 10^{-3})\exp\left(\frac{77500}{RT}\right) \quad \text{(E. 18)}$$

$$k_{13} = k_{0,13}\exp\left(\frac{-E_{13}}{RT}\right) = 43.4\exp\left(\frac{-58900}{RT}\right) \quad \text{(E. 19)}$$

$$K_{p,d} = \exp\left(\frac{104}{R}\right) \times \exp\left(\frac{-88400}{RT}\right) \quad \text{(E. 20)}$$

$$K_{CH4,d} = (2.1 \times 10^{-6})\exp\left(\frac{78000}{RT}\right) \quad \text{(E. 21)}$$

$$K_{r,d} = (5.18 \times 10^{7})\exp\left(\frac{-133000}{RT}\right) \quad \text{(E. 22)}$$

$$k_{14} = k_{0,14}\exp\left(\frac{-E_{14}}{RT}\right) = (3.08 \times 10^{4})\exp\left(\frac{-166000}{RT}\right) \quad \text{(E. 23)}$$

$$K_{H2O,g} = (4.73 \times 10^{-6})\exp\left(\frac{97700}{RT}\right) \quad \text{(E. 24)}$$

$$K_{CH4,g} = 3.49 \quad \text{(E. 25)}$$

$$K_{r,g} = (1.83 \times 10^{13})\exp\left(\frac{-216000}{RT}\right) \quad \text{(E. 26)}$$

$$K_{p,g} = \exp\left(\frac{137}{R}\right)\exp\left(\frac{-126000}{RT}\right) \quad \text{(E. 27)}$$

$$k_{15} = k_{0,15}\exp\left(\frac{-E_{15}}{RT}\right) = (8.37 \times 10^{10})\exp\left(\frac{-312000}{RT}\right) \quad \text{(E. 28)}$$

$$K_{CO,g} = (37.8 \times 10^{-6})\exp\left(\frac{100000}{RT}\right) \quad \text{(E. 29)}$$

$$K_{CO2,g} = (8.17 \times 10^{7})\exp\left(\frac{-104000}{RT}\right) \quad \text{(E. 30)}$$

$$K_{p,g,CO2} = \exp\left(\frac{178}{R}\right)\exp\left(\frac{-169000}{RT}\right) \quad \text{(E. 31)}$$

$$\frac{dq_{CO2}}{dt} = k_{carb}(X_{max} - X)\left(\upsilon_{CO2} - \upsilon_{CO2,eq}\right) \quad \text{(E. 32)}$$

$$\upsilon_{CO2,eq} = (4.137 \times 10^{7})\exp\left(\frac{-20474}{T}\right) \quad \text{(E. 33)}$$

9.6 APPENDIX F

Table F.1: Summary of the experimental conditions used for the modelling of NiO reduction [43]

Temperature	800-900 °C
Pressure	1 atm
Oxygen transfer material [OTM]	15% NiO/Al_2O_3
Particle size, d_p	140 μm
Specific surface area	102 $m^2\ g^{-1}$
CH_4 composition	10% in Ar
Gas flow rate	$1.67 \times 10^{-6}\ m^3\ s^{-1}$
Bulk density	1040 $kg\ m^{-3}$
Bed porosity	0.37
Reactor internal diameter	4 mm
Bed depth	7.652 mm
Space velocity	2017 $s\ g_{NiO}^{o}\ g_{CH4}^{-1}$
Peclet number, Pe	> 200

9.7 APPENDIX G

Table G.1: Summary of the experimental conditions and values of physical properties used in the modelling of Ni oxidation [241]

Temperature	450-550 °C
Pressure	1.5 atm
Oxygen transfer material [OTM]	15% NiO/Al_2O_3
OC load	0.1 g
Particle size	140 μm
O_2 composition	8% in Ar
Catalyst density	5000 kg m^{-3}
Porosity	0.80
Bed depth	6.5 mm
Thermal conductivity of gas	$1.6x10^{-2}$ W m^{-1} K^{-1}
Thermal conductivity of solid	100 W m^{-1} K^{-1}
Viscosity of the gas	$0.031x10^{-3}$ kg m^{-1} s^{-1}
Heat of oxidation reaction	$-4.8x10^5$ J mol^{-1}

9.8 APPENDIX H

Table H.1: Summary of the average physical properties and operating conditions used in the modelling of fuel/reforming reactor

Feed temperature	700 °C
Pressure	30 bar
Oxygen transfer material [OTM]	15% NiO/Al_2O_3
OC load	0.1 g
Particle size	0.01 m
Length of bed	7.0 m
Bed Porosity	0.50
Particle Porosity	0.64
Catalyst density	550 kg m^{-3}
Sorbent density	1125 kg m^{-3}
Bed density	1675 kg m^{-3}
Heat capacity of bed	980 J kg^{-1} K^{-1}
Initial specific area of OTM	102 m^2 $kg_{carrier}^{-1}$
Thermal conductivity of gas	3.0×10^{-2} W m^{-1} K^{-1}
Thermal conductivity of solid	13.8 W m^{-1} K^{-1}
Viscosity of the gas	0.018×10^{-3} kg m^{-1} s^{-1}
Standard heat of carbonation	-178,000 J mol^{-1}
Initial concentration of CH_4 and H_2O [mol m^{-3}]	CH_4 H_2O 74.159 222.476
Gas mass flux	3.5 kg m^{-2} s^{-1}

9.9 APPENDIX I

CODING OF SE-CLSR MODEL

MODEL

- **PARAMETER**

COMPONENTS AS ORDERED_SET

REACTIONS AS INTEGER

VOID_BED AS REAL # PACKING BED POROSITY

Reactor_Length AS REAL

av AS REAL # External catalyst surface area per unit volume of catalyst bed (m^2/m^3)

Rho_cat AS REAL # Density of the catalyst pellet (kg/m^3)

Rho_bed AS REAL # Density of the catalyst bed (kg/m^3)

Cp_bed AS REAL # Specific heat of the catalyst bed (J/(kg K))

Hrxn AS ARRAY (reactions) OF REAL # Heat of reaction (J/mol)

Eta AS ARRAY (reactions) OF REAL # Effectiveness factor of reaction j

nu_g AS REAL # Average gas viscosity (kg/(m s))

dp AS REAL # Catalyst particle diameter (m)

Dm AS REAL # Average molecular diffusivity (m^2/s)

Gs AS REAL # Gas mass flow velocity ($kg/(m^2s)$)

lambda_g AS REAL # Average gas thermal conductivity (W/m K)

lambda_s AS REAL # Average solid thermal conductivity (W/m K)

k_o AS ARRAY (reactions) OF REAL # Reference temperature dependent kinetic rate constant of reaction j

E AS ARRAY (reactions) OF REAL # Activation energy of reaction j (J/mol)

Gas_constant AS REAL DEFAULT 8.314 # Universal gas constant (J/mol K)

K_large_o	AS	ARRAY (components) OF REAL # Reference adsorption constant of species i
H	AS	ARRAY (components) OF REAL # Heat of adsorption of species i (J/mol)
LHV_H2,LHV_CH4	AS	REAL
Mav	AS	REAL
a,b,ce,de	AS	ARRAY (components) OF REAL
Mol	AS	ARRAY (components) OF REAL

 # Adsorption

Rho_ad	AS	REAL
pore_bed	AS	REAL
Rho_p	AS	REAL
D_p	AS	REAL
mCO2	AS	REAL
Hcarb	AS	REAL

 # Reduction

MNiO, MNi	AS	REAL
ao	AS	REAL

- **DISTRIBUTION_DOMAIN**

Axial	AS	[0 : Reactor_Length]

- **VARIABLE**

C	AS	DISTRIBUTION (components, Axial) OF Concentration # concentration of species i in the gas phase (mol/m^3)
C_o	AS	ARRAY (components) OF Concentration
u	AS	DISTRIBUTION (axial) OF notype
T	AS	DISTRIBUTION (Axial) OF Temperature # Gas phase temperature (K)
T_o	AS	Temperature # Initial gas phase temperature (K)

P AS DISTRIBUTION (Axial) OF notype

Pin AS notype

r_small AS DISTRIBUTION(components, Axial) OF Rate # Rate of consumption or formation of species i (mol/(kgcat s))

R_large AS DISTRIBUTION (reactions, Axial) OF Rate # Rate of reaction j (mol/(kgcat s))

p_p AS DISTRIBUTION (components, axial) OF notype # Partial pressure of gas species i (bar)

K_eq AS DISTRIBUTION (reactions, Axial) OF notype # thermodynamic equilibrium constant of reaction j

Omega AS DISTRIBUTION (Axial) OF notype # Denominator term in the reaction kinetics

K_large AS DISTRIBUTION (components, Axial) OF notype # Adsorption constant of species i

lambda_f AS Conductivity # Effective thermal conductivity (W/m K)

Rho_f AS DISTRIBUTION (Axial) OF notype

Cp_g AS notype # Specific heat of the fluid (J/(kg K)

D_z AS DISTRIBUTION (Axial) OF notype

hf AS notype # Gas to solid heat transfer coefficient (W/(m2 s))

Pr AS notype

jH,Re AS notype

X_CH4 AS DISTRIBUTION (Axial) OF notype

yi AS DISTRIBUTION (components, axial) OF notype

y AS DISTRIBUTION (components, axial) OF notype

Adsorption

Rcarb AS DISTRIBUTION (Axial) OF notype

qi AS DISTRIBUTION (Axial) OF notype

kCO2 AS notype

qeq AS DISTRIBUTION (Axial) OF notype

Reduction

CNiO AS DISTRIBUTION (Axial) OF notype

CNi AS DISTRIBUTION (Axial) OF notype

Rred_1	AS	DISTRIBUTION (Axial) OF notype
Rred_2	AS	DISTRIBUTION (Axial) OF notype
Rred_3	AS	DISTRIBUTION (Axial) OF notype
Rred_4	AS	DISTRIBUTION (Axial) OF notype
k1,k2,k3,k4	AS	DISTRIBUTION (Axial) OF notype
X	AS	DISTRIBUTION (Axial) OF notype
CNiO_o,CNi_o	AS	Concentration

- **BOUNDARY**

 # At inlet, z = 0

C(,0) = C_o;

T(0) = T_o ;

P(0) = Pin;

 # At outlet, z = Reactor_Length

PARTIAL (C (,Reactor_Length),Axial) = 0 ;

PARTIAL (T (Reactor_Length),Axial) = 0 ;

- **EQUATION**

 # Mass balance in the gas phase and solid phase

```
FOR i IN components DO
        FOR z := 0|+ TO Reactor_Length|- DO
        Void_bed*$(C(i,z))
        + PARTIAL(u(z)*C(i,z),Axial)
        - 0.3*(1-Void_bed)*1000*Rho_cat*r_small(i,z)
        + (1-Void_bed)*Rho_ad*Rcarb(z)
        = 0 ;
        END
END
```

 # Adsorption

```
FOR z := 0 TO Reactor_Length DO
Rcarb(z)          = 1000*(0.3/56)*$qi(z);
$qi(z)            = kCO2*(0.4-qi(z))*(yi('CO2',z)-qeq(z));
qeq(z)             = 1.737E7*EXP(-20474/T(z));
END
```

 # NiO and Ni

```
FOR z := 0 TO Reactor_Length DO
$CNiO(z)          = -(2*Rred_1(z)+Rred_2(z)+Rred_3(z)+Rred_4(z))*MNiO;
$CNi(z)           =  (2*Rred_1(z)+Rred_2(z)+Rred_3(z)+Rred_4(z))*MNi;
END
```

 # Energy balance in the gas phase and solid phase

```
FOR z := 0|+ TO Reactor_Length|- DO
        Void_bed*Rho_f(z)*Cp_g*$T(z)
        + u(z)*Rho_f(z)*Cp_g*PARTIAL(T(z),Axial)
        = Rho_cat*(1 - Void_bed)*SIGMA(-Hrxn()*R_large(,z))
        -(1-Void_bed)*Rho_bed*Cp_bed*$T(z)
         -(1-Void_bed)*Rho_ad*Rcarb(z)*(Hcarb);
END
lambda_f/lambda_g      = (Void_bed + (1-Void_bed)/(0.139*Void_bed-
0.0339+(0.667)*(lambda_g/lambda_s))) + (0.75*Pr*Re);
```

 # Pressure Drop

```
FOR z := 0|+ TO Reactor_Length DO
PARTIAL(P(z),axial)        = (-150*nu_g*((1-Void_bed)^2)*u(z)/((dp^2)*(void_bed^3))
                             -1.75*(1-void_bed)*Rho_f(z)*(u(z)^2)/(dp*void_bed^3))*1E-5;
END
```

 # Density

```
FOR z := 0 TO Reactor_Length DO
Rho_f(z)          = (P(z)*Mav/Gas_constant/T(z))*100;
END
```

 # Axial dispersion

```
FOR z := 0 TO Reactor_Length DO
D_z(z)          = 0.73*Dm + (0.5*u(z)*dp)/(1+9.49*Dm/u(z)/dp);
END
```

 # Equilibrium constants

```
FOR z := 0 TO Reactor_Length DO
K_eq(1,z)
        = EXP(-26830/T(z) + 30.114);
K_eq(2,z)
        = EXP(4400/T(z) - 4.036);
K_eq(3,z)
        = K_eq(1,z)*K_eq(2,z);
K_eq(4,z) = 1;
K_eq(5,z) = 1;
K_eq(6,z) = 1;
K_eq(7,z) = 1;
END
```

 # Adsorption constant

```
FOR i IN components DO
        FOR z := 0 TO Reactor_Length DO
        K_large(i,z) = K_large_o(i)*EXP(-H(i)
                        /
                        (Gas_constant*T(z))) ;
        END
END
FOR i IN components DO
        FOR z:=0 TO Reactor_Length DO
        p_p(i,z) =C(i,z)*Gas_constant*T(z)*1E-5;
        END
END
```

 # Velocity

```
FOR z:=0 TO Reactor_Length DO
u(z)      = Gs/Rho_f(z) ;
END
```

 # Heat Transfer Coefficient

```
hf        = (jH * Cp_g * Gs)/(Pr^(2/3));
Pr        = Cp_g * nu_g/lambda_g ;
```

 # Reynold's number

```
Re        = Gs * dp/nu_g ;
jH        = 0.91 * Re^(-0.51) ;
FOR z:=0 TO Reactor_Length DO
X_CH4(z)          = (C('CH4',0)-C('CH4',z))/(C('CH4',0))*100;
yi(,z)            = C(,z)/SIGMA(C(,z));
END
```

 # Dry mole fraction [%]

```
FOR z:=0 TO Reactor_Length DO
y('H2',z)         = C('H2',z)/(C('CH4',z)+C('H2',z)+C('CO',z)+C('CO2',z))*100;
y('CH4',z)        = C('CH4',z)/(C('CH4',z)+C('H2',z)+C('CO',z)+C('CO2',z))*100;
y('CO',z)         = C('CO',z)/(C('CH4',z)+C('H2',z)+C('CO',z)+C('CO2',z))*100;
y('CO2',z)         = C('CO2',z)/(C('CH4',z)+C('H2',z)+C('CO',z)+C('CO2',z))*100;
y('N2',z)         = 0;
y('H2O',z)        = 0;
END
```

PROCESSES

- **UNIT**

Flowsheet	AS	Reforming_SECLR

- **SET**

WITHIN flowsheet DO

Components	:=	['CH4', 'CO', 'H2', 'H2O', 'CO2','N2'];
Reactions	:=	7;
Void_bed	:=	0.5 ;
Reactor_Length	:=	7 ; # m
av	:=	300 ; # m^2/m^3
Cp_bed	:=	980; # (J/(kg K))
nu_g	:=	0.0181E-3; # (kg/(m s))
dp	:=	0.01; # m
Dm	:=	1.6e-5 ; # m^2/s
Gs	:=	3.5 ; # (kg/(m^2 s))
lambda_g	:=	3E-2 ; # W/m/K
lambda_s	:=	13.8 ; # W/m/K
LHV_CH4	:=	800;
LHV_H2	:=	240;
Mav	:=	20.002; # g/mol

 # Adsorption

pore_bed	:=	0.65;
Hcarb	:=	-178000;
D_p	:=	3.3E-7;
mCO2	:=	0.65;

 # Reduction

MNi	:=	58.69; # g/mol
MNiO	:=	74.69; # g/mol

ao := 102; # g/m^2

 # Discretization Method

Axial := [BFDM, 1, 100];

END

- **ASSIGN**

WITHIN Flowsheet DO

C_o := [15.325, 0, 0.4241, 30.650, 0, 15.325]; # (mol/m^3)

T_o := 873.15; # K

Pin := 4.45; # bar

kCO2 := 0.35;

END

- **INITIAL**

WITHIN Flowsheet DO

FOR z := 0|+ TO Reactor_Length|- DO

C(,z) = C_o() ; # (mol/m^3)

T(z) = 873.15; # K

END

FOR z := 0 TO Reactor_Length DO

qi(z) = 0;

CNiO(z) = CNiO_o;

CNi(z) = CNi_o;

X(z) = 0;

END

END

- **SOLUTIONPARAMETERS**

DASolver := "DASOLV" [

"OutputLevel" := 2,

```
        "VariablesWithLargestCorrectorSteps" := 2
    ]
PESolver := "MAXLKHD" [
        "MINLPSolver" := "SRQPD" [
        "OutputLevel" := 3,
        "Scaling" := 1
      ],
        "OutputLevel" := 2
]
```

- **SCHEDULE**

```
Sequence
        #sendmathinfo
        Continue for 2000
END
```

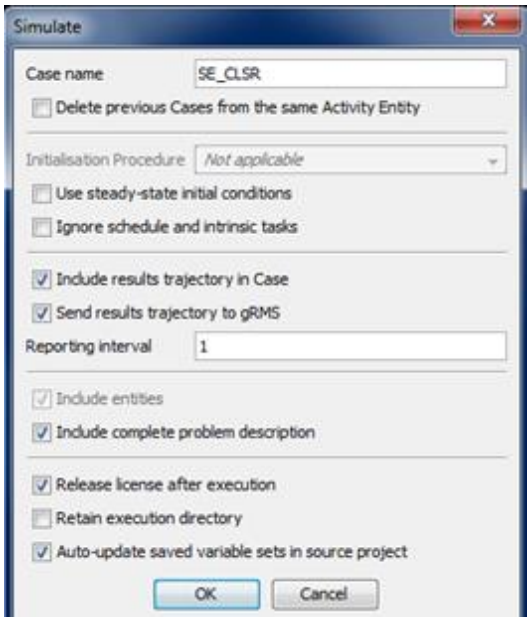

Figure I.1: Execution of Simulation of developed mathematical model of SE-CLSR process